COST MODELLING OF OFFSHORE WIND ENERGY SYSTEMS IN NORTHERN EUROPE

TIMOTHY THOMAS COCKERILL

A thesis submitted in partial fulfilment of the requirements of the University of Sunderland for the degree of Doctor of Philosophy

June 2005

Acknowledgements

A thesis produced on a part time basis is particularly painful for all involved. I am particularly grateful to my supervisor, Professor Harrison for his support, advice and council over rather more years than he expected. Other members of the University of Sunderland have also provided direct support for his work, notably Robin Murphy, Kevin Kelly, Dr. Alan Judd, Peter Claiden and Dr. Nadia Ligdas. I am also grateful for the encouragement offered by my colleagues Professor Tony Alabaster, Dr. Monica Price, Dr. Mary Argyraki, Dr. Julia Walton and Karen Blakey.

Certain elements of the work described were undertaken within the scope of several NERC and European Commission JOULE funded projects. Their financial support is acknowledged with thanks. Other aspects of the work would have been impossible without additional financial support provided by the School of Health, Natural and Social Sciences.

Inspiration for some aspects of this thesis was obtained through discussion with JOULE project collaborators. The expertise of Dr. Martin Kühn (Delft University of Technology, Netherlands), Murray Ferguson (Kvaerner Oil and Gas Limited, UK) and Peter Fuglsang (Riso National Laboratory, Denmark) proved particularly valuable in this regard. The work reported in this thesis was not undertaken in collaboration, and is entirely that of the author except were noted otherwise.

Declaration

While registered as a candidate for the University's research degree, the author has not been a registered candidate or enrolled student for another award of a University or other academic or professional institution.

Aspects of the work reported herein were carried out within the context of several externally funded collaborative projects including:

- Site specific design of wind turbines using numerical cost optimisation, CEC Joule funded project JOUR-CT98-0273 (1998-2001),
- An integrated study of carbon dioxide disposal in the UK, Tyndall Centre Funded Project (2002-2005).

While there are areas of commonality with the funded projects, the study described in this thesis is separate from them, and except where noted, is entirely the original work of the author.

Elements of the work underlying this thesis have contributed to the publications listed in appendix T.

Summary

Locating large wind farms offshore avoids many of the social and environmental conflicts that limit development on land. The major disadvantage is that the costs associated with offshore construction tend to make any energy produced more expensive than that from comparably sized onshore farms. In view of the marginal economics of even the most competitive wind farms, there is a need to identify economically efficient configurations for offshore farms. This requires an understanding of the parameters that drive both the cost and the design of offshore farms, together with knowledge of the relationships between them.

This thesis develops a cost modelling methodology for the analysis of bottom mounted offshore wind farms located in northern European waters. The approach attempts to replicate in simplified form elements of the design process for an offshore farm. Starting with environmental and overall engineering parameters, the methodology 'sizes' the components required for a farm, estimates their cost and energy production performance, and hence predicts the cost of energy.

While all major farm components are considered, the focus of the work described here is on structural aspects. This is because the support structure is directly influenced by local environmental conditions and must be custom designed for each location. Only bottom-mounted structures are examined in this thesis, and analysis is further constrained to mono-tower designs with piled or gravity-type foundations.

The cost modelling methodology is implemented as a computer code and used for a series of parameter studies. The sensitivity of the cost of energy from offshore farms to changes in environmental and overall engineering parameters is investigated. The studies suggested that the wind resource should be the main driver in site selection for good economics.

During the design of an offshore wind farm, the various overall engineering parameters can in principle be chosen independently. In contrast, environmental parameters are linked through geography. While locations can be chosen arbitrarily, environmental parameters do not vary independently in practice. Good wind conditions for example, may be found far offshore. To allow a realistic investigation of the impact of location and combinations of environmental parameters on farm economics, a Geographic Information System (GIS) of offshore conditions has been coupled with the model. Further parameter studies using the GIS demonstrated that environmental parameters other than the wind resource must be accounted for in the process of selecting a site with good economics.

Contents

List of Figures

List of Tables

List of major symbols

The study reported in this thesis draws on an range of engineering disciplines. So far as possible, notations compatible with the 'host' discipline have been maintained. Where a range of symbols are conventionally associated with a particular quantity, choices have been made so as to minimise the scope for confusion. Inevitably there are a number of symbols with multiple definititions, but the particular meaning should always be clear from the context.

The symbols defined here are limited to those used several times in the teaxt. There are a number of other quantities that are only used one ot two times, and these are defined at the point of first use.

Latin script

A	Area
a	Axial flow induction factor, annuity factor
C_d	Drag coefficient
C_l	Lift coefficient
C_m	Inertia coefficient
C_p	Rotor power coefficient
C_t	Thrust coefficient
C_{xxx}	Cost of component xxx
c	Damping coefficient, Weibull shape parameter, unit cost; Charnock constant
D	Fatigue damage
d	Depth
$d_T\,(h)$	Tower diameter (function of height)
$\mathbf{f}$	Force vector
E	Young's Modulus
F	Force
F_S	Factor of safety
f	Frequency
g	Acceleration due to gravity
H	Wave height, transfer function
H_S	Significant wave height
$H_{S,50}$	Significant wave height, 50 year return period
$H_{S,1}$	Significant wave height, 50 year return period

h	Height, vertical co-ordinate
I	Second moment of area
k	Stiffness coefficient; Wave number; Weibull shape parameter
L	Wave length; Lifetime
M	Bending moment
m	Mass, Mass coefficient
N_b	Number of blades
n_e	Economic lifetime
P	Probability; Blade passing frequency
$\mathbf{p}$	Applied force vector
q	Displacement of structure node
R	Radius
Re	Reynolds number
r	Test discount rate
$S(f)$, $S(\omega)$	Spectral density
S_{aa}	Acceleration spectrum
S_{ff}	Force spectrum
S_{qq}	Modal deflection spectrum
S_{uu}	Velocity spectrum
S_{yy}	Nodal deflection spectrum
$S_{\eta\eta}$	Sea surface displacement spectrum
T	Time period
T_Z	Zero up-crossing time period
t	Elapsed time; Construction time
$t(h)$	Tower wall thickness (function of height)
u	Flow speed
u_*	Friction velocity
Z	Section modulus
z	Height, Vertical dimension
z_O	Surface roughness

Greek script

γ	Soil unit weight
κ	Von Karman constant
η	Efficiency
ξ	Damping factor as a fraction of critical damping
ρ	Density
ρ_a	Density of air
ρ_w	Density of water
ρ_T	Density of tower material
λ	Tip speed ratio
σ	Stress
σ_a	Stress amplitude
σ_r	Stress range

σ_u	Standard deviation of turbulence intensity
ϕ	Angle of friction
Ω_R	Rate of rotor rotation
ω	Angular frequency ($= 2\pi f$)

Chapter 1

Introduction

1.1 Role of wind in meeting energy demand

Traditional electricity production techniques rely on combustion of fossil fuels which inevitably releases carbon dioxide into the environment. Over the past three decades there has been increasing concern that rising concentrations of carbon dioxide in the atmosphere have the potential to cause significant changes in the climate by trapping more incident solar energy. While experimental evidence is still inconclusive, there is general agreement of the need to take action in an effort to reduce the ultimate concentration [1].

A difficulty with this policy is that there are few large-scale means of electricity production that do not require fossil fuels. The scope for further deployment of those that do is severely constrained, in the developed world at least. While fusion may ultimately offer a solution, the anticipated timescale of its development is such that it can make little contribution to climate change avoidance. In principle energy saving measures can help, but the practical experience is that it is difficult even to offset the annual growth in demand (see [2] for UK energy statistics and [3] for world figures).

Attention has turned to the less well developed renewables. In part as a result of their immaturity, these technologies are not well suited to electricity production on a scale comparable to fossil plant and tend to be expensive. Low energy densities also mitigate against their economics. Of these technologies, wind energy is arguably in the strongest position to provide substantial quantities of power within the near term. Recent years have seen rapid growth of turbine rated power and total installed capacity in Europe [4].

1.2 Advantages and disadvantages of offshore wind

Rapid expansion has highlighted some 'unexpected' problems with wind. In some EU countries, particularly the UK, public opposition via the planning process has become a major obstacle to development. In Denmark and the Netherlands, expansion has been such that there are only a limited number of good sites with relatively high wind speeds still undeveloped.

Constructing wind farms offshore is a potential solution to these problems. The offshore wind resources of the EU are 'truly enormous' [5] and there are few neighbours to be disturbed. Offshore work is expensive however, meaning that the construction and maintenance cost of an offshore farm is considerably greater than for an equivalent capacity onshore installation. Given the already marginal economics of wind energy production there is therefore no direct economic motivation for moving offshore.

If offshore farms are to be a successful means of circumventing the problems of onshore wind, they must be designed and located so as to produce energy at the lowest possible cost. This in turn requires an undestanding of the factors that influence the energy cost. Developing such an understanding forms the subject of this thesis.

1.3 Overview of offshore farm design

The key feature of any offshore wind farm is the *turbine*. Its interaction with the wind produces electricity, which must be taken ashore via a *grid connection*[1] for sale to consumers. Wind/turbine interaction also produces loads which are transmitted to the *support structure* which comprises both *tower* and *foundation*. A wide range of design solutions are possible for each, and details are discussed further in the next chapter. The choices made, in conjunction with the characteristics of the location, have a direct impact on the cost of the energy produced.

Energy cost may also influenced by other design choices. An important decision is the total capacity of the farm, particularly as it is hoped that economies of scale may lower the energy production cost. The topology of the turbine layout has some influence on the total energy production, thanks to wake interference, and on the grid connection cost, as widely spaced turbines require longer interconnections. Maintaining the wind farm has the potential to be a significant cost, and unexpected failures can result in substantial lost energy production. A major

[1] The literature contains proposals for hydrogen producing offshore farms [6], but these are beyond the scope of this work.

difficulty in the design of economic offshore farms is the interaction between the components.

1.4 State of the art: Projects and studies

Table 1.3 summarises the main environmental and economic features of some existing offshore wind energy converter systems (OWECS), whereas Table 1.2 deals with some of the 'older' feasibility studies. Details of some more recent studies are tabulated at Table 1.1. Where possible energy costs have been calculated from published investment costs, on-going cost and energy production values using a discount rate of 5% and an economic lifetime of 20 years, to provide a consistent basis for comparison. In cases where suitable data was not available the cost of energy and specific investment costs quoted are those stated in the literature. For two of the operating farms information on the on-going costs was not available, and it has been assumed that the annual ongoing costs represent 20% of the final energy costs (see chapter 3 for justification of this value). Where difficulty has been experienced in obtaining complete information, missing data is marked as not known (n/k).

Study	**Scroby Sands**	**Nearshore**	**Omo**	**Horns Rev**	**Gedser**
Reference	[7]	[8]	[9]	[9]	[9]
Date proposed	~ 2000	~ 2000	~ 2002	~ 2003	~ 2006
Site	Norfolk coast, UK	IJmuiden, NL	Omo, DK	Horns Rev, DK	Gedser, DK
Capacity (MW)	25 x 1.5	100	144	120	144
Distance to shore (km)	3	9-16	n/k	n/k	~ 17
Water depth (m)	6	17	n/k	n/k	8-10
S.I.C. (EURc/kW)	1230	1800	1430	1521	1612
Energy cost (EURc/kWh)	6.4	6	4.8	4.6	4.9
Discount rate (%)	n/k	5	5	5	5
Economic life (years)	n/k	20	20	20	20

Table 1.1: Some published commercially oriented OWECS design studies.

Study	**RES Study**	**Thyssen Study**	**SK Power Study**
Reference	[10]	[11]	[12]
Date	1993	1995	1994
Site	Skegness, UK	Baltic Sea, DE	Baltic Sea, DK
Capacity	40 x 500 kW	140 x 1.4 MW	180 x 1 MW
Distance to shore (km)	5	4	17
Water depth (m)	15	5 - 10	8 - 10
S.I.C. (EUR/kW)	4908	1413	1823
Energy cost (EURc/kWh)	17	7.9	6.7
Discount rate (%)	5	n/k	6.7
Economic life (years)	20	n/k	20

Table 1.2: Some older offshore wind design studies.

The studies are presented primarily to provide historical context. Of particular note is the reduction in both specific investment (S.I.C.) cost and energy cost from 1993 to the more recent studies. There are more recent studies not included in the tables, but the increasingly commercial nature of the industry means that cost data are difficult to obtain. In any case it is more informative to examine data from real projects rather than relying on paper studies.

To aid comparison of the projects, the final two rows of Table 1.3 contain specific investment costs and energy costs updated to 2002 values, assuming inflation equal to the UK manufacturing output costs index (PLLU)[2]. The reduction in cost achieved between the first farm in 1991 and the more recently commissioned projects is clearly shown in figure 1.1. A range of factors are likely to be responsible for the reduction in S.I.C., particularly the use of larger turbine units, requiring fewer support structures to be built, and better understanding of the behaviour of support structures in the marine environment, allowing less conservative design. Figure 1.2 shows that in general projects with lower S.I.C. produce more economic energy, however this is a far from clear relationship and in any

[2]There is no certainty that the costs experienced by the offshore wind industry scaled with the UK PLLU, but cost analysis over a 12 year period must take some account of inflation. There is no clearly established way of assessing the inflation experienced by a newly developing industry that relies on multinational expertise and equipment. The UK PLLU is used in the absence of better information.

Project	Vindeby	Lely	Tuno-Knob	Dronten	Gotland	Blyth	Middel-grunden	Utgrun-den	Yttre Sten-grund	Horns Rev	Samso
Reference	[13]	[14] [15] [16]	[17] [18]	[19] [14] [15]	[20] [14] [15]	[14] [21] [15]	[22] [23] [24] [15]	[25] [14] [15] [26] [19]	[14] [15] [19]	[27] [28] [15]	[19] [29]
Completion date	1991	1994	1995	1996	1997	2000	2001	2001	2001	2002	2003
Site	Baltic DK	Ijsselmeer NL	Baltic DK	Ijsselmeer NL	Bockstigen SE	Blyth UK	Middel-grunden DK	Kalmar Sound SE	Yttre Sten-grund SE	Horns Rev DK	SE
No of Turbines	11	4	10	19	5	2	20	7	5	80	10
Capacity (MW)	0.45	0.5	0.5	0.6	0.55	2	2	1.5	2	2	2.3
Distance to shore (km)	1.5	1	6	0.03	4	1	2-3	8	5	14-20	6.2
Water depth (m)	3-5	5-10	3.1-4.7	1-2	5.5-6.5	8.5±2.5 tide	3-6	7.2-10	8	6-14	11-18
Hub height (m above MSL)	35	39	40.5	50	41.5	58	64	65.5	60	70	61
Annual output (MWh/y)	11200	3800	12600	36700	8250	12000	99000	36900	30000	600000	78000
S.I.C. (EUR/kW)	2076	2286	2028	n/k	1290-1455	1420	1217	n/k	n/k	1684	n/k
Energy cost (EURc/kWh)	7.9	11.7	7.5	n/k	4.27-4.81	7.1	5.69	n/k	n/k	4.3	n/k
Discount rate (%)	n/k	5.0	5.5	n/k	5.0	n/k	5.0	n/k	n/k	5.0	n/k
Economic life (years)	n/k	20	20	n/k	20	n/k	20	n/k	n/k	20	n/k
Estimated O&M					Yes					Yes	
Cost year	1991	1994	1995		1997	2000	2000			2001	
2002 Cost	10.22	13.87	8.69		4.92-5.32	7.44	5.96			4.61	
2002 S.I.C.	2685	2710	2351		1426-1609	1487	1275			1723	

Table 1.3: Existing offshore farms with more than a single turbine. Data sources are listed in the table. In some cases a range of values are quoted in the literature, particularly for the older farms. The single values stated here are taken from the literature source that was closest to the project owners, typically written by their staff. Where there was no obvious correct source, a range is quoted. Where no data is available, the entry is marked n/k. In some cases, where shown the O&M costs have been estimated. This list was compiled at the end of 2003. Subsequent constructions are listed in appendix S.

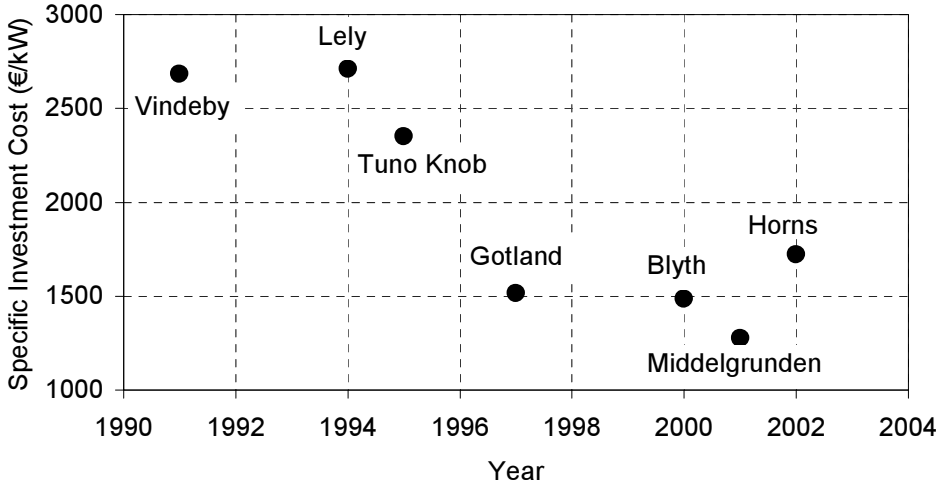

Figure 1.1: Adjusted specific investment cost against year of completion for several offshore wind farms.

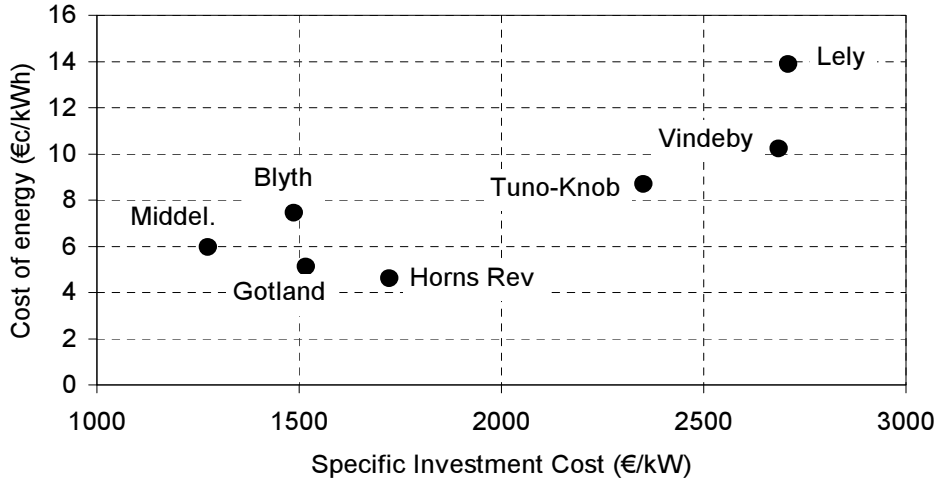

Figure 1.2: Adjusted specific investment cost against cost of energy for several offshore wind farms.

case there are too few data points to draw strong conclusions.

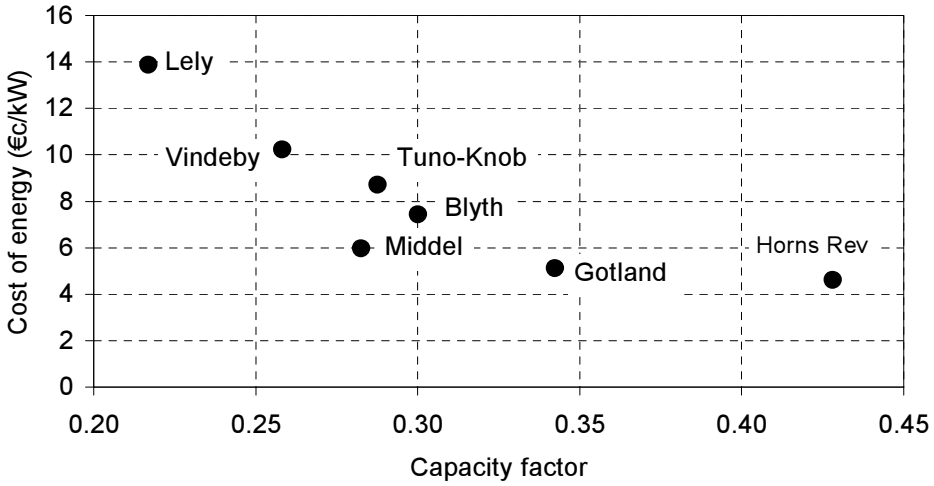

Figure 1.3: Capacity factor against cost of energy for some offshore wind farms. The capacity factor was calculated by dividing the estimated annual output from table 1.3 by the installed turbine capacity.

The first three farms built were intended primarily as experiments to demonstrate the concept of offshore wind, and were very conservatively designed. As such, their relative expense is not surprising, and they should perhaps be considered separately from the more recent plant. Dronten is also something of a special case as it is barely offshore with turbines constructed at the very edge of the IJsselmer inland sea.

The farms built since 1997 have a more commercial focus. Of them, Horns Rev is in a location with a much stronger offshore character than the others, being relatively far from the shore and in deep water. As a result it has a comparatively high S.I.C. The farm still achieves a good energy cost in 2002 prices, and this is due at least in part to the high capacity factor (Figure 1.3), which in turn arises because of good wind conditions at the turbine hub (see Figure 1.4). The hub height wind speed is dictated by the quality of the site wind resource and the tower height. To investigate the influence of the wind resource figure 1.5 plots cost of energy against wind speed measured at 10 m above mean sea level (MSL), showing that for the more modern farms at least, better resource in broad terms produce results in cheaper energy. Figure 1.6 plots both normalised S.I.C and energy cost to demonstrate the importance of the hub height. Broadly speaking higher hubs tend to produce cheaper energy (C.O.E.), but have a more unpredictable impact on the S.I.C. Both the economic performance and the capacity factor are influenced by factors other than wind speed, as the scatter in figures

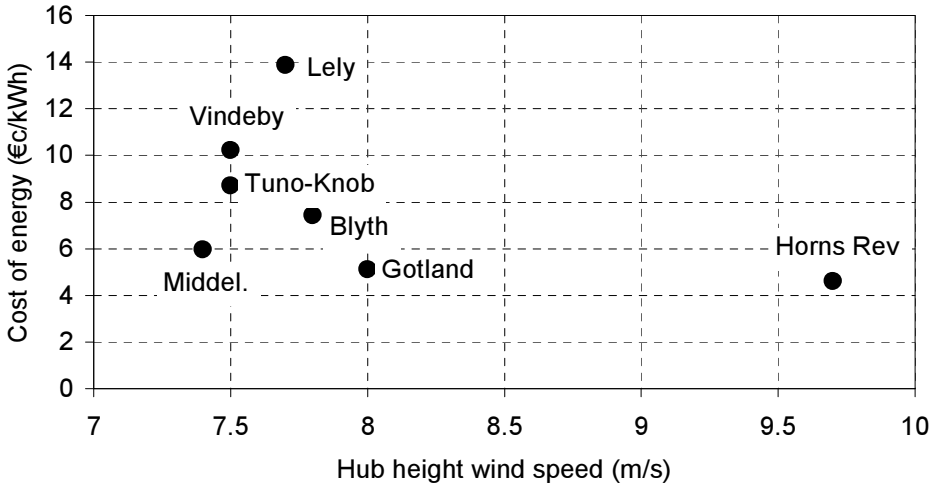

Figure 1.4: Energy cost plotted against hub height wind speed for some offshore wind farms. See figure 1.7 for further information on the sources of the hub height wind speed data.

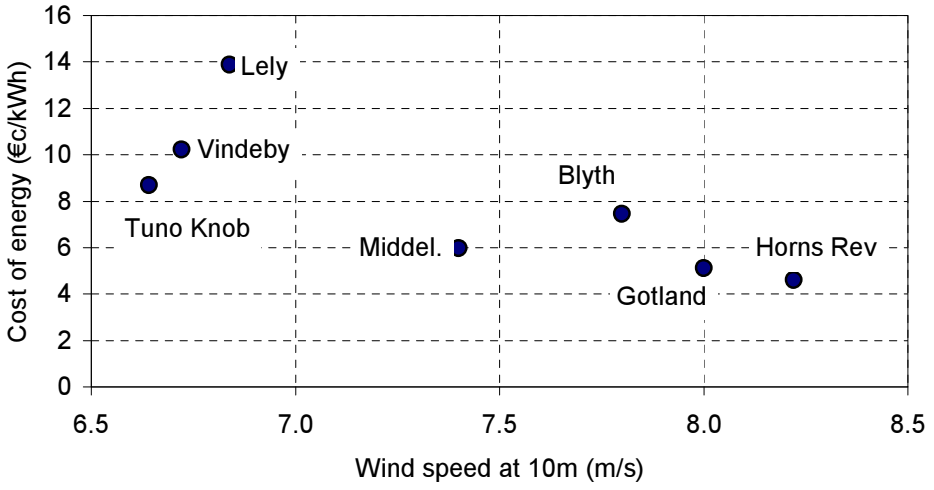

Figure 1.5: Energy cost plotted against wind speed at 10 m above MSL for some offshore wind farms. See figure 1.7 for further information on the sources of the wind speed data. Where 10 m data was not available it has been estimated from hub height data.

1.4 and 1.7 demonstrates but insufficient data is available to take a simple analysis any further.

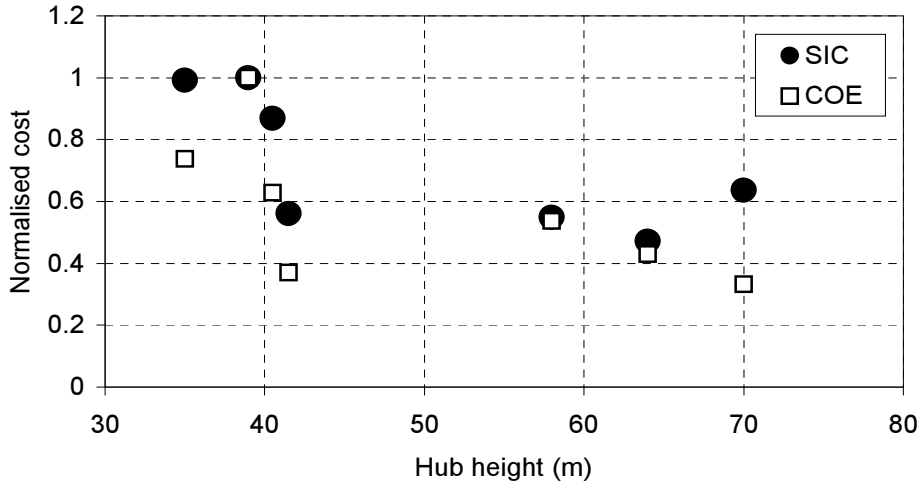

Figure 1.6: Normalised specific investment cost (SIC) and normalised energy cost (COE) plotted against hub height above MSL for some offshore wind farms.

Middelgunden and Gotland also show relatively good economic performance. In these cases the wind resource, measured at hub height, is rather poorer than that at Horns Rev. The relatively low energy cost is due to the low S.I.C. achieved.

1.5 Rationale

As the discussion above illustrates, the offshore environment interacts with wind farm design and performance to influence the economics in a complex way. If the economic performance of offshore wind is to improve further, there is a need for better understanding of the relationships between wind and wave conditions, efficient support structure design, energy production, farm configuration and the cost of energy for offshore farms. Parameter studies are a practical means of developing such understanding, and the need for further work of this sort was recognized in a report by the Concerted Action on Offshore Wind Energy project [14].

Investigation of the inter-relation between these issues is difficult with conventional design tools. There is a need therefore for simplified, quick running, integrated design tools that can be used for rapid parameter studies, resource assessments and initial feasibility studies. Calculations using such simplified tools will necessarily be much more approximate than detailed modeling work. Their

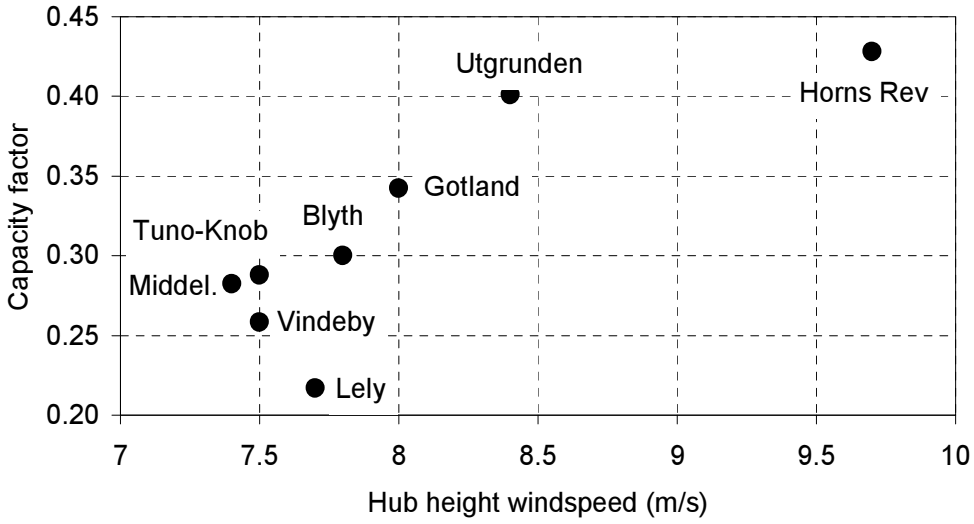

Figure 1.7: Capacity factor plotted against hub height wind speed for some offshore farms. All the hub height speeds were taken directly from references cited except for : (i) Middelgrunden (Middel.) where only data for a height of 50 m were available and the value was scaled to the hub height, and (ii) Blyth where a value for 10 m above sea level was taken from the database of [5] and scaled to the hub beight.

main value lies in the rapid comparison of a range of possibilities, allowing time consuming more detailed work to be better focused.

1.6 Aims and objectives

This work aims to develop a design and cost model for structural aspects of bottom mounted offshore wind farms. It is widely beleived that the economics of future offshore wind farms will be improved by increasing their size in comparison to those already discusses. The model will be formulated for larger farms, of approximately the size of Horns Rev, therefore.

The finished model will be used to investigate the impact of the range of environmental conditions found in Northern Europe waters on the economics of OWECS support structures. Wind farm energy production as a function of environmental conditions will also be calculated, so that the inter-relation between environment, support-structure and energy production may be studied. A precompiled Geographic Information System (GIS) database of marine conditions around Northern Europe [5] will be used to facilitate investigation of a range of possible wind farm locations, and general conclusions will be drawn as to which

locations are the most attractive economically.

In order that sensible economic conclusions may be drawn some attention must be given to all components of a farm. Grid connection and O&M costs will be included in the study, but in a relatively simple way. Details of turbine design are not considered here, except in as much as general parameters influence the design of the support structure. Throughout the work all analysis is undertaken assuming one of two turbines are deployed, specifically a 4 MW concept based upon the Kvaerner-Turbin WTS-80 and a generic 1.5 MW 'Danish-style' machine. The decision to limit analysis to these two turbines was made on pragmatic grounds to constrain the scope of the work. The methodology developed is able to model any turbine in principle.

Specific objectives are:

- Formulate a methodology to allow integrated cost modelling of an entire offshore farm. As future offshore farms are likely to be larger than existing prototypes, the methodology will be oriented towards farms with at least 25 turbines.
- Identify the principles underlying the design of offshore wind farms and particularly their support structures.
- Develop a detailed cost and design model for the support structure that is able to account for the range of environmental conditions found in Northern Europe. The model is implemented in FORTRAN to allow use of existing libraries, to ensure compatibility with a range of computer systems and to produce short run times.
- Include the support structure model in a wider 'broad brush' offshore wind farm cost model.
- Demonstrate the utility of the model through a limited set of investigations of the influences on the energy production, capital cost and energy poduction cost of offshore wind farms.

The developed model is intended to form a tool that can be used for the outline design of, and site selection for, OWECS. Its use in this thesis however will be limited to generalised parameter studies that are intended to demonstrate its value, rather than a comprehensive design optimisation study.

1.7 Outline

The text begins with a review of the fundamentals underlying the modelling and design of offshore wind energy converter systems. The discussion also draws some immediate conclusions regarding the feasibility of some design concepts and practical modelling approaches. Using this information chapter 3 identifies the capabilities required for a useful design and cost model and presents an overall methodology for implementation. Chapter 4 describes in detail the approach taken to modelling the dynamics of and forces exerted on the support structure. Chapter 5 describes how the internal forces calculated by the methodology of chapter 4 are used by the model to design a support structure. The cost model is used in chapter 6 to investigate relationships between environmental conditions, wind farm energy production and economics.

Chapter 7 discusses how the cost model is integrated into a GIS database of offshore conditions. In chapter 8 the use of the combined model and GIS for a survey of selected Northern European offshore wind resources is described. Finally in chapter 9 some overall conclusions are drawn.

Chapter 2

Review of literature and preliminary analysis

2.1 Introduction

There is little formal literature that discusses design of offshore wind systems or the cost modelling of renewable energy systems explicitly. However both fields represent extensions of well documented methods, and thus most attention here will be paid to the underlying principles.

The chapter begins by considering the principles of cost modelling and their application to renewable energy systems, and offshore wind in particular. In order to predict the cost of any farm, a good description of its design is required, and so the chapter continues by discussing the principles of offshore wind farm design and identifying the disciplines that must be tackled. Finally, since the cost of energy depends at least as much on the power produced as the cost of the farm, resource assessment methods are examined.

2.2 Cost modelling of energy systems

2.2.1 General background

There are two broad approaches to modelling the costs of systems as complex as a wind turbine. The parametric technique [30] seeks to identify a (small) set of parameters that effectively act as a proxy for the cost. To model the cost of a wind farm, C, using this approach for example, it might be proposed that

$$C = f\left(n, D, h, s, l_{grid}\right) \tag{2.1}$$

where

D	Rotor diameter
h	Hub height
l_{grid}	Distance from grid
n	Number of turbines
s	Turbine spacing ratio.

Fitting a prototype expression, based on the functional relationship, to a large data set of data will produce an equation that can be used to 'predict' the cost from the specified parameters. When done for a complex system, such as a wind turbine, the parametric approach is necessarily very approximate. Resulting expressions are adequate for broad scaling studies, such as comparing the economic performance of a 500 kW turbine with that of a 1 MW turbine. The considerable uncertainties in the predictions make detailed comparisons impractical.

Power law parametric models are frequently used for estimating wind turbine costs, such as

$$C = kD^n. \tag{2.2}$$

where k and n are empirically determined constants. Fitting this expression to 25 cost-diameter data points taken from [31], yields k=0.465 and n=1.88, producing the relationship shown in figure 2.1. The correlation co-efficient (R^2) for the fit is good at 0.977. Nevertheless it is clear that the relationship would be a poor choice for estimating the cost of an individual turbine of between 4 0m and 50 m rotor diameter. Figure 2.2 shows the percentage error in the cost prediction for each individual machine. While the range of deviations depends on the local density of data-points, it is notable that differences range from approximately –30% to +20%.

An alternative approach to cost modelling complex systems is to decompose the system into several of its constituent components (see for example [32]). The component costs can then be modelled either using parametric techniques, as described above, or using a functional approach that attempts in some way to 'simulate' the design process for the component. This technique is adopted in the current work, and later chapters discus the models developed for each component.

2.2.2 General cost modelling of energy systems

Cost modelling has a long history in the design and optimisation of energy systems (consider [33, 34, 35, 36]). It is of particular value when tackling the design of complex, large and very expensive systems with constrained budgets, for which

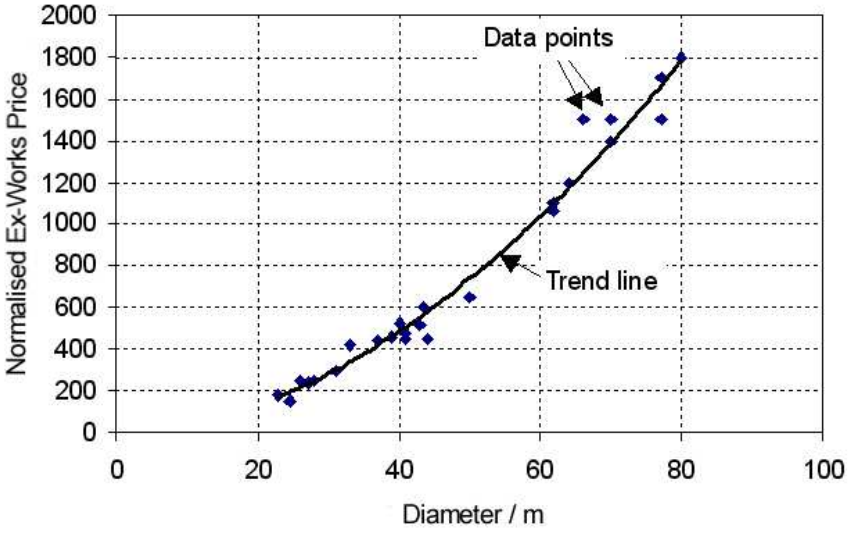

Figure 2.1: Simple cost model for wind turbine ex-works prices.

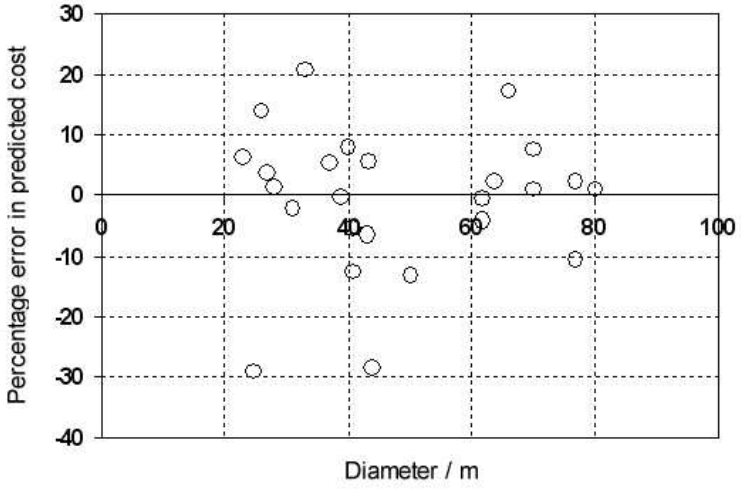

Figure 2.2: Errors in the simple cost model.

it is not feasible to build prototypes or a scale model. Constructing a cost model allows the designer to experiment with design changes and observe the effects.

A 'pure' cost model predicts the cost of components from set of parameters. On its own this is not particularly useful, as unless changing a component has implications for the performance of a system beyond cost alone, why use anything other than the cheapest? In most cases a cost model is combined with some other prediction of performance, in order than optimum designs, providing the greatest performance for the least cost can be identified (e.g. [30]). Furthermore, one approach to calculating costs is to first design components that meet specified criteria. In such cases the performance prediction may well be a direct part of the cost estimation process. This text therefore uses the term 'cost model' to refer to what might more properly be called a 'cost, performance and design model', in other words any tool that allows some aspect of an engineering system to be optimised with respect to costs.

The underlying theory and design of a system being modelled must be well understood. Data should also be available to allow costs to be estimated reliably. In order to collect together such information, there have been efforts to establish a common costing methodology for renewable energy, drawing together information from different industries [37, 38, 39].

Techniques related to cost modelling found early application in the aerospace industry. Initial activity was driven by the need to optimise designs with respect to mass rather than cost, in order to maximise carrying capacity. However cost estimating was a natural development, and the highly competitive nature of the civil aircraft industry puts it at the cutting edge of cost estimation technique (e.g. [40]). Space technology makes wide use of cost (and mass) estimation and optimisation, although the nature of the field makes this inevitably more speculative and less rigorous than civil aviation (e.g. [41]). One of the best-known cost estimation manuals is published by a body spanning both the aviation and space fields, namely NASA [42]. The military, particularly in the USA also make wide substantial use of cost modelling in operation planning to optimise the use of resources (e.g. [43, 44]).

2.2.3 Previous wind cost modelling studies

Turning to wind turbine design, one of the first reported uses of cost modelling techniques was during the NASA MOD projects [45]. However, the studies conducted were tied very closely to the MOD design work and their wider applicability is limited.

One of the best-known 'general' wind turbine models is Harrison-Jenkins

model [46, 47], developed during the late 1980s and early 1990s. It exploited the (then) newly available spreadsheet technology to include elements of numerical analysis, and model much more detail than had previously been practical. The model was essentially mass-based, calculating the masses of components initially and using multipliers to estimate costs. A wide ranging study by MacRae [48] found a good correlation between the mass of major wind turbine components and their costs, thereby validating the mass-cost multipliers approach.

A deficiency of the Harrison-Jenkins approach was that all calculations were based upon extreme loads alone. At the time of development this practice was common among machine designers. However, it is now quite clear that wind turbine design is partly driven by fatigue. While obsolete in this respect, the model still contains many useful component design and costing features. Of particular interest here is the 'bottom' up approach employed, designing components according to engineering principles as far as possible, before resorting to correlations.

The Harrison-Jenkins model also included little in the way of design optimisation. It was intended mainly for parameter studies to investigate general trends rather than as a design tool. A study in 1996 [49] used elements of the model to try to optimise HAWT design using a more automated system. A model [50] for turbine blades alone was among the first to introduce detailed engineering principles into wind cost modelling, going considerably beyond the more general analysis of the Harrison-Jenkins model. The work includes a fairly sophisticated load calculation, uses a bottom up-approach, and applies automated optimisation procedures in determining most of the local dimensions. The study only investigates the relationship between mass and design, without calculating costs and still no explicit account is taken of fatigue loads. The Opti-OWECS study [51], used cost modelling techniques to identify optimum designs for offshore wind farms. This was one of the first attempts to incorporate the difficulties of fatigue in the cost modelling of wind energy systems.

More recent work has integrated large-scale aero-elastic calculations and cost assessment approaches with the objective of optimising designs [52, 53]. However, the complexity of the whole procedure has usually meant that comparatively simple cost models, with much less detail than the Harrison-Jenkins model have been practical. The SITEOPT [54, 55] study of 1998-2001 married a much more sophisticated cost model with several commercial wind turbine dynamics simulation codes [56, 57] with the objective of economically optimising turbine design for particular types of site with widely differing wind conditions.

2.3 Fatigue analysis

Repeated cyclic loading of components causes cracks in the microstructure of materials to grow until either the crack extends across the entire component or the remaining intact material is no longer able to support the design load and failure occurs [58].

Early wind turbine designers largely ignored fatigue as until recent years, with the advent of inexpensive powerful computers, it was difficult to generate the data required for fatigue based design. Furthermore, with the small turbines that were common until the mid-1980s, fatigue was not a major design driver. Things changed with newer generations of large machines, and inadequate treatment of fatigue led to many failures [59]. The role of fatigue in wind turbine design has grown considerably over the last twenty years, with many large projects devoted entirely to understanding it. Design procedures for onshore machines are now well established [59] and recent work has sought to introduce concepts such as reliability based design [60] into the wind energy field. There is though still considerable uncertainty about their application to offshore farms, and in particular the way in which cyclic wind loads interact with cyclic wave loads [25, 5].

The treatment of fatigue in cost modelling studies largely mirrors its role in 'real' turbine design, but with a substantial time lag. Even work more recent than the Harrison and Jenkins study [46] has ignored its impacts, including one tower design optimisation study where including it may have fundamentally altered the conclusions [61]. Such simplifications are usually justified on pragmatic grounds, but nevertheless mean that a major design driver is not considered. Structural and mechanical engineering design standards (e.g. [62]) provide simplified means of assessing fatigue, but their direct application to onshore and particularly offshore wind turbines is often unclear due to the specialised nature of the problems. In a cost modelling study of offshore wind, Pauling [63] employs a simplified procedure relying on trapezium shaped load spectra based on German wind energy standards [64].

Fatigue theory either tackles the fundamental physics of the microstructure cracking process, or concentrates on predominantly empirical methods to predict component lifetimes. While there are of course strong connections between the branches, only the latter is of interest here as the fundamental work is not yet developed to a stage useful for design. The theory of fatigue divides component loading regimes into two classes – low cycle and high cycle [65]. In a wind turbine, loading falls clearly into the high cycle regime, and is amongst the most demanding experienced by any large plant.

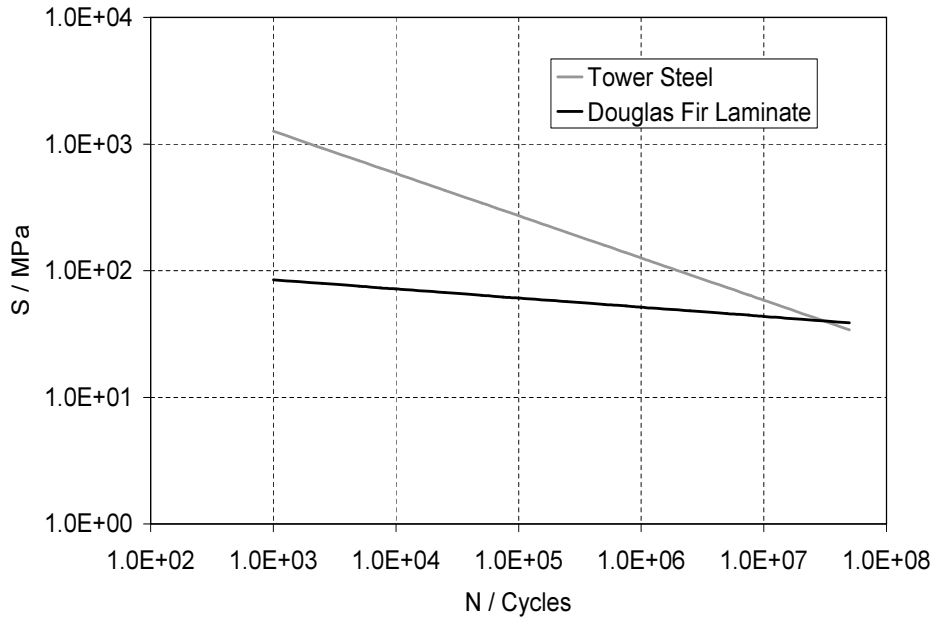

Figure 2.3: Fatigue stress endurance (S-N) curves for tower steel used by Kvaerner-Turbin [68] and for Douglas-Fir Wood/Epoxy laminate [59]. The vertical axis shows the applied alternating stress and the horizontal axis depicts the corresponding lifetime in cycles of application.

The designer is either interested in how many cycles a component is able to withstand, or more usually the inverse question of what component dimensions are necessary to withstand a particular loading regime. Experiment shows that the lifetime in cycles N decreases with increasing stress range s of the fatigue cycles, usually modelled with a modified version of a relationship proposed by Basquin [66]:

$$N = \frac{A}{(\Delta\sigma)^m} \tag{2.3}$$

where k and m are constants for particular materials. Experimental data is typically presented as a fatigue endurance, or so called S-N, curve, illustrated for a range of materials in figure 2.3. For some materials the Basquin law provides a rather poor fit and many design standards [64, 67] recommend modified forms that divide the stress response into a number of regimes each modelled separately.

S-N relationships are generally based on laboratory-produced data under ideal conditions with no mean loading on the test component. This is a rather unusual situation as in practice components carry mean stresses on top of oscillating forces. A tensile mean stress reduces the lifetime in comparison with the unloaded ideal cases. There are two limiting conditions, which are well known for most materials:

- Failure due to cyclic loading with uniform stress amplitude σ_0

- Failure during the first cycle, i.e. at the yield stress $\sigma_y$or the tensile strength σ_{TS}.

However behaviour at intermediate combinations is less well known and in common practice is modelled by one of three relationships predicting the stress amplitude σ_a at a mean stress σ_m that gives the same lifetime as stress cycles of amplitude $\sigma_0$with no mean stress. The relationships are compared in table 2.1 and figure 2.4.

Name	**Equation**	**Comments**
Soderberg [69]	$\sigma_a = \sigma_0 \left\{1 - \frac{\sigma_m}{\sigma_y}\right\}$	Based on the lower yield stress and generally conservative
Modified Goodman [70]	$\sigma_a = \sigma_0 \left\{1 - \frac{\sigma_m}{\sigma_{TS}}\right\}$	Good for brittle metals, conservative for ductile alloys, not conservative for compressive mean stresses [71]
Gerber [70]	$\sigma_a = \sigma_0 \left\{1 - \left(\frac{\sigma_m}{\sigma_y}\right)^2\right\}$	Good for ductile alloys with tensile mean stress. Does not distinguish between tensile and compressive mean stresses [71]

Table 2.1: Comparison of fatigue relationships.

The modified Goodman relation is arguably the most commonly used. A difficulty is that the expression is not conservative for cases with mean compressive stress, but as compression is generally beneficial to the fatigue life, a safe compromise is simply to neglect the benefits [71]. In fact, for many preliminary studies the issue of mean stress is often ignored completely. This approach has been used in other offshore and onshore wind studies [72] and is adopted here.

A further practical complication is that components in service are generally subjected to varying amplitude stress cycles rather than the uniform amplitude used in testing. Palmgren [73] and Miner [74] separately proposed a linear damage summation rule to deal with such cases, which may be written

$$\sum_{i=1}^{M} \frac{n_i}{N_i} = D \tag{2.4}$$

where total damage D is sustained by a component that undergoes n_i stress cycles at stress level s_i, and N_i is the number of cycles to failure for cyclic loading at stress level s_i only (taken from the S-N diagram). It is usually assumed that failure occurs when the linear damage sum D is equal to unity, however more rigorous

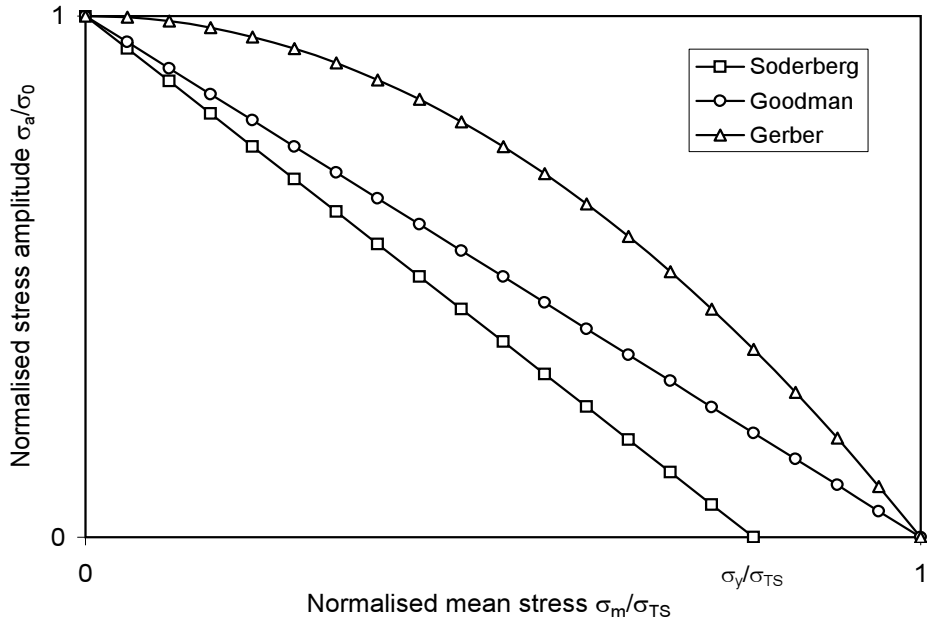

Figure 2.4: Comparison of three models for fatigue endurance in components subjected to non-zero mean stress. The mean stress values on the horizontal axis are normalised by the material tensile strength σ_{TS}, with σ_y representing the yield stress. On the vertical axis, the stress amplitude values are normalised by the stress amplitude that can be sustained in the absence of mean load, σ_0.

studies have shown failure occurring over a range of values. Veers [75] for example finds that the computed damage at failure from a wide range of references varies between 0.79 and 1.53. It is well known that the offshore environment tends to accelerate fatigue crack growth and for design purposes it may be prudent to assume failure at a sum of 0.5, or where there is no access for inspection, 0.33 [76].

Measured loading histories from wind turbines reveal a complex time signal. Even relatively simple simulations show complex load signals and it is not immediately obvious how to identify a cycle and its amplitude. There are many, largely empirical techniques. Most popular in the wind industry is rainflow counting. In fact there are many implementations of the rainflow counting technique, but they all produce the same result if the data being analysed meet certain conditions. The algorithm proposed by Downing and Socie [77] is common in the wind industry, although can be inconvenient as it requires a multipass technique. The result of the rainflow analysis is a "rainflow matrix" that lists the number of cycles at combinations of mean and alternating stress. The matrix can be used directly with the Palmgren-Miner rule and a model of the impact of mean stresses to calculate fatigue life.

It is often convenient to represent loading time histories in the frequency domain as spectra. A fair body of work considers how to estimate fatigue damage

from such spectra. The 'obvious' procedure, as described by Sutherland [59] and others [78] is to use Fourier techniques to synthesise corresponding time domain signals and then employ a more-or-less conventional cycle count. This however is a time consuming and cumbersome process. Several authors [79, 80, 81, 82, 83, 84] have investigated means to directly estimate fatigue damage directly from spectra. In general they are only suitable for data that meets very limiting constraints, although the most generally applicable [85], the expression originally due to Dirlik [86] and further developed by Bishop [87, 88] is widely employed within the wind energy field where it has met with reasonable success [5].

2.4 Dynamic simulation of wind turbines

Fatigue driven design is only possible if the engineer has detailed knowledge of the loading history that will be experienced by turbine components. One way to obtain such information, of course, is to build a prototype turbine at the proposed location, and record the loads experienced using a datalogger. While this may be acceptable to 'prove' a new machine, cost and time considerations make it impractical for design purposes. A more realistic approach is to simulate in detail the response of the turbine components to operating conditions using a computer, generating load histories that can be used for fatigue design. An additional benefit is that the simulations may well be able to predict the peak loads experienced by components.

There are three aspects to the simulation of an in-service turbine. Firstly a model of the incident wind, accounting for short term fluctuations and tubulence is required. Secondly there must be a treatment of the loads generated by the incident wind. Thirdly a model of the dynamic response of the system when subjected to wind generated loads is necessary. It turns out that whole system dynamic turbine models are computationally intensive, such that even with the easy availability of computer power, simulations prove time-consuming[1]. It is not practical to simulate the entire lifetime of the machine, and thus means of compressing the extent of the simulations while still producing realistic time histories is required, described here as loading regimes.

At the time of writing, most available simulation codes either do not include offshore specific aspects, or include them in only a preliminary manner. The discussion here will focus therefore on the dynamic analysis of onshore machines.

[1]Running even a relatively simple code such as FASTAD on an PC with an AMD Athlon 1.73 GHz processor, simulation of 1 minute of operating time takes approximately 1 minute of processor time.

Most of the techniques described can be extended to encompass the offshore environment, and any offshore specific analysis will be dealt with in later discussion.

2.4.1 Dynamic response of turbine and support structure

The fundamental principles of wind turbine structural dynamics are no different from those for more conventional structures. Behaviour is reduced to a coupled set of ordinary differential equations (ODEs) [89] of the form:

$$M\ddot{v} + C\dot{v} + Kv = P(t) \tag{2.5}$$

where $\boldsymbol{v}$ is the displacement of the structural degrees of freedom. The left hand side of equation 2.5 is the structural model with $\boldsymbol{M}$ being the mass matrix, $\boldsymbol{C}$ representing the damping, and $\boldsymbol{K}$ the structural stiffness matrix. On the right-hand side of the equation are the external loads $\boldsymbol{P}$ which primarily arise from the aeroelastic response of the blades to the applied wind, although of course in offshore locations wave loads may also be very important. A dynamic model may also include the response of the drivetrain and any controller by adding further ODEs to the LHS that include appropriate parameters for these subsystems, although this may increase the overall order of the model. From a purely dynamic viewpoint, the drive train and controller simply modify the response of the structure to any applied wind, although their practical significance for the effective operation of the turbine is rather more important.

Solution of equations of the form of 2.5 is a common engineering problem. In the case of wind turbines this is complicated by the fact that the rotation of blades makes the coefficient matrices periodic, which is rather unusual in structural dynamic analysis. In most wind turbine analysis codes, a time domain approach using an algorithm such as Runge-Kutta (see for example [90]) is used to 'time-step' through the turbine behaviour from moment to moment. This is a computationally intensive approach but deals naturally with the periodic coefficients. In the wider structural field, frequency domain approaches are by far the most common thanks to their much greater efficiency (see for example [91]). Application of such methods to wind turbine analysis is limited by the time varying coefficients, but subject to a number of approximations, has been attempted by several authors with reasonable success [5, 92, 93].

2.4.2 Derivation of structural model

Many wind turbine structural models rely on the modal approach, wherein the mode shapes of free oscillation of the structure are identified and it is assumed

that forced vibration is composed of these modes. The displacement of the structure in time and space is represented as [89]

$$Q(x,t) = \Phi(x)Y(t) \tag{2.6}$$

where Φ is a matrix representing the mode-shapes and Y is a generalised co-ordinate vector representing the state of the structure as a function of time. The mode shapes are calculated using conventional eigenvalue analysis, typically using a finite element model. While necessarily approximate, modal decomposition embracing only a limited number of modes provides a good enough representation of the tower dynamics, as it is unusual for higher modes to play an important role [94].

Several more recent codes include a finite element model directly as part of the dynamic simulation. This requires substantially more computer time than the modal approach, but allows more detailed refinements of the support structure to be investigated. Other recent codes use a 'multi-body system' to model the behaviour of the structure. Again this is relatively expensive with respect to computer power, but permits more detailed investigations in the later stages of design. Tables 2.2 and 2.3 compare the approaches taken by some well-known codes.

2.4.3 Blade aeroelastics and other forces

The interaction of the blades with wind is responsible for both the energy production and the major part of the mechanical loads experienced by all the turbine components. Blade element momentum theory (BEM), due to Glauert [95], is the 'standard' means of calculating both loads and energy production in the wind turbine community. Each blade is divided into a number of elements, with the rate of change of both axial and angular momentum of the incident wind considered at each to calculate forces. Where the blade is flexible its motion may also contribute to the forces experienced. The rotation means that aerodynamic conditions vary substantially along the length of each blade and a detailed knowledge of lift and drag coefficients over a wide range of angles of attack (AOA) is required for successful use of BEM in wind turbine simulation. The range of AOA experienced is far beyond that normally encountered in aviation, from where most aerofoil experimental data originates, and makes suitable performance information hard to obtain for many aerofoils. Well known information sources, such as the tests co-ordinated by Selig at UIUC [96], rarely include data for AOA outside the range encountered in normal aircraft flight (approximately –20^o to +20^o) and in general resort must either be made to analogies with flat plates or to

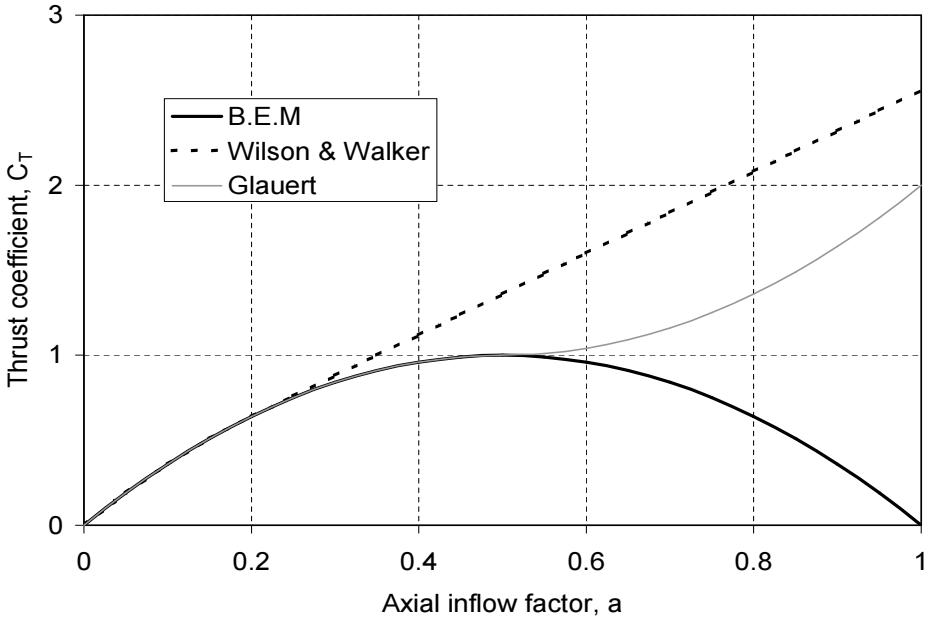

Figure 2.5: Comparison of corrections to B.E.M. The solid line shows the thrust coefficient as predicted by equation (2.7). The light line depicts an emprical correction to B.E.M. proposed by Glauert, as reported by Hansen [100], and the dotted line a correction by Wilson and Walker, reported by Spera [101].

computer models such as XFOIL [97] to obtain a full data set. In the longer term it may be possible to replace standard aerofoil theory with Computational Fluid Dynamics (CFD) based on first principles, but while there have been tentative movements in this direction [98, 99], present day computer power is insufficient to make this practical as part of a full turbine model.

A major deficiency with BEM arises with heavily loaded machines. The theory predicts areas of reversed flow, whereas in practice the flow remains unidirectional, but separates from the blades giving a turbulent wake behind the turbine. BEM predicts a simple expression for the blade thrust coefficient C_t in terms of the axial flow induction factor, a, which in effect is a measure of the loading on a turbine

$$C_t = 4a(1-a). \tag{2.7}$$

Beyond $a = 0.5$ reversed flow is predicted and the theory is not valid although in practice it begins to break down at lower values of a. Resort has to be made to empiricism to provide a workable model in these circumstances. Figure 2.5 compares some commonly used corrections.

BEM was originally formulated for airscrew and wind calculations, and subsequently adapted for helicopter rotor design. A possible concern is that BEM has never been comprehensively and explicitly validated for wind turbine use and the unusual flow regimes encountered [102]. There is though no reason to

suspect any failure of the theory or its assumptions, and twenty or more years of use have failed to reveal any major discrepancies. However it is worth keeping in mind that even sophisticated wind turbine modelling codes are only reliable as intermediate design tools.

Other issues with BEM relate to the practicalities of implementing the calculation. Firstly the theory assumes infinitely long blades, where as real blades of course are finite. Air driven by the pressure difference between the 'lower' and 'upper' surfaces of the blade spills over at the tips, reducing the left force generated. There are several corrections for this so called 'tip-loss', the best known being due to Prandtl [103] and Goldstein [104]. The Prandtl correction is more widely used because it is expressed in a closed form while the Goldstein solution relies on an infinite sum of modified Bessel functions.

BEM implicitly assumes that an instantaneous equilibrium exists between the flow field approaching the blades and the forces they exert, such that the impact of changes in the blade pitch is immediately reflected by the inflow. In modern turbines the rotor configuration is continuously changing [102], and in practice the flow field will lag slightly behind that predicted by the instantaneous equilibrium assumption. To account for this so called 'dynamic inflow' effect, some calculations include a linear first order lag model [100] for the induced velocities.

A third issue, the subject of much active research relates to the two dimensional character of the flow assumed by BEM. Drag and lift coefficients are conventionally measured with no component of the flow velocity along the length of the blade, and the usual BEM approach ignores any such component. This is adequate for most aeronautical applications, but with wind turbine blades cross flow is very common particularly near the hub, and it is well known that such cross flow components do have an impact on the performance. The full impact of this three dimensional aspect to the flow is relatively poorly understood, and most wind turbine applications rely on empirical corrections to account for it such as those due to Snel [105] and Viterna and Corrigan [106].

Although of lesser direct importance for the current study, the issue of 'dynamic stall' is also poorly understood. In essence re-attachment of the boundary layer to an aerofoil occurs at a different angle of attack from the initial separation, such that the true drag and lift co-efficients follow a hysteresis curve. This has impacts on both the energy capture and the loads. Again a number of empirical techniques are used to model these effects (e.g. [107, 108]), but they usually require specific experimental data for particular aerofoils.

Code	ADAMS/WT	BLADED	DUWECS	FAST	FLEX4/FLEX5
Main references	[109],[110]	[111],[5]	[25]	[94],[110]	[25],[102],[100]
Main developers	NREL, USA	Garrad-Hassan, UK	DUT, Netherlands	NREL, USA	TUD, Denmark
Tower					
Dynamics approach	Multi-Body	Modal	Finite Element	Modal	Modal
Fore/Aft modes	Yes	3	Yes	2	1
Lateral modes	Yes	3	Yes	2	1
Torsion modes	?	No	No	No	1
Rotor					
Structural dynamics	Multi-Body or Hinge	Modal	Hinge	Modal	Modal
Lead-lag modes	Yes	6	1	1	2
Flap modes	Yes	6	1	1	2
Torsion modes	?	No	No	No	Yes
Aerodynamics					
Loads	BEM or GDW (uses Aerodyn [110])	BEM	BEM	BEM or GDW (uses Aerodyn [110])	
Induced velocities	Axial & Tangential	Axial & Tangential	Uniform axial	Axial & Tangential	Axial & Tangential
Tip effects	Prandtl[95] or GTech[112]	Prandtl[95]	Lift loss factor	Prandtl[95] or GTech[112]	Prandtl[95]
Turbulent wake	?	Garrad-Hassan in-house method	Johnson[113]	?	Glauert[95]
Dynamic inflow	GDW or 1^{st}-Order DE	Pitt & Peters	First-Order	GDW or 1^{st}-Order DE	?
Dynamic stall	Beddoes[107] & Gormont[114]	Beddoes[107]	ONERA[102]	Beddoes[107] & Gormont[114]	Stig-Øye[115]
3D effects	Viterna & Corrigan[106]	?	Viterna & Corrigan[106], Snel[105]	Viterna & Corrigan[106]	Yes

Table 2.2: Comparison of wind turbine simulation codes (Part 1). In the developers section, NREL is the US National Renewable Energy Laboratory, DUT represents Delft University of Technology, TUD the Technical University of Denmark, ECN the Netherlands Energy Research Foundation and NTUA the National Technical University of Athens. Caption continues in table 2.3

Code	FOCUS/FLEXLAST	HawC	GAST	PHATAS-IV
Main References	[102],[116]	[54]	[102],[117]	[102],[54]
Main developers	Stork & DUT, Netherlands	Risø, Denmark	NTUA, Greece	ECN, Netherlands
Tower				
Dynamics approach	MSD	Finite Element	Multi Body System	MSD
Fore/Aft modes	1	Yes	Yes	1
Lateral modes	1	Yes	Yes	1
Torsion modes	No	?	Yes	1
Rotor				
Structural dynamics	Hinge	Finite Element	Multi Body System	Finite element
Lead-lag modes	1	Yes	Yes	Yes
Flap modes	1	Yes	Yes	Yes
Torsion modes	No	?	?	Yes
Aerodynamics				
Loads	BEM	BEM	BEM	BEM
Induced velocities	Axial	?	Axial & Tangential	Axial & Tangential
Tip effects	Prandtl[95]	?	Prandtl[95]	Prandtl[95]
Turbulent wake	No	?	Emprical	Wilson[101]
Dynamic inflow	1st Order DE	?	1st order DE	Yes
Dynamic stall	Stig-Øye[115]	?	ONERA[102]	Yes
3D effects	Snel[105]	?	Snel[105]	Snel[105]

Table 2.3: Comparison of wind turbine simulation codes (Part 2). Caption continued from table 2.2: The Hinge model of rotor dynamics treats the blades as rigid but attached to the hub via a damped, sprung hinge allowing a single degree of freedom. BEM stands for Blade element momentum model, which in some cases is used in modified from (not noted here). GDW stands for Generalised dynamic wake model [110, 118] which can optionally be used in place of BEM in the Aerodyn code that performs the aerodynamic calculations for both ADAMS/WT and FAST. The GDW approach accounts explicitly for flow induction and dynamic inflow. GTech stands for a tip effects model developed at Georgia Institute of Technology. Other terms are discussed in the main text or the cited references.

2.4.4 Wind field generation

An accurate turbine dynamic model must be complemented by a good description of the wind, as this of course is ultimately responsible for the loads experienced. Examination of long term wind spectra shows a spectral gap between periods of approximately 10 minutes and 2 hours [119]. Wind speed fluctuations may be considered on two separate time scales therefore:

- short term, with time scales under ten minutes encompassing both microscopic turbulence and coherent gusts
- long term, due to larger changes in meteorological conditions

This sub-section is concerned with modelling the shorter term, smaller scale influences, with longer term issues discussed in the next section.

Even when subjected to a 'steady' wind, the wind field experienced by a turbine is variable in time and space, as illustrated in figure 2.6. Every part of the rotor plane may be subject to slightly different wind speed at any instant. The blades move at relatively high speed through the non-uniform fields, and as they do so the structure of the wind turbulence generates excitation at integer multiples of the rotation speed, known as 'rotational sampling' [31].

A common approach to modelling this small-scale variation is through division into deterministic and stochastic components. The most important deterministic variations across the rotor plane are wind shear, and tower shadow. Wind shear is the increase of wind speed with height arising from the viscous boundary layer formed by the moving air [121]. In principle this is no different from any other boundary layer and as such may be treated with Prandtl's logarithmic law model [103]

$$\overline{U}(z) = \frac{u_*}{k} \ln\left(\frac{z}{z_o}\right) \tag{2.8}$$

where

U	Mean wind speed at height z
z	Height above the ground
k	Von Karman constant
u_*	Friction velocity
z_0	Roughness length characteristic of terrain.

A difficulty in the practical use of this expression is the need for a terrain roughness length. For the open sea the roughness length depends on the sea state, which in turn depends on the mean wind speed. The Charnock relation [122]

$$\frac{u_*^2}{z_o g} = c \tag{2.9}$$

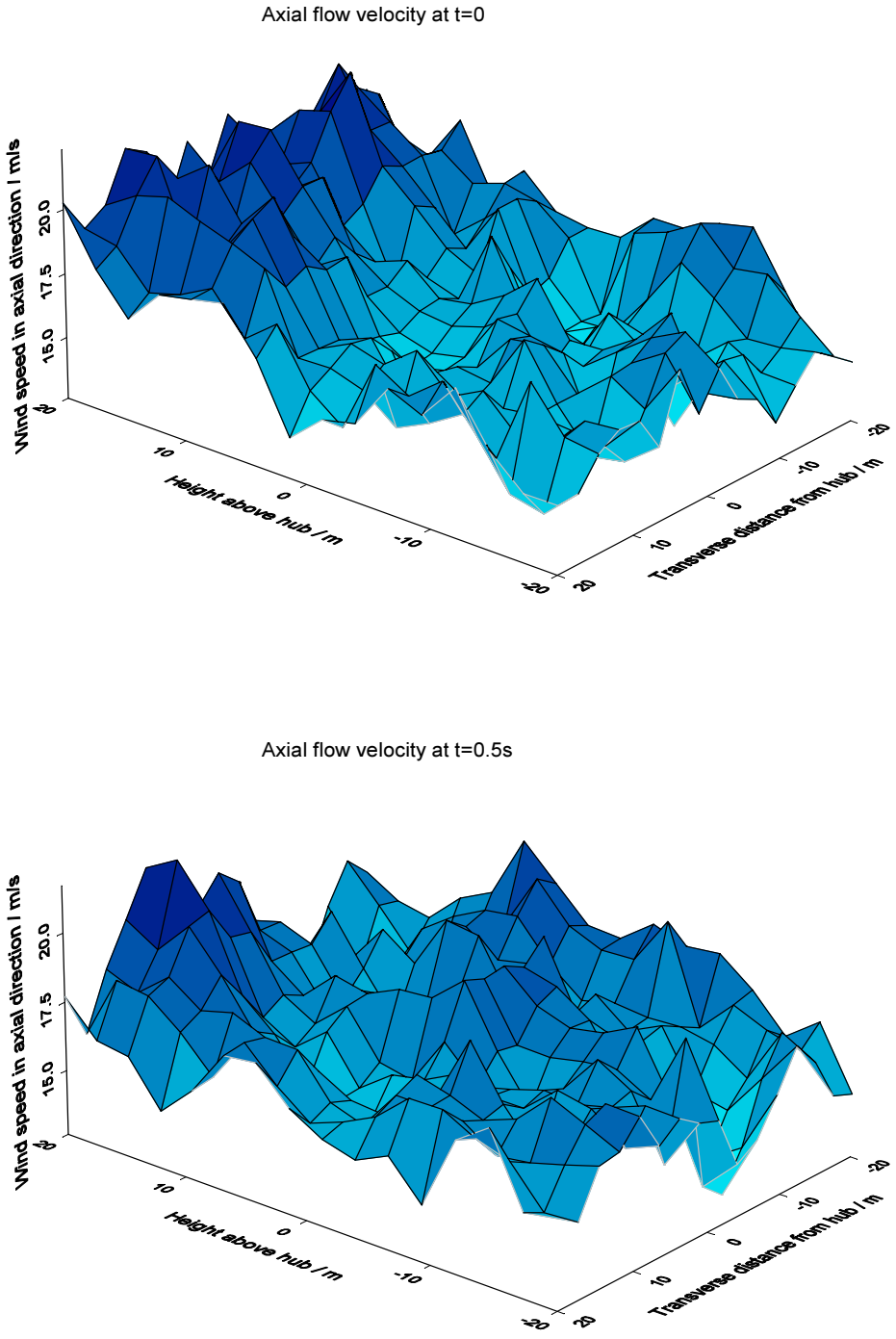

Figure 2.6: Illustration of the variable wind field experienced by a turbine. The diagrams show the incident wind velocity field in the direction of the turbine axis, at times 0.5 s apart. The upper plot shows the field that reaches the turbine first. Data was generated using SNWind [120] over a 20 m x 20 m rectangular plane centred on the rotor hub axis, for a mean flow velocity of 20 m/s at a hub height of 80 m, and assuming turbulence according to IEC Class A using the Von Karman model. No account is taken of tower shadow, but wind shear is modelled as can be seen from the general increase of velocity with increasing height.

is commonly used to relate the surface roughness and the friction velocity, and must be solved iteratively with the Prandtl law. The Charnock constant c is approximately equal to 60 for a fully developed sea state. Where the wind is not in equilibrium with the waves, for example over a short fetch or for a recently developed wind field, the value of c depends on the wave age.

The atmospheric boundary layer exhibits several differences from the idealised cases underpinning Prandtl's work, and empirical modifications have been proposed to improve predictions in the lower regions of the atmosphere where wind turbines operate [123]. With increasing height above the ground coriolis forces arising from motion of the wind in the Earth's rotating reference frame become more important in comparison to the viscous forces that dominate in the lower 'surface' layer. In the Ekman layer, typically at least one hundred meters above the surface [119], the direction of the wind begins to change with increasing height, in addition to its speed. However even the very largest wind turbines barely enter this region.

'Tower shadow' refers to the area of reduced wind speed found immediately upstream of the tower where the incoming flow diverges around the obstacle caused by the tower (figure 2.7). The velocity deficit can be easily estimated using a conventional potential flow calculation [124]. For simplicity, some workers assume that the tower shadow velocity deficit, shown in figure 2.8, follows a $(1 - cos)$ or $(1 - cos^2)$ profile [102].

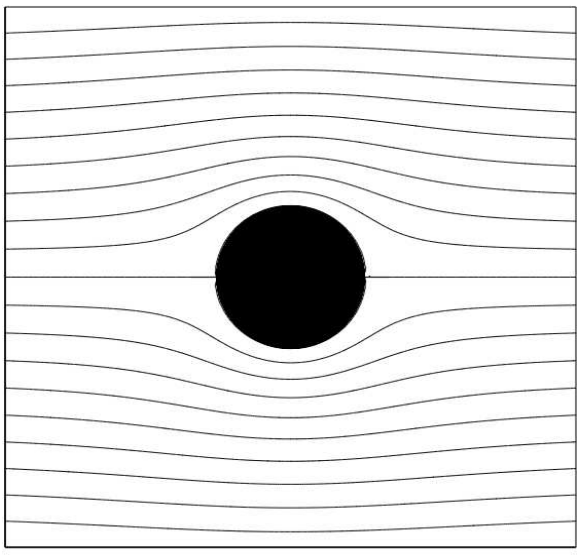

Figure 2.7: Potential flow streamlines for a tower in a uniform flow, produced by a potential flow solution written in Mathcad.

For simulation purposes, the stochastic wind turbulence must be treated numerically, typically using a model that generates a three dimensional turbulent

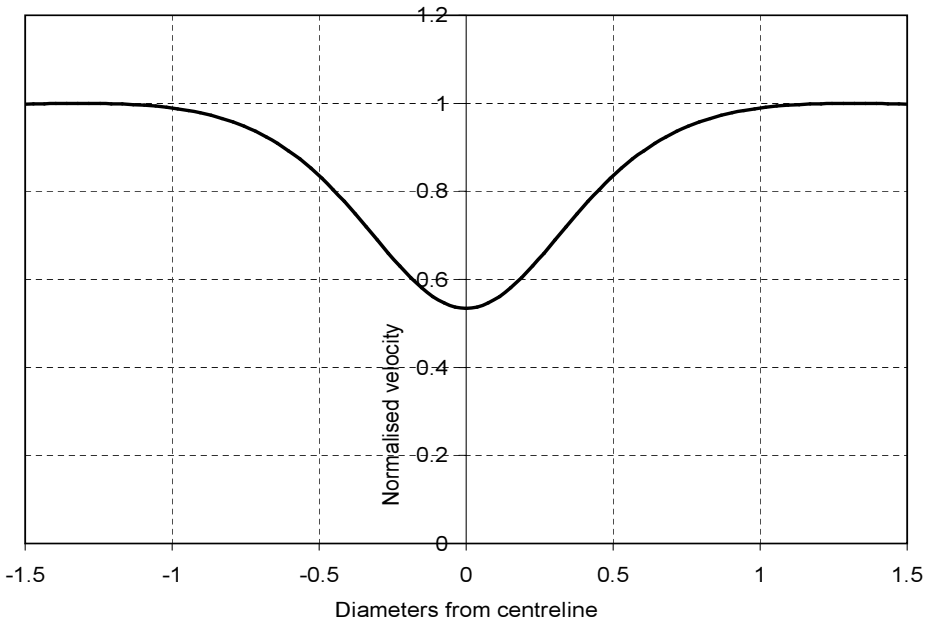

Figure 2.8: Velocity profile behined a tower of circular cross section calculated using the potential flow approach, illustrating tower shadow.

wind field. Many numerical codes are used in practice including SNWind [120], SWING [125] and others. Most implement the Von Karman (see for example [126]) or Kaimal [127] turbulent spectra specified in the IEC design standards [128].

2.4.5 Loading regimes

Over its years of operations a wind turbine will experience many meteorological conditions ranging potentially from dead calm to violent storms. As a result of the spectral gap in wind spectra, each meteorological condition can be considered to last a finite period of time after which long-term changes in weather bring about a new wind regime.

For fatigue design purposes ideally the entire lifetime of the turbine would be simulated using a numerical code with the meteorological conditions being varied with time. The fatigue damage over the lifetime for each component could then be readily evaluated. This, however, is an impractical objective both in view of the inordinate amount of computer time required and because it is not possible to precisely predict meteorological conditions over a turbine's future life. To account for longer-term changes in wind conditions, a set of representative load cases is defined including turbine start-up and shut-down, normal operation across the range of likely wind speeds, and similarly for fault conditions [59]. Simulations are conducted for between 10 minutes and 1 hour of turbine operation under each of these cases. The proportion of the turbine's life for which each

of these load cases will pertain is estimated using the Weibull distribution for normal operation and experience for the other cases. Assuming that each 10 minute simulation is representative of longer operation at that load case, the damage is extrapolated according to the proportion of the turbine lifetime spent subject to each load case, and hence the total fatigue damage calculated in the normal way.

For extreme load design only the peak loads experienced by components are required. An 'obvious' way to obtain these is to trace through a lifetime loading history and identify the maximum load, but as already noted generation of such a loading history is impractical. Again a load-case approach is frequently adopted, with peak loads identified from simulation of say 10 minutes of turbine operation subject to each of a number of load case conditions. Naively it might be expected that peak loads would always be experienced under the most extreme conditions, but with modern compliant designs this is not always true (see for example [25]). The load cases must extend beyond the extreme conditions therefore and suitable sets of conditions are specified in several design codes [62, 128], although the theoretical basis for the selection is not always clear.

2.5 Support structure design

2.5.1 Fundamentals

At the simplest level, support structure design optimisation represents a trade off between the increasing cost of a taller tower and the greater energy production resulting from higher wind speeds at height. Detailed design however is much more complex as the tower plays a crucial role in the dynamics of the system.

2.5.2 Onshore design

Traditionally the designer chooses between a stiff tower, with an eigenfrequency significantly above that excited by the turbine, and a soft tower, with a natural frequency below the turbine excitation range. A stiff tower will never experience substantial resonance, and will exhibit limited deflection under normal operation. In contrast a soft tower will experience brief resonance producing large deflections during turbine start-up, but will ultimately experience lower loadings from turbine operation. Figure 2.9 illustrates the point by showing the transfer function for a single degree of freedom system between driving force as input and displacement as output for a range of ratios of forcing frequency to natural frequency (after [129]). In effect opting for a tower below the forcing frequency substantially decouples the rotor and tower dynamics during normal operation

of the turbine.

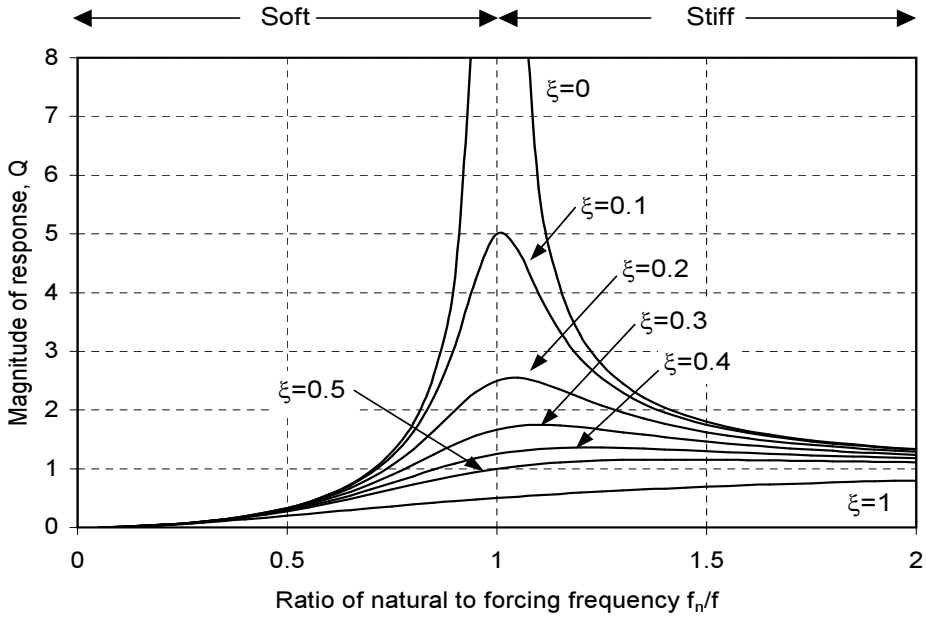

Figure 2.9: Transfer function for a damped dynamical system with a single degree of freedom. The horizontal axis shows the natural frequency of the system f_n divided by the forcing frequency f. This is the inverse of the conventional way of plotting this diagram. However it allows the effect of increasing tower frequency (i.e. increasing stiffness) to be more readily understood, as the stiffness increases from left to right. The vertical axis shows the magnitude of the response to the forcing normalised by the steady state response. The separate curves represent the response of systems with different damping ratios ξ.

With the increasing dominance of fatigue in the design of wind turbine components, softer towers potentially offer better economics than stiffer designs, as the loads experienced over a lifetime of operation are lower. One way of looking at this is that soft towers allow transient loads to be absorbed by inertia in contrast to stiffer designs which resist loads by elastic stiffness. A soft tower in general can be much lighter, and therefore cheaper than an equivalent stiff design [47], although the details of course depend on the turbine and the local wind climate.

2.5.3 Offshore design

Aside from the difficulties presented by the more corrosive environment, many of the design issues offshore are similar to those onshore. A preliminary analysis is presented by Sinclair and Clayton [130].

Offshore there are three sources of excitation, with the turbine providing periodic loading at perhaps 30 Hz, interactions between wind turbulence and the blades providing excitiation at a range of frequencies and waves impacting at

periods typically ranging between 1 s and 20 s [131]. The major design decision is where to place the tower eigenfrequency relative to these drivers. There are three options, which it has become common to refer to [132] as soft-soft (f_n below both excitation frequencies), soft-stiff (f_n between the frequencies) and stiff-stiff (f_n above both frequencies). The relative properties are illustrated in figure 2.10. The softest towers again produce the lowest loads in principle, but the wave driving frequency can be very variable [131] and a soft-soft design may be difficult to achieve in some locations.

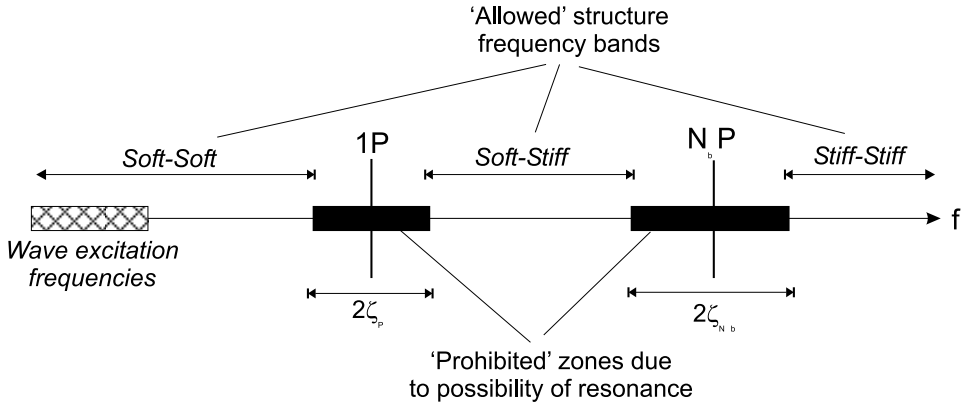

Figure 2.10: Comparison of natural frequency options for offshore wind turbine support structures. The diagram shows support structure frequency f increasing from left to right. The thick black rectangles represent bandwiths in which the structure frequency must not lie, due to the danger of resonance either with the rotor frequency, P, or the blade passing frequency N_bP where N_b is the number of blades. The width of the excluded bands ζ_P and ζ_{N_b} must established on a case by case basis but is often taken as equal to 5% of the central frequency [25]. The hatched region is also unavailable due to excitation provided by the incident waves.

A practical design solution must account for the uncertain dynamic properties of any offshore foundation. Difficulties both in offshore surveying and construction make it impractical to predict the stiffness of an offshore pile to an accuracy greater than 20% at best [25]. The behaviour of the support structure must not be crucially dependent on the structural properties of the foundation; otherwise the expected soft-soft structure may turn out to have soft-stiff properties. Ultimately this may have consequences for the fatigue lifetime of the installation.

If a soft-soft or stiff-stiff structure is adopted, designing a very soft or very stiff foundation so that there is no danger of the final assembly having a natural frequency in an unexpected band may circumvent this difficulty. Such an approach was used at the Lely farm, although the final stiffness deviations proved so large that one of the units responds in the soft-stiff band rather than the expected soft-soft regime [133]. The problem is more pronounced with a soft-stiff design and

one solution is to build in a facility for final tuning of the structure in situ. Where a variable speed turbine is used there may be some scope for retrospective modification of the control algorithm to accommodate the foundation uncertainty [25].

2.5.4 Modelling of sea derived structural forces

The diameter D of pile foundation offshore wind support structures is small in comparison to the wavelength L of typical sea waves. The structures can be regarded as hydrodynamically transparent therefore, having little impact on the passing waves. Gravity structures for offshore wind turbines typically require horizontal dimensions an order of magnitude larger than piled foundations [134]. With $\pi D/L$ approaching unity, the influence of the structure on passing waves becomes more significant and a diffraction analysis, usually requiring a numerical solution of the Poisson equation, is required [131, 135].

In the absence of diffraction the support structure members are subjected mainly to forces from two sources:

- Inertia forces derived from the pressure gradient caused by accelerating fluid
- Drag forces caused by flow separation around the member and viscosity

It is common practice to model this loading with the Morison [136] equation which in elemental form for a vertical cylinder of diameter D in a flow of speed u may be written [131]:

$$dF = C_m \rho_w \frac{\pi d_T^2}{4} \frac{du}{dt} + C_d \rho_w \frac{d_T}{2} |u| \, u \tag{2.10}$$

where

dF Elemental force
ρ_w Fluid density

The inertia and drag coefficients, C_M and C_D, must be derived empirically, although there are several documents [137, 76] that provide values suitable for common situations.

The Morison equation is valid both for currents and passing waves, with the total force calculated by integration up to the water surface. Clearly for this to be possible knowledge of the water particle kinematics is essential, and resort is made to analytic wave theory.

Wave slope	Classification
$\varsigma < 0.5$	spilling
$0.5 < \varsigma < 3$	plunging
$\varsigma \geq 3$	surging

Table 2.4: Classification of breaking waves.

2.5.5 Wave kinematics

Analytic theories for trains of regular waves are based on solutions of the Laplace equation for velocity potential [138], which is a standard model for the incompressible, irrotational flow that water waves comprise. Small waves in deep water are adequately treated by so called linear or Airy wave theory [139], which is characterised by applying boundary conditions at the undisturbed water surface rather than on the wave surface itself. Steeper waves in shallower water require more sophisticated higher order stream function solutions [140] or Stokes wave theory [141].

2.5.6 Breaking waves

Breaking waves present a difficult problem, especially since many proposed sites for offshore wind farms are in locations where breaking waves may from time to time occur [5]. A convenient 'rule of thumb' to identify waves prone to breaking is that the height to depth ratio is equal to 0.78 in shallow water, or in deep water, the height to wavelength ratio approaches 0.14 [137]. Some sources [131] note that these simple relations are not adequate in all situations, but the complexity of more rigorous criteria presents an obstacle to their use.

Breaking waves occur when the particle speed in the wave crest exceeds the wave celerity, and can be classified as shown in table 2.4 according to the non-dimensional slope

$$\varsigma = \tan\alpha \sqrt{{gT^2}/{2\pi H}} \tag{2.11}$$

where

g Acceleration due to gravity
H Wave height
T Time period.

In the North Sea coastal regions, breaking waves are clearly a concern since the depths in which the literature suggest it is feasible to construct offshore farms range from 5 to 40 metres (see [16] for example). In all cases modelling the forces

exerted by breakers presents considerable difficulty. Spilling breakers, at the onset of breaking, may be adequately treated by certain stream function theories. Other cases, particularly after breaking, can only be dealt with using CFD techniques, which is clearly beyond the scope of the modelling in the current work.

2.5.7 Description of the wave climate

The preceding sections have discussed calculation of the forces exerted by a specified wave or wave train on an offshore structure. A real structure will be subjected to a range of wave conditions over its lifetime. For design purposes, techniques to assess the influence of the range of conditions on the loading of the structure are required for the identification of design giving critical cases, be they due to extreme or fatigue endurance. The application of the available techniques is necessarily closely coupled with description and modelling of the wave climate.

There are two basic approaches used by the offshore industry, which mirror the treatment of wind conditions in wind engineering. For the design wave approach the largest wave likely to impact on the structure over a specified interval, known as the return period, is determined. A relatively simple statistical analysis, fitting an analytic distribution such as the Weibull or Gumbell distribution to measured data is used to estimate the design wave. This wave is considered to act on the structure concurrently with similarly determined design wind and currents (if they provide significant loading), assuming they all originate from the same direction. The structure is designed to resist this combined loading. While relatively easy to apply, this approach has several disadvantages. Firstly, the design wave may not cause the largest structural loads, particularly if resonance occurs with smaller waves of a different frequency. In principle at least this can be over come with a parameter study of wave heights and frequencies, and some design codes [137] suggest schemes for such an analysis. Secondly, and most importantly there is no means to account for fatigue. For this reason, the design wave approach is not usually employed in isolation.

An alternative approach involves developing a more sophisticated statistical description of wave variability based on the well-established theory of random processes. As with the wind, there is a spectral gap in the frequencies at which energetic waves are found (figure 2.11 [135]), and thus the long-term and short-term statistics of waves may be treated separately. Over a long period a structure will experience a large number of sea states, which might be characterised by the significant wave height and associated period. The variation of sea states with time can be modelled using probability distributions.

It is conventionally assumed that each sea state lasts for between 20 minutes

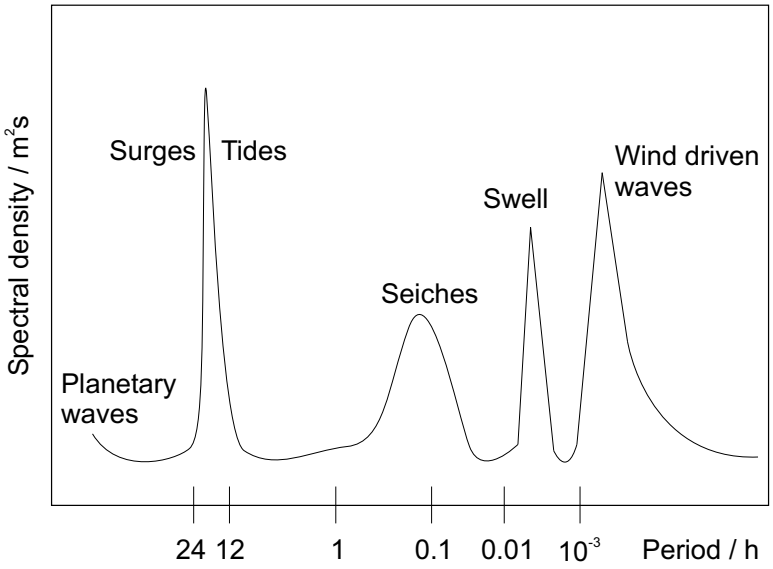

Figure 2.11: Spectral gap in energetic waves. The diagram is based on information taken from references [25, 135].

and 3 hours, during which the statistical properties of incident waves are stationary. Short-term statistics, for long-crested (i.e. uni-directional) waves, may be characterised with parameterised expressions for their power spectral density. This provides a frequency domain description of the sea state which is convenient for frequency domain calculations of the structural response.

The statistical, frequency domain, approach allows account to be taken of both fatigue and extreme loads, as the extreme conditions are included in the statistical description. It does however rely on the linear superposition of the influence of incident waves, since in effect the environment has been decomposed into its Fourier components. The action of small waves on large structures is very nearly linear, but the validity of the approach reduces as waves become larger and structures become smaller. This is a particular issue for extreme wave loading of relatively slender offshore wind turbine structures. A common design practice, adopted in this work, is to use both techniques, relying on the design wave approach for extreme analysis and statistical approaches for fatigue.

2.5.8 Long term statistics: sea states

The wave climate at a location may be regarded as a series of seas states, during each of which the wave statistics remain constant. It is conventional to assume that a sea state lasts for 3 hours [137]. Specification of the climate therefore requires a description of the sea states experienced over an appropriate period of time, at least a year and ideally the lifetime of the structure.

Sea states are often characterised by the significant wave height H_S and an as-

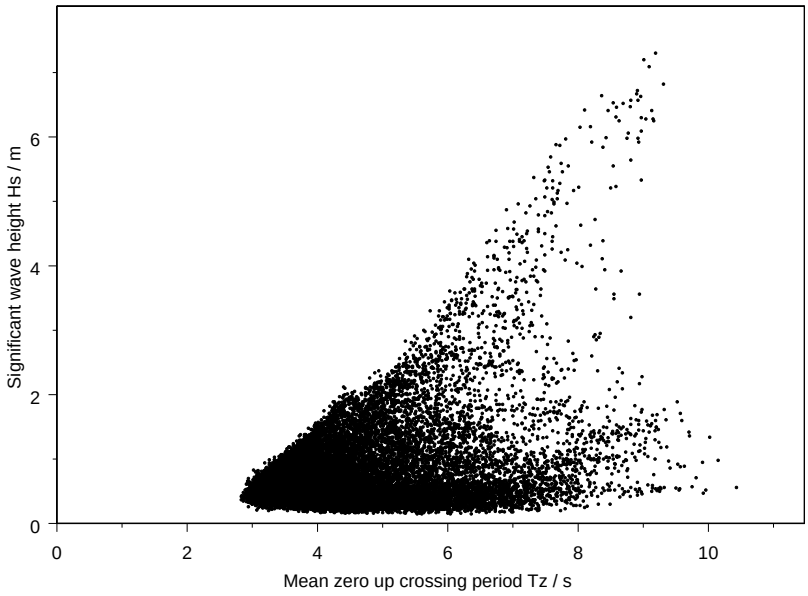

Figure 2.12: Scatter diagram of sea states. The data represents hourly average values collected from measurement buoy 44103 operated by the NOAA [144] in the North Atlantic.

sociated wave period, usually the average zero up-crossing period T_Z. A scatter diagram of these two properties, such as that shown in figure 2.12, can represent the full range of sea states encountered at any location, although for analysis purposes similar sea states are 'lumped' together to produce a limited number of cases. There are many databases that collect together such information (e.g. NESS [142, 143] NOAA [144]), however commercial sensitivities mean that the data is often not readily available. The coverage of such data is usually limited to areas of interest to the database owner, and extrapolation to other areas is not straightforward. While invaluable for final design work, the accuracy they provide is probably excessive for a study such as this where there are considerable uncertainties in many of the parameters at each location.

Simpler representations of sea state are more appropriate for use here, such as the Weibull distribution parameters for significant wave height derived from Voluntary Observer Fleet information calculated by Garrad et al [5] and other similar data sources [145, 146]. This data does not provide period information, but empirical correlations exist which can be used to estimate these values for different sea regions.

A further issue is the correlation between sea states and wind conditions, such as that shown in figure 2.13. Ideally a three dimensional scatter diagram of significant wave height, zero up-crossing period and mean wind speed would be

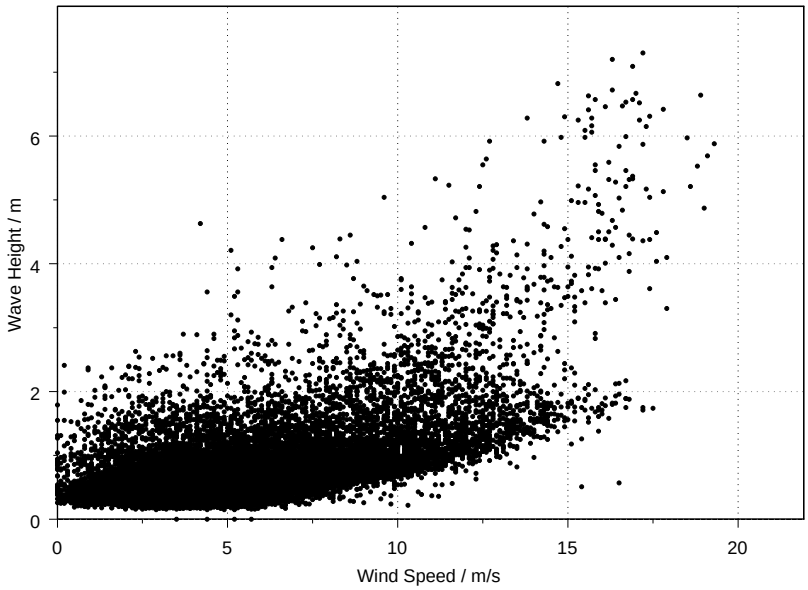

Figure 2.13: Scatter diagram of wind and sea states. The data represents hourly average values collected from measurement buoy 44103 operated by the NOAA [144] in the North Atlantic.

available for all locations, and the lumping procedure suggested by Kühn [25] used to identify a manageable number of load cases. More generic methods are required for initial design purposes using limited data.

For conventional offshore structures the influence of the correlation on fatigue is largely ignored thanks to the low importance of wind loads, and hence design codes provide little guidance. A means of relating longer term sea state parameters to wind conditions is required. Neumann and Pierson [147] give a suitable empirical correlation (equation 2.12) valid for fully developed[2] sea states:

$$\begin{aligned} H_s &= \tfrac{0.21}{g} U_{19.5}^2 \\ T_Z &= 0.81 \left(\tfrac{2\pi}{g} U_{19.5} \right) \end{aligned} \tag{2.12}$$

where $U_{19.5}$ is the wind speed measured at a height of 19.5 m above the water surface.

The relations allow the sea state parameters to be correlated with the mean wind speed (described by a Weibull distribution), and hence a series of loads cases defined. Kühn [25] notes that these relations are excessively conservative for most fetch limited situations, as found in the North Sea. He suggests that

[2]The notion of a fully developed sea state is discussed in section 2.5.9.

where data is available, a better approach would be to formulate a monotonic relation between wind speed and significant wave height by equating their cumulative probability. This could be based on, for example, independent Weibull distributions of each, or $H_s - T_z$ scatter diagrams.

For extreme load calculation[3] estimates of the extreme conditions are required, and it is conventional in offshore design to use 50-year return period values. Suitable values may be obtained from the climate descriptions required for the fatigue analysis. However, since individual gusts and waves are uncorrelated, simultaneous combination of 50-year return period extreme values for both wind and wave is excessively conservative. UK design codes [137] recommend consideration of the 50-year return extreme wave applied simultaneously with the 50 year return 1 minute average wind speed. This guideline was written with large offshore platforms in mind, where wind loading is of a secondary importance. Application to wind turbines requires extension to take better account of wind loading and Garrad et al [5] evaluate two procedures as follows:

1. Extend the UK guidelines by adding a second load case where the 50 year extreme gust is combined with the wave height that gives the same combined probability of return as the specified case

2. A methodology suggested by Simpson [148] that assumes the 50 year return extreme state occurs at the same time as a storm with mean wind speed equal to the 50 year return hourly mean wind speed, but wind gusts and waves are uncorrelated over the hour duration of the storm and sea states and both have a Gaussian distribution.

Application to a range of studies found that the results correspond to within three percent, and thus either may be applied.

2.5.9 Short term statistics: wave spectra

In any given sea state an offshore structure will experience waves of differing heights and periods. Several empirical wave spectra have been developed that describe the wave frequency content in any short-term sea-state.

The Pierson-Moskowitz spectrum [149] is commonly used to describe the spectral content in fully-developed seas. It appears in many forms in the literature,

[3] As in other studies [5], we will assume here that the extreme loads occur under 'extreme' conditions, although this may not be strictly correct where compliant structures are deployed. The problem of identifying appropriate combinations of wave and wind conditions to calculate the extreme load is considerably complicated if the extreme wind loads occur during operation. However in this case the extreme wind load will occur in conditions far from those that give extreme wave loads, and thus the procedures here are likely to be too conservative.

but the most convenient for practical application is expressed as a power spectrum in terms of the sea state parameters, that is

$$S_{\eta\eta}(f) = \frac{H_S^2}{4\pi T_z^4 f^5} e^{-\frac{1}{\pi (f T_z)^4}} \tag{2.13}$$

where H_s is the significant wave height, T_z the zero-up crossing wave period and $S_{\eta\ eta(f)}$ is the spectral density of water surface elevation at frequency f.

A fully-developed sea is one in which the spectral content of the sea does not change with increasing fetch. The conditions under which such a state arises can be understood by considering the physical processes through which waves are formed. The origin of waves lies in the shear stress and pressure fluctuations exerted on a calm sea by a wind blowing over it. Of the ripples that arise, those that travel the most slowly, and consequently have a high frequency and short wavelength are further excited by the wind due to the large difference in speed. Further energy is transferred from the wind to the waves, and their height continues to grow until the deep water breaking limit is reached. Energy is then transferred most effectively to the shortest wavelength remaining waves, which in turn reach the breaking limit. Eventually the only remaining waves travel close to the speed of the wind and absorb little energy from it so that there is no further evolution of the wave spectrum.

A long fetch and consistent wind conditions are required for a fully developed sea state to be achieved, typically a constant wind blowing for several hours over a fetch of hundreds of kilometres. In the constrained area of the North Sea these conditions rarely arise and the frequency content is better represented by the JONSWAP spectrum, written by Hasselman et al [150] as

$$S_{\eta\eta}(f) = \frac{\beta g^2}{(2\pi)^4 f^5} e^{-\frac{5}{4}\left(\frac{f_p}{f}\right)^4} \gamma^a \tag{2.14}$$

where γ is the so called 'peak enhancement factor, f_p is the frequency of the spectral peak and

$$a = e^{\frac{-\left(\frac{f}{f_p}-1\right)^2}{2\sigma^2}} \tag{2.15}$$

with

$$\begin{aligned} \sigma &= 0.07 \quad f < f_p \\ \sigma &= 0.09 \quad f \geq f_p. \end{aligned} \tag{2.16}$$

Values for the parameters β, f_p and γ can be related to the sea state descriptors H_s and T_z through fitting to experimental data. Comparison of equations 2.13 and 2.14 reveals similar forms. Performing the fitting process to data for a fully developed sea will yield the Pierson-Moskowitz expression, which may be considered

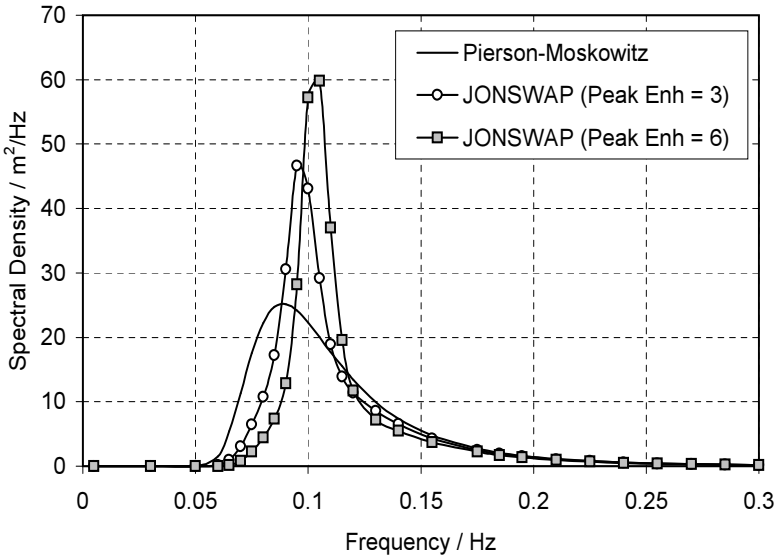

Figure 2.14: Comparison of the Pierson-Moskowitz spectrum with the JONSWAP spectrum for two values of the peak enhancement factor, γ. The spectra are plotted for the same nominal sea state, specifically a significant wave height H_s of 5 m and a zero up- crossing time period T_z of 8 s.

a special case of the JONSWAP formula with a peak enhancement factor of unity.

Barltrop [139] presents a modified form of the JONSWAP formula in which Hasselman's parameters are explicitly related to H_s and T_z by a series of empirical expressions valid for the fetch limited North Sea. However the basis for predicting γ from H_s and T_z is open to question and it is preferable to use measured data for the location of interest.

The modified JONSWAP form was used to plot figure 2.14 in which comparison is made with the Pierson-Moskowitz spectrum for various values of the peak enhancement factor. The diagram shows that, for the same nominal state, the energy content of the sea is more tightly concentrated around a peak for the fetch limited cases modelled by the JONSWAP spectrum than for the fully developed states. The peak energy content also occurs at a higher frequency for the fetch limited states, increasing with the peak enhancement factor.

In principle the JONSWAP spectrum is the more representative of the conditions to be found in candidate locations for bottom mounted offshore wind farms. However the limited data available makes determination of the peak enhancement factor difficult. Thus, this work adopts the common practice [25] of using the Pierson-Moskowitz spectrum for fatigue calculations.

2.5.10 Directional phenomena

In any sea state real waves are rarely perfectly unidirectional, and measure of their direction shows some scatter. This variation, known as "short crestedness" is often neglected for analysis purposes. This is conservative so far as fatigue is concerned, as in reality the damage will be distributed around the loaded object, where as the analysis assumes loading is always applied from the same direction. A simple approach to accounting for it is to analyse the structural response assuming waves arrive from each of perhaps eight sectors [137].

Another directional phenomenon is misalignment between the wind and wave direction. This is potentially serious as when the turbine is in operation, much of the structure's damping is derived from aerodynamic effects which operate in the fore-aft direction. Lateral waves excite a response that is not contained by this damping. Kuhn [25] found that the impact was small for misalignments of up to 30 degrees, but that for larger misalignments the structural response to waves could exceed that in co-linear cases, which in turn would have implications for the fatigue life. Fortunately the role of the wind in generating waves means that large mis-alignments are relatively rare, with design guidance suggesting it is acceptable to assume that waves and wind are in the same direction in the absence of more specific information [137].

2.6 Foundation design

2.6.1 The first decision: floating or bottom mounted?

A fundamental decision is whether to construct a floating or a fixed base foundation. The limited work on floating designs [72, 151, 152, 153] has suggested they are expensive compared to fixed base options for relatively shallow water. Their advantages become more apparent in very deep water, however such locations tend to be very far from the shore which increases connection and maintenance costs. There is general agreement that near to shore bottom mounted designs are intrinsically more economic than floating concept. As such there is little interest in floating turbines at present, and they are not considered here.

One suggestion to improve the economics of floating turbines is through combination with wave energy capture mechanisms [154]. However this may prove impractical due to the contradictory nature of the concepts: wave energy machines aim to capture as much energy from the sea as possible, whereas good turbine support structures are as transparent as possible to this energy.

2.6.2 Pile, caisson or gravity base?

A cursory analysis suggests that a gravity base would be considerably cheaper than a piled base, since the effort of installation is reduced. Gravity foundations could be floated into place, potentially with the tower and turbine already attached. This requires much less expensive offshore work than for the piled alternative where the pile must the constructed, and the tower and turbine all attached offshore.

Unfortunately the large dimensions required for stability and the shallow water conditions mean that gravity bases are not in general hydrodynamically transparent and are subject to substantial diffraction forces under extreme wave conditions. This can produce large heave loads, potentially able to displace the foundation, unless very heavy ballasting is used, which in turn offsets most of the expected advantages [134].

Skirted or caisson (so called 'Spudcan') foundations are a relatively recent innovation [155] that rely on generating suction in an upturned 'bucket' to transmit horizontal loads to the seabed. While they have found quite some favour with designers of large offshore platforms their suitability for offshore wind turbine use has been questioned because of the very different loads. There is currently work underway to evaluate these issues further [156, 157, 158].

Of the existing offshore farms, the majority use pile foundations.

2.6.3 Design and modelling of foundations

The principles of both pile and gravirt foundation design are well understood, and the literature [159, 160] describes methods for evaluating the static vertical and lateral loading capacity, along with means of calculating internal forces. Calculations are necessarily approximate, even with a good description of the soil properties relying on techniques ranging from, at the simplest level, analytic formulae, to integration of differential equations at the most complex [135]. Such complexity is only worthwhile if the soil properties as a function of depth are well known, which for preliminary offshore design will in general not be the case. There is little readily available detailed engineering data on the nature of the seabed in Northern European waters, beyond qualitative descriptions of the types of material found such as those provided in map form by the British Geological Survey [161]. In consequence it is appropriate to use relatively simple methods for the preliminary design of foundations.

2.7 Design and costing of non-structural components

2.7.1 Overview

While the main costs, and the focus of this work, are the structure and the turbine, there are many other farm components which cannot be ignored in any cost study (the breakdown of offshore wind farm costs is analysed in more detail in chapter 3). The individual turbines must be connected collectively to the power grid in order to supply electricity. Provision must also be made for maintaining the turbines. The treatment of these systems for the current work is described briefly in chapter 3 with more detail in appendices D and E, while this section surveys their design and costing.

2.7.2 Operation and maintenance

Annual operation and maintenance for onshore wind farms represents perhaps 2.5% of the investment cost [31]. Using a discount rate of 5% and a lifetime of 25 years, this accounts for approximately 23% of the energy cost. Experience [24] and calculation [132] demonstrates that it is a more important consideration offshore, contributing as much as 30% of the overall energy costs. The difficulty of working offshore is largely responsible for this. Offshore work requires expensive equipment, including boats and possibly helicopters or floating cranes for lifting, than onshore where a land rover and mobile crane will be sufficient for almost all operation. More people are necessary to operate the equipment than onshore, and they are required for a longer time, as travel to and from the farm will in general be more time consuming offshore. Wind and sea conditions may prevent some or all the operations planned on any day from taking place, further increasing the overall expense [162]. Marine standards [131] give maximum conditions for particular operations.

The importance of operation and maintenance goes beyond simply the direct cost however. In some locations, the winter North Sea being a good exemplar, weather conditions may prevent maintenance access for months at a time [163]. Were turbines to fail at the beginning of such a period, they would remain out of service, not generating revenue until conditions improved. There may be a net benefit to the cost of energy in operating a vigorous preventive maintenance schedule in order to improve availability by minimising incidents of failure during periods of poor weather and the subsequent extended down time.

Determining the optimum maintenance schedule for any farm is a difficult problem, depending on the failure characteristics of the machines, the local climate, the distance from a harbour and the costs of staff and operations. The most

successful analyses to date rely on Monte-Carlo type [90] simulations of machine failure and weather conditions [163] to test the availability produced by different maintenance strategies.

2.7.3 Electrical connections

The major choice in designing the grid connection to shore is between an AC and a DC connection. Which is the most economic depends on the cost of construction, and the power lost in transmission. As a rule of thumb, AC connections tend to be more attractive over short distances [132]. With increasing distance to the grid, however, the dielectric losses incurred due to the capacitance of the insulation material increase [164]. Coupled with the requirement for a separate core, or possibly even separate cable, for each of the three phases, AC transmission rapidly becomes more expensive as distances increase. DC transmission, on the other hand, needs expensive conversion equipment for connection to the power grid. This is a fixed cost independent of transmission distance, and hence DC becomes more economic with longer distances. The crossover point between which scheme offers the best economics is difficult to estimate and location dependent, but most estimates for offshore wind applications place it between 30 and 250 km [164]. HVDC connection technology is the subject of much active work [165], and costs are expected to fall over the next decade. Nevertheless, for farms just a few kilometres from the coast, using AC is clearly the most attractive, and all the existing farms use this technology. For future developments, such as the proposed UK Western Offshore Transmission Grid [166], the decision is less clear.

Before transmission to shore, the power must be collected from the individual turbines. In principle the internal collection may be based on either AC or DC, irrespective of the transmission system. Onshore, AC collection coupled with AC transmission systems (AC-AC) are by far the most common. Typically wind turbine induction generators operate at 690 V, with a nacelle or tower based transformer stepping the voltage up to 11 kV or, in newer systems 33 kV for collection [167]. Using the higher voltage permits direct connection to most distribution grids, removing the need for an expensive site transformer. For long distance grid connection 132 kV is used since losses reduce with increased voltage. As turbine based transformers are essentially limited to 33 kV, a site transformer is then necessary irrespective of the collection voltage.

DC power collection in conjunction with AC transmission has also been used successfully. While experience is very limited, there do not seem to be any fundamental issues with combining DC collection with DC transmission [167]. Combining AC collection with DC transmission to form an ‘AC Island’ may give sta-

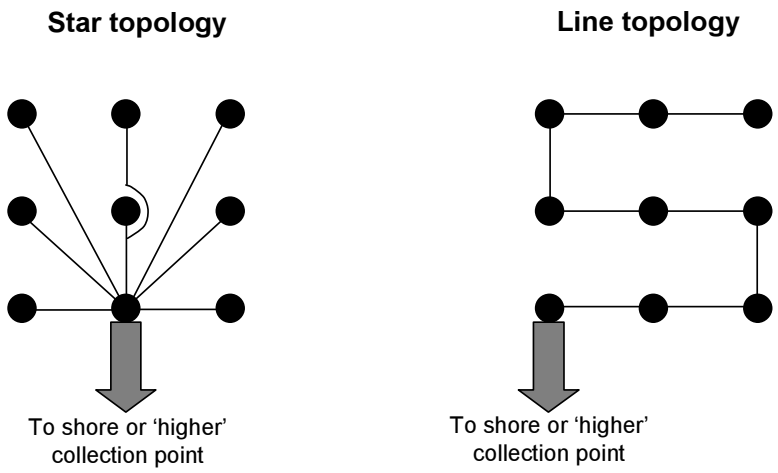

Figure 2.15: Connection topologies for offshore wind farms.

bility and start-up problems however.

In view of the difficulties of offshore maintenance work, the reliability of the power collection and transmission system is an important consideration. Connecting the turbines together in a circuit or using star formation (figure 2.15) gives increasing levels of redundancy but with increasing capital costs. The cheapest to construct linear connection could result in a large number of turbines being disconnected if even a single cable fails.

Failure of the grid connection itself would have very serious consequences. This risk is significant [168], and potentially could disconnect the wind farm for months. One solution is to treat a large offshore farm as a collection of smaller blocks, connecting each directly to shore using 33 V AC cables and then directly to the power grid, as is now common onshore. This avoids the need for a difficult offshore site transformer, in part offsetting any additional cabling costs. However for farms larger than 200 MW capacity or relatively far from the shore a single HVDC or 132 kV AC link becomes essential. Both of these will require isolated conversion equipment and switchgear to be located at sea which is without precedent and therefore risky.

In principle modelling the costs of offshore grid connection should be straightforward [169]. Most of the electrical design principles are well understood, and the initial design process can be broken down into a series of decisions. There have been attempts to formulate decision support tools for this purpose [170]. While automating the major technical decisions is possible, the availability of cost information presents a serious difficulty. Most of the equipment required is not available 'off-the-shelf' [167], and manufacturers are unwilling to provide data except as part of a quotation for a job [171].

2.8 Offshore wind resource assessment

2.8.1 Principles

The objective of wind resource assessment is to identify locations likely to maximise energy production from a proposed wind farm. Gathering suitable data conventionally relies on direct measurement techniques and modeling, sometimes used in combination. Anemometry lies at the root of resource assessment, but while most European countries have networks of weather stations reporting suitable data, their distribution is too sparse to account for local factors that influence the wind speed [172].

Several models have been developed to 'interpolate' between the measured data by solving the governing equations of the flow (usually in simplified form), subject to a description of the intermediate land. An early attempt was NOABL [173], which was used to produce a wind atlas of the UK with an approximately 1 km resolution. Most commonly used today is the well-known WAsP [174] model which accounts for geostrophic effects, variations from neutral stability, changes in roughness, shelter and orography. WAsP has been updated to improve its performance for the treatment of offshore cases [175], and extended to provide more detailed engineering information beyond that required for resource assessment [176].

Output from combined measurement and modelling programmes has been found adequate for the initial selection of candidate sites. Ultimately, unless there are existing meteorological stations near by, there may be no alternative but to carry out a detailed measurement programme at candidate sites [177].

2.8.2 Offshore studies of the EU

The data required for resource assessment is closely linked with that needed for the structural design of offshore farms, although less detailed descriptions of the wind environment are generally acceptable and clearly there is no need for sea state information. There are many detailed sources of raw wind speed that include offshore measurements, such as the NERC sponsored British Oceanographic Data Centre [178] and the British Atmospheric Data Centre [179]. Since the data was not collected for use in wind energy assessments, their coverage is incomplete. Where there is wide coverage, the data is generally unsuitable for resource assessment work without large scale processing, beyond the scope of this project.

There have been numerous studies of the wind conditions around individual countries (see [180] for a discussion of UK studies) specifically to assess the off-

shore wind resources. These would seem a good place to start any large scale source assessment, but as reported by Garrad et al [5], inconstancies in the approaches taken by each study make combining the data a formidable objective. Even converting the data into a form compatible with modern analysis tools, like GIS, represents a considerable effort. To overcome these difficulties, Garrad produced a new 'broad-brush' database of wind conditions by combining Voluntary Observer Fleet data (analysed by DWD) modified by 'WAsP-Type' calculations to better represent inshore conditions.

Recently the POWER [181, 182] project has sought to improve on the Garrad-Hassan approach, predicting offshore wind characteristics from pressure based calculations of geostrophic winds in conjunction with WAsP calculations and a coastal discontinuity model to properly account for inshore effects. At the time of writing this data is not available to the community, although the long-term intention is to release it.

The available resource is reduced by constraints on wind farm construction. These may be considered as falling into one of three classes. Physical constraints are those natural features that make offshore farm construction impractical. In principle they could all be overcome with technological solutions, but there are some cases where this would clearly be so expensive that the features should be regarded as a constraint. An important example is depth, where there is consenus that depths greater than 40-50 m are too deep to make offshore wind installations viable. Seabed conditions have the potential to be an important constraint also. Man-made constraints arise because of existing construction, such as oil rigs and pipelines which an offshore farm might interfere with. They are not a major concern here, due to the focus on engineering design and cost, but where data is readily available it is sensible to account for them. Finally there will be socio-political constraints, which in practice are likely to be the most severe, but will not be considered here in any detail.

Information on the physical and man-made constraints is readily available, but as with the wind data, collecting it together is a substantial task. The Garrad work provides consistent data on the constraints. As such it still represents the best wide ranging source of data on European wind for resource assessment, and was used as the basis of parts of the current work, although supplemented from other sources. Chapter 7 discusses the formulation of the constraints and composition of the GIS data.

Chapter 3

Modelling approach

3.1 Engineering economic analysis of energy projects

3.1.1 Fundamentals

Following IEA guidelines [183], the cost of energy from wind energy conversion systems in this work is evaluated using a discounted cash flow approach. A net present value is calculated from the total investment (or capital) cost, I_{tot} ,and the total annual on going costs, M. This is converted to an annualised payment and divided by the estimated annual energy production E to produce the minimum cost per energy unit at which the produced energy can be sold. The calculation is encapsulated in equation 3.1

$$C = \frac{I_{tot}}{aE} + \frac{M}{E} \tag{3.1}$$

where the annuity factor a is calculated from the test discount rate r and the economic lifetime n_e in years,

$$a = \frac{1 - \left(\frac{1}{1+r}\right)^{n_e}}{r}. \tag{3.2}$$

The purely economic parameters, r and n_e are not a focus of this study and will be treated as constant. For comparison of technologies with similar variations of cost over time their values do not have an impact on the conclusions so long as each case is treated consistently (see appendix A). The precise values employed are not critical therefore, although it is preferable that the parameters to some extent reflect 'real world' conditions so that cost of energy values stand qualitative comparison with those from other sources. Academic studies of wind energy costs frequently assume discount rates of 5% and a lifetime of 20 years, and these values will be adopted here.

This analysis ignores any end of life costs and benefits such as decommis-

sioning or the salvage value of any decommissioned equipment. With a 20 year project lifetime and 5% discount rate, end of life costs contribute 37% as much to the project net present value in comparison to comparably sized initial costs, as can be seen from figure 3.1 which shows how the contribution to the net present value made by equal costs occurring in each year of operation declines with time. This omission potentially represents a significant error. Assuming, for the purposes of illustration, that initial costs represent 70% of the energy cost and that net decommissioning costs are half those of the initial construction, the cost of energy will be undervalued by approximately 13%. Currently, however, there is little understanding of the decommissioning measures that will be required for offshore farms, and their associated costs. As such any treatment would necessarily be very approximate, and it was considered better to neglect them completely in this study.

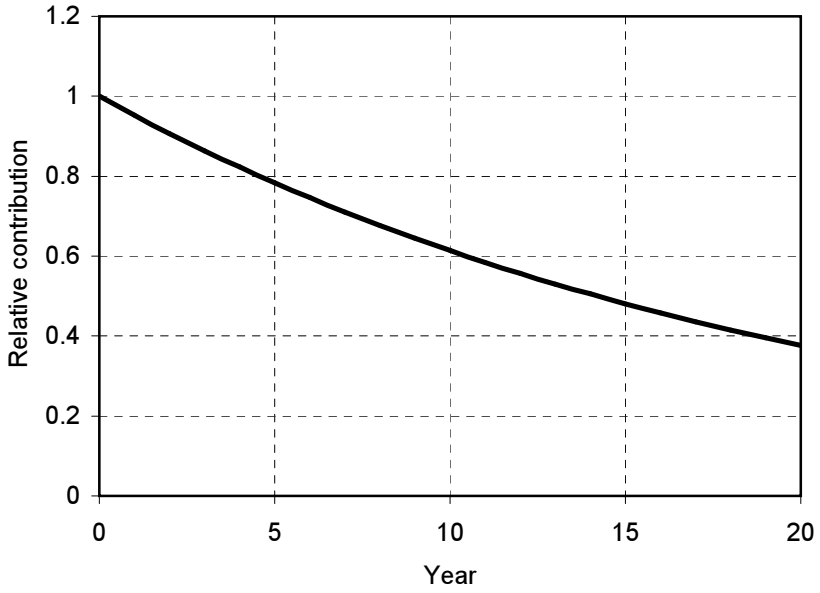

Figure 3.1: Contribution of equal annual future costs to cost of energy.

No provision is made for retrofit costs, such as might occur if the support structure life was much greater than that of the turbine, and the original turbine was replaced by an upgraded version. While the analysis can be easily extended to include such circumstances, they are not considered here.

3.2 Breakdown of energy costs from existing farms

3.2.1 Opening remarks

To obtain some insight into the parameters that influence the cost of the energy from an offshore wind farm, it is worth re-examining data relating to existing farms in more detail. This section will analyse costs relating to all components of an offshore farm, even though the support structure is the focus of the study. The limited information available means that cost breakdowns will necessarily be fairly coarse, limited to turbine, grid connection / electrical equipment, support structure. This is sufficient to draw some general conclusions however, which are carried over into the cost model development. A further issue arises because the increasingly commercial nature of offshore wind has discouraged farm developers from publishing detailed cost information in recent years. In consequence the analysis relies on data from older projects and studies.

3.2.2 Analysis

Figure 3.2 compares breakdowns of the major investment costs for five constructed farms and four desk studies completed within approximately the last 10 years. Values are expressed in terms of the proportion of total investment cost to try to mask the effect of widely differing installed capacities.

Data was taken from the sources listed in table F.1 of appendix F, being updated to 2002 Euro values as described in the appendix. The cost data from the studies must be treated with some caution in comparison to that from real farms for two reasons. Firstly the predicted cost may not be realised in practice, and secondly some of the estimates rely on data from the existing farms. However the limited experience of offshore farm construction means it is difficult to proceed without including the desk study data. It must also be kept in mind that none of the real farms can be considered 'truly commercial' [184] and as such the value of the data for cost predictions for large farms is questionable. Furthermore the data represent different design concepts in many cases, which could better be treated separately if more information was available. Only very limited data was obtained for the Horns Rev farm, where the 'other' category includes all investment costs excluding the grid connection.

The figure shows that none of the components can be ignored in estimating offshore wind farm investment costs. The support structure consistently represents about one third of the overall cost with the other components varying considerably in their importance between farms.

The absolute cost of the support structure varies by a factor of approximately

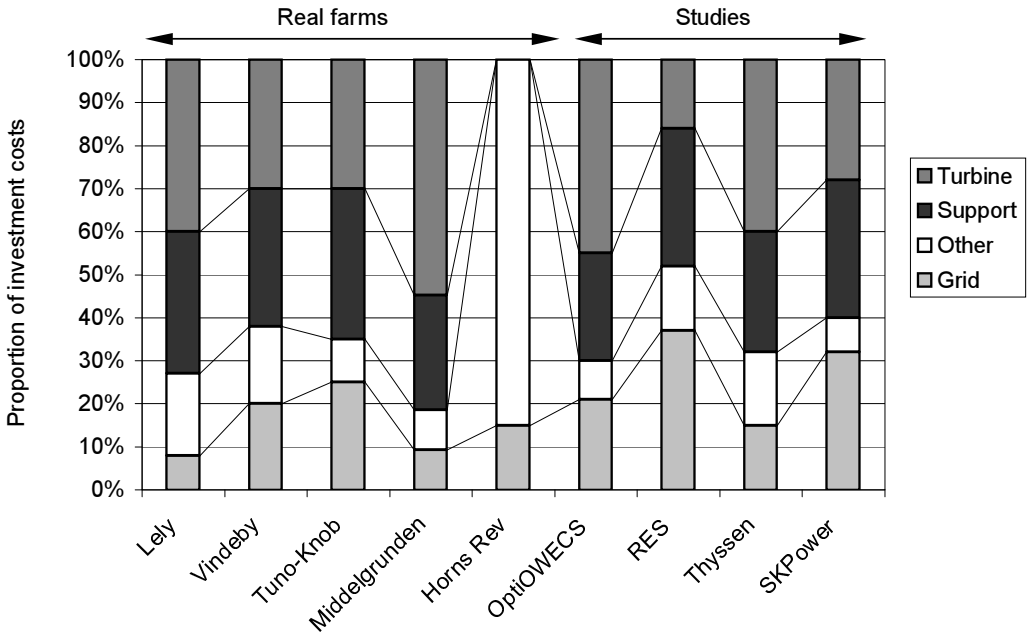

Figure 3.2: Breakdown of investment costs for some offshore farms and studies.

2.5 from the cheapest to the most expensive case. Figures 3.3 to 3.5 show some evidence that the support structure cost is influenced by the turbine choice, the total height of the structure above the seabed and the local wind climate. The limited data and its scatter are not sufficient to allow a simple correlation based cost model to be formulated for the support structure that would provide more than very general estimates. The data shows that design drivers interact in a complex way to influence the support structure configuration and costs. Also local conditions do play a strong role in the support structure design.

There is no reason to expect a strong site-specific component in the cost of the turbine, since all farms and studies considered have essentially employed modified onshore machines. Plotting turbine cost against rated power (figure 3.6) shows a good correlation, demonstrating that offshore machines to date follow the broad onshore pattern wherein the rated power chosen by the designer dominates the investment cost trend. This may change in future as the offshore market grows and manufacturers tailor their designs to the peculiarities of offshore operation, or even to local conditions if very large numbers of machines are required for a single massive project. This possibility will not be considered any further however.

Plots of turbine cost against environmental parameters (figure 3.7) do not

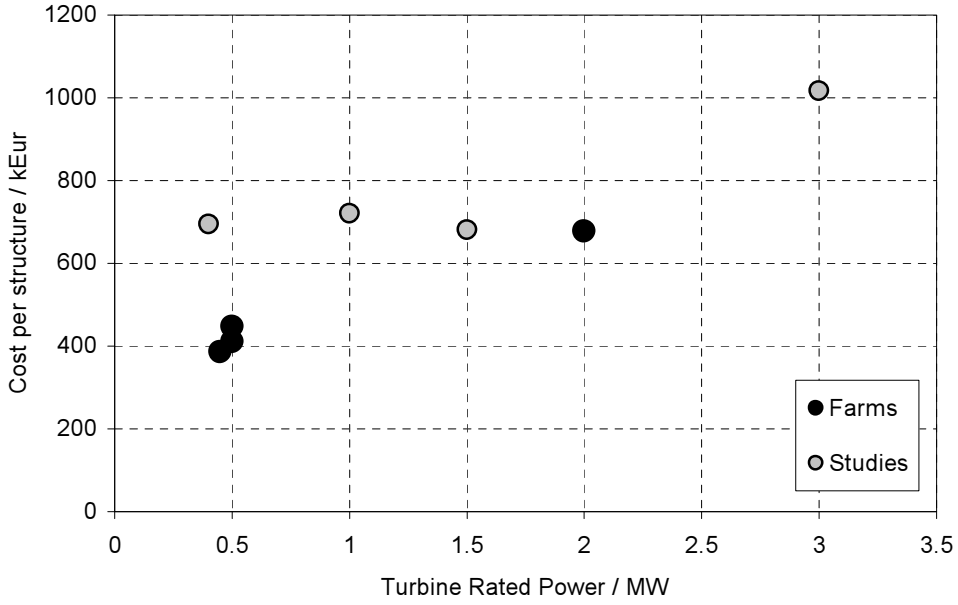

Figure 3.3: Influence of turbine rated power on support structure cost.

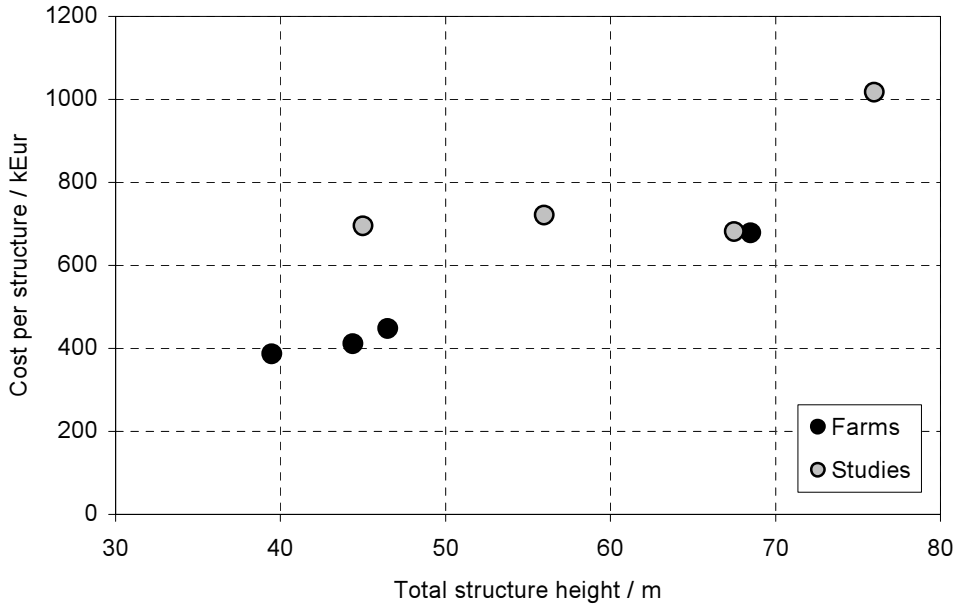

Figure 3.4: Influence of total support structure height on structure cost.

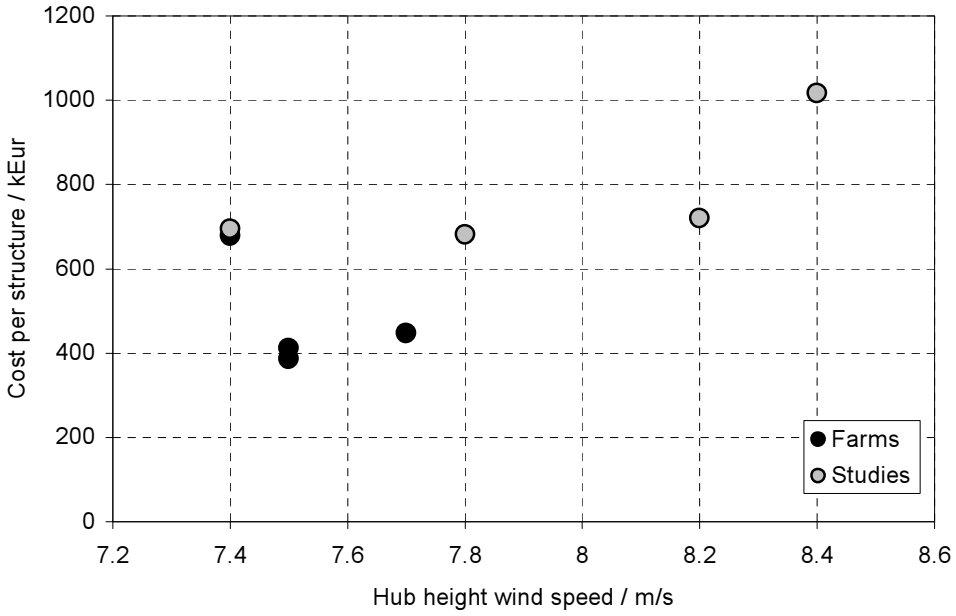

Figure 3.5: Influence of hub height wind speed on support structure cost.

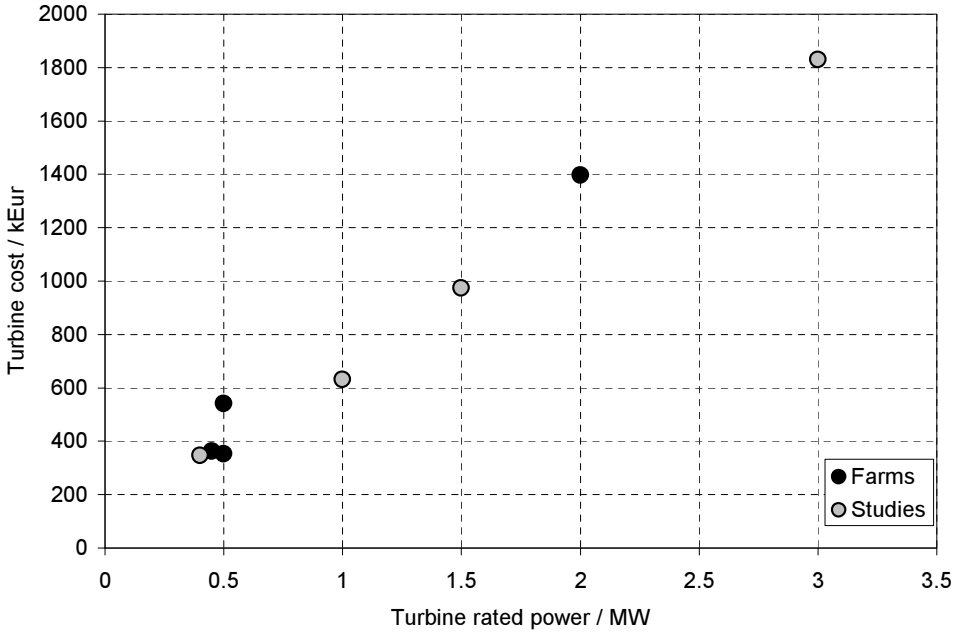

Figure 3.6: Relationship between turbine rated power and capital cost.

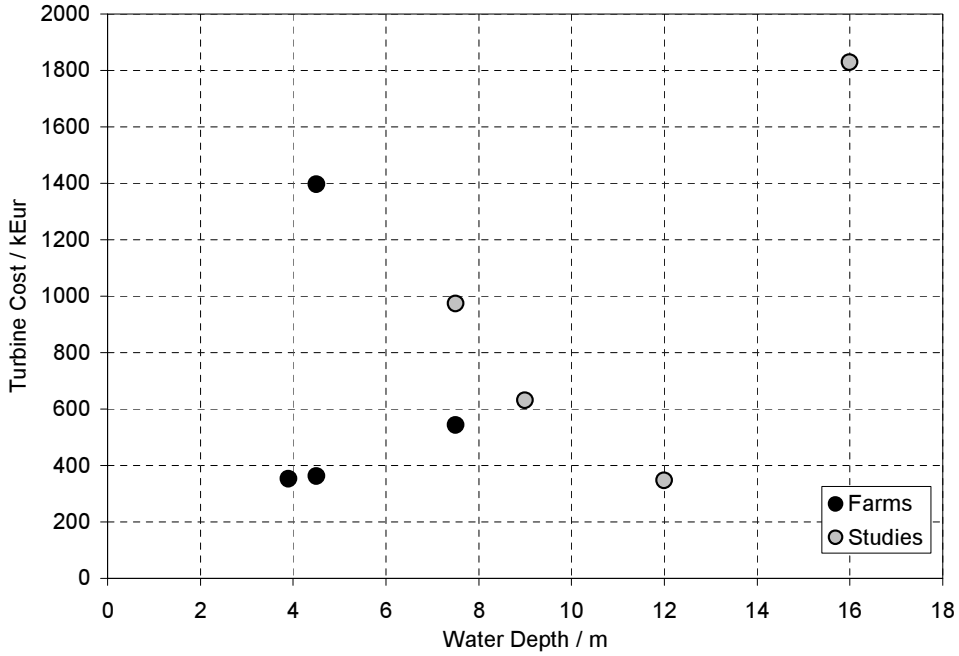

Figure 3.7: Influence of water depth on turbine cost.

show clear relationships, confirming that to date turbine costs have not been influenced by the local environment. Despite this, there may well be a strong environmental component in the selection of an economically *optimal* wind turbine for a specific location. It is well accepted that for onshore use, where the turbine is by far the largest investment cost, larger machines can provide better value in terms of their specific cost [11]. For the turbine in isolation, there is no reason why this rule should not remain true offshore. The turbine however represents only one-third to one-half of the investment cost for an offshore farm, and selection of an optimal turbine requires that the implications for the support structure and other costs be considered. Since the environment has an impact on the structure cost, it follows that there may be an environmental influence in the choice of an optimal turbine.

Plotting the grid connection cost against the installed capacity and the closest distance from the shore (figures 3.8 and 3.9) shows the expected evidence of relationships. As with the support structure there is considerable scatter and formulating a statistical cost model is not practical with the data available. In general the grid connection accounts for between nine and thirty-eight percent of the total investment costs. It is notable that in the two most recent farms listed, Horns Rev and Middelgrunden, the grid represents less than fifteen percent of the overall investment cost. This is all the more remarkable as Horns Rev is a

comparatively distant 14 km from the coast. If this trend is representative grid connection costs will not be dominant in bottom mounted coastal offshore farms, and for this reason are not a major focus of the work presented here.

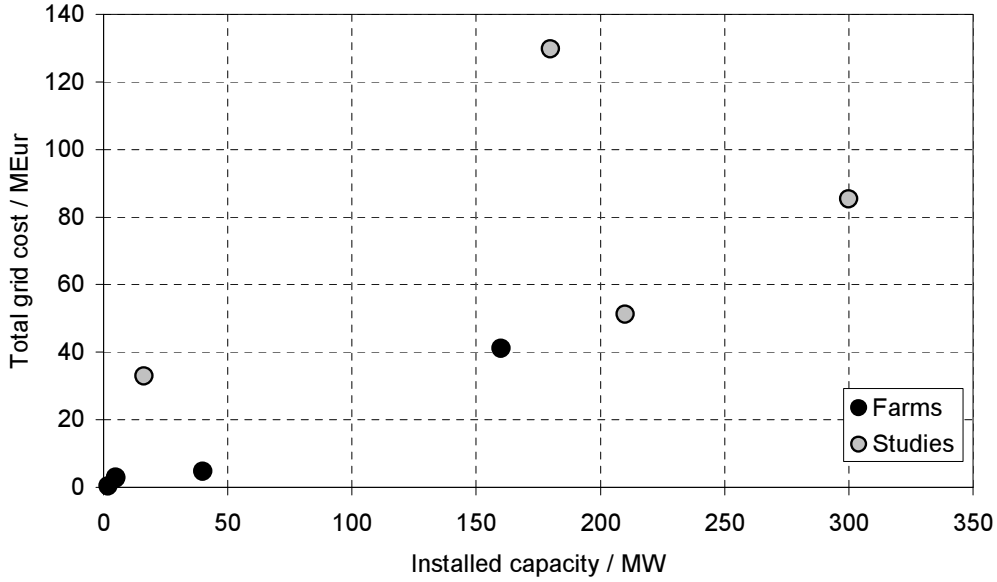

Figure 3.8: Relationship between grid connection cost and farm rated power.

Operation and maintenance costs represent between 13% and 22% of the overall energy cost for the farms/studies examined in appendix F. Since the maintenance cost is a function of environmental conditions [163], variations must be accounted for when seeking optimum wind farm locations and configurations.

3.2.3 Conclusions

The cost of the turbine in an offshore wind farm, is unsurprisingly driven mainly by the rated power. Cost modelling of the turbine could be reasonably dealt with through parametric techniques or indeed with established 'bottom-up' models. The turbine in general is the most expensive or second most expensive farm component.

Depending on the environment, the support structure is the most expensive or second most expensive farm component. It is clear that there are a number of factors that influence the support structure cost in a difficult to predict way. While there is evidence that some of the variations may be attributed to experiential learning there is nevertheless some value in attempting to understand the factors that influence the cost. The only realistic way to attempt this is through a bottom-up cost model.

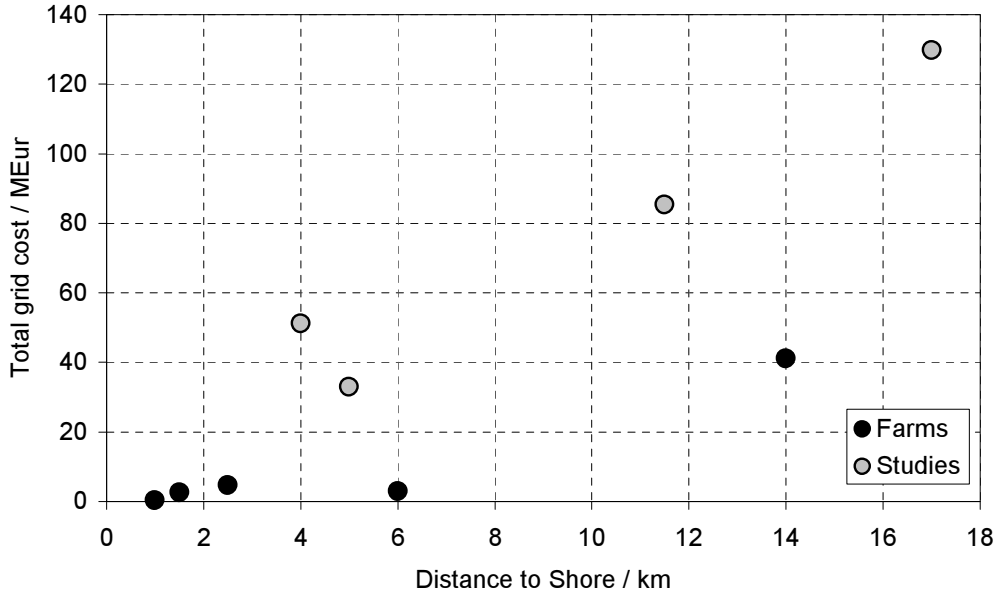

Figure 3.9: Relationship between grid connection cost and distance from shore.

Grid connection costs are less important than those of the turbine and the support structure. However they are still significant. The plots suggest that the primary cost drivers are the distance to shore and the farm installed capacity, although there is significant scatter.

3.3 Modelling the major economic parameters

In principle the major parameters needed to estimate the cost of energy, I, M and E, can be calculated from a sufficiently detailed description of the farm, the location and associated wind/wave climate and the external economic factors (such as the cost of materials, labour and plant).

The investment cost I, on-going costs M and annual energy E production are inter-related. In general, substantially increasing the energy production from a farm requires an increase in investment cost, and the overall implication for the economic performance is not immediately clear. Design changes necessary to increase the energy production will also impact on the maintenance requirements and thence the on-going costs in a way that is difficult to predict. The relationship between the values is also influenced by the choice of technology (e.g. fixed or variable speed wind turbines), the details of the location (e.g. wind and wave climate, distance from the shore), and external economic factors. With a specified technology, location and set of external economic factors, one-to-one rela-

tionships could be formulated between I,M and E for changes in farm design parameters, such as rotor diameter and support structure. When combined using equation 3.1 these relationships can be used to identify economically attractive design configurations. Separate "families of curves" could be plotted for different combinations of technology, location and external economic parameters as suggested by the sketch in figure 3.10. Alternatively, the farm design parameters could be held constant and the environmental conditions varied to identify the characteristics of locations to which a particular design is well suited.

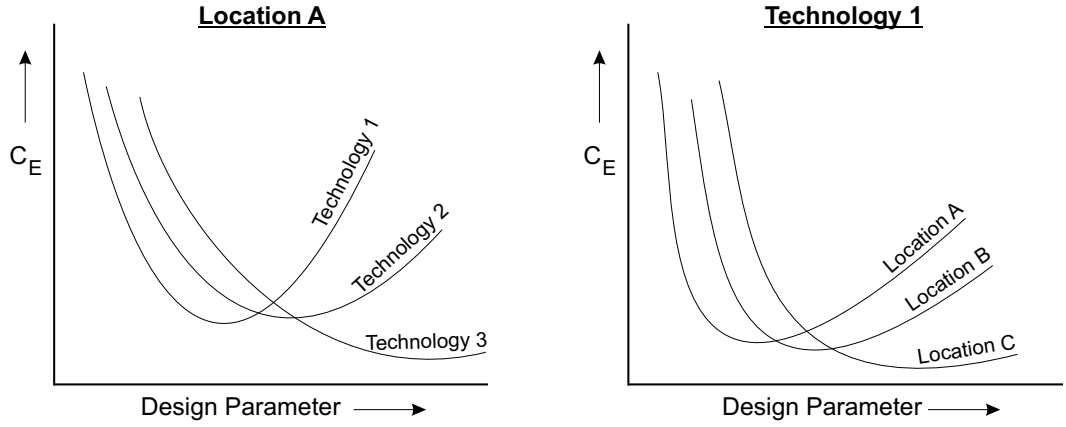

Figure 3.10: Sketch of relationships between technology, location and cost.

Identifying economically optimal farm designs may be reduced therefore to the problem of calculating I,M and E as a function of design parameters, location/climate parameters and economic parameters. The primary interest in this study is to examine the tradeoffs between support structure cost and energy production, for large bottom mounted offshore farms subjected to Northern European wind/wave climates. To achieve this objective, direct calculation of the support structure contribution to the investment cost forms the bulk of the work. The complexity of the structure, and the many factors that can influence its design mean that only a 'bottom-up' modelling approach is realistic, attempting to 'size' and then cost each component.

If economically optimal configurations are to be found, the support structure cannot be treated in isolation. Many of the support structure parameters also influence the energy production and the cost of other wind farm components. Most of this chapter therefore develops an overall framework for an offshore wind farm cost model, describing how the other investment cost, ongoing costs and the energy production can be evaluated in order to calculate a levelised production cost. Interactions between the support structure and other farm systems are identified,

and a methodology to account for them is formulated.

The final sections of the chapter discuss approaches to modelling the support structure cost based on overall structural parameters, turbine characteristics, location parameters (particularly wind and wave climates) and external economic parameters. Chapters 4 and 5 continue by developing these ideas into a detailed support structure cost model.

3.4 Cost model framework

To evaluate the cost of a energy for an offshore farm the cost model must calculate the major economic parameters E, I and M based on a set of input information describing the location and the overall farm specification. Discrete modules deal with each of the three parameters. As the preceding discussion demonstrated, the only practical means to treat the investment cost is through a component-by-component approach, wherein the farm components are effectively designed and then costed by the model. The investment cost calculation is further divided into a number of sub-modules that deal with specific farm components therefore. In order to make the separate calculations consistent, there are interdependencies between the cost model modules. Figure 3.11 shows the main information flows that the model must accommodate, and forms the basis for the structure of the numerical model. For clarity important interactions within the support structure itself have been omitted and will be discussed separately in section 3.8.

Shaded boxes in the diagram represent the major parameters that must be specified as model inputs, referred to here as 'external' parameters. Non-shaded boxes represent values that are calculated by the model termed 'internal' parameters. The quantity of information 'contained' within each box varies widely. For example, the "average annual energy delivered" is a single value, whereas the "support structure design" represents a large collection of data required to fully define the structure.

Many of the terms in the diagram are intentionally vague as there is some arbitrariness in the information required to describe each component, and also in the choice of internal and external parameters. The following sections identify the internal and external parameters in detail and outline the calculation approached used by the cost model modules.

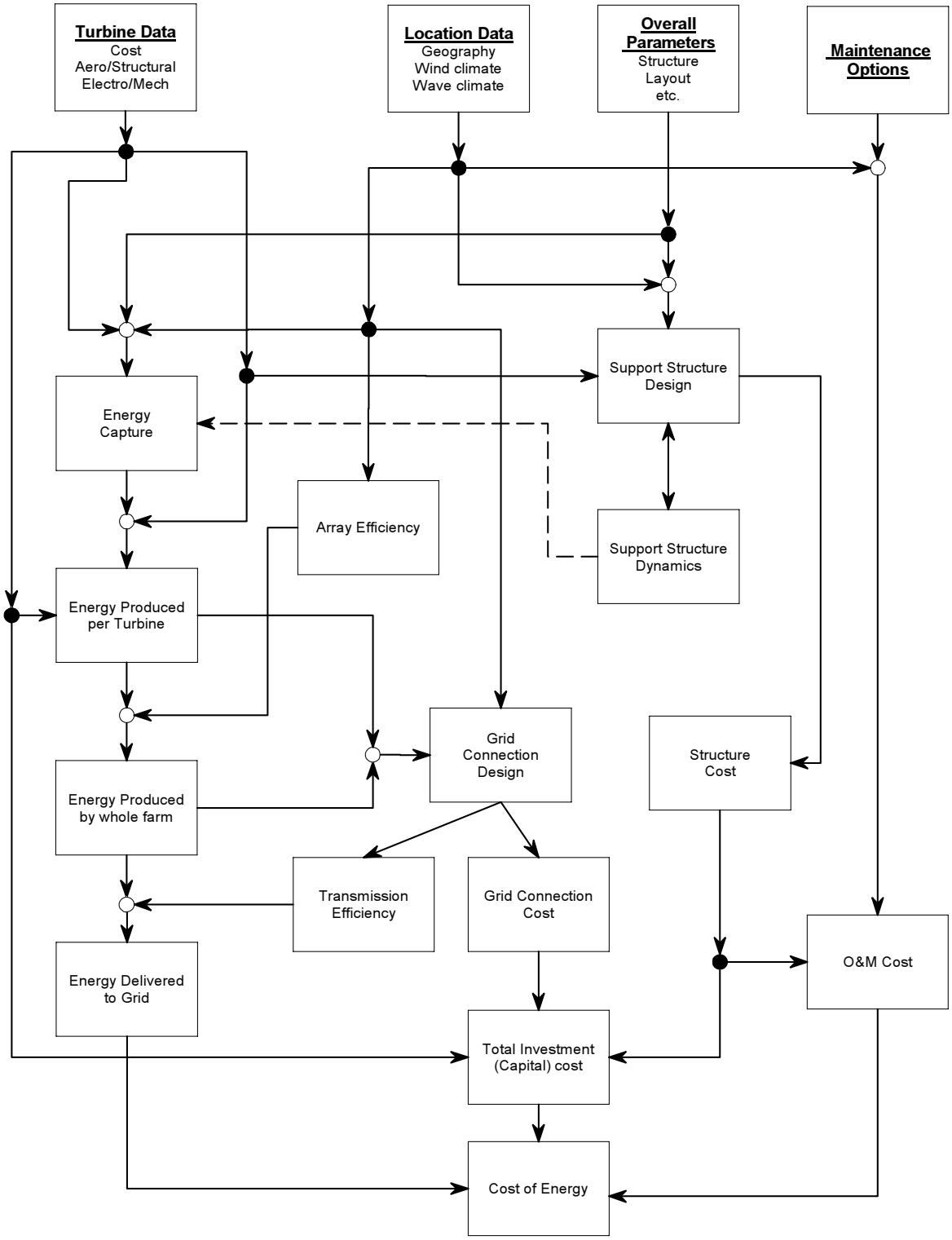

Figure 3.11: Information flows in offshore farm design.

3.5 Investment cost calculation

The model framework assumes three components for the investment cost. Costs associated with site assessment and installation are largely dependent on the support structure and are dealt with in the following chapters where the approach to support structure modelling is also discussed. Approaches used to determine the other two capital costs, specifically the cost of the turbine and the cost of the grid connection are described here.

3.5.1 Turbine selection and cost

To limit the scope of the work, the cost model does not attempt to estimate turbine parameters directly. As the preceeding analysis has demonstrated, influences on turbine costs could easily be deal with using parametric techniques and there is no value in pursuing them further here. Instead, a set of turbine data including the capital cost must be supplied to the model. The data set necessary is rather complex.

To further constrain the scope, the model is provided with complete data sets for only two contrasting turbines with the main features compared in table 3.1 and complete details in appendix B. All the calculations in this thesis have been performed using one of these two data sets. The methodology presented and the computer code implemented for the structural cost model are perfectly general however, and it would be relatively straightforward to extend the model to other turbines.

Concept represented	Generic 1.5 MW turbine	4 MW offshore specific turbine
Based on	Micon 1.5 MW production turbine.	Kvaerner-Turbin WTS-80 4 MW prototype/concept.
Rated power (MW)	1.5	4
No. of blades	3	2
Rotor diameter (m)	64	80
Mass (inc blades) (te)	75	141
Rotation speed (rpm)	20	20
Control system	Full span pitch	Full span pitch
Unit cost (2002 Euro)	1,000,000	2,550,000

Table 3.1: Summary details of the two turbines considered in the study.

3.5.2 Grid connection cost

The grid connection is designed and costed using a simplified version of a 'bottom-up' model originally developed for the Opti-OWECS study [132]. It is influenced by the annual energy production, and geographical features including the distance to shore. Appendix D provides a more complete description of the modelling approach.

3.5.3 Other costs

Figure 3.2 shows an 'other' component to farm investment costs. Except for Horns Rev, these comprise management costs and minor capital items, and are difficult to evaluate explicitly. Clearly such 'other costs' will be related to the size of the farm and thus it makes sense to look for correlations based on the proportion of the investment cost. However, the other costs (excluding Horns Rev) do not show a good correlation with any of the specific component costs, expressed as a proportion of the total investment cost. Figure 3.12 relates the other costs to the support structure costs by way of illustration.

Taken across all the projects shown, again excluding Horns Rev, the average other cost, as a proportion of the total investment cost, is 13%. Other costs within the cost model are estimated on this basis.

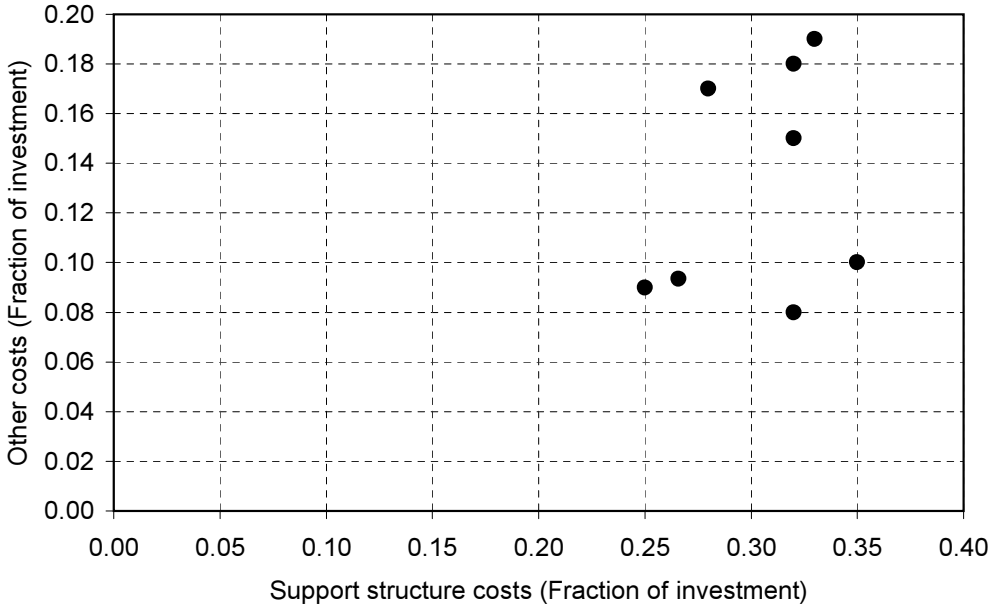

Figure 3.12: Correlation between support structure and other costs.

3.6 Energy production calculation

At any instant the energy captured by each turbine depends on the aero-elastic properties of the blades and the incident wind. The control system also plays an important role. To calculate the annual energy production for each wind turbine, the control system parameters and blade aerodynamic properties are used to generate a Cp-λ curve for the turbine. The instantaneous electrical output of the turbine is then given by

$$P_e = \left(\frac{1}{2}\rho_{air}\, v^3 A_{swept}\, C_p\right) \eta_{gb}\eta_{gen} \tag{3.3}$$

where η_{gb} and $\eta_{gen}$are the efficiencies of the gearbox and generator respectively and are functions of the power input to them. This is then integrated over time to give the annual energy production for a single turbine $E_{a,turb}$, that is:

$$E_{a,turb} = 8766 \int_{v_{cut-in}}^{v_{cut-out}} P_e(v) f(v) dv \tag{3.4}$$

where $f(v)$ is the probability that the wind has speed v at any instant and is derived from the description of the wind climate at the location. In this expression $E_{a,turb}$ has units of kWh if the instantaneous energy production is measured in kW.

There are two main interactions between the support structure and the energy production. Firstly the hub height influences the incident wind speed. This is accommodated by scaling the wind speed distribution so that the mean follows the Prandtl law (equation 2.8) with the surface roughness estimated according to the Charnock relation (equation 2.9) using a constant specified in the model input. Secondly, the motion of the turbine on top of the tower potentially has an impact on energy production, however this is widely considered to be relatively small and is not included in the cost model.

The model assumes that each turbine in the farm performs identically at all times. Losses due to wake interactions are accounted for using an array efficiency η_{array}. The efficiency is estimated from the turbine diameter and spacing using a simple model [185]. Transmission losses are ignored in the work presented here, such that the transmission efficiency η_{trans} is taken to be unity.

Unexpected failures of the turbines, together with planned maintenance outages will mean that turbines are not always available to generate power when wind conditions are suitable. This will further reduce the annual output and is incorporated using an availability factor $\eta_{farm,avail}$ which must be calculated by

the operation and maintenance model, and will typically be a function of the local climate, the distance from the shore and the O&M spend. With a number $N_{turbines}$ turbines in the farm, the total energy delivered to the shore is given by

$$E_{a,delivered} = N_{turbines} \times \eta_{farm,avail} \times \eta_{array} \times \eta_{trans} \times E_{a,turb}. \quad (3.5)$$

3.7 On-going costs

Despite their relative importance, there are no widely accepted means of estimating on-going costs. Successful approaches to date have relied on statistical analysis of historic wind farm failures combined with Monte-Carlo climate simulations and information on the cost of corrective actions. In principle fundamental approaches based on knowledge of the properties of particular wind farm components may be possible. However developing such an approach is a substantial undertaking, and on-going costs are not considered in detail here.

On-going costs are estimated using a published analytic relationship derived by a curve fit to data generated by a stochastic model written at the University of Delft [132]. The on-going costs are a function of the distance to the shore, the number and size of turbines employed, and a parameter representing the maintenance strategy employed. The methodology also provides corresponding turbine availability for use in the energy production calculation.

In practice, the maintenance cost and availability must depend on the local climate, as this affects access to the machines [163]. To provide such as simple relation, some assumptions must be made regarding the variation of weather conditions with distance from the shore. Consequently, the relation employed is only valid for Northern European waters. Appendix E, which contains a full description of the on-going costs model discusses these issues in more detail.

3.8 Support structure components

3.8.1 Concept

The support structure consists of the tower and the foundation, which are separate but interdependent components. Loads exerted by the turbine, environmental loads exerted directly, and the farm specification drive design of both components.

Two of the three major externally specified parameters are the tower and foundation design concepts. For the former, the model only considers mono-tower

type designs of the type shown in figure 3.13. Two types of foundation are examined, specifically a single pile and a gravity base, also illustrated in the figure. While real offshore turbine foundations are generally more complex, they combine elements of the contrasting fundamental approaches these two concepts represent. Modelling these two relatively easy to analyse concepts will provide insight into the general applicability of gravity and fixed foundation elements for offshore wind turbine use.

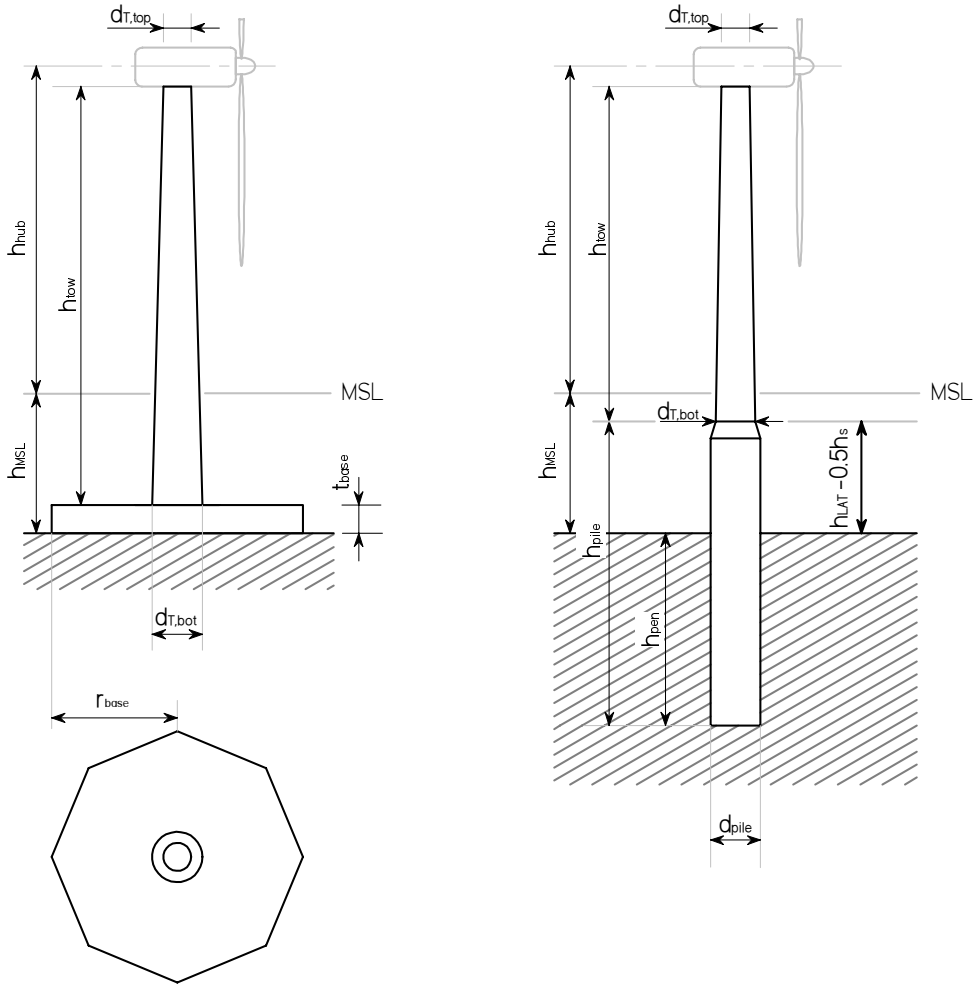

Figure 3.13: Support structure configurations considered.

The final major externally specified parameter is the turbine hub-height. In principle the model could determine the hub-height internally, as for any circumstance there will be a value that provides least cost energy. This would be a time consuming calculation, requiring repeated evaluation of many slightly different support structures. Moreover, the hub height is an important parameter in the design and evaluation of almost all the mechanical components of an offshore farm,

influencing the details of the wind climate experienced by the turbine and hence the energy produced and loads generated, and the practicality of the installation method to name a few. The form of the relationship between the hub-height and the energy-cost cannot be anticipated for all circumstances therefore. This in turn makes devising an automated optimisation algorithm difficult. As a result, the hub-height is treated here as an external parameter, and the optimum value must be determined 'by-hand'.

3.8.2 Interactions and modelling approach

Figure 3.14 illustrates the major design interactions between the two support structure components and the other components of an offshore farm, essentially expanding the dotted box of figure 3.11. It must be emphasised here that the diagram is *not* a flow chart for a design procedure. Instead the arrows represent physical interactions between properties of components, with solid lines denoting strong interactions that a model must account for and dotted lines standing for weaker interactions that designers often ignore. Alternatively the diagram may be thought of as representing the information flows that a design process, and by implication the cost model, must account for.

The 'information flow' diagram for the entire wind farm has a direct "top-to-bottom" form, wherein data mostly flows from earlier stages of design to later stages. In contrast figure 3.14 contains many feedback loops where properties of components considered later in the design have an important impact on those considered earlier[1].

One important loop in the diagram connects the tower design, the tower dynamics and the loads experienced by the tower. For the purposes of the model, the design of circular cross section tower will be characterised by the vertical distributions of outer diameter and wall thickness. Both these dimensions, which can vary along the height of the tower, are evaluated on the basis of the loads experienced. All the loads experienced however are in turn dependent on the tower dimensions. The direct wind and wave loads depend on the outer diameter, and the loads from the turbine depend on the tower dynamics, which in turn are dictated by the dimensions (discussed in detail in the two chapters that follow). One practical way of dealing with this interdependence is through iteration using a design procedure such as that illustrated in the flowchart of figure 3.15.

[1] In view of the strong interactions between the components, the order in which the tower and foundation are treated in figure 3.14 is arbitrary. As shown, the diagram considers the tower before the foundation, on the basis that the loads exerted by the tower drive the foundation design. However it could be argued that the foundation dynamics directly influence the loads experienced by the tower, and thus the foundation should be treated first.

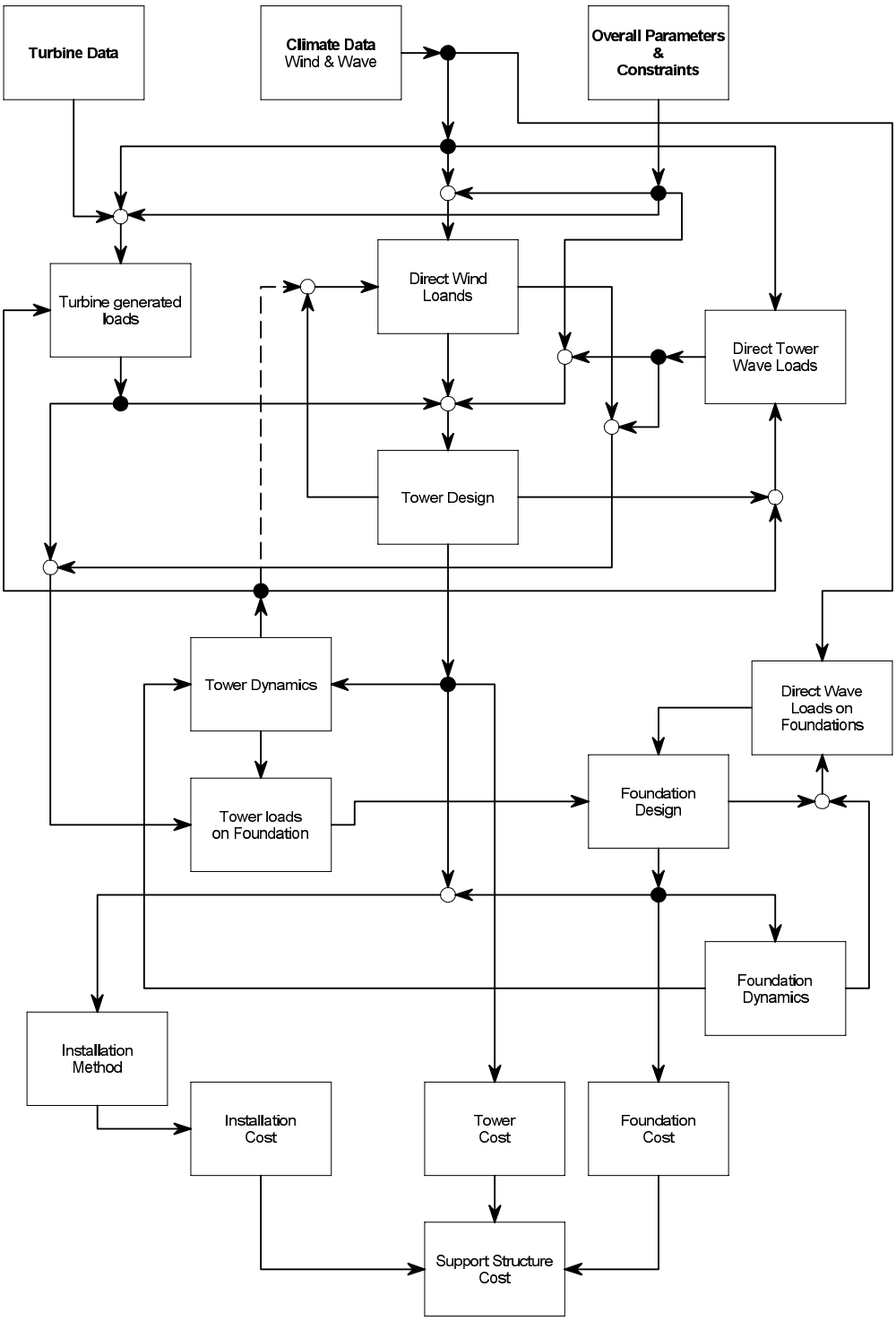

Figure 3.14: Interactions between the support structure and other offshore farm components.

Loads are initially evaluated using an assumed 'starting' tower design. The tower design parameters are then re-evaluated using the newly calculated loads. This allows a second calculation of the loads using the properties of the re-designed tower, which in turn allows a further re-evaluation of the tower parameters with the iteration continuing until subsequent changes in loads and design parameters become small.

The other important loops in the diagram centre on the foundation. As with the tower, the foundation dimensions influence both the loads exerted directly by the environment and the loads received from the tower via their impact on the overall dynamics of the support structure. The dimensions however must be determined from the calculated loads. Iteration allows a practical design procedure to be devised, in a manner similar to that proposed for the tower. For the pile concept the model characterises the foundation by the penetration depth, overall pile length, outer diameter and wall thickness. The latter two dimensions are treated as constant over the entire pile. The gravity foundation is characterised by the density of the filling material, and its horizontal and vertical dimensions.

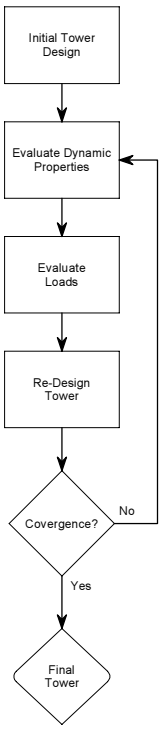

Figure 3.15: Iterative support structure design approach.

With iteration required for both foundations and tower design, the issue arises of how best to co-ordinate the design of these strongly interlinked components.

The obvious approach is to use nested iteration of the form shown in figure 3.16. With this procedure the foundation/tower combination output by the support structure routine is always consistent in that the foundation has been designed to support the loads exerted by the tower.

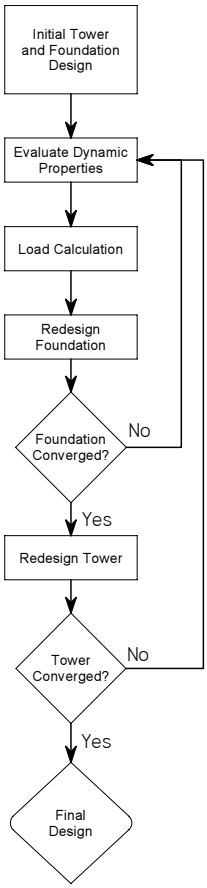

Figure 3.16: Approach to the combined iteration required for consistent tower and foundation design.

3.8.3 Structural design optimisation and resonance

For any situation defined by a set of external parameters, there is a wide range of possible structures, as characterised by the 'internal' design parameters identified above, that are capable of supporting the turbine throughout its lifetime. An alternative, but equivalent viewpoint is that the internal support structure parameters are not uniquely defined by the external support structure parameters.

Any tower section must resist a design-giving fatigue or extreme load determined from the dynamic calculations, and there will be a range of combinations

of diameter and wall thickness capable of achieving this. In general, the combination of wall thickness and diameter at each point in the tower that results in the cheapest overall structure is to be preferred. Determining these optimum values is not straightforward thanks to the feedback between the dynamics and the loads. Similarly there will generally be a range of internal parameter combinations that produce a functionally satisfactory foundation.

Many of the physically possible support structure designs will be much more costly than the optimum design. A human designer can rely on experience to select 'good', economic designs. While the human is unlikely to design a 'true' optimum tower, the outcome is certain to avoid the most expensive possibilities and will probably be a 'good-enough' approximation to the optimum.

The model must include a mechanism to identify (near)-minimum cost support structure configurations. To achieve this, the internal parameters are classified either as 'independent' parameters, which may be varied arbitrarily, or 'dependent' parameters, which are completely defined by the external parameters and the loads. By way of example, the tower outer diameter is treated as independent, while the wall thickness is then dependent.

An optimiser routine in the model varies the independent internal parameters to identify the least cost support structure configuration, using the procedure outlined by the flowchart in figure 3.17. Continuing with the tower as an example, the optimiser tries out alternative outer diameter distributions. In each case the loads are estimated, and then used to calculate a thickness distribution. The tower dynamics are re-evaluated, the loads re-calculated and the iterative procedure of figure 3.16 continued until the wall thickness and loads do not change significantly between passes. After trying a number of diameter distributions, that which provided the least cost support structure is selected as the optimum solution. Foundation parameters are optimised in a similar manner. Chapter 5 describes the developed procedures in full.

An advantage of this approach is that it can implicitly account for all forms of resonance, so long as the treatment of the interaction between the support structure dynamics and the generated loads is sufficiently detailed. If a trial support structure design were prone to resonance, then the estimated loads would be relatively high, producing a substantial, and therefore expensive structure. In practice, implementing a model of the turbine generated loads sufficiently detailed to account for resonance with the support structure is difficult without resorting to a full simulation of the turbine dynamics, which would be too demanding of computer time for practical use in the cost model. Instead the support structure optimiser checks whether there is a risk of resonance with the turbine (the prohibited zones of figure 2.10) and dismisses any such structures irrespective of their

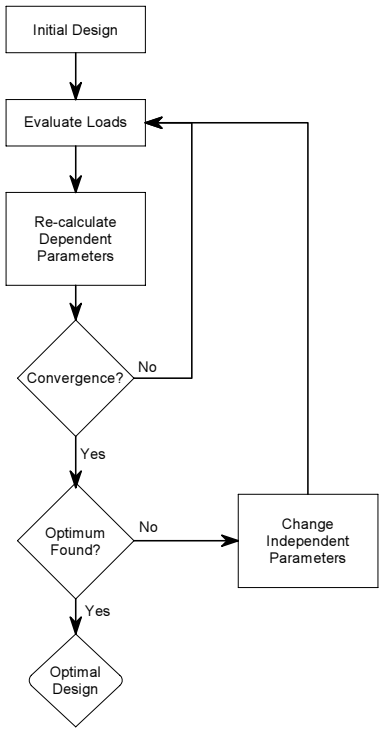

Figure 3.17: Approach to support structure design optimisation.

cost.

The optimisation procedure described will find the most economic non-resonant support structure design. To allow investigation of relationships between dynamics and cost, it is desirable that the model can be forced to design a structure in one of the three acceptable frequency ranges, soft-soft, soft-stiff, stiff-stiff. The frequency band is therefore an additional external parameter that must be supplied to the model.

Not all support structure frequency bands are achievable in every case. This is particularly true with relatively short towers where it may not be possible to design a soft structure that is capable of supporting the turbine. By way of illustration the lower surface of figure 3.18 shows the minimum achievable frequency for a steel conical tower to support a three-bladed 1.5 MW turbine with a 30 rpm rotation speed as a function of bottom radius and tower height. Calculations were performed on a static basis only using the extreme wind load exerted on the turbine, accounting for bending strength and buckling resistance only and assuming a perfectly rigid foundation[2]. Frequency is plotted as a proportion of the rotor speed, such that 'forbidden bands' lie around unity and the blade passing frequency which is 3. It is clear that a soft-soft design can never be achieved with the shortest, 50 m towers and a wide base diameter. Minimum strength taller towers are naturally softer than shorter ones. Stiff-stiff taller towers are easily achievable by either increasing the bottom radius or using thicker walls, with the upper surface showing the frequency of towers designed using double the minimum wall thickness.

3.9 Cost model overall structure

This chapter has discussed the features required of a cost model for offshore wind farms, and developed methods by which those features may be implemented. Figure 3.19 summarises the chapter by providing an overall flow chart for the operation of the model. The flowchart reflects the structure of the model as implemented in FORTRAN-90 computer code. Some practical details of the code are discussed in appendix L.

Most of the model elements have been fully described in this chapter and its associated appendices and will not be discussed further. The support structure model has been discussed only in outline and will be fully developed in the following two chapters.

[2]The simple MathCad model used for this analysis is in appendix G.

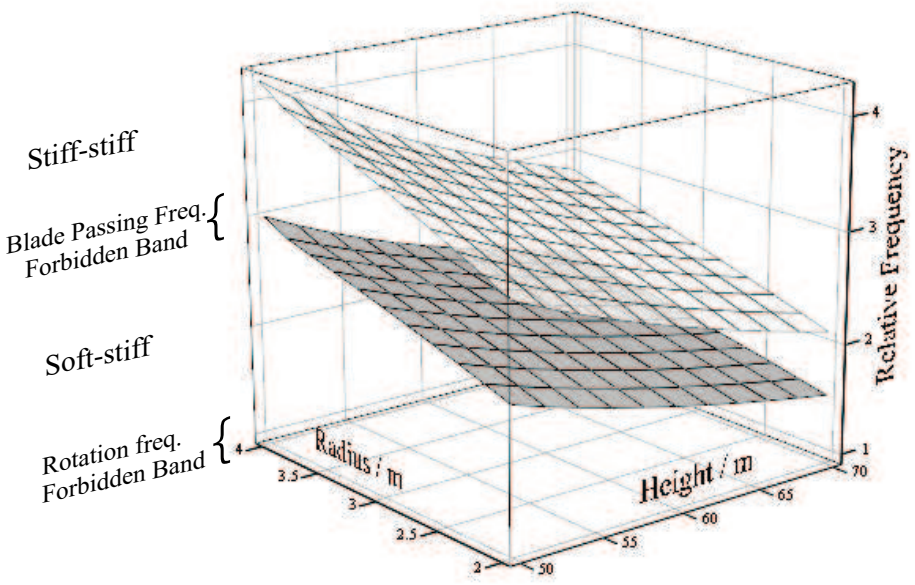

Figure 3.18: Minimum achievable frequency for rigidly fixed steel conical support towers as a function of height and bottom diameter. The lower surface shows the minimum achievable tower eigenfrequency, demonstrating the impossibility of constructing a soft-soft tower in the case modelled. The upper surface shows the eigenfrequency of a tower with double the minimum wall thickness.

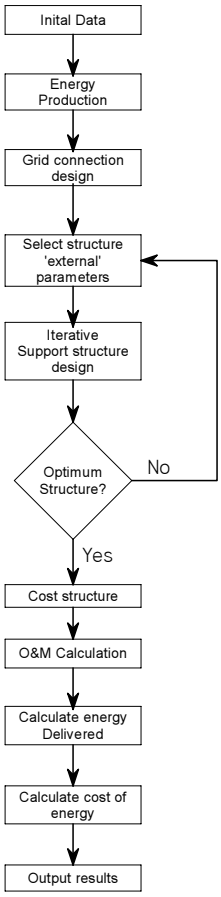

Figure 3.19: Summary of cost model operation.

Chapter 4

Modelling of environment, dynamics and loads

4.1 Introduction

This chapter discusses the loads experienced by the support structure as a result of the action of wind on both the turbine and structure, and waves on the structure alone. How the calculated loads are translated into real dimensions and costs forms the subject of the next chapter.

Discussion begins by reviewing how the offshore environment is represented in a form suitable for use in modelling work. This representation influences the techniques used to estimate the loads, which are considered next. Finally, recognizing that comprehensive environmental information is unlikely to be available for the preliminary studies the model is intended for, a simplified representation, still compatible with the modelling approach is developed.

4.2 Description of the environment

4.2.1 Climate

A complete description of the offshore climate is conventionally provided as a set of wave height, wave period and wind speed scatter diagrams, usually associated with eight direction sectors. The incident direction of the weather is less important for the design of offshore wind farms than more conventional offshore structures because of symmetry. The support structure itself is symmetrical, and the major source of asymmetry, the turbine, rotates to face the weather such that the dynamic properties of the system remain constant in the direction of the weather. To simplify the analysis, the impact of directionality is ignored therefore, and the

climate is represented by an omni-directional scatter chart.

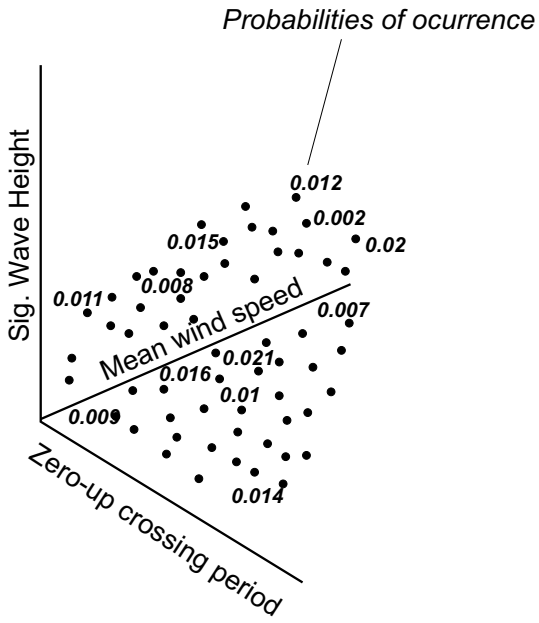

Figure 4.1: Illustration of general form of omni-direction wave scatter chart required by the cost model.

For the design evaluation, it is assumed that the weather described by the omnidirectional chart always arrives from the same direction. Thus there is no possibility for fatigue damage to be distributed around the circumference of the support structure. At locations where the climate is strongly directional this assumption will have little impact on the results. Where the incident weather does not have a prevailing direction it will produce a rather conservative design, that over-estimates support structure costs. In many of the coastal regions considered for offshore farm development there is a distinct prevailing climate direction, such that the impact on the results should be small.

The cost model is written to design structures starting primarily from an omnidirectional scatter chart for a proposed location, reduced to the general form shown in figure 4.1 relating frequency of occurrence of significant wave height, zero-up crossing period and mean wind speed combinations. As will become apparent in later sections, the design calculations also require values for the one and fifty year return period mean wind speeds and significant wave heights. These cannot reliably be estimated from a scatter chart and must be provided in addition, together with upper and lower limits on the wave periods in the sea states.

Ideally, the supplied wind speed values will have been measured at the turbine hub height. However in practice this is unlikely to be the case. Furthermore

one of the purposes of the model is to allow investigation of changes in design parameters, such as the hub height. Wind speeds at other heights are estimated therefore using the Prandtl relation with the surface roughness estimated using the Charnock relation as described in section 2.4.4. The value of the Charnock constant can be specified in the input to the cost model, but, unless noted otherwise, all the calculations here use a value of $c = 60$.

The wind induced fatigue loading is influenced by the turbulence, which is also dealt with using standard relationships. The treatment is closely coupled to the modelling of the fatigue loads and is described in section 4.6.2.

4.2.2 Seabed conditions

In principle the model can use any physically reasonable set of soil parameters, such as may be obtained from a site investigation. As discussed in chapter 2 however, only qualitative descriptions of the seabed are readily available over wide areas. To accommodate some measure of the impact of the seabed, the model itself accepts a qualitative seabed description, which is converted in to representative quantitative parameters according to table 4.1. It is assumed that there is no vertical variation in seabed composition.

Description	Saturated density kg/m^3	Cohesion kPa	Angle of friction degrees	Undrained shear strength	Data sources
Sand	2000	0	37	0	[139]
Clay	1800	27.5	25	75	[139]

Table 4.1: Assumed sea bed geotechnical properties.

4.3 Overview of support structure treatment

4.3.1 Geometry

The structure geometry as treated by the cost model is shown in figure 4.2, and represents an approximation to the concepts of figure 3.13. For the purposes of the dynamic modelling developed here, the tower is defined as the entire structure above the sea bed for the piled concept and the structure above the foundation for the gravity concept, as shown in figure 4.2. The design calculations of chapter 5 however reflect the true configuration of the piled design, with the

tower/pile interface affected by a transition piece above the mean sea level. The definitions of the major geometrical parameters of figure 3.13 are maintained.

4.3.2 Main design considerations

The support structure design may be driven by fatigue or extreme load considerations, and the design driver may change with position in the structure. For design, the fatigue and extreme loads must be evaluated at several locations in the structure, and the most demanding selected. The tower is treated as a truncated hollow cone, the diameter and wall thickness of which vary continuously throughout its height, as shown in figure 4.2.

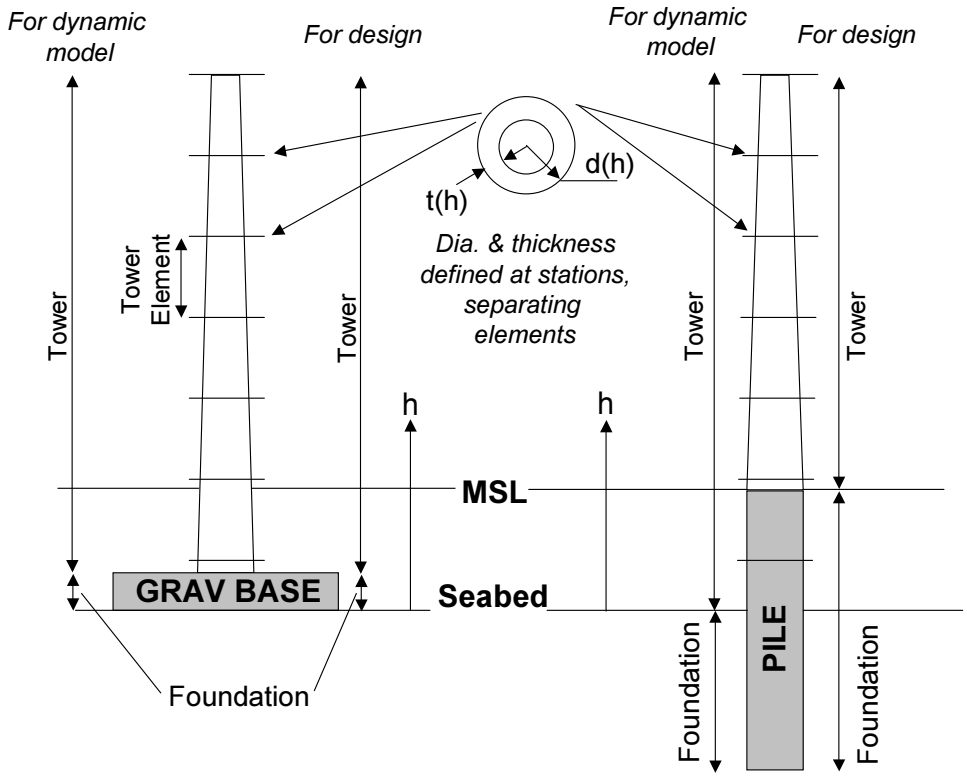

Figure 4.2: Tower as represented in the model.

4.3.3 Fatigue

Fatigue is accumulated over the lifetime of the structure predominantly from wave loads and loads from the operating turbine. Direct wind loads on the structure play only a small role in fatigue [25] and are ignored here. The approach taken is to evaluate the behaviour of the structure for each combination of wind

speed, wave height and wave period listed in the offshore climate scatter diagram, and calculate the damage accumulated over a known period during which the climate remains constant, say an hour. Total damage accumulated over the lifetime is calculated by combining the effects of each climate regime in proportion to the period of the lifetime it is expected to last, using the Palmgren-Miner rule.

4.3.4 Extreme loads

There is some uncertainty in the community [5, 25] over how best to evaluate extreme loads on offshore wind turbine structures. For modern wind turbines, peak loads may occur not in extreme conditions when the turbine is shut down, but during operation. This presents many difficulties, meaning the only way to determine the extreme loads is through a series of very detailed simulations of turbine operation. This is too complex for a 'broad-brush' study such as this. In any case the focus of the work is on offshore aspects, and it is clear that the extreme wave load will occur under extreme conditions. Hence it is assumed that the extreme structural loads do occur under extreme conditions.

4.4 Formulation of dynamic model

4.4.1 Model requirements

This section discusses the analytic formulation of the model of the structural response of the turbine. Treatment of the excitation forces is tackled in later sections.

The model is provided with a description of the support structure generated by the routines of chapter 5 which comprises the stiffness and mass per unit distance as a function of height, together with the lateral and rotational stiffness and damping provided by the foundation at the mudline. Geometric parameters such as the diameter and wall thickness are also available, but these do not directly influence the dynamics.

4.4.2 Sophistication of model

Most wind turbine dynamic models, such as those discussed in chapter 2, include a coupled treatment of the support structure and blade dynamics. This study focuses on differences in support structures and their cost arising from differing environmental conditions. Several studies [5, 25] have demonstrated that

the blade response has little impact on the wave induced tower loads, and thus a simplified treatment neglecting the blade-tower interaction would be justified.

So far as fatigue is concerned most of the differences between locations will arise from the wave climate. The wave fatigue loads, particularly in the more expensive lower parts of the structure will be little influenced by the blade response. Wind fatigue loads are significantly affected by blade and tower interactions. However, the main comparisons to be made here involve identical turbines in different locations, and thus tower-blade dynamics interactions are unlikely to differ so much between cases as to be dominating.

Thanks to these considerations, together with a desire to avoid making the cost model any more complex, the impact of the blades on the tower structural response is completely ignored in the dynamic model. Instead the entire tower-top is modelled as a point mass equal in magnitude to the sum of the masses of the nacelle components and the blades, located at the nacelle centre of mass. As shown in figure 4.3, the tower top mass is considered to be rigidly connected to the top of the tower.

The tower, and protruding part of the pile where applicable, is treated as being composed as a series of sections, with the second moment of area I and the mass per unit length m varying with height. Forces generated by the turbine are assumed to act directly on the point tower top mass, while wave loads are distributed over submerged sections of the structure. Both types of foundation are modelled in the same simplified manner, with the dynamics represented as lateral and rotational spring-damper systems linking the tower to the rigid seabed.

4.4.3 Fundamental analysis

Analytic approaches are used to formulate a model of the dynamics of the simplified structure of figure 4.3. As the analysis largely follows standard practice in structural dynamics, only the major points are described here together with specialisation to the specifics of the problem.

A generalised multiple degree of freedom equation of motion for a structure may be written as [89]

$$\mathbf{f_I} + \mathbf{f_D} + \mathbf{f_S} = \mathbf{p}\,(t) \tag{4.1}$$

where

$\mathbf{f_I}$	Inertia force vector
$\mathbf{f_D}$	Damping force vector
$\mathbf{f_S}$	Elastic force vector
$\mathbf{p}\,(t)$	Time varying applied force vector.

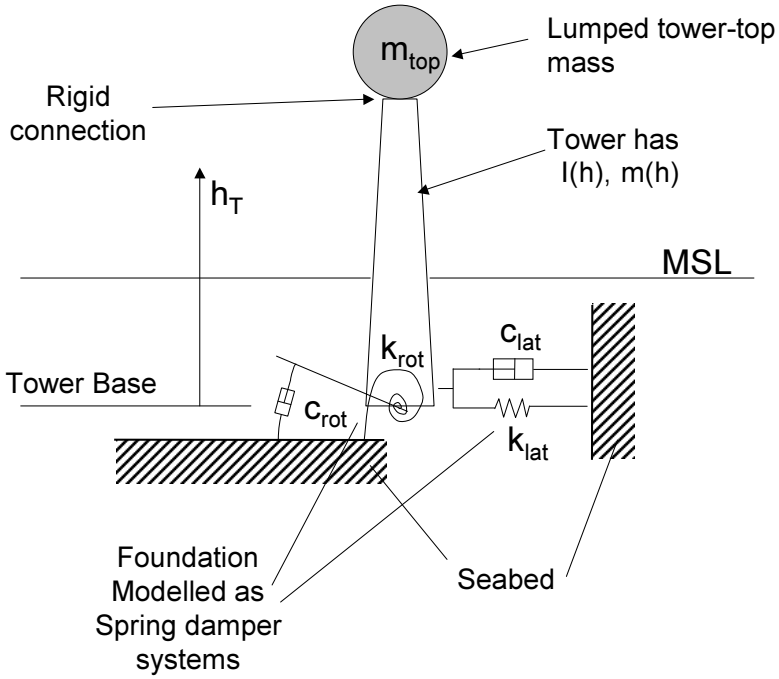

Figure 4.3: Simplified dynamic model of support structure.

Each vector comprises the forces evaluated at a set of N discrete nodes distributed over the structure. The lateral displacement of the i^{th} node is represented by q_{2i}, and the rotational displacement by q_{2i+1}.

To derive a specialised equation for the offshore support structure, the modelled sections are first divided into a large number of equal height elements, as shown in figure 4.3. It is assumed that the properties of the structure remain constant across each element, adopting the value they have at the midpoint of the element. The only exception to this is the element at the very top of the tower, which is extended to the centre of mass of the nacelle. The precise number of elements is not crucial and can be specified in the cost model input file. For good results however, there must be sufficient elements that the properties of the real tower do not change greatly across each, and all the analyses in this work use twenty.

Following the finite element approach of appendix H a stiffness matrix is formulated for each element that relates the elastic forces and moments at each end of the element to the corresponding rotational and lateral deflections. For the element of the support structure bounded by nodes at i and $i + 1$, the relation has

the form

$$f_{S,i} = \begin{bmatrix} k_{i,11} & k_{i,12} & k_{i,13} & k_{i,14} \\ k_{i,21} & k_{i,22} & k_{i,23} & k_{i,24} \\ k_{i,31} & k_{i,32} & k_{i,33} & k_{i,34} \\ k_{i,41} & k_{i,42} & k_{i,43} & k_{i,44} \end{bmatrix} \cdot \begin{bmatrix} q_{2i} \\ q_{2i+1} \\ q_{2(i+1)} \\ q_{2(i+1)+1} \end{bmatrix} \tag{4.2}$$

where the stiffness coefficients $k_{i,xx}$ depend on the length, Young's modulus and second moment of area of each element, adopting the values shown in the appendix.

A similar analysis produces values for the inertial forces at each node. Taking the i^{th} element yields

$$f_{I,i} = \begin{bmatrix} m_{i,11} & m_{i,12} & m_{i,13} & m_{i,14} \\ m_{i,21} & m_{i,22} & m_{i,23} & m_{i,24} \\ m_{i,31} & m_{i,32} & m_{i,33} & m_{i,34} \\ m_{i,41} & m_{i,42} & m_{i,43} & m_{i,44} \end{bmatrix} \cdot \begin{bmatrix} \ddot{q}_{2i} \\ \ddot{q}_{2i+1} \\ \ddot{q}_{2(i+1)} \\ \ddot{q}_{2(i+1)+1} \end{bmatrix} \tag{4.3}$$

with the mass coefficients being functions of the element mass and length. Damping is not considered explicitly at this stage, but it will be noted that the damping force vector could be written in a manner analogous to the inertial and elastic forces, that is

$$f_{D,i} = \begin{bmatrix} c_{i,11} & c_{i,12} & c_{i,13} & c_{i,14} \\ c_{i,21} & c_{i,22} & c_{i,23} & c_{i,24} \\ c_{i,31} & c_{i,32} & c_{i,33} & c_{i,34} \\ c_{i,41} & c_{i,42} & c_{i,43} & c_{i,44} \end{bmatrix} \cdot \begin{bmatrix} \dot{q}_{2i} \\ \dot{q}_{2i+1} \\ \dot{q}_{2(i+1)} \\ \dot{q}_{2(i+1)+1} \end{bmatrix} \tag{4.4}$$

The general equation of motion for the structure 4.1 can then be written as

$$\mathbf{M}\ddot{\mathbf{q}} + \mathbf{C}\dot{\mathbf{q}} + \mathbf{K}\mathbf{q} = \mathbf{p}\,(t) \tag{4.5}$$

where the mass matrix M has the form

$$\mathbf{M} = \begin{bmatrix} m_{1,11} & m_{1,12} & m_{1,13} & m_{1,14} & 0 & 0 & \dots \\ m_{1,21} & m_{1,22} & m_{1,23} & m_{1,24} & 0 & 0 & \dots \\ m_{1,31} & m_{1,32} & m_{1,33} + m_{2,11} & m_{1,34} + m_{2,12} & 0 & 0 & \dots \\ m_{1,41} & m_{1,42} & m_{1,43} + m_{2,21} & m_{1,44} + m_{2,22} & 0 & 0 & \dots \\ 0 & 0 & m_{2,31} & m_{2,32} & m_{2,33} + m_{3,11} & m_{2,34} + m_{3,12} & \dots \\ 0 & 0 & m_{2,41} & m_{2,42} & m_{2,43} + m_{3,21} & m_{2,44} + m_{3,22} & \dots \\ 0 & 0 & 0 & 0 & m_{3,31} & m_{3,32} & \dots \\ \vdots & \vdots & \vdots & \vdots & \vdots & \vdots & \ddots \end{bmatrix} \tag{4.6}$$

with the damping matrix $\mathbf{C}$ and stiffness matrix $\mathbf{K}$ constructed in a similar manner.

4.4.4 Boundary conditions

The foundation stiffness and damping, as shown in figure 4.3 are included directly in the modelling process, with the zeroeth node representing the ground. Only two boundary conditions apply therefore, specifically that the zeroeth node has zero lateral and rotational displacement, or

$$q_0 = 0 \tag{4.7}$$

and

$$q_1 = 0. \tag{4.8}$$

In the solution procedure, the deflection at each point in the structure is calculated as a linear combination of modal shapes (section 4.4.5). The boundary conditions are enforced therefore by ensuring that the modal shapes used in the solution method have zero deflection at the ground node. Appendix H describes in more detail how this is achieved.

4.4.5 Modal decomposition

The deflection profile of the structure at any time can be written as a linear combination of the structure's eigenvectors, that is the deflection at node i is

$$q_i = y_1\phi_{1,i} + y_2\phi_{2,i} + \dots \tag{4.9}$$

where $\phi_{j,i}$ is the normalised deflection of node i in eigenvector j and y_1, y_2, y_j are the modal co-ordinates. This may be written in matrix format for all the nodes of the structure

$$\mathbf{q} = \mathbf{\Phi Y} \tag{4.10}$$

with $\mathbf{\Phi}$ representing a matrix of the normalised eigenvectors and $\mathbf{Y}$ a column vector of the nodal co-ordinates.

Substituting expression 4.10 into 4.5, allows the equation of motion to be approximately decomposed into a series of decoupled equations each representing the motion of a single mode of the structure, and having the form

$$m_{ii}\ddot{y}_i + c_{ii}\dot{y}_i + k_{ii}y = p_i\left(t\right). \tag{4.11}$$

Each term in the decoupled equation is related to the coefficients of equation 4.5

according to

$$m_{ii} = \mathbf{\Phi}_i^T \mathbf{M} \mathbf{\Phi} \tag{4.12}$$

$$k_{ii} = \mathbf{\Phi}_i^T \mathbf{K} \mathbf{\Phi} \tag{4.13}$$

$$c_{ii} = \mathbf{\Phi}_i^T \mathbf{C} \mathbf{\Phi} \tag{4.14}$$

and

$$p_i(t) = \mathbf{\Phi}_i^T \mathbf{p}(t) \tag{4.15}$$

with $\mathbf{\Phi}_i$ being the normalised vector representing the i^{th} eigenmode of the structure.

As noted in the literature [135], the analysis does not strictly separate the modes as some coupling remains via the damping co-efficients. However formulating an accurate damping matrix $\mathbf{C}$ is difficult due to uncertainties in the physical processes involved. The error caused by neglecting the damping coupling is small compared to that due to the uncertainty in the damping matrix itself. It is therefore common practice to assume that the modes can be modelled independently using a series of equations of the form of expression 4.11. The decomposition analysis is used only to identify the mass and stiffness coefficients for the modal equations, with damping coefficients calculated using a pragmatic approach described in a later section.

4.4.6 Applied forces

External forces are applied to the structure at the very top node (representing the thrust load from the wind turbine) and over a number of nodes in the wet area (representing wave loads). The forcing vector $\mathbf{p}(t)$ therefore is of the form

$$\mathbf{p}(t) = \begin{bmatrix} p_N(t) \\ 0 \\ 0 \\ 0 \\ \vdots \\ p_m \\ \vdots \\ p_3(t) \\ p_2(t) \\ p_1(t) \\ 0 \end{bmatrix} \tag{4.16}$$

where p_j represents the force at node j and p_m is the force at the highest node that encounters water.

Following modal decomposition the forcing term for each mode is given by equation 4.15. Expanding this shows that the forcing term for mode i is equal to the sum of the forces applied at each node, multiplied by the normalised modal deflection at that node, that is

$$p_i(t) = \phi_{i,N} p_N + \phi_{i,m} p_m + \ldots + \phi_{i,3} p_3 + \phi_{i,2} p_2 + \phi_{i,1} p_1. \tag{4.17}$$

4.4.7 Implementation

The cost model automatically calculates the mass and stiffness matrices of equation 4.5 for the modelled structure. A specially written finite element routine (Appendix H) is used to calculate the eigenmodes of the structure, which are expressed as normalised vectors of the relative deflection at each finite element. Using these values, mass and stiffness coefficients are calculated for the first modes of the structural response. In principle, the model can deal with muliple modes. However the extra precision of using multiple modes in the cost model calculations is not warranted in view of the many uncertainties in the input data. Thus all the calculations reported here use only the first mode.

Damping factors are defined for each mode as a fraction ξ_c of critical damping. For all modes above the first, only structural damping, arising from the internal friction of the tower material and joints is accounted for. A range of values are employed in the literature, with 0.8% as suggested by Burton et al. [186] adopted here. For the first mode, damping from both structural and aerodynamic sources is included. Aerodynamic damping is estimated as described in appendix B, with the values used in table 4.2.

Turbine	Aerodynamic damping
1.5 MW	1.31 % critical
4 MW	1.02 % critical

Table 4.2: Value of aerodynamic damping of first mode of structure.

Details of treatment of the loads differ between the extreme and fatigue calculations described in the following sections. In general terms wave theory and the Morison equation are used to calculate loads at each of the wet nodes. For the fatigue calculation, tower top forces are estimated using a simple model of the response of the wind turbine to turbulence. The full set of loads are combined using equation 4.17 and the resultants used to drive the modal tower response.

4.5 Wave theory and treatment of wave loads

4.5.1 Theoretical approach

Wave loads on the structure are calculated using the Morison equation [136], with the elemental horizontal force on a vertical element of length dz with circular cross section of diameter d_T in a flow of speed u given by

$$dF_x = \frac{1}{2}\rho_w C_d d_T \mid u \mid u dz + C_m \rho_w \frac{\pi {d_T}^2}{4}\frac{du}{dt}dz \tag{4.18}$$

Non-dimensional force coefficients are chosen in accordance with published data [137] as shown in table 4.3.

Drag coefficient	C_d	1.25
Inertia coefficient	C_m	2.0

Table 4.3: Force coefficients used in the Morison equation.

Estimation of the wave forces requires a description of the wave kinematics. Airy's linear wave theory [187] is used here. It should be noted that it assumes wave amplitudes are low and thus provides a poor description for some of the extreme waves encountered by wind farms in shallow water. However the complexity of more accurate descriptions make the use of linear wave theory common in outline studies of the type undertaken here.

The only interest here is the behaviour of the horizontal velocity and acceleration of water particles as a wave passes. According to linear theory, for a wave of time period T and height H, the horizontal velocity u and corresponding acceleration at time t are given by

$$\begin{aligned} u &= \frac{\pi H}{T}\frac{cosh\left(\frac{2\pi}{L}(z+d)\right)}{sinh\left(\frac{2\pi}{L}d\right)}cos\left(-2\pi\frac{t}{T}\right) \\ \frac{du}{dt} &= \frac{2\pi^2 H}{T^2}\frac{cosh\left(\frac{2\pi}{L}(z+d)\right)}{sinh\left(\frac{2\pi}{L}d\right)}sin\left(-2\pi\frac{t}{T}\right) \end{aligned} \tag{4.19}$$

where L is the wave length, d the water depth and z the distance below the surface.

4.5.2 Extreme loading

Extreme wave loads on the structure are determined through a time-domain calculation of the effects of a passing deterministic wave at the extreme wave height.

The cost model time-steps through the kinematics of the passing wave as given by equations 4.19. At each step, the Morison equation is used to calculate the corresponding force distribution up the height of the submerged part of the support structure. Thanks to the limitations of linear wave theory, the calculation only proceeds to the mean water level rather than the true height of the crest above the sea bed.

With the force distribution $f(h)$ known, the bending moment m_e on each tower element at height h_e above the tower base is calculated by integrating the force distribution up to the mean sea level

$$m_e = \int_{h_e}^{h_{msl}} (h - h_e) f(h) dh. \tag{4.20}$$

The wave overturning moment at the sea bed is determined in a similar manner. Calculations are repeated for each time step, with the maximum moment at each tower section and the tower base over the course of a wave cycle recorded.

4.5.3 Fatigue loading

Fatigue analysis within the cost model is based on spectral calculations. The sea state is described by a surface elevation spectrum $S_{\eta\eta}(f)$, the form of which is discussed in section 4.6. For application in dynamic calculations, a wave force power spectrum $S_{ff}(f)$ for each node on the support structure model must be generated from the surface elevation spectrum.

A linearised version of the Morison equation is used to calculate loads. This first requires that velocity and acceleration spectra are generated from the elevation spectrum, and for this linear wave theory is again employed. At each structure node below the mean water level, the wave length L associated with a range of wave frequencies f is calculated by an iterative solution of the linear wave theory result

$$L = \frac{g}{2\pi f^2} tanh\left(\frac{2\pi d}{L}\right). \tag{4.21}$$

The maximum velocity associated with a unit height wave of each wavelength is then calculated from equations 4.19, that is

$$u_{max} = \frac{\pi}{T} \frac{cosh\left(\frac{2\pi}{L}(z+d)\right)}{sinh\left(\frac{2\pi}{L}d\right)} \tag{4.22}$$

$$\left(\frac{du}{dt}\right)_{max} = \frac{2\pi^2}{T^2} \frac{cosh\left(\frac{2\pi}{L}(z+d)\right)}{sinh\left(\frac{2\pi}{L}d\right)}. \tag{4.23}$$

Repeating the calculation across the range of wave frequencies encountered pro-

duces a numerical representation of the transfer functions for velocity $H_u(f)$ and acceleration $H_a(f)$ such that the velocity spectrum is given by

$$S_{uu}(f) = [H_u(f)]^2 S_{\eta\eta}(f) \tag{4.24}$$

and the acceleration spectrum by

$$S_{aa}(f) = [H_a(f)]^2 S_{\eta\eta}(f). \tag{4.25}$$

The Morison equation is linearised according to the procedure of Borgman [188] to produce a transfer function from velocity and acceleration to member forces. If equation 4.18 is written as

$$dF_x = f_D dz + f_I dz \tag{4.26}$$

the inertial force can be calculated in the normal manner

$$f_I = C_m \frac{\pi d_t^2}{4} \frac{du}{dt}. \tag{4.27}$$

The drag force f_D with the non-linear $\mid u \mid u$ term is more problematic. Borgman suggests a linearisation of

$$f_d = \frac{1}{2} \rho_w C_d d_t k_d u \tag{4.28}$$

where

$$k_d^2 = \frac{8}{\pi} \int_0^\infty S_{uu}(f)\, df. \tag{4.29}$$

The linearisation allows a force spectrum $S_{ff}(f)$ to be calculated from velocity and acceleration spectra at each submerged node of the support structure.

4.6 Details of fatigue load calculations

4.6.1 Approach

Kuhn [189] and others [14] have shown that it is not adequate to treat wind and wave effects separately in the evaluation of fatigue in offshore wind turbine structures. To do so results in over designed structures as the wind and wave loads interact in such a way that the structural fatigue life is not used linearly. An integrated treatment is necessary for evaluation of the fatigue lifetime, but as already noted this has the potential to be computationally expensive if undertaken in the time domain. For this reason, a spectral approach is employed. This introduces an additional complication in that spectra for the turbine generated tower top

loads are required. A method taken from the literature is employed to estimate these that relies on an assumption that the tower top loads arise exclusively from the 'sampling' of wind turbulence by the rotating blades.

To calculate the fatigue damage over the lifetime of the support structure, stress spectra for each node are required for each combination of environmental parameters specified in the climate scatter chart provided to the cost model. In principle account should also be taken of the operational status of the turbine at each of the climate combinations including the effects of start-up and shut-down, together with treatment of cases where the turbine is shutdown. Detailed inclusion of these effects considerably complicates the calculation and is not warranted for a generalised study of the type described here. The following simplified approach was applied:

- If the wind speed is between the start-up and shut-down speed for the turbine, it is assumed that the turbine always operated normally.
- If the wind speed is above the shut-down speed, it is assumed that the turbine is shutdown. To ease the analysis the contribution of any tower top loads to the support structure fatigue is assumed to be the same as that of the turbine at the shutdown speed.
- If the wind speed is below the start-up speed, it is assumed that there are no tower top loads and the structure is only subject to wave fatigue.

The stress spectra can be calculated from nodal deflection spectra, as described in section 4.6.4. Nodal deflection spectra in turn can be computed by solving the structural dynamics in the frequency domain using the methodology discussed in section 4.6.3. For each state in the sea-state wind speed scatter diagram therefore, force spectra for each underwater node and the turbine must be formulated. Direct wind loading on the tower is ignored for the fatigue calculations.

4.6.2 Tower top fatigue loads

A simple model for tower top fatigue loads is used drawing on the work of Tarp-Johansen and Frandsen [190] and Madsen and Frandsen [191]. It is assumed that the rotor is stiff, and the sole source of fatigue loads is the sampling effect of the rotor on passing wind turbulence. It is also assumed that turbulent fluctuations may be modelled as a Gaussian process.

Neglecting tower top motion, the thrust force generated by the rotor may be divided into a mean and turbulent component. The power spectrum of the fluctuating thrust component may be written approximately as

$$S_\omega(f) = \nu_{rot}^2 F_{rot}(\omega) S_u(\omega) \tag{4.30}$$

in which $S_u(\omega)$ is the spectrum of the longitudinal turbulent wind component at hub height and $F_{rot}(\omega)$ is an admittance function representing the filtering of wind turbulence by the rotor. This function may be approximated by

$$F_{rot}(\omega) = \frac{1}{\left(1 + \frac{\gamma R \omega}{u_{10,h}}\right)^2} \tag{4.31}$$

with R being the rotor radius, $u_{10,h}$ the 10 minute average wind speed at hub height, and γ related to the force distribution over the submerged pile as described by Tarp-Johansen and Frandsen [190].

The aerodynamic damping coefficient ν_{rot} is given by

$$\nu_{rot} = \rho_a C_t u_{10,h} A \tag{4.32}$$

where C_t is the rotor thrust coefficient. In general the thrust coefficient will be a function of the windspeed, and Tarp and Frandsen suggest that a representative relationship is

$$C_t = \frac{5}{u_{10,h}}. \tag{4.33}$$

Tarp-Johansen and Frandsen use an expression for the turbulence spectrum recommended by Danish standards, and that practice is adopted here with

$$S_{uu}(\omega) = \frac{1}{4\pi} \frac{\sigma_u^2 l}{u_{10,h}\left(1 + \frac{1.5\omega l}{2\pi U_{10,h}}\right)^{\frac{5}{3}}}. \tag{4.34}$$

The standard deviation of the turbulence is estimated from the approximate expression [186]

$$\sigma_u = 2.5 u^* \tag{4.35}$$

with the friction velocity calculated as described elsewhere, and the length scale l taken as a constant 150 m as recommended by the Danish standards [192].

4.6.3 Frequency domain solution

For each sea state considered wave force spectra for the submerged nodes are calculated following the methodology of section 4.5.3, and the tower top load spectrum as in section 4.6.2. Deflection spectra for points in the tower are calculated from a frequency domain solution of the modal equations of motion represented

by expression 4.11.

For each modal equation, the spectrum of the forcing term S_{ff} is calculated by superposing the modal force spectra for each node according to the relationship obtained by taking the Fourier transform of relation 4.17, that is

$$p_i(\omega) = \phi_{i,N} p_N(\omega) + \phi_{i,m} p_m(\omega) + \ldots + \phi_{i,3} p_3(\omega) + \phi_{i,2} p_2(\omega) + \phi_{i,1} p_1(\omega). \quad (4.36)$$

The deflection spectrum for each mode is then given by

$$S_{yy}(\omega) = H^2(\omega) S_{ff}(\omega) \quad (4.37)$$

where the transfer function is

$$H = \frac{1}{K - \omega^2 M + i\omega C} \quad (4.38)$$

with the coefficients representing the behaviour of the mode, K,M and C calculated according to expressions 4.12 to 4.14. Deflection spectra for each station in the support structure are calculated from the modal deflection spectrum and the structure mode shape produced by the finite element analysis.

4.6.4 Calculation of stress spectra

Once deflection spectra have been calculated at each node, stress spectra are calculated by means of the structure stiffness matrix.

4.7 Extreme load calculations

Estimation of extreme loads is based around several load cases, each representing a set of circumstances likely to produce the maximum loading on the structure. In each case, extreme wind and wave loads are evaluated separately. The effects are combined using the principle of superposition to provide bending moment and hence stress distributions throughout the tower and foundation. Results from each load case are compared and the maximum loading at each point in the structure taken across the whole set identified. The extreme loading in different parts of the same structure may therefore be driven by different load cases.

4.7.1 Wind loads

For each load case, the tower top wind load is initially calculated quasi-statically by summing the loads on each of the major external components using

$$F_{ex,tt,qs} = \frac{1}{2}\sum_{i=1}^{n} C_{d,i} A_i u_i^2 \tag{4.39}$$

where

i	Component index (each blade, nacelle, spinner)
n	Number of components
$C_{d,i}$	Drag coefficient of component i
A_i	Frontal area of component
u_i	Mean wind speed over extent of component i.

The height above the seabed of the line of action of the net tower top force $z_{tt,qs}$is also calculated so that moments down the support structure can be evaluated.

4.7.2 Wave loads

Each load case provides an extreme wave height and a range of periods associated with the extreme wave.

A purely static calculation is performed, for a range of wave periods between the maximum and minimum associated with the wave, timestepping through the effects of each passing wave section (4.5.2). The maximum value obtained at each point down the support structure, taken across the range of frequencies considered, is returned as the peak load. A number of authors suggest that a static calculation is adequate for estimating extreme loads on offshore wind turbine installations below the water line.

Above the water line the static calculation clearly implies a wave induced bending moment of zero. Accounting for wave loads above the water line and also for the possibility of resonant behaviour requires a calculation that encompasses the dynamic response of the structure. Since the fatigue calculation fully accounts for wave-structure dynamics, it is unlikely that a support structure likely to exhibit wave resonance would turn out to be the most economic. To avoid any possibility of resonance, the first eigenfrequency of the structure is checked against the range of possible extreme wave frequencies. If the structural period is found to lie within the range of wave periods, then the structure is 'flagged' and avoided during the design optimisation process.

4.7.3 Load cases considered

Two load cases associated with the configuration of the shutdown turbine are considered based on recommendations in Germanischer-Lloyd guidelines [62] . For the first, the turbine is treated in its normal shutdown configuration, with blades yawed out of the wind and subjected to 50 year return period environmental conditions. With the second case, it is supposed that a fault has prevented the blades from being yawed out of the wind, and that the pitch angle is set at an operating condition (taken to be 0 degrees), but that only 1 year return period environmental conditions are present. For modelling purposes, the distinction between the turbine configurations is contained entirely in the component drag factors and frontal areas used for the load calculation of equation 4.39. Appropriate values were supplied by the turbine manufacturers and are listed in table 4.4 and appendix B.

Component	1.5 MW Turbine	4 MW Turbine
Rotor (parked & feathered)	0.4	0.4
Rotor (fault condition)	1.3	1.3
Nacelle	1.2	1.2

Table 4.4: Drag co-efficients used for extreme load calculations.

Drag co-efficients for the tower sections are estimated using a published [193] correlation for the drag of cylinders

$$C_d = 1.2 + \frac{0.18log\left(\frac{10k_T}{d_T}\right)}{1 + 0.4log\left(\frac{Re_{d_T}}{10^6}\right)} \tag{4.40}$$

where

k_T Tower surface roughness
d_T Tower section mean diameter
Re_{d_T} Reynolds number of tower section.

4.7.4 Combinations of environmental parameters

There remains the question of which combinations of wave and wind parameters represent 50 year and 1 year return period conditions to be employed with the load cases in section 4.7.3.

UK Department of Energy guidelines [137] specify that the 50 year return period extreme wave be assumed to occur simultaneously with the 50 year one

minute average wind speed. Garrad et al [5] point out that this guidance was formulated for conventional offshore structures where wind loading is of secondary importance. Following Garrad, a second, 'wind oriented' case is defined to account for the greater importance of wind loading for offshore wind installations. This second case combines the 50 year return extreme 3 second gust wind load with a wave height that results in the same combined probability of occurrence as the first case.

Table 4.5 summarises the four extreme load cases considered by the cost model, together with values for the corresponding wind gust speed and wave heights. Wind speed gust factors u' were evaluated relative to hourly mean extreme wind speeds, using a relation due to Wieringa [194]

$$\frac{u_{T_2}}{u_{T_1}} = 1 + 0.42 I_u ln\left(\frac{T_1}{T_2}\right) \tag{4.41}$$

where T_1 and T_2 are the averaging periods for the wind speeds and I_u is the turbulence intensity. Wave height factors $w' = \frac{H}{H_s}$ for the wave oriented load cases were obtained by the conventional assumption [5] that the probability of occurrence is 10^{-3} and using the result that the probability of a wave in a sea state exceeding a certain height is given by

$$P(w') = e^{-2(w')^2}. \tag{4.42}$$

This relation can be derived from an assumption that wave heights in a sea state follow a Raleigh distribution. To obtain the wave factor for the wind oriented case, it is assumed that gust wind speeds follow a Gaussian variation around the hourly mean, and a wave factor derived using equation 4.42 such that the probability of occurrence of the two cases was identical.

The maximum height of waves at any location is constrained by the phenomenon of breaking, which is discussed a little further in section 4.8. In essence the maximum wave height may be estimated as 0.78 of the local depth, and the extreme wave height values from table 4.5 are limited to this criterion by the cost model.

Calculation of the wave loads also requires knowledge of the range of periods that the extreme waves might adopt. The raw climate data that must be input to the cost model (section 4.2.1) includes specification of upper and lower limits on the wave periods that arise in the two extreme sea states, and this information is used to set the range of periods considered.

Turbine status	Operational		Failed	
Climate return period	50 year		1 year	
Load case orientation	Wave	Wind	Wave	Wind
Wave height	$1.86H_{s,50}$	$1.32H_{s,50}$	$1.86H_{s,1}$	$1.32H_{s,1}$
Wind gust	$1.343u_{m,50}$	$1.595u_{m,50}$	$1.343u_{m,1}$	$1.595u_{m,1}$

Table 4.5: Extreme conditions load cases showing values of extreme wave heights and wind speed gusts used. In the table $H_{s,x}$ represents the x year return period significant wave height and $u_{m,x}$ represents the x year return period hourly mean wind speed. A turbulence intensity of 20% has been assumed.

4.8 Simplified climate representation

4.8.1 Rationale

To drive the design calculations, the cost model assumes the availability of a climate scatter chart and extreme weather data as described in section 4.2.1. At the feasibility stage of a project, only limited environmental data are likely to be available. To facilitate application in the early stages of a project, the cost model has been extended to accept a simplified representation of the climate that relies on a restricted range of data.

Even the limited data may only be available at a relatively few locations, hindering assessment of areas. A means of estimating the climate parameters at more inshore locations from those at relatively nearby, more offshore locations is included therefire. The approach attempts to account for the influence of increasing proximity to the shore on the climate experienced by the wind farm.

4.8.2 Description of climate at a known location.

Both the wind speed and significant wave height variation are described by Weibull distributions with cumulative form

$$P(y < y_o) = 1 - e^{-\left(\frac{y_o}{c}\right)^k} \tag{4.43}$$

where y is the physical parameter and k and c are empirically determined shape and scale parameters respectively. A relationship between wind and wave conditions is obtained using Kuhn's [25] suggestion of equating cumulative probabilities of occurrence.

The approximate climate description should ideally include explicit specification of the extreme wave and wind, obtained from other sources or a Fischer-

Tippet analysis of the available annual extreme data. In the absence of this information, estimates are made from the Weibull distribution. Equation 4.43 is solved for the parameter value that gives a probability equivalent to the required return period. Wind speeds are treated as hourly means, giving 8766 wind 'events' per year. The n-year return period hourly extreme wind speed has a probability of $1/(n \times 8766)$ therefore. The duration of the sea states fitted by the Weibull distribution is less well defined than for the wind speeds. Here we follow Garrad et al [5] in assuming a time interval of 6 hours making the probability of an n-year return period event equal to $6/(n \times 8766)$.

Wave time periods for fatigue calculations may be described with reference to their steepness by using an empirical correlation of the form

$$T = K\sqrt{H} \tag{4.44}$$

There are a number of published values for K, with the UK Department of Energy [137] suggesting $K = 4$ in the absence of better information. Wave steepness tends to vary with wave height however, so an empirical function of the form

$$K(H) = A_0 + A_1\sqrt{H} \tag{4.45}$$

may be developed by fitting the modal wave period at each height class of historic measured data, and facility for using this relation is included in the model code.

Periods for extreme waves are more difficult to model. One approach is to specify a minimum and maximum likely K and examine the full range during the structural analysis, that is

$$K_{ex,lo}\sqrt{H_{S50}} < T_Z < K_{ex,hi}\sqrt{H_{S50}} \tag{4.46}$$

where H_{S50} is the fifty-year return period significant wave height. The model considers extreme waves with periods distributed across this interval. The upper and lower constants $K_{ex,lo}$ and $K_{ex,hi}$ may be specified in the input to the cost model. In the absence of specific information, it is assumed here that periods lie in the range specified by UK Department of Energy guidance [137], that is: $K_{ex,lo} = 3.2$ and $K_{ex,hi} = 3.6$.

4.8.3 Estimation of inshore wave climate from data at a nearby more offshore location

It is assumed that the wave climate at a nearby inshore point can be estimated from the simplified representation at points for which data is available. Whether

this is true depends on the extent to which conditions at the known point are 'propagated' to more inshore locations, and some judgement must be used before using the methodology at arbitrary locations.

As waves travel towards the shore, they are subject to three main effects, breaking, shoaling and refraction, all of which are dominated by changes in depth. Refraction only influences the wave direction and thus is ignored here. Breaking constrains the height of waves in shallow water. The physical processes are poorly understood, and several authors [135, 139] suggest that breaking of regular waves may be predicted empirically using

$$H_{s,\max} = 0.78d. \tag{4.47}$$

Shoaling is the tendency of waves to increase in steepness as they enter shallower water. Using linear wave theory and assuming that the average rate of energy transfer as the wave progresses is constant, it may be shown that a wave starting with height H_1 in water with depth d_1 has a height of $H_2$when moving to water with depth d_2 given by

$$\frac{H_1}{H_2} = \sqrt{\frac{\left(1 + \frac{2k_2d_2}{\sinh(2k_2d_2)}\right)\left(\frac{\tanh(k_2d_2)}{k_2}\right)}{\left(1 + \frac{2k_1d_1}{\sinh(2k_1d_1)}\right)\left(\frac{\tanh(k_1d_1)}{k_1}\right)}}. \tag{4.48}$$

The wave number of the wave at each depth, k_1 and $k_2$respectively may be calculated using the conventional assumption that there is no build-up of waves, such that the time period T remains constant. Thence the wave number k and depth d are related by

$$kd\tanh(kd) = 4\pi^2\left(\frac{d}{gT^2}\right) \tag{4.49}$$

which is solved using numerical iteration. As shoaling occurs the waves may break on reaching the height limit in expression 4.47.

Expressions 4.47 to 4.49 are used to transform the wave heights of a Weibull distribution at the known deeper water location to give a distribution for a shallower location. If the shallower location is sufficiently deep that no breaking occurs, the new distribution remains Weibull in form, but an analytic solution cannot be stated due to the need to calculate wave numbers numerically. If breaking does occur then the new distribution is no longer truly Weibull.

4.8.4 Estimation of inshore wind climate from data at a nearby more offshore location

Moving onshore will also have some impact on the wind Weibull distribution. However the wind speed distribution is not subject to clear physical constraints in the same way as the wave height distribution. As a result a simple treatment is not practicable, and the changes are ignored here.

The vertical profile of the wind speed is also influenced by proximity to shore due to the very different surface roughness of the onshore and offshore environment. Again this is difficult to model without very detailed calculations, and furthermore depends on the wind direction. It too is ignored here, such that the wind climate is assumed to be unchanged as the shore is approached from the known point.

4.8.5 Generation of sea and wind states for use within the cost model.

The structural calculations require climate data in the form of a 'scatter diagram'. This is generated from the simplified representation by first dividing the hub height wind speed into 1 m/s width bands of 0-1 m/s, 1-2 m/s and so on, for compatibility with the wind fatigue calculation method. The bands are then scaled down to the height at which the wind Weibull distribution is valid, and the cumulative probability of each boundary value is calculated. The cumulative probabilities are then used with the wave Weibull distribution to define corresponding wave height bands. This produces a table of corresponding hub height wind speed bands and wave height bands, together with the number of hours per year for which each condition pertains, of the form shown in table 4.6 for a case with the parameters of table 4.7. This is then supplied to the cost model.

Hub Height Wind Speed		Wave height		Hours per year
Lower	Upper	Lower	Upper	
1	2	0.01	0.04	134
2	3	0.07	0.11	256
3	4	0.14	0.19	363
4	5	0.24	0.29	453
5	6	0.35	0.41	523
6	7	0.47	0.54	574
7	8	0.61	0.68	604
8	9	0.75	0.83	616
9	10	0.90	0.98	611
10	11	1.07	1.15	590
11	12	1.24	1.33	558
12	13	1.42	1.51	518
13	14	1.60	1.70	471
14	15	1.80	1.90	420
15	16	2.00	2.10	369
16	17	2.20	2.31	319
17	18	2.41	2.52	272
18	19	2.63	2.75	228

Table 4.6: Wind speed - wave height relation generated as described in the text.

Parameter	Value
Hub height	80m
Charnock constant	60
Wave Weibull shape parameter	1.3
Wave Weibull scale parameter	1.5
Wind Weibull shape parameter	2
Wind Weibull scale parameter	10
Height at which wind parameters specified	10

Table 4.7: Parameters for the generated wave height - wind speed relation.

Chapter 5

Modelling of support structure components

5.1 Support structure design approach

5.1.1 Use of calculated loads

The models described in the previous chapter provide extreme loads and fatigue spectra down the extent of the tower and the protruding part of any pile foundation. The extreme forces that must be carried by the foundation are also calculated. These loads must now be converted into component dimensions, and the means by which this is achieved forms the subject of this chapter.

5.1.2 Iterative approach

As mentioned in chapters 2 and 3, a complication is introduced by the interdependence of the loads and the component dimensions. Since the model is already numerical in nature, a conceptually simple iterative approach has been used to accommodate this. An outline of the approach to integrating the load calculation and design parts of the model was discussed in chapter 3, and this will be developed further here. Figure 5.1 illustrates how the various levels of iteration fit into the overall design procedure.

Initially, load calculations are carried out using an assumed foundation and tower. The assumed designs represent a practical configuration but are essentially arbitrary and are unlikely to be satisfactory for the case in hand. Results of the first load calculations are used to design a new foundation, using the methods described later in this chapter. A new structure is also designed from the initial calculations. For subsequent iterations, only the foundation is updated until convergence is achieved. Once this point is reached, the foundation is held constant

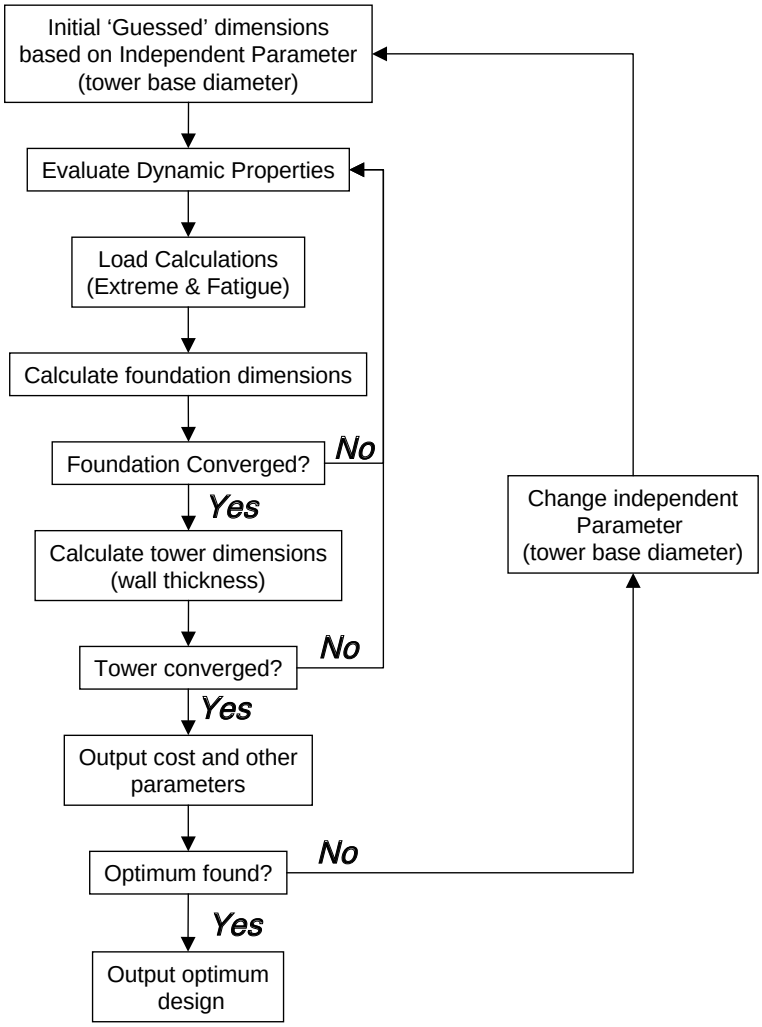

Figure 5.1: Support structure design procedure.

and only the tower updated, again until convergence. Attention then returns to the foundation and so on until both the tower and the foundation are converged. An important question is how to determine when components are converged. The main interest here is in cost assessment, which in turn is influenced strongly by component mass (see section 5.5). For this reason, components are regarded as converged if the change in mass between subsequent iterations is less than five percent.

5.2 Tower model

5.2.1 Description and dimensions

For design purposes, the tower is treated as a truncated hollow cone as shown in figure 5.2. At the upper end, the outer diameter is set by the need to interface with the turbine, and thus is specified by the turbine data. The lower diameter is the only arbitrarily variable parameter, and can be set either as an input to the model or by an automated design optimisation routine described later. It is assumed here that the diameter varies linearly with distance from the tower base between the two extremes, although the methodology can deal with any profile. This leaves only the wall thickness to be calculated from the applied loads.

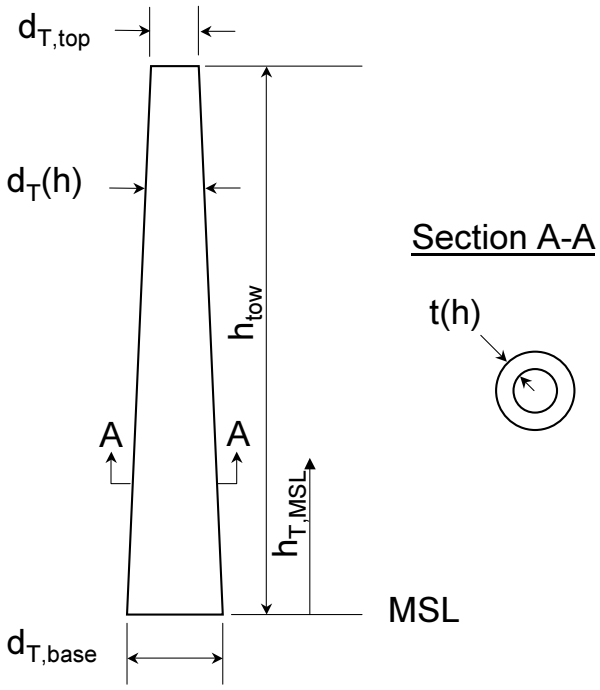

Figure 5.2: Support structure tower geometry.

The dynamic modelling treats the protruding part of the pile and the tower as a single system, with the foundation parameters describing only the buried part of the pile. This convenience is not carried forward to the design sections of the model, which use different algorithms for the two components.

5.2.2 Design approach

Tower design is driven by the fatigue and extreme loads calculated according to the methodology in chapter 4, and by buckling considerations. Initially fatigue considerations are employed to calculate a minimum wall thickness. Next overall buckling is considered, with wall thickness being increased as necessary, and finally yield and local buckling are treated.

Wall thickness is evaluated at several stations down the tower, corresponding with the locations at which load spectra are calculated. The algorithm starts with the top, and proceeds down the tower, calculating the wall thickness based on fatigue at each station in turn. On reaching the last station, the algorithm returns to the top to consider overall buckling, and completes this at every station before treating the other criteria in the same way.

The order in which the design criteria are treated is important because all except the fatigue are influenced by the tower mass above the design node. An iterative procedure is employed therefore wherein overall buckling is reconsidered if yield or local buckling has required thickening of the tower wall, as illustrated by the flow chart in figure 5.3. Experimentation has shown that in most cases neither yield or local buckling are design drivers, and thus the iterative procedure considered both of these before re-evaluating loads.

5.2.3 Fatigue load design

The fatigue oriented calculations described in section 4.6 compute bending moment spectra at every tower station for each of the climate combinations. Bending spectra are initially converted to single sided stress spectra, based on the current section modulus Z using the standard expression for maximum stress due to bending

$$\sigma = \frac{M}{Z} \tag{5.1}$$

where M is the bending moment and σ the stress induced at the outer wall.

The Dirlik [86] expression is then used to calculate rainflow stress range probabilities $p_{RF}(o_r)$ directly from the stress spectra. Appendix I discusses the form of the Dirlik expression used here and details of its numerical implementation. Next, the rate of fatigue damage associated with each spectrum is calculated from

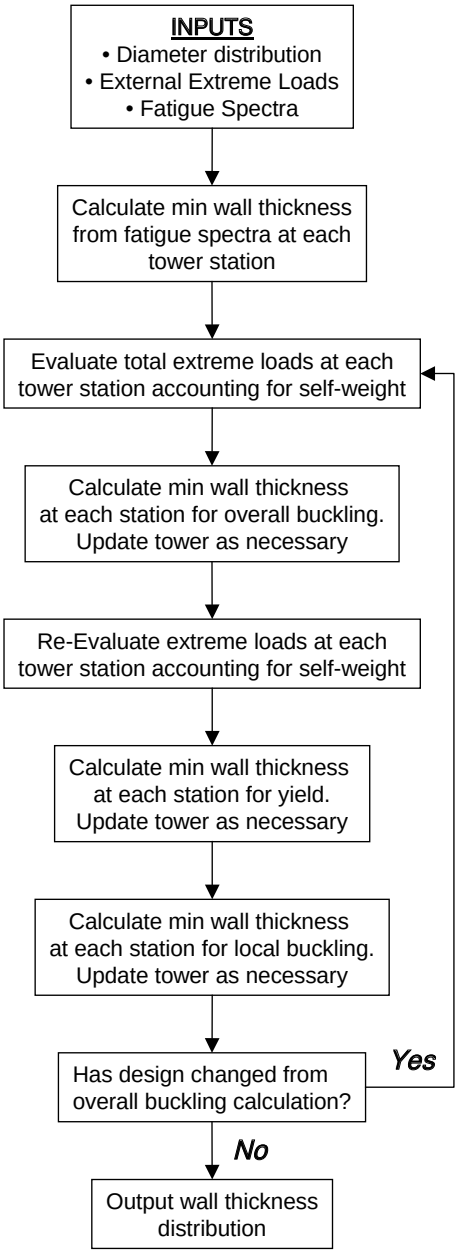

Figure 5.3: Flow chart showing treatment of overall buckling.

the rainflow range probabilities by numerical integration of [139]

$$D_i = \frac{1}{AT_c} \int_0^\infty \sigma_r^m p_{RF}(\sigma_r)\, d\sigma_r \tag{5.2}$$

where the subscript i indicates that this is the damage rate for spectrum i. The mean time between peaks in the time history of the loading, T_c, can be evaluated from moments of the original stress spectrum, again as described in appendix I. It is assumed that the tower material has a fatigue endurance curve of the Basquin form, that is

$$N = A(\Delta\sigma)^{-m}. \tag{5.3}$$

For the calculations here the material fatigue parameters were provided by offshore engineers Kvaerner Oil and Gas [195], and are listed in appendix C.

For each spectrum, the calculations yield damage rate $D_{m,i}$. To calculate the total damage accumulated during the lifetime, the damage rate for each spectrum is multiplied by the total time for which it will be experienced, as predicted by the simplified climate representation of the previous chapter. Summing the result for every spectrum at each tower station produces the total damage for that station, that is

$$D_m = \sum_i D_{m,i} p(i)\, L \tag{5.4}$$

where L is the lifetime of the structure and $p(i)$ is the probability of the climatic conditions that produce spectrum i arising, estimated as described in section 4.8.

It is assumed that failure occurs when the total damage D is equal to unity, although the model allows use of a fatigue safety factor $F_{S,fatigue}$. The value of the fatigue safety factor follows conventional practice in offshore engineering [195], and depends on the location of the components concerned as shown by the values in appendix C. Clearly the required section modulus is given by

$$Z = \frac{D_m}{F_{S,fatigue}}. \tag{5.5}$$

A new wall thickness t can then be estimated using

$$t = \left(\frac{4 \times Z \times 2.236}{\pi d_T^2} \right)^{\frac{1}{1.25}} \tag{5.6}$$

which is derived by solving the definition of the section modulus of a hollow cylindrical section in terms of the outer diameter and thickness, that is,

$$Z = \frac{\frac{\pi}{64}\left(d_T^4 - (d_T - 2t)^4\right)}{d_T} \tag{5.7}$$

for t.

5.2.4 Extreme load design

The calculations described in chapter 4 provide extreme bending moments at all the 'design' stations in the tower. These are used to assess three modes of failure due to extreme loading. Firstly overall buckling is treated. The maximum compressive stress at each node is calculated using

$$\sigma_{c,\max} = \frac{d_T M}{2I} + \frac{F}{A} \tag{5.8}$$

where

d_T	Outer diameter of segment
M	Extreme bending moment
I	Second moment of area of section
F	Vertical load
A	Cross sectional wall area.

The area and second moment of area are initially calculated using the wall thickness from the fatigue calculation. The maximum vertical load for this calculation is taken to be the weight of the turbine combined with the weight of the tower above the point of calculation. If the compressive stress exceeds the material maximum divided by a safety factor $F_{S,c}$, as specified in the input to the cost model, the wall thickness is increased to reduce the stress to the maximum permissible value.

Secondly, the tower section is checked for yield, with the maximum tensile stress calculated using an expression comparable to 5.8. Again the value is checked against a material maximum divided by a safety factor, and the wall thickness increased if necessary. Finally the structure is checked for local buckling against the criterion that for stability

$$\frac{t}{d_T} > \frac{1}{175} \tag{5.9}$$

and the thickness adjusted as necessary.

5.2.5 Physical characteristics for dynamic calculations

The structural dynamics routines require stiffness EI and mass per unit length, m, distributions for the designed tower. For the former, the second moment of area at each station is calculated using

$$I = \frac{\pi(r_o^4 - r_i^4)}{4} \tag{5.10}$$

while the latter is given by

$$m = \rho_T \pi \left(r_o^2 - r_i^2 \right) \tag{5.11}$$

where r_o and r_i are the outer and inner radii respectively. The relevant material properties were obtained from the same source as the fatigue characteristics and are listed in appendix C.

5.3 Pile foundation

5.3.1 Design approach

The pile is considered to be a hollow cylinder with protruding length h_{prot}, penetration depth h_{pen}, outer diameter d_{pile} and wall thickness t_{pile}, as shown in figure 5.4. In contrast to the tower, where dimensions can vary with height, practical constraints mean that the pile must have the same properties over its entire length. As a result, the dimensions are determined to withstand the most strenuous demands found in any point of the foundation. The dimensions must also depend on the properties of the seabed in which the pile is constructed. In later chapters several classes of seabed are identified and physical properties associated with each, however the analysis described here is general and can be applied across the range of seabed types.

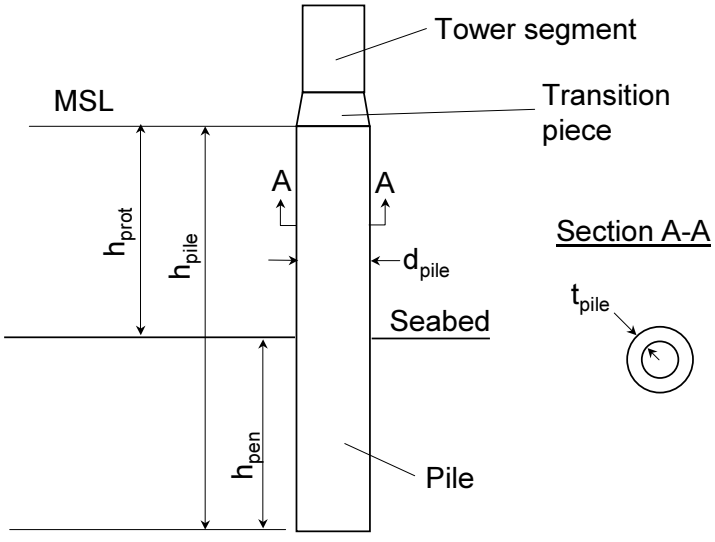

Figure 5.4: Geometry of pile foundation.

The protruding length is set by the geometry of the situation, but the other dimensions depend on the loads and, to complicate the problem, are to some extent

interdependent. There are several design drivers for the pile. Of primary importance is the ability to transmit the maximum vertical and lateral forces, calculated by the extreme load analysis, to the seabed. These drivers establish a relationship between the pile length and diameter. The pile material itself must be able to resist the internal moments set up when the foundation is subjected to the maximum overturning moment, which establishes a minimum pile wall thickness. Fatigue also plays a role, with need for sufficient material being available to withstand lifetime accumulated damage also setting a minimum wall thickness as for the tower. Fatigue is only considered for the protruding part of the pile, at nodes where the dynamic analysis has calculated spectra.

Several ancillary components are required in addition to the pile itself. Specifically these are a j-tube, outfitting and cathodic protection. As with the pile, these components are costed on the basis of their masses m_{j-tube}, $m_{tower-outfit}$ and m_{cath} respectively. However they are not designed in detail in every case. Instead it is assumed that their masses scale linearly from a reference case with the pile mass m_{pile}, that is

$$m_x = \frac{m_{pile}}{m_{pile,ref}} m_{x,ref} \tag{5.12}$$

where x represents one one of the components. The reference case was designed in detail by experienced offshore engineers [134]. Finally each unit incorporates a landing platform for boat access. This is treated as a fixed design with cost $C_{platform}$.

A transition piece connects the pile to the tower proper, as shown in figure 5.4. For the purposes of the model, the details of the transition piece are neglected. The design and dynamic calculations are performed assuming the pile connects directly to the tower at the point where in reality the top of the transition piece would be.

5.3.2 Vertical load calculation

The vertical load resistance of a pile comprises a component from skin friction on the curved surface of the pile with the remainder provided by the end of the pile. The cost model calculates the skin friction contribution using the λ-method described by Bowles [160] as having been successfully applied in North Sea design work. The resistance force per unit surface area of pile is

$$f_s = \lambda \left(\overline{q}_{\frac{1}{2}} + 2s_u \right) \tag{5.13}$$

where

s_u Undrained shear strength of soil
$\overline{q}_{\frac{1}{2}}$ Effective overburden pressure at half full depth
λ Empirically derived coefficient, function of depth.

The effective overburden pressure at half full depth may be estimated using

$$\overline{q}_{\frac{1}{2}} = \gamma \frac{h_{pen}}{2} \tag{5.14}$$

in which γ is the unit weight of the soil and h_{pen} is the total pile depth.

The contribution of the pile end to the vertical load resistance is calculated using the Hansen method as described by Bowles [160]. The ultimate load bearing capacity per unit area of the sea bed under the pile end is given by

$$q_u = cN_c d_c + \overline{q} N_q d_q + \frac{1}{2}\gamma d_{pile} N_g \tag{5.15}$$

where

$$N_q = e^{\pi \tan\phi} \tan^2\left(45 + \frac{\phi}{2}\right) \tag{5.16}$$

$$N_c = \frac{(N_q - 1)}{\tan\phi} \tag{5.17}$$

$$N_g = 1.5\,(N_q - 1)\tan\phi \tag{5.18}$$

$$d_c = 1 + 0.4 \tan^{-1}\left(\frac{h_{pen}}{d_{pile}}\right) \tag{5.19}$$

$$d_q = 1 + (2\tan\phi)\,(1 - \sin\phi)^2 \tan^{-1}\left(\frac{h_{pen}}{d_{pile}}\right) \tag{5.20}$$

$$\overline{q} = \gamma h_{pen} \tag{5.21}$$

in which

c Cohesion of soil beneath pile point (i.e. s_u)
ϕ Angle of friction
γ Soil unit weight

The bearing capacity of the pile is then given by

$$F_{pile} = f_s A_c + q_u A_e \tag{5.22}$$

where

A_c Curved surface area of pile in sea bed
A_e Area of pile end

5.3.3 Maximum lateral load

The maximum lateral load that can be carried by the pile is dictated by soil failure, and can only be estimated using semi-empirical methods. The approach adopted here is that proposed by Meyerhof [196] as reported by Das [159].

Firstly, the relative stiffness k_r of the pile is calculated from

$$k_r = \frac{E_p I_p}{E_s h_{pen}^4} \tag{5.23}$$

where

E_p	Young's modulus of pile
I_p	Second moment of area of pile
E_s	Horizontal soil modulus of elasticity
h_{pen}	Length (i.e. depth) of pile.

Piles with a relative stiffness of less than 0.01 are known as short, or rigid piles, where as other piles are termed long.

In sandy beds, the ultimate lateral load $F_{horiz,u}$ is determined from

$$F_{horiz,u} = 0.12\gamma d_{pile} {h_e}^2 K_{br} \tag{5.24}$$

where

γ	Soil unit weight
d_{pile}	Pile diameter
h_e	Effective pile length
K_{br}	Net soil pressure coefficient.

The net soil pressure coefficient is function of the ratio $\frac{h_{pen}}{d_{pile}}$ and is obtained by means of a look up table drawing on data presented in graphical form by Das [159]. For short piles, the effective pile length is simply equal to the true pile penetration depth, and for long piles

$$h_e = 1.65 {k_r}^{0.12} h_{pen}. \tag{5.25}$$

Where clay conditions dominate, the ultimate lateral load is given by

$$F_{horiz,u} = 0.4 c_u K_{cr} d_{pile} h_e \tag{5.26}$$

where c_u is the undrained shear strength of the sea bed, and the net soil pressure coefficient K_{cr} is again obtained by means of a look up table. Again for short piles

$h_e = h_{pen}$, and for long piles

$$h_e = 1.5{k_r}^{0.12} h_{pen}. \tag{5.27}$$

5.3.4 Fatigue

Fatigue is treated as for the tower, with a minimum section modulus being evaluated at each location where loading spectra have been produced. A minimum wall thickness is then calculated based on the pile outer diameter.

5.3.5 Internal bending moments

In the protruding part of the pile, internal bending moments are dealt with in the same way as for the tower with minimum wall thickness calculated at each station. For the penetrating pile section, extreme bending moment distributions are calculated from the extreme base bending moment and horizontal force. In an elastic soil with modulus E_s, the behaviour of a pile with second moment of area I_p and Young's Modulus E_p can be described using simple beam theory by balancing the reaction of the soil with the lateral force exerted by the pile at any point, that is

$$E_p I_p \frac{d^4 x}{dz^4} = E_s x \tag{5.28}$$

where x is the deflection of the pile and z is position along the penetrating section of the pile measured from the top. An numerical solution to equation 5.28 has been formulated assuming both that the buried end of the pile is free and that the soil modulus E_s remains constant with both depth and compression. While this is unlikely to be true in practice [135], the limited seabed data available means that more sophisticated modelling is not worthwhile. The formulation of the numerical solution is described in more detail in appendix J.

Once the deflection profile is known, bending moments at stations down the penetration length of the pile are calculated from the bending moment – deflection relationship

$$M = E_p I_p \frac{d^2 x}{dz^2}. \tag{5.29}$$

Checks are then made for buckling and yield failure in a manner similar to that used for the tower. In the event that failure is found the wall thickness is increased such that the failure criteria are satisfied. This of course changes the pile second moment of area, and thus the bending moments are recomputed, and the thickness re-evaluated, with the process continuing until subsequent changes in wall thickness are less than one percent.

5.3.6 Optimisation

For any set of seabed soil properties and specific vertical and horizontal loads to be supported, there is a unique relationship between a given pile diameter d_{pile} and the length of pile that must be embedded h_{pen} to support the load. Figure 5.5 shows the procedure used to establish pile parameters, starting from a specified penetration depth. The cost model searches over pile embedded lengths from a minimum of 15 m up to a maximum of 40 m in order to determine the dimensions of the most economic pile. A further constraint is that the pile diameter must not be less than the tower base diameter, as other configurations could cause difficulty in construction. As discussed in section 5.5, for the cost model the most economic pile is that with minimum material volume. The search process employs the FORTRAN routine sfmin [197] from the Netlib GO library to locate the minimum cost pile.

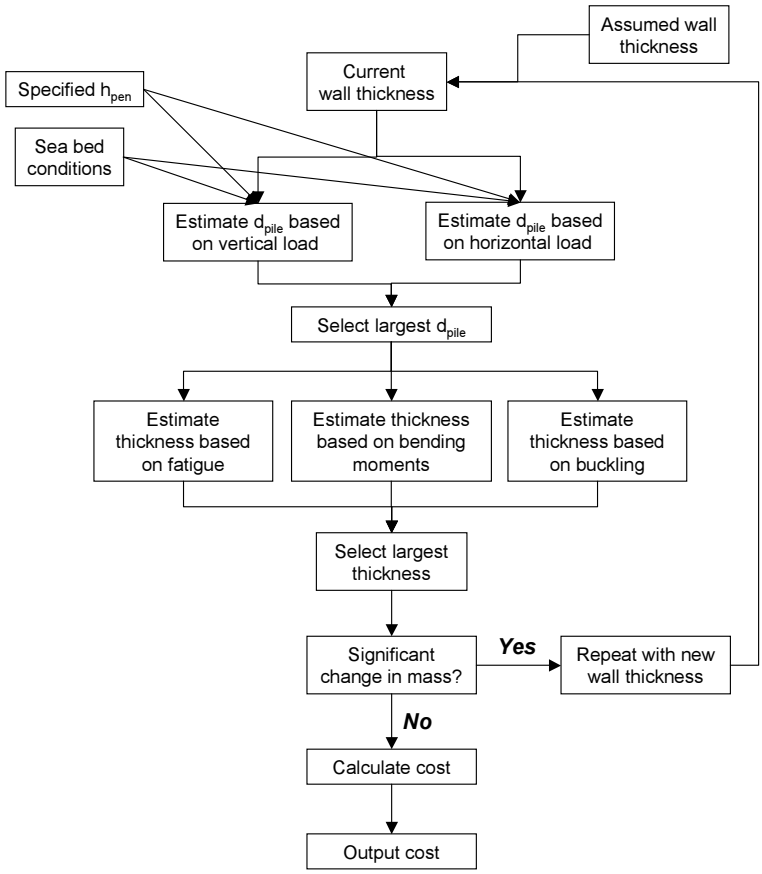

Figure 5.5: Elements of the pile design procedure.

5.3.7 Pile foundation stiffness

The developed model can account for the influence of foundation stiffness on the dynamic properties of the structure. Details of how the pile stiffness is estimated are in appendix. However the calculations in this thesis have assumed a rigid foundation below the sea bed as accounting for foundation stiffness greatly increased the model run time.

5.4 Gravity foundation

5.4.1 Design approach

The gravity foundation comprises an octagonal shaped steel caisson filled with concrete as a ballast material, as in figure 5.6. Design is carried out in a simplified manner, and results are only intended for comparison with the piled foundation when employing 4 MW turbines.

Three overall design criteria are used. Firstly the maximum vertical loading must be distributed over sufficient area that the seabed is able to support the foundation. Secondly the diameter must be large enough to provide resistance to overturning. Both these criteria are evaluated using the vertical loading, determined from the total mass, and maximum overturning moment, predicted by the calculations of chapter 4. The third criterion is that the weight of the structure must be sufficient to resist uplift due to diffraction of passing waves. This issue is only treated approximately, as discussed in section 5.4.4.

Iteration is required to determine suitable dimensions because the self-weight of the foundation is significant. Thus it is not sufficient to perform sizing calculations on the basis of the applied loads alone. Thanks to the role of the self-weight, increasing the foundation diameter also increases the load to be supported and the necessary diameter cannot easily be expressed as a function of the maximum applied vertical load. To solve this a routine was written that returns the maximum load that can be supported as a function of diameter, and a numerical search algorithm used to identify the smallest acceptable diameter.

A second issue is the linking between foundation thickness and diameter. Assuming constant density of materials, increasing the thickness also increases the mass per unit area, and influencing the result of the search described in the previous paragraph. However the minimum thickness is itself an indirect function of the diameter. Changes in the diameter influence the maximum shear forces in the foundation and the uplift caused by diffraction. Both of these potentially impact on the minimum thickness which in turn has implications for the diameter.

The iterative procedure of figure 5.7 determines compatible foundation dimensions. An initial diameter and thickness are assumed, and alternately updated until consecutive calculations result in only small changes. As with the pile foundation, the dimensions depend on the local seabed properties.

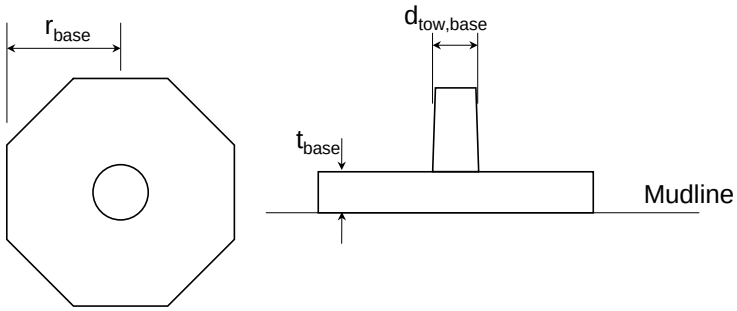

Figure 5.6: Configuration of the gravity foundation.

5.4.2 Bearing capacity

The foundation diameter required to distribute the maximum vertical load, including the foundation self-weight, over a sufficient area of the seabed depends on the ultimate bearing capacity q_u. The design criterion used is

$$\frac{F}{A} - \frac{q_u}{F_{Sq_u}} = 0 \tag{5.30}$$

where

F	Applied vertical load (tower, foundation and turbine weight)
A_{grav}	Area covered by foundation
F_{Sq_u}	Safety factor on undrained shear strength

The ultimate bearing capacity is estimated using the Hansen method, as described for the pile end bearing capacity in section 5.3.2.

A complication is that when subject to an overturning moment, as will always be the case here the load is not distributed evenly over the whole base. Bowles [160] suggests that an effective area be used for A_{grav} in place of the true area, and provides a purely geometric calculation method. Treating the base as a circle of equal area to the octagon, considerable algebra shows the load bearing area to be

$$A_{grav} = \frac{1}{240}\phi_E \pi R^2 + \frac{1}{2}\left(R - 2e_x\right) R sin\left(\frac{\phi_E}{2}\right) - \frac{1}{8}R^2 tan\left(\frac{\phi_E}{2}\right) \tag{5.31}$$

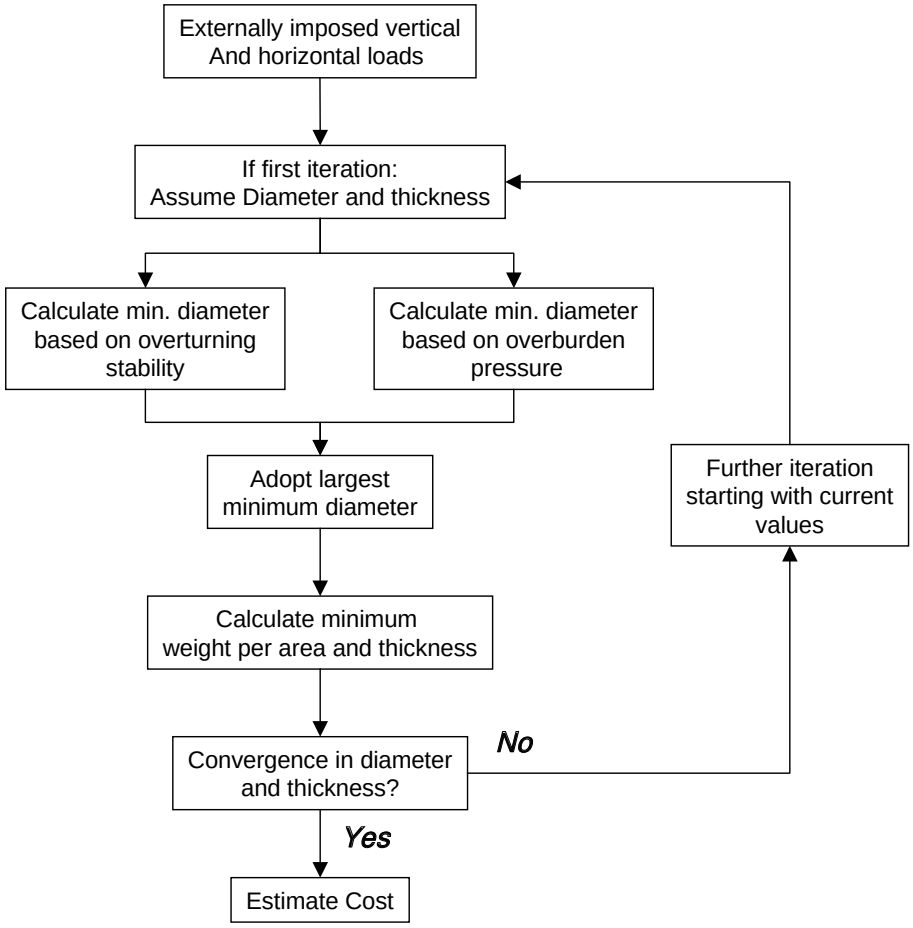

Figure 5.7: Gravity foundation design procedure.

where

$$\phi_E = 2cos^{-1}\left(\frac{R}{e_x}\right) \tag{5.32}$$

and

$$R = 0.5421 r_{base} \tag{5.33}$$

The 'eccentricity' of the loading, e_x is the ratio of the overturning moment to the vertical load. A value for the maximum overturning moment is determined from the extreme loading cases considered in chapter 4, and the vertical load is equal to the total weight of the installation.

A root finding routine (seroin) from the Netlib GO library [197] is used to identify the minimum base radius that satisfies equation 5.30. A difficulty arises because there are multiple values of the radius that satisfy the pressure requirements for certain loading conditions. In general, only the smallest radii, which produce the most economic foundations, are of interest here. There is however no mechanism in the standard search routine to control which root is returned in cases with multiple solutions. Further investigation revealed that in general the 'other' root was substantially larger than the required value. A detailed parameter study demonstrated that for the range of conditions encountered here, the smallest radius satisfying equation 5.30 was always less than 10 m, and the seroin routine was modified to only return roots below this value.

5.4.3 Overturning moment

Once a base diameter that meets soil pressure requirements has been determined, the base is checked for stability to overturning. The extreme overturning moment from chapter 4 multiplied by a safety factor SF_{om} must be balanced by a righting moment arising from the weight of the foundation, the tower and the turbine itself. A static assessment is performed, by considering a small rotational displacement of the foundation about a point on the perimeter. If the current base diameter is too small for stability, a new minimum value is determined assuming that the foundation thickness and mass per unit area is maintained constant.

5.4.4 Diffraction force

With a diameter of up to 10m [134], gravity foundations for offshore wind turbines in the relatively shallow locations of interest here cannot be considered as hydrodynamically transparent. The ratio of the wavelength to base diameter is less than 5 for at least some incident waves, and as a result diffraction effects should be taken into account [76].

A comprehensive physically based analysis requires solution of a Poisson equation to predict the flow field around the base for a range of incident wave conditions, followed by integration of the pressure field to calculate the net force exerted on the foundation. Such calculations are beyond the scope of this study. Instead diffraction is accounted for using a simplified method that relies on modifying a foundation designed in detail for a 4 MW turbine of the type described here [134]. The major difficulty encountered in this design was that the uplift due to diffraction of passing wave was sufficiently large to dictate the weight of the foundation, with additional ballast required to ensure the structure would remain in contact with the sea bed. The methodology therefore focuses on estimating the total mass required to overcome diffraction uplift.

A detailed parameter study of diffraction driven uplift on the gravity foundation [198] demonstrated that the plan area was the main influence on the uplift force, with wave height, base height, water depth and wave spectrum playing an increasingly secondary role. Building on the analysis in the study, it may be shown that the maximum uplift force in a sea state is proportional to the significant wave height and approximately proportional to the base plan area. Appendix K describes the analysis which relies on a number of approximations and assumes that the shape of the wave spectrum remains the same in each sea state. The relatively small influence of water depth is also ignored.

With the uplift being proportional to the plan area of the foundation, maintaining the weight per unit area of the original foundation is sufficient to resist the force, assuming identical wave conditions. To account for the effect of differing wave heights, the minimum mass per unit area is scaled linearly with the extreme significant wave height from that for which the original foundation was designed. The model calculates the required total weight based on the data for the original design in table 5.1, and adds sufficient ballast to achieve the calculated weight. Increasing the weight per unit area requires a thicker foundation to contain the ballast and hence the foundation thickness is also scaled.

Weight per unit area	2.16 tonnes/m^2
Design extreme wave height	5 m
Base height	2 m
Diameter	20 m

Table 5.1: Data for the base case gravity foundation.

5.4.5 Foundation stiffness

As with the pile, the model can account for the rigidity of the gravity foundation using the methodology in appendix M. However the calculations presented here assume a rigid foundation.

5.5 Capital cost calculation

5.5.1 Introduction

In this discussion, the capital cost of the support structure is defined as the materials and manufacturing costs of the tower and foundation, together with all the costs of installing the structure and the turbine, along with site investigation and preparation costs. The site investigation costs relate only to the detailed engineering studies necessary for foundation and structural design that occur *after* the general location for the wind farm has been chosen. Any costs associated with the initial site selection are not included.

The costing methodologies described were developed through consultation with offshore engineers [195]. In general there are many operational costs, such as those for equipment mobilisation, that are shared among all the structures in an offshore farm. For this reason the algorithm focuses on calculating the total construction and installation cost for a whole farm rather than for individual structures. The installation techniques assumed are based on descriptions from the literature [134] and are outlined as the costing algorithms are developed.

The minimum capabilities of the offshore plant required for installation work, for example the lifting capacity of floating cranes, will be influenced by the size and weight of the support structure. In principle the hire costs of the offshore plant will be a function of its capabilities, with more capable plant costing more to hire. A number of factors however make it difficult to model how the cost of offshore plant varies with capacity. The limited availability of suitable equipment means that quoted costs reflect current overall demand for offshore work. Furthermore, most operators view offshore wind as an immature market, and quotations reflect their desire to obtain experience in the field, with a view to obtaining future contracts, as much as the real costs of such operations. In addition, very little recent data is available thanks to the relatively small number of operations and the confidential nature of contracts. To complicate matters further, it has been suggested that it may be more economic for developers that intend to build several large-scale offshore farms to purchase offshore plant rather than hire it. Consideration of how to share the cost of such purchased equipment over a number of offshore farms is beyond the scope of this work.

In the light of these difficulties, the costing methodology uses representative values for the operating costs of the offshore plant. These have been obtained through discussion with consultants, and represent the costs of the smallest capacity equipment that could deal with the entire range of support structures considered here. Clearly, since the equipment costs do not vary with the tower size, this approach will in principle over-estimate the construction costs of the smaller towers and turbines. This error is unlikely to impact on the value of the results, in the main because a continuous range of offshore plant capabilities is not available. A reduction in tower height or mass does not necessarily mean that smaller plant can be used therefore. Since the range of heights and masses considered here is relatively small, compared to most offshore equipment, the impact of this simplification will be minor relative to variations in the market price of the offshore equipment.

5.5.2 Costing the piled foundation

Costing for the monopile structure assumes that the pile is installed first, using either a piling hammer or drilling equipment as dictated by the sea bed. The tower, with turbine already attached, is subsequently lifted into place from a flat bottom barge with a sheerleg crane, as described in the literature [134]. Due to the limitations of flat bottom barges, this installation procedure will only be able to proceed in relatively calm weather conditions, and thus will be susceptible to weather delays. The impacts of delays are not modelled explicitly.

Costs for the tower and the pile foundation are dealt with separately. The foundation cost comprises site investigation, procurement and installation. Total procurement costs are calculated as follows:

$$C_{pile,proc} = [(m_{pile} \times c_{pile}) + (m_{j-tube} \times c_{j-tube}) + (m_{cath} \times c_{cath}) + C_{platform}] \times n_{turbines} \tag{5.34}$$

with definitions and values as given in section 5.5.5. Note that to assist in understanding these expressions, capital C is used for absolute costs, while lower-case c stands for costs per unit, and m terms represent masses of individual components. Foundation installation costs are evaluated using

$$C_{pile,install} = (c_{pile,install} + c_{scour}) \times n_{turbines} + C_{pile,install-mob} \tag{5.35}$$

and site investigation costs with

$$C_{pile,site} = C_{pile,geophys} + (c_{geotech} \times n_{turbines}) \,. \tag{5.36}$$

Tower costs are themselves divided into procurement, assembly and installation. Materials procurement costs are evaluated with the following expression

$$C_{pile,towerproc} = [(m_{tower} \times c_{tower}) + C_{tower-outfit}] \times n_{towers} \tag{5.37}$$

with assembly and installation costs from

$$C_{pile,towerassy} = C_{pile,assy-mob} + c_{pile,assy} \times n_{towers} \tag{5.38}$$

The total pile and tower cost is then given by

$$C_{structure} = C_{pile,pileproc} + C_{pile,install} + C_{pile,site} + C_{pile,towerproc} + C_{pile,towerassy}. \tag{5.39}$$

5.5.3 Costing the gravity foundation

With the gravity foundation, the entire foundation/turbine/tower structure is assembled in a dry dock specially constructed close to the wind farm site. Completed structures are floated into position in $N_{batches}$ batches of $n_{turbs,batch}$ turbine, each supported by custom designed barges pulled by tugs. The batch process, together with the need for custom facilities means that it is not possible to identify clear costs for each unit in the same way as for the piled structures. As a result a different approach to costing must be used that explicitly considers the labour costs of the construction.

The total structure cost is broken down into tower procurement, foundation procurement, dry dock operation, offshore work and geophysical survey costs such that

$$C_{structure} = C_{grav,towerproc} + C_{grav,foundproc} + C_{grav,drydock} + C_{grav,offshore} + C_{geophys}. \tag{5.40}$$

Of these components, the survey cost is treated as a constant, and has the same value as for the piled case. The tower procurement cost is essentially that of the associated materials such that

$$C_{grav,towerproc} = (c_{tower} m_{tower})\, n_{turbines} \tag{5.41}$$

and similarly the foundation procurement cost

$$C_{grav,foundproc} = (c_{ballast} m_{ballast} + c_{caisson} m_{caisson})\, n_{turbines}. \tag{5.42}$$

The dry dock operations include the cost of constructing a nearby dry dock facility, the cost of maintaining it for the duration of the offshore farm construction,

and the labour associated with actually building the structures, such that

$$C_{grav,drydock} = C_{dock,construction} + C_{dock,ops} + C_{dock,labour}. \tag{5.43}$$

A fixed price is used for the dock construction cost, and a fixed annual operation cost is assumed $C_{dock,annops}$, scaled according to the total construction period to give the actual operation cost $C_{dock,ops}$. The labour cost is estimated mainly from the materials masses and the construction time per unit of material denoted by t according to

$$\begin{aligned} C_{dock,labour} \quad = \quad & [(m_{tower} t_{dock,towerlab} c_{dock,towerlab}) \\ & + (m_{caisson} t_{dock,cassonlab} c_{dock,caissonlab}) \\ & + (m_{ballast} t_{dock,ballastlab} c_{dock,ballastlabcost})] \times N_{turbines} \\ & + (c_{floataway} N_{batches}) \,, \end{aligned} \tag{5.44}$$

which also includes the cost of preparing each batch of machines to be floated away.

Offshore work costs include those associated with the tug to pull the floated structures to the farm site, the necessary offshore equipment, and the installation operations at the site giving

$$C_{grav,offshore} = C_{offshore,tug} + C_{offshore,eqpt} + C_{offshore,ops}. \tag{5.45}$$

Tugs are hired by the day and are required both during transportation and installation of the structures. There is also a mobilisation period for the tugs, each time a batch of turbines is to be transported, and hence the total tug cost is

$$C_{offshore,tug} = N_{batches} \left(t_{tug,ops} + t_{tug,mob}\right) \times c_{tug,day}. \tag{5.46}$$

where the number of operational tug-days per batch is given by

$$t_{tug,ops} = n_{turbs,batch} \times t_{tug,install}. \tag{5.47}$$

The tug time required to install an individual turbine, $n_{tug,install}$ must include time spent towing and on-site, as well as an allowance for weather interruptions and is assumed constant. In principle the towing time will vary with the distance of the farm from the shore. With the limited range of distances considered here, in practice an entire day will be required for the outward journey, and an entire day for the return, and thus $t_{tug,install}$ is treated as a constant. The mobilisation time $t_{tug,mob}$, which applies to the whole group of tugs is also considered a constant.

The offshore operations are those associated with placing the structures in position and including labour and other costs. As with the tugs, there is a mobilisation effort that applies to the whole batch of structures and an individual effort to locate individual machines such that

$$C_{offshore,ops} = N_{batches}\left(t_{ops,ops} + t_{ops,mob}\right) \times c_{ops,day} \tag{5.48}$$

with the number of operational days per batch being

$$t_{ops,ops} = n_{turbs,batch} \times t_{ops,install}. \tag{5.49}$$

The mobilisation and installation times are also treated as constants, estimated using data provided by offshore engineers.

Finally the capital cost of the offshore barges and other equipment required for each turbine installation must be evaluated. For barges a mass based cost estimate is used, while the costs of other equipment are taken to be constant such that

$$C_{offshore,eqpt} = n_{turbs,batch} m_{barge} c_{barge} + n_{turbs,batch} c_{eqpt}. \tag{5.50}$$

Barges are not designed in detail for each case. Instead the barge mass is assumed to scale from a reference case [134] with the total mass of the support structure

$$m_{barge} = m_{barge,ref} \frac{m_{tower} + m_{found}}{m_{tower,ref} + m_{found,ref}}. \tag{5.51}$$

5.5.4 Management and certification costs

Charges for management and certification are estimated as percentages of the *total* farm construction cost, according to the data in appendix C.

5.5.5 Definition of symbols and values used

Values for each of the terms in sections 5.5.2 and 5.5.3 are shown in tables 5.2 and 5.3 respectively. The quantities were obtained from discussion with an offshore engineering consultant [195] and were originally provided in 1998 financial year Pounds Sterling. The tables show 2002 financial year values, the original data having been updated according to the variation of UK manufacturing output costs index (PLLU) provided by the UK Office of National Statistics.

Symbol	Description	Value	Unit
c_{pile}	Unit cost of pile	423	GBP/tonne
c_{j-tube}	Unit cost of j-tube	2,115	GBP/tonne
$c_{pile,install}$	Installation cost for single pile	79,313	GBP
c_{scour}	Scour protection cost per unit	5,288	GBP
c_{cath}	Unit cost of cathodic protection	2,643	GBP/tonne
$C_{pile,mob}$	Mobilisation cost for pile intallation	370,127	GBP
$C_{geophys}$	Cost of geophysical survey	158,626	GBP
$c_{geotech}$	Geotechnical survey cost per pile	2,115	GBP
c_{tower}	Unit cost of tower material	423	GBP/tonne
$c_{tower,outfit}$	Tower outfitting cost per pile	52,875	GBP
$C_{pile,assy-mob}$	Pile/tower assembly mobilisation cost	1,586,257	GBP
$c_{pile,assy}$	Assembly cost for single unit	68,737	GBP
$C_{platform}$	Landing stage cost	29,610	GBP
$m_{pile,ref}$	Pile mass for reference case	280	Tonnes
$m_{j-tube,ref}$	J-Tube mass for reference case	2.5	Tonnes
$m_{tower-outfit,ref}$	Outfit mass for reference case	10	Tonnes
$m_{cath,ref}$	Cathodic mass for reference case	0.5	Tonnes

Table 5.2: Definitions and values for the pile support structure. Unlike the gravity structure, the pile cost calculation does not explicitly include labour costs, and thus the unit costs of the pile and other components must include an allowance for manufacturing effort. It is also assumed that the unit costs account for delivery of the component to the proximity of the construction site.

Symbol	Description	Value	Unit
c_{tower}	Unit cost of tower material	423	GBP/tonne
$c_{caisson}$	Unit cost of caisson material	423	GBP/tonne
$c_{ballast}$	Unit cost of ballast material	106	GBP/tonne
c_{barge}	Unit cost of barge per tonne	2,115	GBP/tonne
c_{eqpt}	Cost of offshore equipment set	528,752	GBP/set
$c_{dock,towerlab}$	Hourly tower labour cost	32	GBP/hour
$c_{dock,caissonlab}$	Hourly caisson labour cost	32	GBP/hour
$c_{dock,ballastlab}$	Hourly ballast labour cost	32	GBP/hour
$c_{tug,day}$	Daily cost of tug	3,701	GBP/day
$c_{ops,day}$	Daily cost of offshore operations	10,575	GBP/day
$c_{floataway}$	Cost of preparing batch for floataway	158,626	GBP/batch
$C_{dock,construction}$	Total dry dock construction cost	2,643,762	GBP
$C_{dock,annops}$	Annual dock operation cost	528,752	GBP/year
$C_{geophys}$	Cost of geophysical survey	158,626	GBP
$t_{dock,towerlab}$	Tower constuction time per tonne	50	Hours/tonne
$t_{dock,caissonlab}$	Caisson constuction time per tonne	50	Hours/tonne
$t_{dock,ballastlab}$	Ballast construction time per tonne	5	Hours/tonne
$t_{tug,mob}$	Tug mobilisation time in days	3	Days
$t_{tug,install}$	Tug time in days for installation of a unit	5	Days
$t_{ops,install}$	Offshore eqpt. time for unit installation	2.5	Days
$t_{ops,mob}$	Offshore eqpt mobilisation time	5	Days/batch
$m_{barge,ref}$	Barge reference mass	500	Tonnes
$m_{tower,ref}$	Tower mass for ref. barge	380	Tonnes
$m_{found,ref}$	Foundation caisson mass for ref. barge	100	Tonnes

Table 5.3: Definitions and values for the gravity base support structure. All labour times quoted represent person-hours of effort.

5.6 Overall optimisation

Once the materials properties have been chosen, there are only two support structure parameters that can be varied arbitrarily within the design framework described. These are the tower top height and the base diameter. As discussed in chapter 3, it is informative to be able to vary the tower height in order to investigate trade-off between costs and energy production. For this reason, the tower height is specified in the cost model input.

The tower base diameter, however, is not as interesting. In practice the only value of significance is that which provides the most economic support structure. An automated optimisation procedure has been developed.

Experiments with simple gradient optimisation techniques proved problematic because the support structure cost is not always a smooth function of the base diameter. As a result, a pragmatic solution to determining a near optimum diameter has been formulated.

The pragmatic method is practical only because the range of tower base diameters is relatively constrained, and outside of resonance bands, the structure cost is not very sensitive to changes. The minimum feasible bottom diameter is equal to the tower top diameter. Manufacturing and other practical constraints limit the maximum base diameter, with the precise value depending on the details of the processes involved, but taken as 4 m here.

For each case treated by the model, towers are designed for several base diameters across the possible range, and the minimum cost example ouput. Figure 5.8 shows an example sweep across a range of tower base diameters. The number of diameters considered can be specified as an input to the model, but in all the cases presented here ten calculations were performed. The designed towers are classified according to their frequency band following the approach of figure 2.10.

5.7 Overall validity of model

The model contains many calculations, and before it can sensibly used for studies some validation is required. It is not practical to assess the prediction accuracy of the model as there are few suitable prototypes against which it can be benchmarked. Furthermore, data from most of those prototypes played a role in the development of the model.

There are, nevertheless, a number of validation measures that can be undertaken to try to produce some confidence in the results, and in particular to ensure:

- That the design methods chosen are suitable and capture the design drivers

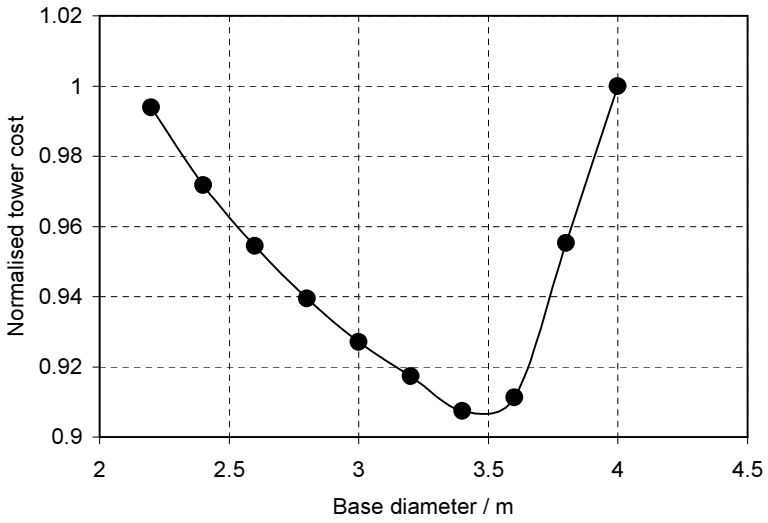

Figure 5.8: Sample sweep of tower cost against base diameter. Circles show the cases evaluated.

for the cases considered,

- That the programmed model algorithms perform correctly, for example that the numerous optimisers do identify optimum cases,
- That the model code is free from errors so far as possible, so that various physical calculations programmed produce correct results,
- That the scope of the utility of the model is defined, to avoid the risk of drawing overly detailed conclusions unwarranted by the precision of the data.

The treatment of these issues is discussed in appendix N.

Chapter 6

Parameter studies

6.1 Introduction

A series of studies to investigate the impact of climate and overall engineering parameters on the levelised energy cost of offshore wind farms have been conducted using the model described in the preceding chapters. As there are many possible farm designs and locations, to provide some focus the studies have considered parameter excursions centred around eight base cases. The base cases have been chosen to reflect a range of climate conditions and farm configurations currently being considered for development. Since the focus of the model is on structural aspects, the parameters considered here are in the main those that potentially can have some impact on the structural design.

The studies are intended to be useful in their own right, but almost as importantly, to act as a demonstration of the utility of the cost modelling methodology developed in the previous chapters. Some of the studies also provide information for the GIS based investigations of chapters 7 and 8.

For the purposes of insight, all the parameters in this chapter are varied independently. Any linkages between the parameters are ignored, except as noted in the text. The initial focus of the studies is on the energy production and the cost of energy. Later sections look more towards the design of the farm.

6.2 Base cases

The base cases have an engineering and a geographical element to their specification. Two one-hundred unit wind farms, one of 1.5 MW turbines and one of 4 MW turbines are considered at four geographical base locations around Northern Europe. Data defining the engineering and geographical elements are provided in the following sub-sections.

For the purposes of this chapter, the geographical data in general is not intended to represent a precise location, but to be representative of conditions in an area. While wind and wave conditions are likely to be constant over open water in the areas shown, it should be kept in mind that there may be particularly sheltered or exposed locations, especially close to land. Equally water depths may vary considerably over each area, which also will impact on wave breaking.

It has been assumed that the wind farms all lie 15 km from the shore, and that grid connections are available within 5 km of the shore. These are realistic values given that all the base locations are near to relatively industrialised areas with well developed grid networks. Maps of the locations contained later in the text show details of the regional high voltage grid infrastructure taken from data supplied by the US National Imaging and Mapping Agency. The distances will vary with the details of a location, but the primary aim is to ensure some consistency between the studies, which focus on structural aspects, while maintaining realistic grid connection costs for any cost breakdown.

In the data that follows, wind conditions are quoted based on hourly average values measured 25 m above the water level unless noted otherwise. Wave data is stated for significant wave heights. For the studies in this chapter, the cost model was set to use specified extreme conditions, and not estimate values from the Weibull parameters.

Detailed information on the periods of extreme waves is in general difficult to obtain. The model 'default' period calculation has been employed in each base case therefore, with periods estimated from significant wave heights according to UK Department of Energy Guidelines [137]. Similar considerations apply for the estimation of periods for fatigue calculations, with the 'default' $T = 4\sqrt{H}$ being employed in all cases.

6.2.1 Farm design base cases

Introduction

Preliminary studies confirmed the literature reports that gravity foundations were less economic than piled solutions. The analysis reported here therefore is constrained to the more economic pile foundation.

Medium scale farm base case

The base case 1.5 MW farm is configured as in table 6.1, giving a total installed capacity of 150 MW. Farms of this total capacity are currently being constructed, but with larger turbine units. 1.5 MW turbines are now effectively obsolete for

offshore deployment, although when the work reported here was begun, they represented the state of the art. This base case is still relevant however as comparing the trends for 1.5 MW and 4 MW offshore machines may give some insight into the impacts of the even larger turbines currently coming to market.

Parameter	Symbol	Base value
No. of turbines	N_t	100
Spacing ratio	r_s	6.25
Hub height	h_{hub}	80 m

Table 6.1: Medium scale farm configuration.

Large scale farm base case

The base case 4 MW farm is configured as in table 6.2, giving an installed capacity of 400 MW. This represents a very large farm using state of the art wind turbine technology. The spacing ratio selected means that the same area is covered by both of the base case farms.

Parameter	Symbol	Base value
No. of turbines	N_t	100
Spacing ratio	r_s	4.44
Hub height	h_{hub}	80 m

Table 6.2: Large scale farm configuration.

6.2.2 Geographical base cases

UK Irish Sea location (UK-IE)

The UK Irish Sea parameters represent a location off the coast of North Western England (figure 6.1), where the wave climate is driven by incoming weather from the Atlantic, but is sheltered by Ireland. A recent UK Government tendering process invited proposals for further developments in this area, and a farm as already in operation. The data are shown in table 6.3. The tidal range and wind driven sea surge values are not cost model inputs but they do constrain the minimum hub height and are reported here for completeness.

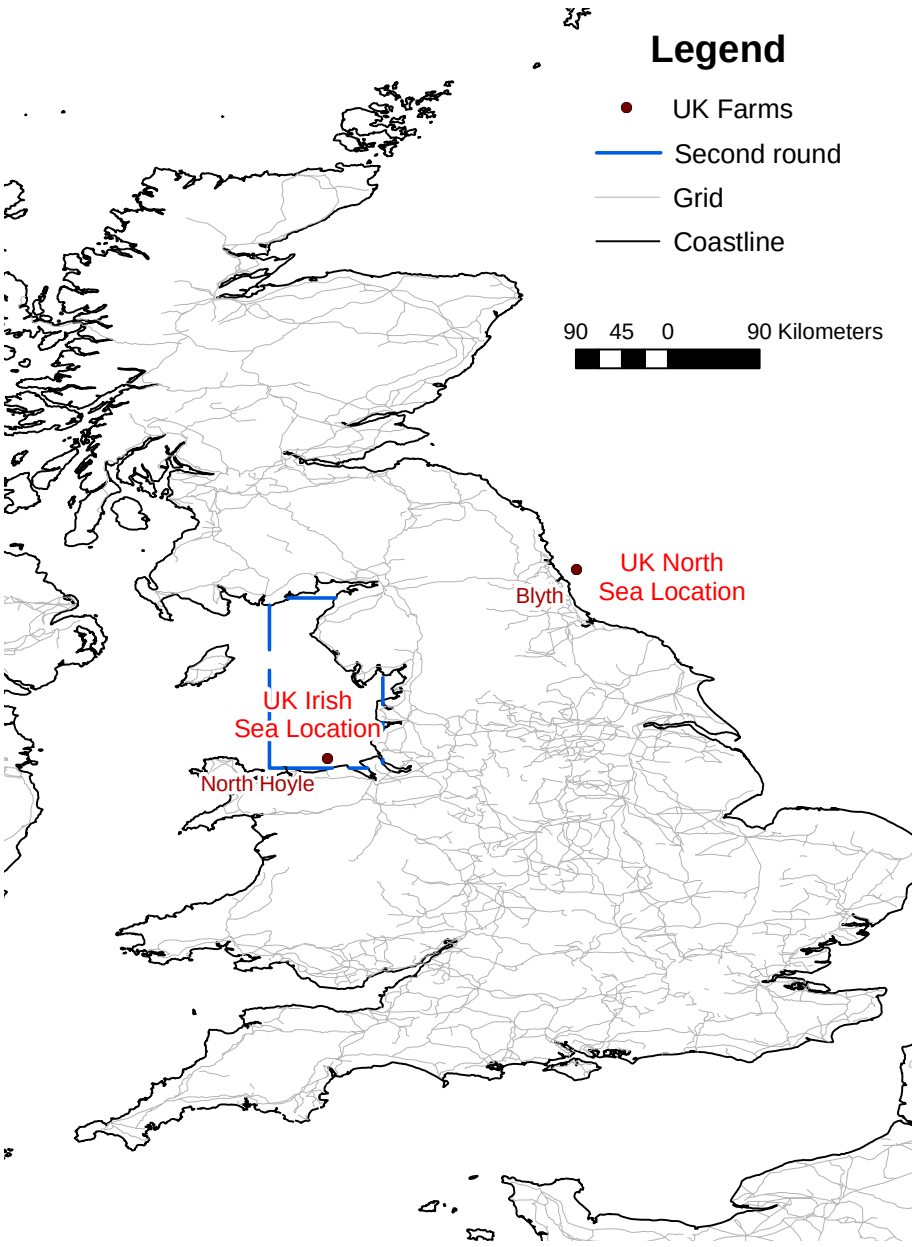

Figure 6.1: Areas considered for the UK studies. The red text indicates the general areas investigated. Grey lines indicate locations of high voltage grid infrastructure, showing that grid connections are potentially available within a short distance of the shore. Also shown, for comparison, are the locations of two operational UK offshore wind farms (brown circles), and the area of the Irish sea (bordered by blue line) available for proposals during the UK Goverments second phase tendering process.

Parameter	Symbol	Base value	Source
Wind climate parameters			
Weibull shape parameter	k_{wind}	1.83 at 25 m	[5]
Weibull scale parameter	C_{wind}	8.9 at 25 m	[5]
50 yr extreme hourly wind	$u_{ex,50}$	40.5 m/s at 25 m	[137]
1 yr extreme hourly wind	$u_{ex,1}$	29.7 m/s at 25 m	Est. [137]
Wave climate parameters			
Height Weibull shape parameter	k_{wave}	1.31	[5]
Height Weibull scale parameter	c_{wave}	1.2	[5]
Wave period for fatigue	T_{fat}	$4\sqrt{H}$	Default
50 yr sig. wave height	$H_{s,50}$	8 m	[5, 137]
1 yr sig. wave height	$H_{s,1}$	5.85 m	Est. [5, 137]
Period of extreme wave	T_{ex}	$3.2\sqrt{H_s} < T_{ex} < 3.6\sqrt{H_s}$	Default
Geographical parameters			
Seabed composition	-	Muddy sand	[199]
Distance from shore	L_{shore}	15 km	-
Distance from shore to grid	L_{grid}	5 km	-
Other-site specific parameters			
Foundation type		Pile	
Water depth	d	12 m	[200]
Tidal range	d_{tide}	± 9 m	[200]
Surge	d_{surge}	1.75 m	[137]

Table 6.3: Description of the Irish Sea location. Where data has been estimated from the sources shown, the citation is prefixed with 'Est.'

UK Northern North Sea location (UK-NS)

The UK Northern North Sea parameters (table 6.4) represent a location off the coast of North East England, near to Teesside, Wearside or Tyneside, as shown in figure 6.1. There is an existing small offshore farm in this area close to Blyth and there are plans for developments near Teesside.

Parameter	**Symbol**	**Base value**	**Source**
Wind climate parameters			
Weibull shape parameter	k_{wind}	2.06 at 25m	[5]
Weibull scale parameter	C_{wind}	8.4 at 25m	[5]
50 yr extreme hourly wind	$u_{ex,50}$	32 m/s at 25m	[5]
1 yr extreme hourly wind	$u_{ex,1}$	24.5 m/s at 25m	Est. [137]
Wave climate parameters			
Height Weibull shape parameter	k_{wave}	1.71	[5]
Height Weibull scale parameter	c_{wave}	1.4	[5]
Wave period for fatigue	T_{fat}	$4\sqrt{H}$	Default
50 yr sig. wave height	$H_{s,50}$	11.16 m	[137]
1 yr sig. wave height	$H_{s,1}$	5.85 m	Est. [5]
Period of extreme wave	T_{ex}	$3.2\sqrt{H_s} < T_{ex} < 3.6\sqrt{H_s}$	Default
Geographical parameters			
Seabed composition	-	Muddy sand	[199]
Distance from shore	L_{shore}	15 km	-
Distance from shore to grid	L_{grid}	5 km	-
Other-site specific parameters			
Foundation type		Pile	-
Water depth	d	20 m	[5]
Tidal range	d_{tide}	± 2 m	[137]
Surge	d_{surge}	1.5 m	[137]

Table 6.4: Description of the Northern UK North Sea location.

Dutch North Sea location(BE-NL)

With the Dutch North Sea location, the objective is to represent a wind farm in the relatively sheltered areas of the North Sea near to the coast of Holland (see figure 6.2).

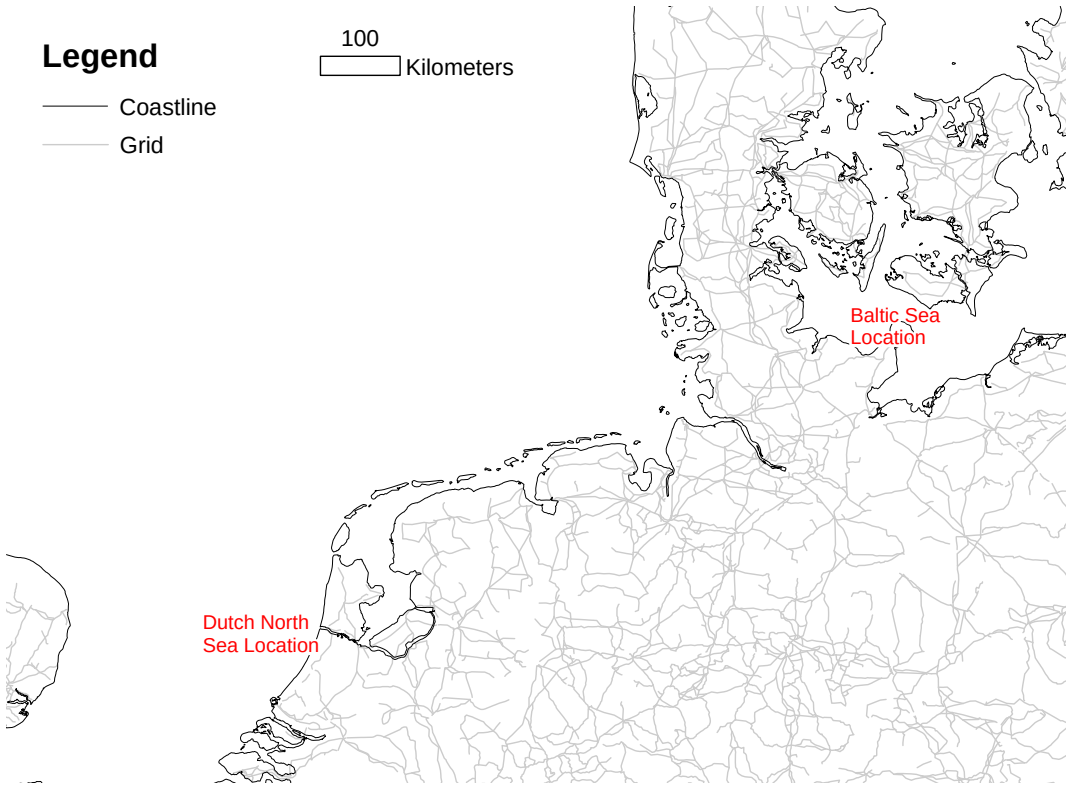

Figure 6.2: General area represented by the Dutch North Sea and Baltic Sea locations. Grey lines represent high voltage grid infrastructure showing that connections are available within a few tens of kilometers of most shores, and thus that the onshore cable cost is unlikely to be a significant factor in the economics of offshore wind farms in northern Europe.

Parameter	Symbol	Base value	Source
Wind climate parameters			
Weibull shape parameter	k_{wind}	2.07 at 25 m	[5]
Weibull scale parameter	C_{wind}	9 at 25 m	[5]
50 yr extreme hourly wind	$u_{ex,50}$	37.6 m/s at 25 m	Est. [134]
1 yr extreme hourly wind	$u_{ex,1}$	26.1 m/s at 25 m	Est. [134]
Wave climate parameters			
Height Weibull shape parameter	k_{wave}	1.24	[5]
Height Weibull scale parameter	c_{wave}	1.2	[5]
Wave period for fatigue	T_{wave}	$4\sqrt{H}$	Default
50 yr sig. wave height	$H_{s,50}$	11.7 m	[134]
1 yr sig. wave height	$H_{s,1}$	6.4 m	Est. [134]
Period of extreme wave	T_{ex}	$3.2\sqrt{H_s} < T_{ex} < 3.6\sqrt{H_s}$	Default
Geographical parameters			
Seabed composition	-	Sand	[201]
Distance from shore	L_{shore}	15 km	-
Distance from shore to grid	L_{grid}	5 km	-
Other-site specific parameters			
Foundation type	-	Pile	-
Water depth	d	15 m	[5]
Tidal range	d_{tide}	1 m	[5]
Surge	d_{surge}	3 m	[134]

Table 6.5: Description of the Dutch North Sea location. Where data has been estimated from the sources shown, the citation is prefixed with 'Est.'

Danish Baltic Coast location (DK)

The Baltic location is intended to represent conditions in the sheltered regions of the middle Baltic near Rostock and close to Denmark and Germany (figure 6.2), where offshore farms have been constructed and are planned. These waters are prone to icing in the winter, but any ice-loads are ignored in this analysis.

Parameter	**Symbol**	**Base value**	**Source**
Wind climate parameters			
Weibull shape parameter	k_{wind}	2.08 at 25 m	[5]
Weibull scale parameter	C_{wind}	8.7 at 25 m	[5]
50 yr extreme hourly wind	$u_{ex,50}$	36.0 m/s at 25 m	[134]
1 yr extreme hourly wind	$u_{ex,1}$	25.0 m/s at 25 m	[134]
Wave climate parameters			
Height Weibull shape parameter	k_{wave}	1.23	[5]
Height Weibull scale parameter	c_{wave}	1.0	[5]
Wave period for fatigue	T_{fat}	$4\sqrt{H}$	Default
50 yr sig. wave height	$H_{s,50}$	6.41 m	[134]
1 yr sig. wave height	$H_{s,1}$	5.41 m	Est. [134]
Period of extreme wave	T_{ex}	$3.2\sqrt{H_s} < T_{ex} < 3.6\sqrt{H_s}$	Default
Geographical parameters			
Seabed composition	-	Sand	
Distance from shore	L_{shore}	15 km	
Distance from shore to grid	L_{grid}	5 km	
Other-site specific parameters			
Foundation type		pile	
Water depth	d	14 m	[134]
Tidal range	d_{tide}	0 m	[134]
Surge	d_{surge}	2.85 m	[134]

Table 6.6: Description of the Baltic Sea location. Where data has been estimated from the sources shown, the citation is prefixed with 'Est.'

6.3 Evaluation of base case farms at base locations

6.3.1 Introduction

The model was used to evaluate the cost of energy for both medium and large scale wind farms at each of the four base case locations. No attempt was made to optimise the designs, beyond the automated procedures built into the model.

6.3.2 Overall Results

Table 6.7 shows the cost of energy predicted for the base case combinations. Figures 6.4 and 6.3 show, for the medium and large scale farms respectively, how the energy cost, and the three parameters that contribute to it vary with location. The locations in these figures are arranged in order of increasing cost of energy, shown by the thick line with circular markers. In both cases the location producing the greatest energy output provides the cheapest energy. The trends for the two farm scales are very similar.

Location	Medium base (1.5 MW)	Large base (4 MW)
UK Irish Sea (UK-IE)	3.54	3.41
UK North Sea (UK-NS)	3.84	3.66
Dutch North Sea (BE-NL)	3.27	3.27
Batic Sea (DK)	3.40	3.40

Table 6.7: Cost of energy for base case farm configurations. The two columns contain results for the medium scale and large scale base case farms with pile foundations. The values shown are in 2002 Euro cents per kWh.

The variation in investment costs clearly plays some role in the relative economics, and figure 6.5 illustrates the breakdown of the predicted investment costs by component, which should in passing be compared with figure 3.2, although this will be considered in more detail later. The base cases have been set up so that only the structure costs vary between location, and thus it is worth looking at these in more detail. Figure 6.6 shows in normalised form the variation of support structure costs with farm size and location. There is a substantial variation in cost from location to location. However, it is particularly noticable that the predicted structure investment cost is not much influenced by turbine size. The reasons underlying these results are discussed further in the following sections.

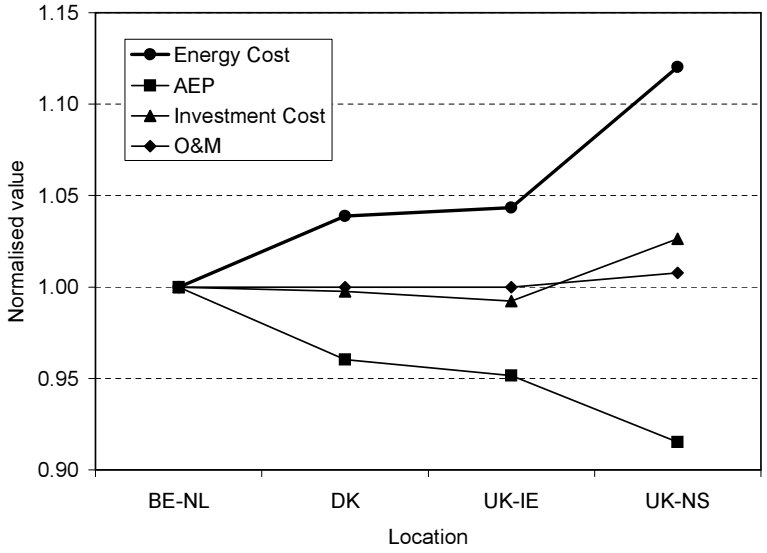

Figure 6.3: Variation of energy cost with location for large scale farms.. The values have been normalised by those for the farm producing the cheapest energy, to reveal the reasons for the change in energy cost. Note that the line labelled AEP shows the annual energy production for each farm, and that labelled O&M plots the optimal annual operation and maintenance expenditure.

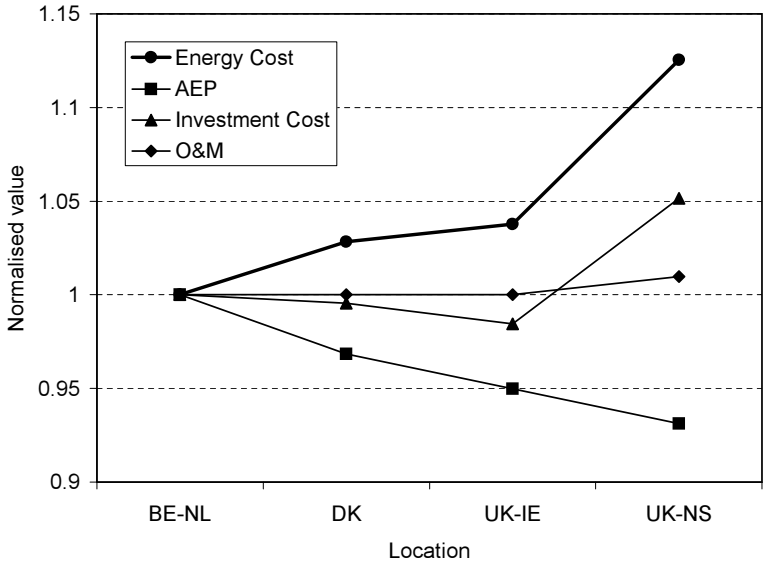

Figure 6.4: Variation of energy cost with location for medium scale farms.. The values have been normalised by those for the farm producing the cheapest energy, to reveal the reasons for the change in energy cost. Note that the line labelled AEP shows the annual energy production for each farm, and that labelled O&M plots the optimal annual operation and maintenance expenditure.

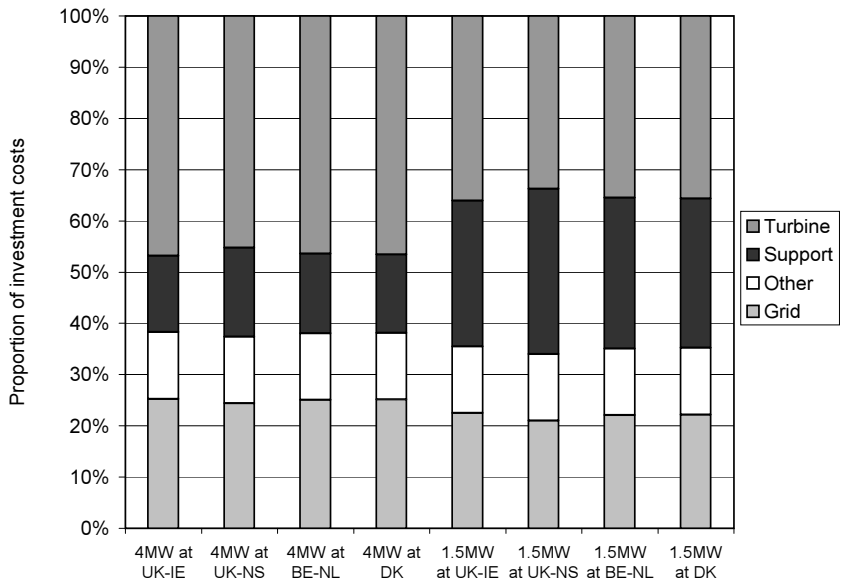

Figure 6.5: Breakdown of energy cost for the eight base case configurations.

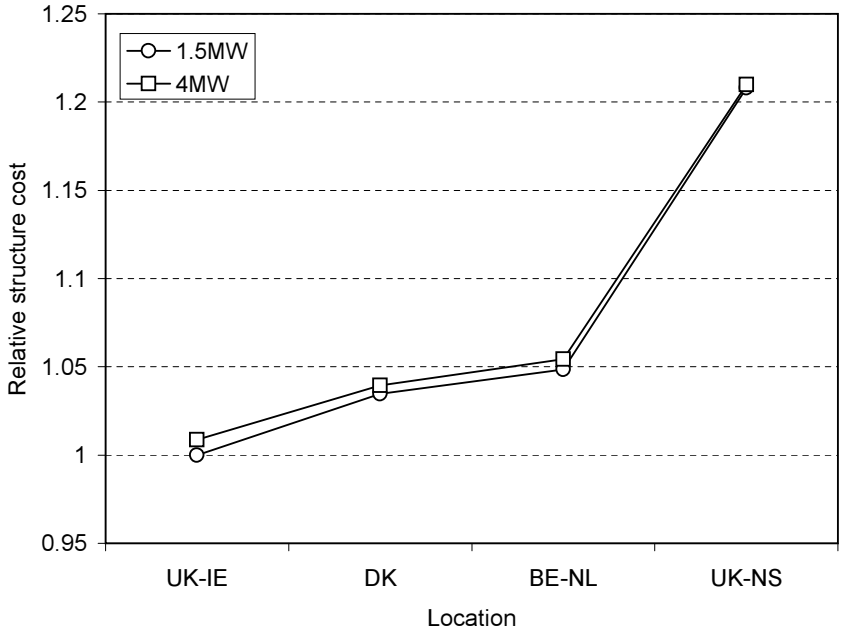

Figure 6.6: Variation of support structure cost with location. Values are normalised by the cheapest base case structure designed by the model.

6.3.3 Qualitative evaluation of overall results

Measures to formally validate the model have already been discussed. Nevertheless, It is informative to compare the overall results to the data presented in chapters 1 and 3, in order to provide a limited degree of confidence in the predictions. In doing so, it should be kept in mind that there has been no attempt to match the bases case parameters to those for the real farms considered in the earlier chapters, beyond the locations considered here being broadly representative of areas in which offshore farm construction might be feasible. In addition the costing approached were formulated assuming construction techniques suitable for farms with many turbines.

The specific investment cost predicted by the model for the base case farms lies in the range 1335 Euro/kW, for the large scale farm at the UK-IE location, to 1976 for the medium scale farm at the UK-NS location. This compares well with the range of specific investment costs displayed in figure 1.1, particularly for the more modern, larger farms.

Figure 6.7 compares the predicted specific energy cost with the predicted cost of energy, in the manner of figure 1.2. The predicted energy costs are all lower than those shown in figure 1.2, although, again, for the most modern, largest commercially oriented farm (Horns Rev), the energy cost is comparable. The capacity factors estimated by the model are larger than those achieved in practice and in part this accounts for the low energy costs. Model capacity factor estimates range between 0.36 for the large scale case at the UK-NS site, to 0.55 for the medium scale farm at BE-NL, which are towards the upper end of those in figure 1.3. In part the larger capacity factors arise because of the 80 m hub height used in the base cases, which is larger than any of the hub heights for the real farms. It is worth noting that the capacity factor of Horns Rev, with a hub height of 70 m is 0.45, which stands comparison with the model predictions for the DK site. Furthermore, the lower capacity factors of the earlier farms reflect their more experimental nature.

Another reason for the seemingly lower energy costs predicted is the scale of the base base farms, which comprise 100 turbines. As will be seen in a later section, reducing the number of turbines in the DK medium scale case to 25 produces an energy cost of approximately 4.5 Euro cents per kWh, which is more comparable with that achieved by the 20 turbine Middelgrunden farm.

Comparing the investment cost breakdowns for the modelled (figure 6.5) and real (figure 3.2) farms reveals broad comparability. The lack of clear trends in the real data makes it difficult to draw many sensible conclusions. However, grid connection costs for the modelled cases are clearly larger than in for the real farms. This is not altogether surprising as the modelled cases are much further

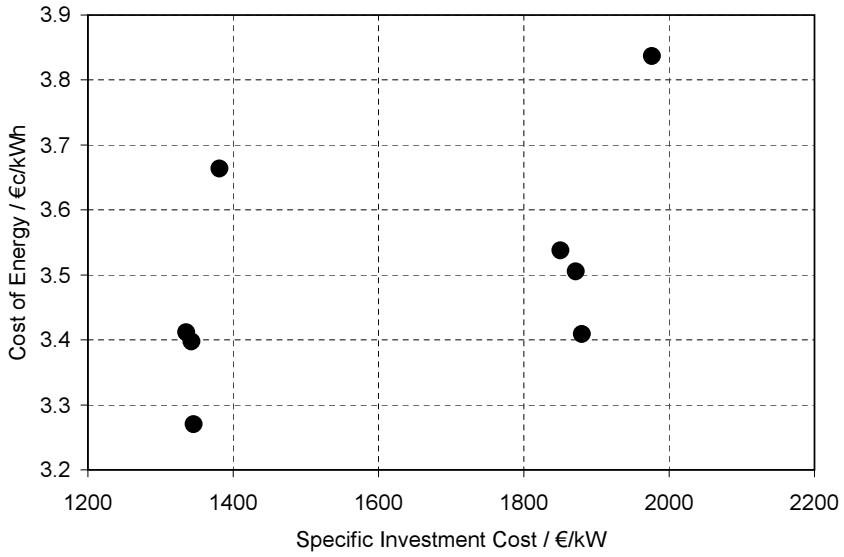

Figure 6.7: Predicted energy and specific investment costs for the base case farms and locations.

from the shore than all the real farms, with the exception of Horns Rev which has a quoted distance of 14-20 km. Modelled grid connection costs range between 21% and 25% of the total investment, while for the projects and studies the range is between 9% and 38%. Modelled support structure costs represent between 15% and 30% of the total investment, which compares reasonably well with the range from figure 3.2 of between 25% and 35%. The figure in chapter 3 also suggests that as turbine size increases, the turbine cost becomes a more dominant component of the total investment cost. This too is seen in the model predictions.

6.3.4 Further analysis of support structure results

In all the cases considered here, the smallest diameter distribution, giving the softest tower, provided the most economic solution. By way of example, figure 6.8 shows the relationship between the tower base diameter and the natural frequency for the large scale farm at the UK-NS location, taking some of the configurations considered by the model tower optimiser. Figure 6.9 shows the relationship between frequency and structure cost for the same case. Also of note from these diagrames is the very small impact of the tower top diameter on the cost and the dynamics. Similar relationships for the medium scale farm at the same location are shown in figures 6.10 and 6.11.

It is worth returning now to the small variation in support structure cost with turbine size (figure 6.6). Since the smallest diameter towers provide the cheap-

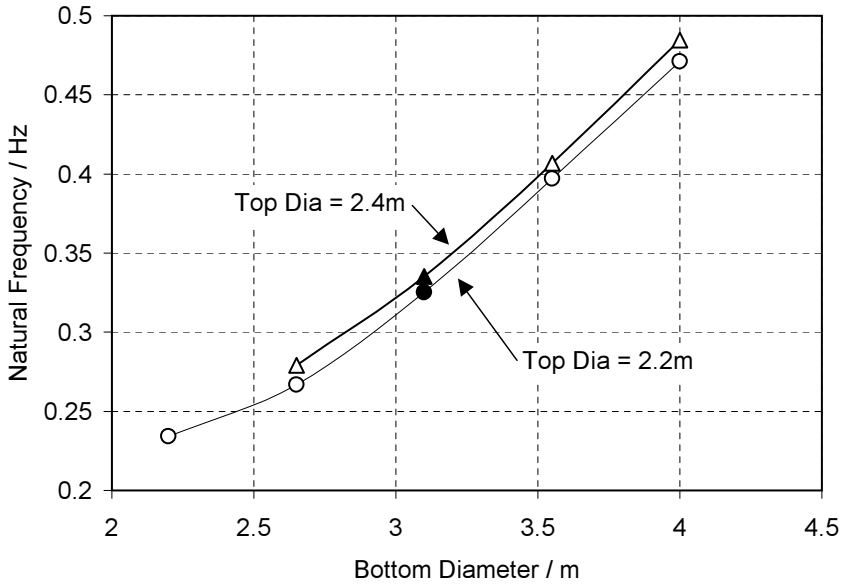

Figure 6.8: Relationship between tower bottom diameter and frequency for the large scale farm at the UK-NS location. The lower line shows the relationship for a tower top diameter of 2.2 m, with the upper diameter giving that for a 2.4 m top diameter. Some of the support structures considered exhibited resonance, with these being denoted by the filled symbols.

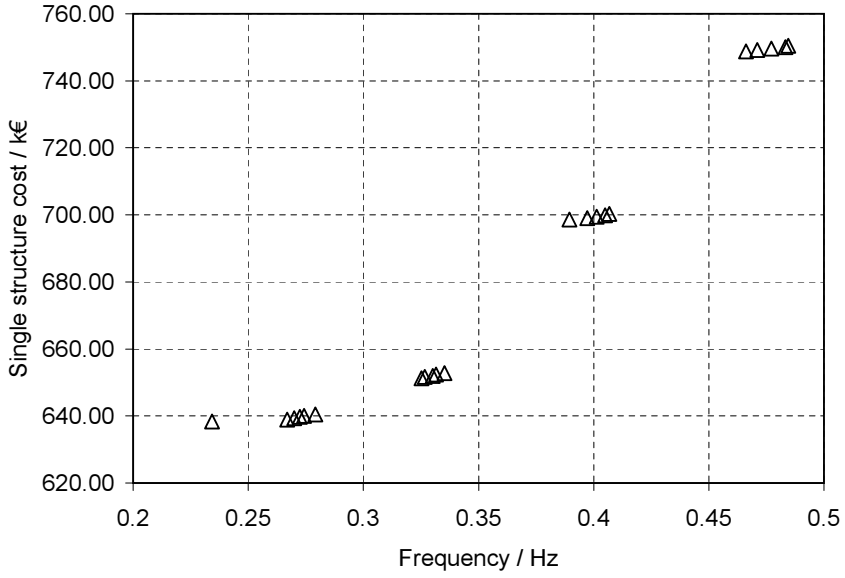

Figure 6.9: Relationship between tower frequency and cost for large scale UK-NS case, showing all cases investigated by the model tower optimiser. The clusters of points represent increasing tower base diameter, with the points in each cluster denoting the effect of changing the tower top diameter.

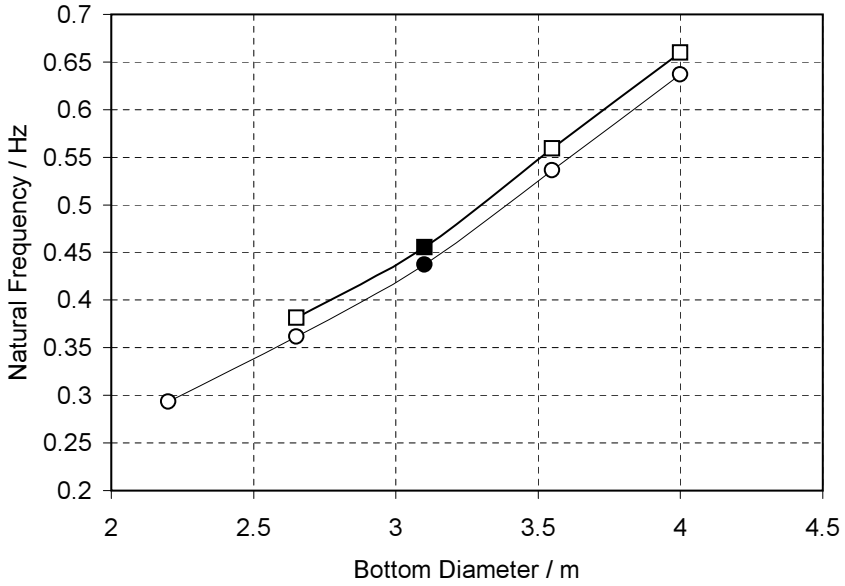

Figure 6.10: Relationship between tower bottom diameter and frequency for the medium scale farm at the UK-NS location. The lower line shows the relationship for a tower top diameter of 2.2 m, with the upper diameter giving that for a 2.4 m top diameter. Some of the support structures considered exhibited resonance, with these being denoted by the filled symbols.

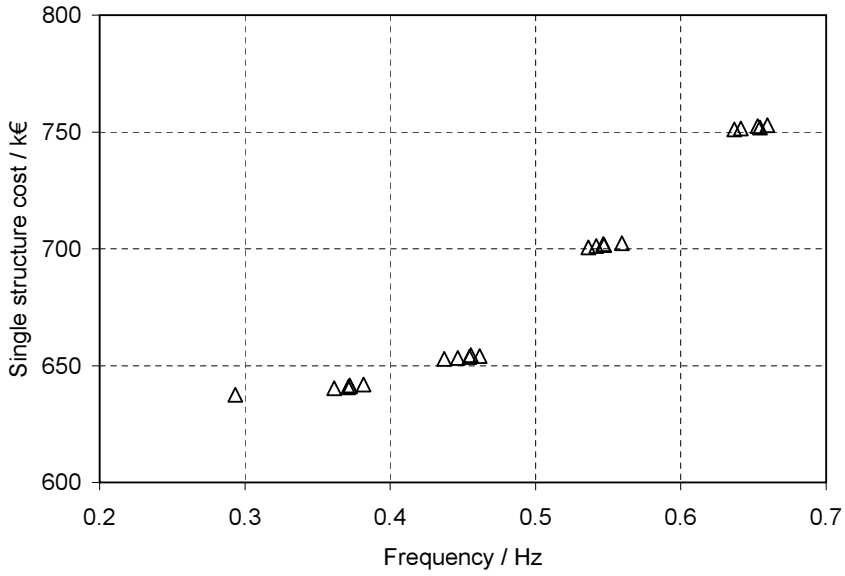

Figure 6.11: Relationship between tower frequency and cost for medium scale UK-NS case, showing all cases investigated by the model tower optimiser. The clusters of points represent increasing tower base diameter, with the points in each cluster denoting the effect of changing the tower top diameter.

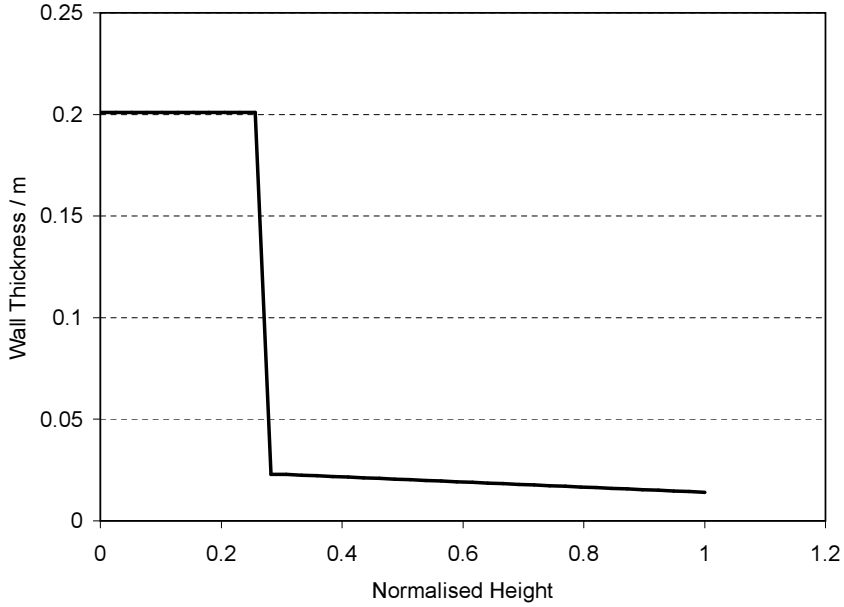

Figure 6.12: Sample tower wall thickness variation.

est design, and there were no resonance issues at these diameters, the optimal outer diameter profiles identified by the model were the same for each turbine. Figure 6.12 shows the outer diameter profile for the large scale UK-NS base case. The only scope for cost differences therefore lies in the pile design and the wall thickness.

The pile design was dominated by wave loading and certain manufacturing/installation constraints imposed on the dimensions. Since the optimum outer diameter distribution proved to be the same irrespective of the turbine selected, the wave loads were also unaffected by the turbine choice. Thus the foundation design was barely affected by the turbine choice. For the cases considered here it turned out that the tower wall thickness was driven, in the upper sections by buckling considerations, with only sections closer to the sea level driven by bending derived from turbine extreme loads. As a result, wall thickness distributions were only slightly increased for the large scale farms in comparison to the medium scale machines. Fatigue was not found to be a significant driver of any of the exposed tower sections for the base case conditions and parameters used here. For these reasons, the structure cost did not vary greatly with turbine choice.

6.4 Sensitivity

In subsequent sections the cost model is used for a series of studies that investigate the sensitivity of the base case results to changes in some of the cost model input parameters. The sensitivity of a value C to a parameter p is defined here as $\frac{1}{C}\frac{dC}{dp}$. The calculated sensitivities can be used to:

- Assess the relative importance of the parameter for the design or site selection process,
- Estimate the uncertainty in a calculation due to uncertainties in the parameters, and
- Estimate the impact of changing a parameter on a calculated value.

For some of the parameters, values can vary over a wide range. In some of these cases sensitivites are evaluated at more than one value to assess if the importance varies over the range of values.

6.5 Parameter studies on energy production alone

The cost model was initially used for a series of studies that investigate the impacts of parameter changes on energy production alone, and in particular:

- Hub height, at three values of hub height
- Charnock constant
- Scale parameter for the wind Weibull distribution C
- Shape parameter for the wind Weibull distribution k

Detailed results are shown in appendix O, with the sensitivity of the energy production to the changes provided in table 6.8.

The first conclusion from the study is the very limited impact of the Charnock constant. As the sensitivities and data in the appendix indicate, varying the value between 40 and 80 had a less than 2% impact on the annual energy production in all cases. For the calculation of the annual energy production from an offshore wind farm detailed evaluation of local wind-wave interaction is not important therefore. The sensitivity of energy production to hub height changes shows the expected form, with the sensitivity decreasing as the hub height is raised due to the wind profile. Perhaps more surprising is the magnitude of the sensitivites, as the energy production is relatively insensitive to the hub height.

Case	Shape	Scale	Charnock	hh(60)	hh(80)	hh(100)
4MW at UK-IE	0.18015	0.12039	-0.00038	0.00298	0.00211	0.00161
4MW at UK-NS	0.09709	0.15986	-0.00042	0.00332	0.00236	0.00181
4MW at BE-NL	0.13911	0.13089	-0.00040	0.00311	0.00221	0.00169
4MW at DK	0.13136	0.14760	-0.00041	0.00322	0.00228	0.00175
1.5MW at UK-IE	0.19540	0.09874	-0.00033	0.00268	0.00190	0.00146
1.5MW at UK-NS	0.13518	0.13039	-0.00037	0.00293	0.00209	0.00161
1.5MW at BE-NL	0.15584	0.10561	-0.00037	0.00277	0.00197	0.00151
1.5MW at DK	0.14292	0.11754	-0.00036	0.00285	0.00203	0.00156

Table 6.8: Sensitivity of annual energy production to changes in parameters. The first column provides the case considered, with '4MW at UK-IE' referring to the base case farm of 4 MW turbines located as the base case UK Irish Sea site. The columns labeled 'hh' provide the sensitivity to changes in hub height, with the number in brackets repesenting the hub height at which the evaluation was carried out.

Unsurprisingly, it is the wind resource, represented by the shape and scale parameters that has by far the strongest influence on the annual energy production, confirming the general trend from the data anaysed in chapters 1 and 3 that good wind resources are important in producing a farm with good economics. Comparing the sensitivities demonstrates that an increase of 0.05 in scale factor provides an improvement in energy production equivalent to an increase in hub height of between 2.6 m and 3.4 m depending on the case (table 6.9). The same increase in the shape factor is equivalent to an increase in hub height of between 1.9 m and 4.3 m.

The extent to which it is worth increasing the hub height at any location in order to improve the energy output depends on the impact on the capital cost which will be considered in the next section.

6.6 Climate parameter studies

Investigation of the impacts of changes in climate parameters is useful to gain insight into the types of location that might be best suited for economic offshore farms. Tables 6.10 and 6.11 list the sensitivity of the cost of energy to changes in climate and other location oriented parameters, with plots of the relevant studies provided in appendix O.

The tables shows that the unit changes in the wind climate parameters have by far the strongest influence on the cost of energy. The values in table 6.11 account for consequent changes in the 50 year and 1 year return period wind speeds

Case	Increased scale parameter	Increased shape parameter
4MW at UK-IE	2.86	4.27
4MW at UK-NS	3.39	1.92
4MW at BE-NL	2.96	3.15
4MW at DK	3.24	2.88
1.5MW at UK-IE	2.60	5.14
1.5MW at UK-NS	3.12	3.23
1.5MW at BE-NL	2.68	3.95
1.5MW at DK	2.90	3.52

Table 6.9: Hub height increase in metres giving an improvement in annual energy output equivalent to a 0.05 increase in the shape and scale parameters for each base case.

Case	$u_{ex,50}$	$u_{ex,1}$	$H_{s,50}$	$H_{s,1}$	d
4MW at UK-IE	5.96×10^{-4}	3.14×10^{-5}	0.0	0.0	3.28×10^{-3}
4MW at UK-NS	1.44×10^{-4}	6.84×10^{-5}	9.65×10^{-3}	0.0	8.07×10^{-3}
4MW at BE-NL	3.35×10^{-4}	0.0	0.0	0.0	4.25×10^{-3}
4MW at DK	2.93×10^{-4}	0.0	0.0	0.0	3.34×10^{-3}
1.5MW at UK-IE	5.96×10^{-4}	3.4×10^{-5}	0.0	0.0	3.28×10^{-3}
1.5MW at UK-NS	1.75×10^{-4}	3.4×10^{-6}	1.75×10^{-2}	0.0	1.47×10^{-2}
1.5MW at BE-NL	3.91×10^{-4}	0.0	0.0	0.0	7.98×10^{-2}
1.5MW at DK	3.96×10^{-4}	0.0	0.0	0.0	6.35×10^{-2}

Table 6.10: Sensitivity of cost of energy to changes in climate and location parameters. The first column provides the case considered, with '4MW at UK-IE' refering to the base case farm of 4 MW turbines located at the base case UK Irish Sea site.

Case	C_{wind}	k_{wind}	C_{wave}	k_{wave}	T_{ex}
4MW at UK-IE	-0.124	-0.189	0.0	0.0	0.0
4MW at UK-NS	-0.168	-0.111	0.0	0.0	0.038
4MW at BE-NL	-0.136	-0.145	0.0	0.0	0.0
4MW at DK	-0.152	-0.128	0.0	0.0	0.0
1.5MW at UK-IE	-0.134	-0.210	0.0	0.0	0.0
1.5MW at UK-NS	-0.134	-0.133	0.0	0.0	0.070
1.5MW at BE-NL	-0.136	-0.161	0.0	0.0	0.0
1.5MW at DK	-0.121	-0.148	0.0	0.0	0.0

Table 6.11: Sensitivity of cost of energy to changes in climate parameters.

resulting from changes in the wind climate. In all cases, the cost of energy would be reduced with a higher mean annual wind speed, despite increases in the structure costs.

Unit changes in water depth have the next most strong influence on the cost of energy at any location. The reason for this is easy to understand, as increased depth requires a greater overall support structure height, but with no increase in energy production. However the difference in sensitivites between the wind and water depth suggests that it is very much a secondary consideration.

The extreme conditions have a surprisingly limited influence on the cost of energy, and their importance varies from case to case depending on which of the load cases has a role in driving the design. The 50 year return period extreme wind speed has an influence on all the cases considered. The 1 year return significant wave has no influence on any of the cases. Together, these two values form the offshore wind oriented load case established earlier. The results show that this load case is indeed important and is dominated by the wind loads.

The conventional marine load case comprises the 1 year extreme wind speed and the 50 year return significant wave height. For the most part, these values have very little impact on the cost of energy, and can essentially be ignored in site selection. However they clearly, can have an impact on support structure design, as the impact on the cost of energy is through increased support structure costs. Thus the marine load case is still important for support structure design.

6.7 Overall WECS configuration

Parameter studies investigated the sensitivity of the cost of energy to changes in three overall farm parameters, specifically,

- Distance from the shore L_{shore}, in kilometers,
- No of turbines in farm N_t,
- Hub height h_{hub}, in meters above mean sea level.

Table 6.12 shows the sensitivity for all the eight base cases considered. Detailed plots of the studies underlying the sensitivity calculations are shown in appendix O.

6.7.1 Distance to shore

The distance to shore exhibits the greatest sensitivity of the three parameters studied in this section, such that moving the 1.5 MW turbine based farm just a kilometer closer to shore could reduce the energy cost by approximately 0.7%. The

Case	N_t	h_{hub}	L_{shore}
4MW at UK-IE	-0.00054	-0.00182	0.0044
4MW at UK-NS	-0.0031	-0.00167	0.0043
4MW at BE-NL	-0.00054	-0.00194	0.0044
4MW at DK	-0.00054	-0.00205	0.0044
1.5MW at UK-IE	-0.00097	-0.00143	0.0071
1.5MW at UK-NS	-0.00091	-0.00161	0.0067
1.5MW at BE-NL	-0.00096	-0.00159	0.0070
1.5MW at DK	-0.00096	-0.00168	0.0070

Table 6.12: Sensitivity of cost of energy to changes in overall parameters. The first column provides the case considered, with '4MW at UK-IE' refering to the base case farm of 4 MW turbines located at the base case UK Irish Sea site.

reduction in energy cost arises from a cheaper grid connection, improved availability thanks to reduced travel time for the maintenance crews, and in cases, slightly reduced optimal annual maintenance expenditure.

6.7.2 Number of turbines

For the configurations investigated the cost of energy was surprisingly insensitive to the number of turbines. In most cases, adding or subtracting 10 turbines from the farm has a less than 1% impact on the energy cost. The sensitivities in the table are calculated from excursions to 75 and 125 turbines from the base case farm size of 100 turbines.

The sensitivity, however, is rather dependent on the number of turbines in the farm. Studies for the 1.5 MW base cases indicated that reducing the number of turbines to 25 gave an increase of 30% in the energy cost. Figure 6.13 shows the wider parameter studies.

6.7.3 Hub height

The sensitivity of cost of energy to the hub height lies between the other two parameters considered here, with the cost of energy slowly reducing with increasing hub height. A 10m increase in hub height provides, at most a 2.05 % reduction in energy cost. This, perhaps surprisingly low sensitivity, appears to arise because for small hub height excursions at least, the tower cost and the energy production change by approximately the same proportion.

Extending the parameter studies to larger hub heights reveals that the increasing tower costs begin to out strip the increase energy production, and there is ev-

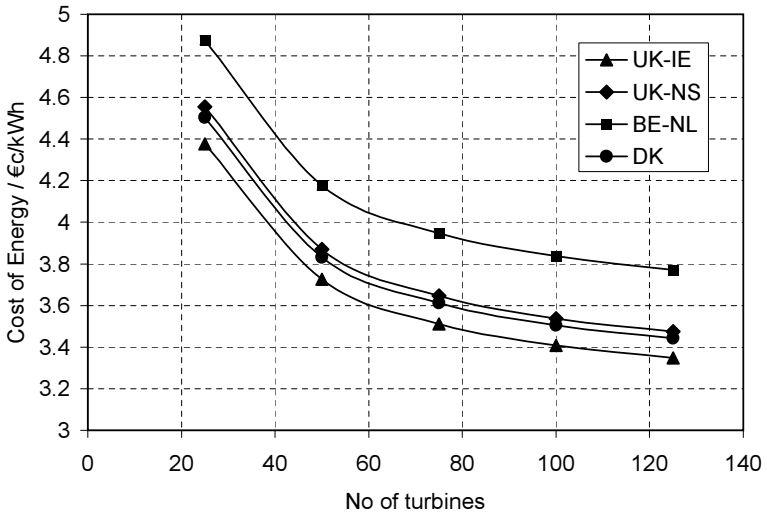

Figure 6.13: Effect of number of turbines on energy cost for 1.5 MW base case farms.

idence of an optimum hub height, considerably higher than the base case value of 80 m. Figure 6.14 shows the behaviour for the 1.5 MW base case at the BE-NL location, with figure 6.15 displaying results for the 4 MW base case at the same site. Optima are visible at hub heights of approximately 130 m and 160 m respectvially. Studies at the other locations reveal that the hub height optima vary with the site conditions. It is not instructive to consider the optima in any detail because the the cost model does not account for any changes in installation costs associated with much taller towers, and thus the numerical values are unlikely to be realised in practice. The identified reduction in cost by using an optimum hub height rather than the base case value barely exceeds 5% in any of the cases, and this is likely to be offset by increased installation costs.

The low sensitivity of the cost of energy to hub height, at least at the base case value of 80 m is an important result. There will be little economic benefit in farm developers considering taller support structures.

6.8 Summary of chapter

In this chapter, the utility of the cost model was demonstrated by the detailed examination of 8 base case offshore wind farm configurations. The results agreed, in qualitative terms with data from real farms presented in earlier chapters. Differences in the concept of the farms treated by the model, and the real farms for which data was avalable meant that only qualitative comparisons were practical.

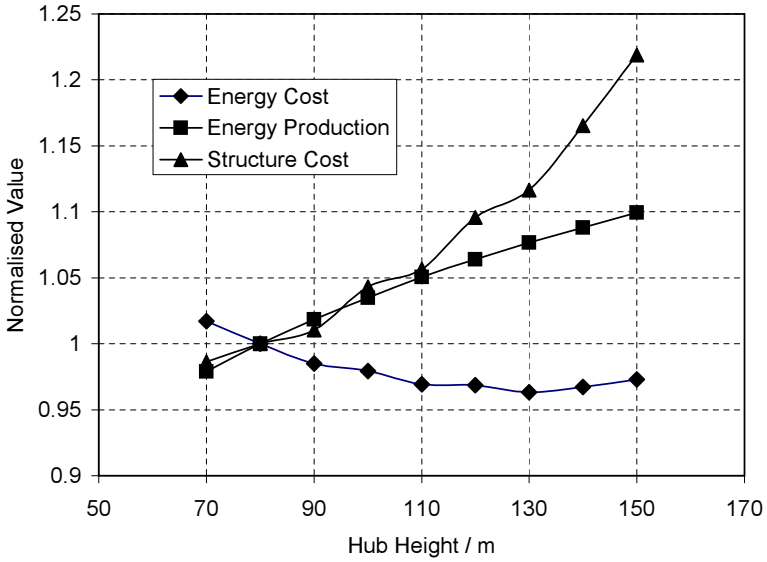

Figure 6.14: Effect of hub height on energy cost for 1.5 MW farm at BE-NL.

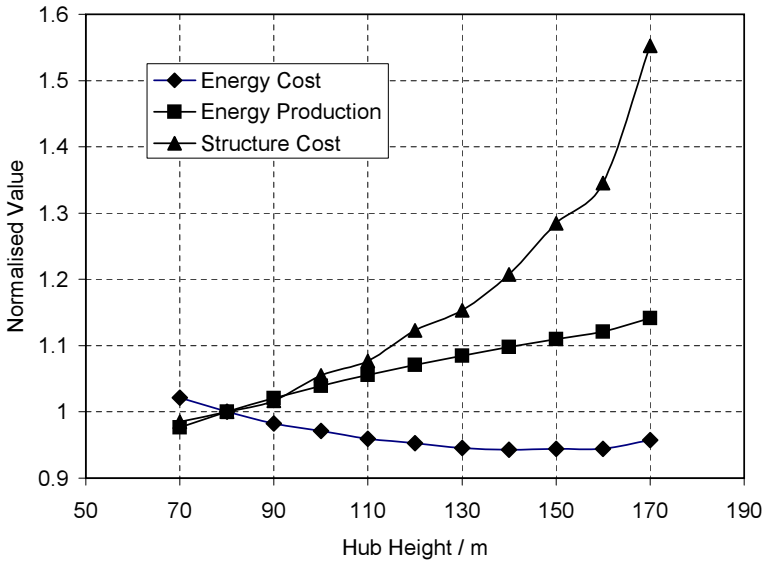

Figure 6.15: Effect of hub height on energy cost for 4 MW farm at BE-NL.

Model predictions from the base cases also suggested that the annual mean wind speed at a location was likely to be the overwhelming driver of the energy cost.

A series of studies further probed the sensitivity of the energy cost to parameter changes. It was confirmed that the annual mean wind speed was the most important driver, suggesting that all other climate parameters can largely be ignored in site selection, at least for small excursions around the base case values. Mean sea level (depth) has the next most important influence on the energy cost, but its impact is small compared to the annual mean wind speed.

The extreme wind speeds and wave heights were found to have a surprisingly limited impact on the cost of energy. In general the most important was the 50 year return period extreme wind speed, which influenced every case considered. The least important was the 1 year return period significant wave height, which had no impact on any of the cases considered.

In general, changes in the wave climate in general were found to have very little impact on the cost of energy. Further examination of the results reveals the reason for this insensitivity. The wave climate parameters C_{wave} and k_{wave} are only able to influence the pile wall thickness, and in all the cases considered here, the wall thickness was driven either by extreme loads or by a minimum wall thickness specified to ensure the pile remains intact during the driving process. Thus the wave climate parameters have no impact on the design of the base case piles, for the ten percent parameter excersions reported here. It is worth noting that very large increases in the wave shape parameter, doubling its value, did impact on the cost of energy, although these results are not reported here for reasons of brevity.

The overall configuration of the offshore farm does of course influence the cost of the energy produced. For large farms, the cost of energy is not very sensitive to the total number of turbines deployed. However, for small farms the sensitivity is greatly increased. Evidence was found that the optimum hub height for most offshore farms may be substantially larger than the 80m assumed for the base case. Limitations with the model meant that exact values could not be sensibly established. Distance to shore is also an important parameter, thanks both to the impact on the grid connection cost and the implications for maintenance expenditure and availability.

Chapter 7

Integrated GIS Survey - Approach

7.1 Objectives

The cost model facilitates parameter studies based on engineering and environmental parameters. While engineering parameters can be varied arbitrarily, the environmental parameters that influence the design of a real farm occur only in combinations that are characteristic of the locations considered.

Geographical Information Systems (GIS) simplify the management of spatially varying data to the extent that it is practical to perform parameter studies for whole areas at a time. This potentially has many advantages for design and site selection purposes. By way of example, contour maps may be produced showing how the cost of energy varies as a function of location for different design concepts, allowing rapid identification of economically attractive locations and the technologies best suited to them.

The GIS based approach has been adopted here. This chapter describes the methodology, including the construction of an offshore database, and the means by which a simplified version of the cost model and the GIS have been coupled. The following chapter discusses the results of studies undertaken with the system to investigate the design and economics of farms based around both the turbines featured in the cost model.

The work developed in this chapter is concentrated on the waters of the UK shown in figure 7.1. Despite this focus, the methodology and numerical tools developed are general and could be applied to any region for which suitable data was available. It should be kept in mind however that the cost estimates used in this thesis were formulated for Northern European practice and may need to be revised for application to other parts of the world.

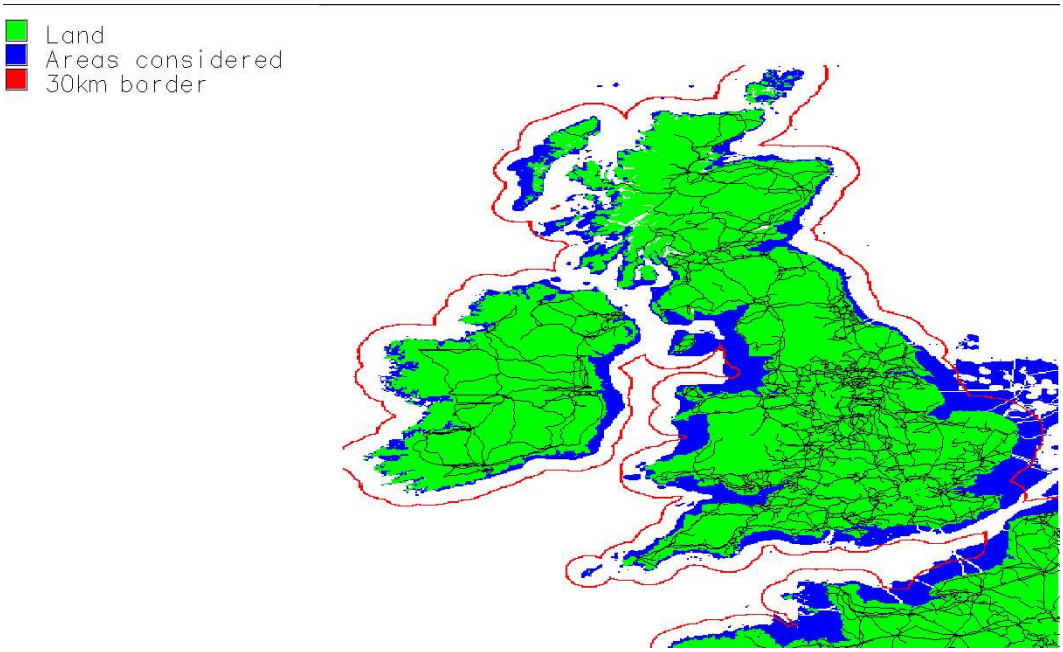

Figure 7.1: Areas potentially available for bottom mounted offshore farms around the UK region, showing 30 km distance from shore to provide an idea of scale. Black lines over the land area represent high voltage transmission lines. The potential areas exclude locations with the constraints listed in table 7.6

7.2 Selection of GIS

A GIS is essentially a combined electronic map and database. Data representing different types of physical features are stored in separate layers. The GIS can return the value in each layer as a function of geographical location. Most systems can process data in two formats: raster and vector. With raster data, the domain of interest is subdivided into a large number of smaller areas on a grid pattern, and each element of the grid is allocated a value representing the property concerned over the whole element. Vector formats represent spatial information as a set of defined points together with information on how those points are connected to form lines, polygons and other features. The GIS database queried by the model comprises raster data entirely, although vector information has been used in the construction of the database.

The open source GIS "GRASS" [202] was adopted for the implementation here thanks to the possibility of integrating the cost model code with the GIS. A number of other systems were used during preparation of the data, particularly ESRI ArcView [203] and IDRISI [204].

7.3 Approach

It was originally planned to integrate the cost model directly with the GIS. The long run times, of several minutes per case, made this impactical as it would have taken many days to have computed cost maps for a single region. Instead a simplified version of the model was constructed.

Thanks to difficulties in devising reliable means to interpolate the available data, analysis has been confined to areas surrounding the two UK base case location discussed in the previous chapter. The areas considered are discussed in more detail in section 7.6. For current purpose however, it is sufficient to note that the constrained analysis area means that conditions do not vary greatly from those in the two UK base cases. The approach therefore is built around calculating deviations in cost from the base case solutions of chapter 6.

7.3.1 Energy production

Using the main cost model, a series of parameter studies were undertaken for the four combinations of base case wind farm and UK location, calculating the annual energy production as a function of annual mean wind speed at 60 m, $\bar{u}_{60}$. The wind speed at 60 m was employed simply because that was the value specified in the database of offshore conditions used for the analysis, and as windshear

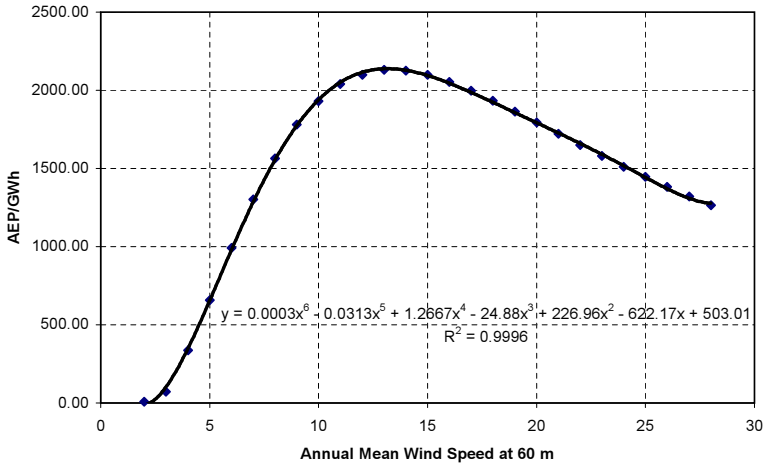

Figure 7.2: Polynomial fit to the annaul energy production data for the 4 MW turbine at the UK Irish Sea location.

is accounted for in the main model this height is of no real significance. The Weibull shape and normalised scale parameters were held constant at the base case values, together with a Charnock constant of 60.

It was found that the relationship between the annual mean wind speed at 60 m and the annual energy output could be well approximated by fitting a polynomial to the sixth power of the annual mean wind speed. Figure 7.2 shows the data and fitted curve for the 4 MW farm at the UK Irish sea location with 80m hub height, by way of illustration.

The fitted curves are for the UK Irish sea case with 4 MW turbines:

$$AEP = 0.0003\bar{u}_{60}^6 - 0.0313\bar{u}_{60}^5 + 1.2667\bar{u}_{60}^4 - 24.88\bar{u}_{60}^3 + 226.96\bar{u}_{60}^2 - 622.17\bar{u}_{60} + 503.01 \tag{7.1}$$

for the UK Irish sea case with 1.5 MW turbines:

$$AEP = 0.0001\bar{u}_{60}^6 - 0.0121\bar{u}_{60}^5 + 0.4801\bar{u}_{60}^4 - 9.1478\bar{u}_{60}^3 + 78.621\bar{u}_{60}^2 - 166.89\bar{u}_{60} + 103.11 \tag{7.2}$$

for the UK North sea case with 4 MW turbines:

$$AEP = 0.0006\bar{u}_{60}^6 - 0.0579\bar{u}_{60}^5 + 2.1824\bar{u}_{60}^4 - 38.889\bar{u}_{60}^3 + 307.88\bar{u}_{60}^2 - 635.64\bar{u}_{60} + 342.8 \tag{7.3}$$

and for the UK North sea case with 1.5 MW turbines:

$$AEP = 0.0002\bar{u}_{60}^6 - 0.0219\bar{u}_{60}^5 + 0.8118\bar{u}_{60}^4 - 14.051\bar{u}_{60}^3 + 104.24\bar{u}_{60}^2 - 149.3\bar{u}_{60} + 41.338. \tag{7.4}$$

The expressions above do not account for any losses. Array losses were accounted for in the GIS calculations using the array efficiencies computed by the cost model for the two base case farms. The impact of availability on the energy output was also accomodated using the predictions of the maintenance model on a site by site basis.

7.3.2 Grid connection cost

The main cost model routines were used directly drawing on data layers detailing the distance to shore. It is assumed that offshore cables are built in a straight line to the nearest shore. As the cost of any land based portion of the grid connection is relatively small, and in view of the fact that none of the shores are very far from grid connections, the costs predicted by the GIS are only for delivery of power to the beach.

7.3.3 Support structure cost

Support structure design is the most time consuming part of the model. To speed the GIS calculations the support structure cost was estimated by assuming linear variation from the base case drawing on sensitivites derived from the studies in the previous chapter, that is

$$\Delta C = C_{base} + \sum_i \left(\frac{dC}{dp_i}\right)_{base} \Delta p_i \tag{7.5}$$

where

C_{base} Cost of base case support structure
p_i Parameter influencing support cost.

Changes in the following parameters are accounted for

- Water depth
- Mean wind speed
- Hub height.

In practice, thanks to the simple modelling of wave propogation included in the main cost model, changes in the water depth implicitly account for the effects of wave shoaling and breaking. For the studies, the model was set to estimate the extreme conditions from the Weibull parameters, and thus changes in the extreme conditions are also accounted for implicitly.

This approach of course constrains the analysis to regions for which sensitivites have been established. As discussed later, the base cases in chapter 6 were in fact chosen so as to form a basis for the analysis described here.

7.3.4 Maintenance cost and availabilty

The main cost model routines were employed directly to estimate the farm availability on the basis of the distance to the shore and the annual maintenance spend.

7.3.5 Integration

Separate GIS raster layers detailing the investment cost, the annual energy production and the annual on-going costs are calculated, and then combined using a discounted cash flow routine of the form described in chapter 3. As elsewhere, the calculations assumed a lifetime of 20 years and a discount rate of 5%, and include 'other' costs comprising 13% of total investment.

7.4 Data requirements

The minimum set of environmental data required to estimate the cost of energy at each location is listed in table 7.1.

Type of data	Comments
Climate description	Required for the energy production calculations. Fixed at the base case value for the structural calculations as described in the text, except for the annual mean wind speed.
Water depth	Influences the support structure cost only.
Distance from shore	Required for estimation of maintenance cost.
Route to grid connection point	Comprising on-shore distance and offshore distance, to estimate grid connection costs.

Table 7.1: Data to be supplied to the cost model by the GIS.

7.5 JOUR0072 GIS Database

A CEC Joule [5] supported project developed a GIS database of information relevant to offshore wind energy across the entire EU, including the data shown in table 7.2.

Data	Comments
Water depth	Taken from digital and printed marine charts, with some post-processing to produce a 'smooth' contour map.
Mean wind speed at 60m above MSL	Produced by combining WASP [205] calculations for the coastal resource with voluntary observer fleet data for the open sea. Wind speed variations reflect the influence of the coast (in an approximate manner).
Seabed slope	Calculated from the water depth map. The coarse resolution means that these values are only a guide to the slope.
Land	Location of land masses A few errors in the land database were detected and corrected.
Location of obstacles	Substantial but incomplete coverage of shipping lanes, military zones, existing cables/pipelines, oil platforms, conservation areas.

Table 7.2: Data provided by the JOUR0072 [5] database.

The database was obtained from Garrad-Hassan and used as a basis for this work. Data was received in a format compatible with the IDRISI system, and subsetted on a country by country basis. It was first converted to be compatible with GRASS, and then the separate data segments were joined to form the regions of interest defined in section 7.1. All the data sets are in raster format, distributed over a grid with 30 cell divisions per degree of longitude and 50 divisions per degree of latitude. Thus the spatial East-West resolution of the data decreases towards the south, from 1.88 km at the north of Scotland to 2.71 km in the French Adriatic. Since meridians of latitude have constant spacing, the North-South resolution remains at approximately 2.2 km throughout. Except where noted, additional raster data generated for the analysis described here maintains this resolution.

7.6 Treatment of climatic conditions

7.6.1 Climatic description

The JOUR0072 database itself contains no information on the time variation of the wind speed or the sea state. To allow more representative calculations, Weibull parameters for distributions approximating the local wind speed and significant wave height variations are required.

7.6.2 Additional sources of information

An analysis performed by DWD [206] of forty years of data collected from voluntary observer fleet (VOF) ships produced wind and wave Weibull parameters for fifty-five European coastal areas. The data points provide fair coverage of the areas available for offshore farms, and reflect the impact of the nearby coast on the conditions.

The DWD data is the result of analysing information reported by ships located over several degrees of latitude and longitude, and thus are representative of 'average' coastal conditions over a wide area. The specific position associated with each data point has been calculated by averaging the co-ordinates of the locations from which each measurement was reported. Since most observations are made by vessels in shipping lanes, these average locations generally lie close to shipping lanes. According to DWD, the climate values are representative of conditions at a distance from the shore equal to the distance of the averaged point from the shore.

In a few locations, where the coastline is particularly convex, the averaged position is on land. For such cases DWD suggest that the values be taken as representative of nearby shipping lanes, where the majority of the traffic will have passed through. Where averaged positions very close to or on land were found, these have been 'corrected' by hand. The arc subtended at the averaged position by the region over which the data has been averaged was identified, and the data point replaced at the intersection of the bisector of the arc and the nearby shipping lane. The whole corrected data set as relevant to this study is shown in figure 7.3.

7.6.3 Comparison and validity assessment of the data

To provide some indication of the validity of the data set, it was checked against other published sources. A recent offshore technology report [207] presented wave height and wind speed exceedences and scatter diagrams based on nine years of hindcast data produced by the NEXT model for forty sites around the UK. A selection of these sites is also shown in figure 7.3. Weibull distributions were fitted to the NEXT data in such a way as to be compatible with the DWD data. Since the DWD data was derived for a 25 m height above MSL, this also involved scaling the NEXT data from a height of 10 m. The entire procedure is presented in Appendix P.

There are three places around the UK where the NEXT and DWD sourced data lie within 40 km of each other. The estimated wind and wave conditions at these locations from the different sources are compared in table 7.3 and 7.4.

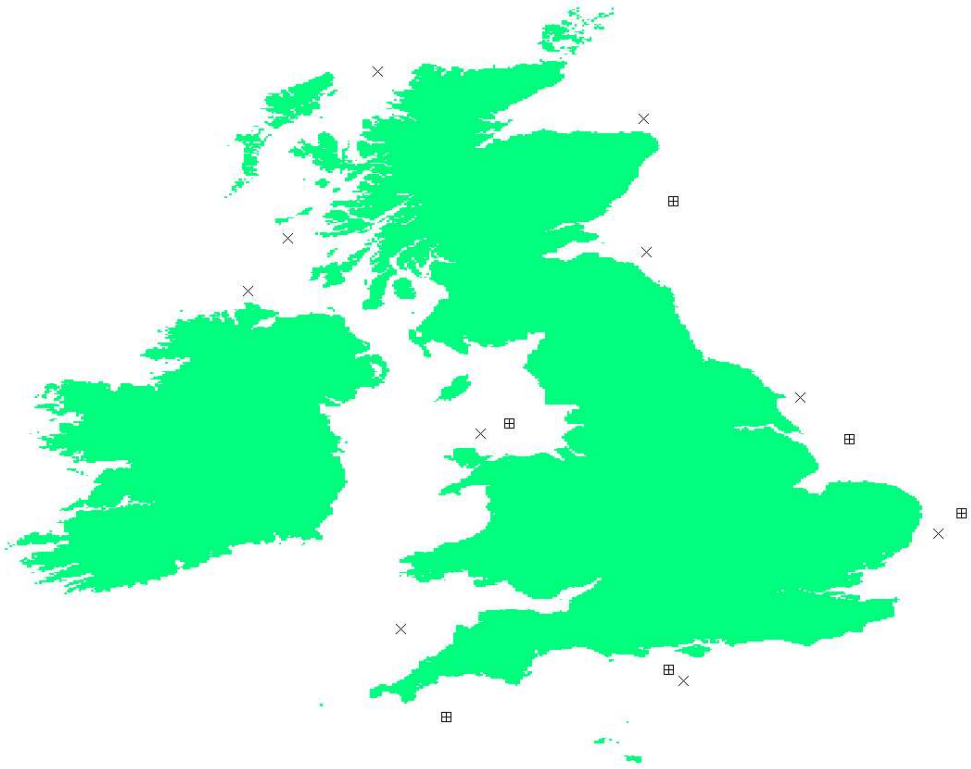

Figure 7.3: Climate data points for the UK region. Simple crosses represent DWD derived data, whereas boxed pluses represent the location of NEXT Data.

Estimates for 50 year extreme values are based on the Weibull parameters using the methodology in chapter 4 and are compared to values taken from UK Department of Energy guidance [137].

k		c		Mean		Extreme			Ref. No.	
NEXT	DWD	NEXT	DWD	NEXT	DWD	NEXT	DWD	DOE	NEXT	DWD
2.40	1.96	1.13	1.13	8.70	7.51	32.3	34.0	35.0	15697	46
2.21	1.93	1.13	1.13	8.36	7.96	33.7	36.0	36.6	16357	60
2.18	1.83	1.13	1.13	8.50	7.91	33.0	39.0	35.8	15920	58

Table 7.3: Comparison of wind speed distribution data at 25 m above MSL. The extreme values represent 50 year return period hourly values. k and c represent Weibull shape and normalised scale parameters respectively. The Ref. No. column identifies the location of each point using the referencing system in the original source.

k		c		Mean		Extreme			Ref. No.	
NEXT	DWD	NEXT	DWD	NEXT	DWD	NEXT	DWD	DOE	NEXT	DWD
1.48	1.20	1.11	1.10	1.21	1.04	6.4	8.0	8.5	15697	46
1.29	1.28	1.08	1.08	1.16	1.30	8.2	9.0	8.5	16357	60
1.32	1.31	1.09	1.08	0.99	1.11	6.8	8.0	7.0	15920	58

Table 7.4: Comparison of significant wave height distribution data. The extreme values represent 50 year return period heights. k and c represent Weibull shape and normalised scale parameters respectively. The Ref. No. column identifies the location of each point using the referencing system in the original source.

Many of wave climate parameters compare well. The wind parameters do not compare as well. The shape parameter and mean wind speed are consistently larger for the NEXT data than for the DWD derived information.

At other locations, extreme values predicted from the DWD data were compared to Department of Energy information with the outcome shown in tables 7.5. In general both the DWD data underpredict the extreme values compared to the Department of Energy data, but this is only to be expected as the calculation estimates extreme values from the Weibull parameters.

7.6.4 Wave periods

Wave periods do not directly influence the GIS calculations, since any assumptions are encapsulated in the cost model calculations of chapter 6. To repeat the assumptions set out in section 4.8.2 for fatigue evaluations, equation 4.44, that is

$$T = K\sqrt{H} \tag{7.6}$$

Wave			Wind			DWD Ref
DWD	DoE	Difference	DWD	DoE	Difference	
8	8	0	33	35	-2	34
10	8	2	36	37	-1	35
10	8	2	34	37	-3	36
10	9.5	0.5	35	37	-2	47
6	8	-2	32	37	-5	48
9	10.5	-1.5	36	41	-5	49
11	14	-3	39	43	-4	52
9	16	-7	39	43	-4	53
12	16	-4	37	42	-5	54
11	12	-1	36	39	-3	59

Table 7.5: Comparison of extreme parameters from DWD and Department of Energy Data. The column DWD Ref refers to the point reference number from the DWD study.

is employed. The practice suggested by the UK Department of Energy [137] (DOE) has been adopted of assuming $K = 4$.

Where NEXT data was available, use of a more sophisticated description for the underlying parameter studies was considered. Empirical relations for K of the form of equation 4.45

$$K = A_0 + A_1\sqrt{H} \tag{7.7}$$

were deduced by a fitting procedure described in Appendix P. At each location two expressions of this form were deduced, one for small waves at the location and one for larger waves, as a result of clear trends in the data. Table P.4 in the appendix shows the values obtained. For larger waves at least, it was found that the developed relationships did not differ greatly from the simpler form suggested by the DOE information. Thus to limit the complexity of the calculations, the DOE relationship was used throughout.

For the periods of extreme waves the default cost model assumptions are used, following the recommendations of the UK Department of Energy [137] such that wave steepnesses are assumed to lie between 1/20 and 1/16.

7.6.5 Spatial variation of climate parameters

Means of interpolating the Weibull parameters to provide a continuous field for analysis were considered. However the factors that drive the climate vary in im-

portance with location[1] and a means of producing a reliable interpolation without resorting to very sophisticated oceanographic modelling techniques could not be identified.

Instead, analysis has been constrained to regions around two DWD data points, as shown in figure 7.4. It is assumed that the Wiebull parameters remain constant over these areas. The UK base cases of chapter 6 were selected so that the climatic conditions examined were identical to those at the two DWD data points, and thus the UK results from that chapter form the basis for the GIS study. The regions were definied on the basis that they lie within 150 km of each DWD point and within 40 km of the shore. The region within the UK Irish sea was further constrained to exclude points outside the 'bay' as the defined DWD point was within the bay and would not be representative of more open waters. The areas shown have also been subjected to the contstraints discussed in section 7.7, but the only one of significance here is a limit on the water depth of 40 m.

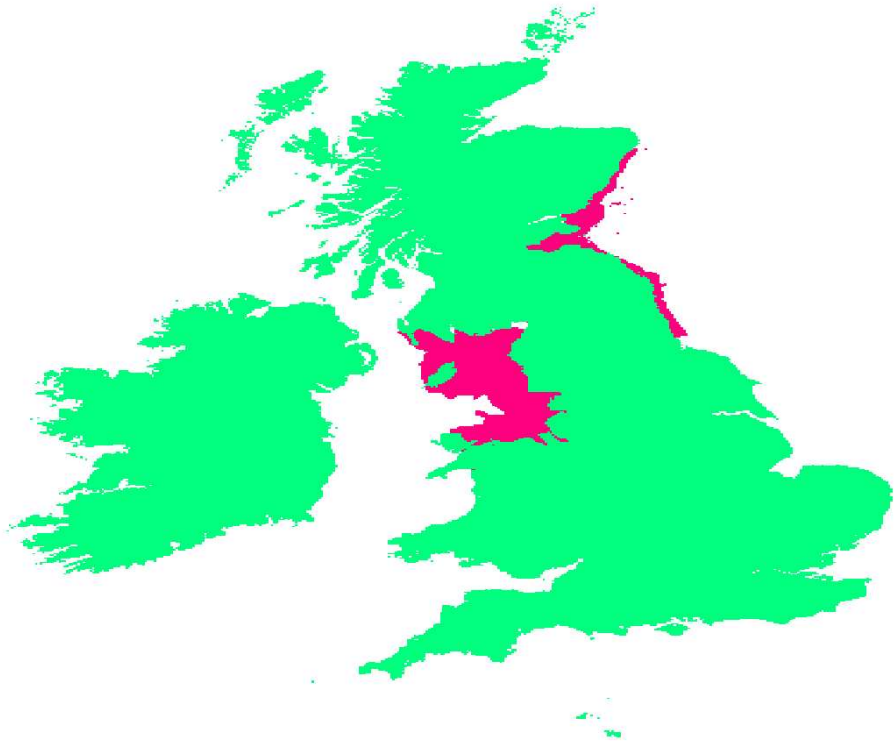

Figure 7.4: Areas analysed with the cost model/GIS for the UK region.

[1]Consider the very different fetches off the coast of North Western Scotland and the Eastern English Channel.

7.7 Constraints on development

Construction of large offshore wind farms may not be possible in many parts of Northern Europe due to conflict with other activities. The JOUR0072 database includes information on the features listed in table 7.6. Neither of the areas considered here is significantly affected by these constraints and thus they have been ignored here.

Feature	**Area excluded**
Major shipping lanes	Marked locations only
Offshore platforms	5 km buffer around platform, due to need for helicopter access etc.
Existing pipes and cables	Marked locations only.
Protected areas	Marked locations only. Area of Wadden sea in Netherlands is the only protected area listed.
Military zones	Marked locations only.

Table 7.6: Areas excluded from consideration using JOUR0072 constraints.

Locations with a highly sloping seabed are poorly suited for bottom mounted wind farm construction. As this is a technical constraint, these locations have been excluded from consideration.

Chapter 8

Results of Integrated GIS Survey

8.1 Introduction

In this chapter, the methodology of chapter 7 is used to plot a series of maps that show the cost of energy, in 2002 Euro cents per kilowatt-hour, from offshore farms as a function of location. For reasons of space, only the UK base case farm configurations described in chapter 6 are considered, but this time at a range of locations. The results are intended to show the impact of real combinations of environmental parameters on the economic performance of offshore farms, and how the methodology can assist in site selection.

The chapter begins by considering the wind resources. Next the results are reported as a series of cost of energy maps, firstly for 1.5 MW turbine based farms and then for 4 MW turbine farms. Finally some conclusions are drawn. Note that the figures in this chapter are grouped together at the end, as this makes it easier to compare the results.

8.2 Wind resources

Figures R.1 to R.4 in appendix R show the annual energy output produced from the two base case farm configurations located in each of the UK study areas. For all the plots shown, the impact of maintenance on availability has been ignored, with the 100% availability assumed. The maps are largely as expected, with inshore areas showing reduced energy production, thanks to the reduced wind speeds resulting from interaction with the land, and the output increasing while moving further offshore. Beyond a few kilometers offshore, it is clear that the annual energy output becomes largely independent of the distance from shore.

Farms comprising 4 MW turbines of course provide greater annual energy

production (AEP) than from 1.5 MW turbines. However the improvement does not reflect the increase in machine capacity, as shown by table 8.1 which compares the average output from the two base case farms in each region.

Region	Ratio of AEP
North Sea	1.97
Irish Sea	1.73

Table 8.1: Ratio of annual energy production from 4 MW and 1.5 MW farms.

8.3 Analysis of medium scale base case farms

Figures 8.1 and 8.2 show how the cost of energy for medium scale farms varies as a function of location in the Irish and North Sea regions respectively. The range of costs is smaller in the North Sea region, but this is largely because the areas considered are closer to the shore. A clear trend for the Irish Sea region is that energy costs very close to the shore are relatively high, thanks to the poorer near shore wind climate. The poorer wind climate reduces the energy production, but as has been demonstrated, yields only a very small reduction in costs. Moving further offshore, energy costs begin to reduce with improving annual mean wind speed.

Trends are different for the North Sea region, with energy costs increasing with distance from shore, even though a much smaller distance from the coast is considered. This appears to be due to the rapidly increasing depth with distance from the shore in this region, which increases the support structure cost quickly with distance to shore, as shown in figure 8.3.

Moving back to the Irish Sea, as figure 8.1 clearly shows, with even further increases in the distance from the shore is increased further, the energy cost begins to rise. As noted in the resource assessment, once away from the influence of the coast, the annual enery production becomes largely independent of the distance from the shore. Depths however increase, making support structures more expensive. The sudden increase in costs to greater than 6 Euro cents per kWh in figures 8.1 and 8.4, however, arises partly from increasing grid connection costs, but more importantly from the impact of maintenance. At the extreme edge of the area considered the distance to shore is such that travel time to the site reduces time available for maintenance operations, and this in turn reduces the availability.

For the North Sea case, the depth constraint on the cost model validity masks

this effect, but careful examination of the figure shows increased energy costs in the very few far offshore locations.

8.4 Analysis of large scale farms

Cost of energy maps for large scale farms are shown in figures 8.4 and 8.5 for location in the Irish and North Sea regions respectively. Many of the trends are very similar to those for the medium scale farms, although, as expected in general the cost of energy is lower.

8.5 Impact of turbine capacity on cost of energy

Figures 8.6 and 8.7 show in quantitative form the difference between the cost of energy from the large scale and medium scale farms in the North and Irish Sea regions respectively. Negative values represent locations in which the large scale farm produces cheaper energy. In most cases the difference is worthwhile, representing a reduction in energy cost of up to 14% depending on the location. Very close to the shore, the benefit of the larger capacity farm is smaller. There are locations where the predicted energy cost for the large scale farm exceeds that for the medium scale case. This arises from the predictions made by the maintenance model for relatively far offshore locations and is discussed further in section 8.7.

For the North Sea location, there is a clear difference in the average energy cost from the two technologies, taken across each considered area as a whole, as shown in table 8.2. For the Irish Sea location, the difference is less clear, however this also arises because of the predictions of the maintenance model in far offshore locations. If the analysis had been constrained to a smaller area, the difference in the average energy costs would have been more pronounced.

Location	1.5 MW farm	4 MW farm
UK-IE	4.599	4.596
UK-NS	4.25	3.09

Table 8.2: Average cost of energy in 2002 Euro cents per kilowatt-hour taken across the areas considered, for the two farm concepts.

8.6 Impact of hub height variation on results

8.6.1 North Sea region

Figures 8.8 and 8.9 show the cost of energy for large and medium scale farms in the North Sea region, with a reduced hub height of 60 m. The energy costs are noticably increased, with the medium scale farm being slightly more influenced than the large scale farm. The difference made by the choice of farm scale is barely effected by the hub height however, as can be seen from comparing figure 8.10 and figure 8.6.

Average energy costs over the region are shown in table 8.3. For the medium scale farm, reducing the hub height produces an increase in average energy cost of 3.3%, with the figure for the medium scale farm being 3.7%.

Location	1.5 MW farm	4 MW farm
UK-IE	4.74	4.77
UK-NS	4.24	3.221

Table 8.3: Average cost of energy in 2002 Euro cents per kilowatt-hour taken across the areas considered, for the two farm concepts, but with 60 m hub height.

8.6.2 Irish Sea region

The influence of reducing the hub height to 60m in the Irish Sea region is shown in figures 8.11 and 8.12 for the large and medium scale farms, with the cost reduction from using 4 MW turbines in place of 1.5 MW technology shown in figure 8.13. Most of the trends are very similar to those for the North Sea case. Again, average energy costs over the region are shown in table 8.3, with the percentage change compared to the base case being -0.23% for the medium scale farms, and 4.23% for the large scale farm.

8.7 Impact of maintenance spend on cost of energy

8.7.1 Introduction

It was noted for the Irish Sea cases that at distances relatively far from the shore, the cost of energy rises dramatically. Analysis of the underlying data shows that this is largely due to decreasing availability, thanks to increased travel time for the

maintenance crews. The calculations assume that for each farm, the annual maintenance cost is maintained at an optimal value identified using the cost model for the appropriate base case combination in chapter 6. At the largest distances from shore treated here, this maintenance expenditure is not sufficient to maintain a good availability factor. The annual energy production falls therefore, and as a result the cost of energy rises. It was notable that the impact on the larger scale farms was greater than on the medium scale installations.

One possibility to progress the work, would have been to recalculate an optimal maintenance expenditure for the further offshore farms and repeat the analysis. However, it was considered of more general value to investigate the effect of reduced maintenance expenditure on the cost of energy from the base case farms. The analysis was repeated therefore with the annual maintenance expenditure set to approximately one third of the optimal value in each case.

8.7.2 North Sea region

Figures 8.14 and 8.15 show cost of energy contour maps for large scale and medium scale farms respectively in the North Sea region, using the reduced maintenance expenditure. There is a clear increase in the cost of energy compared to the results with the optimal maintenance expenditure. The most interesting result, however, is that in most cases medium scale farm now produce cheaper energy than the large scale farms, as shown by figure 8.16. The result is emphasised by the regional average energy costs in table 8.4.

Location	1.5 MW farm	4 MW farm
UK-IE	4.69	6.22
UK-NS	3.74	3.59

Table 8.4: Average cost of energy in 2002 Euro cents per kilowatt-hour taken across the areas considered, for the two farm concepts, but with reduced annual maintenance expenditure.

8.7.3 Irish sea region

Figures 8.17 and 8.18 show comparable results for the Irish Sea region. Again the medium scale farms now produces cheaper energy in most cases, as demonstrated by figure 8.19 and table 8.4.

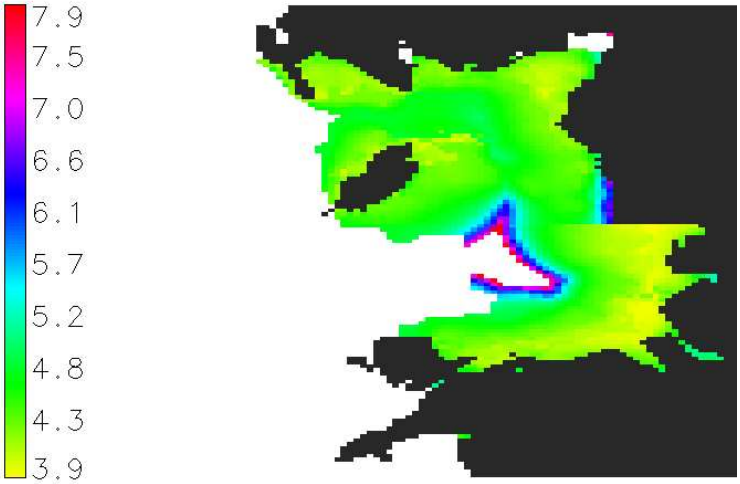

Figure 8.1: Base case 1.5 MW turbine farm energy cost map for UK Irish Sea region.

8.8 Chapter summary

In this chapter, the GIS drawing on results from the main cost model has been used to examine how the cost of energy from the two base case farm concepts would vary as a function of location in two contrasting areas of UK waters. Cost of energy contour maps have been plotted to illustrate the results.

An important conclusion is that, in contrast to the indications of the simple parameter studies, economic site selection for large offshore farms is considerably more complex than merely finding locations with good wind resource. Comparison of the cost of energy maps with the resource maps in appendix R shows that locations with a good resource may still produce relatively expensive energy. Although the cost of energy from a specific farm shows great sensitivity to the annual mean wind speed, other factors, taken together, appear to be capable of offsetting the benefits of a good resource.

Another observation is that in most locations there is a worthwhile cost of energy reduction from using large scale farms based on 4 MW turbines, rather than relying on 1.5 MW turbines. However, this saving was dependent on optimal maintenance being carried out. With ineffective maintenance, the cost saving could be overturned. This in turn goes on to emphasise the importance of efficient maintenance for the economic performance of large offshore farms that has been suggested in the literature.

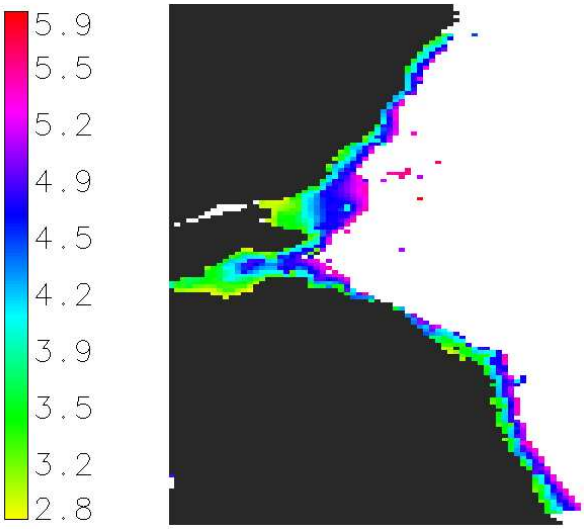

Figure 8.2: Base case 1.5 MW turbine farm energy cost map for UK North Sea region.

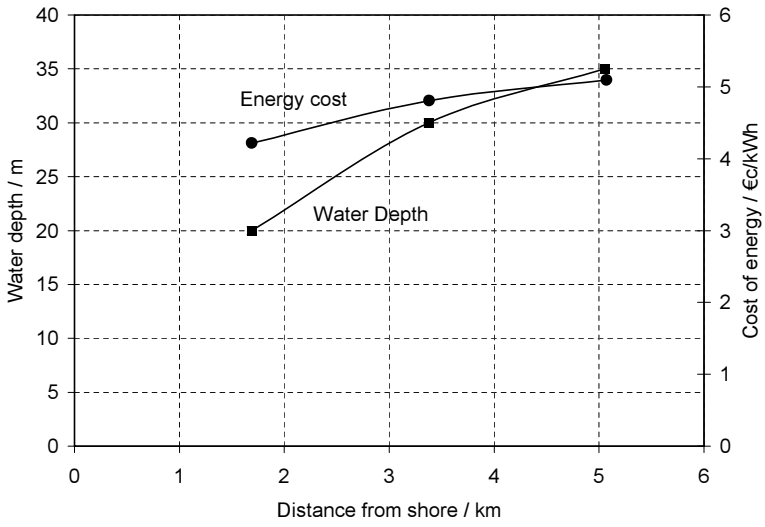

Figure 8.3: Relationship between water depth and energy cost with distance to shore for base case 1.5 MW turbine in UK North Sea region.

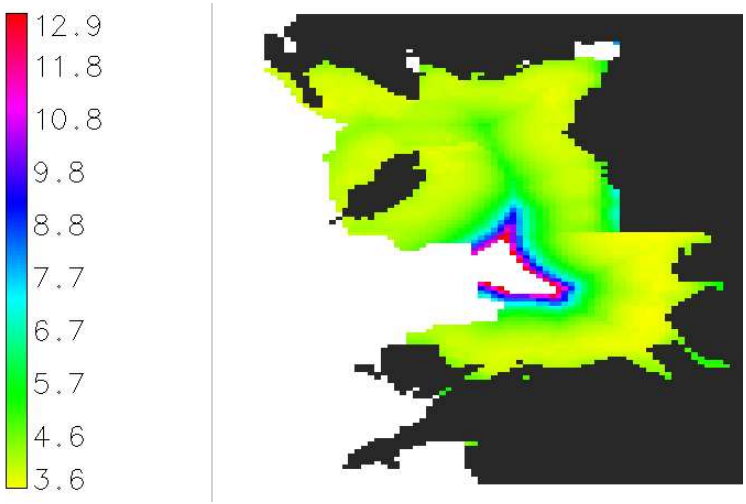

Figure 8.4: Base case 4 MW turbine farm energy cost map for UK Irish Sea region.

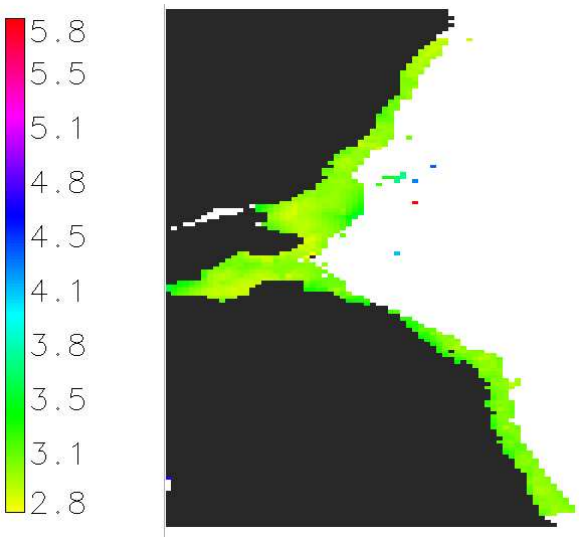

Figure 8.5: Base case 4 MW turbine farm energy cost map for UK North Sea region.

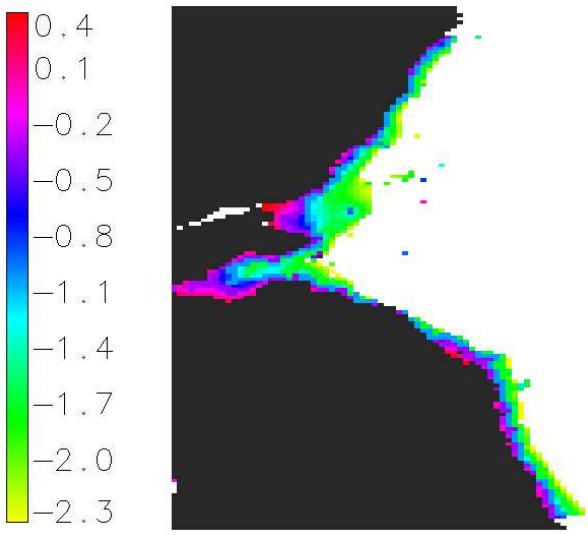

Figure 8.6: Difference in energy cost between farm scales for UK North Sea region.

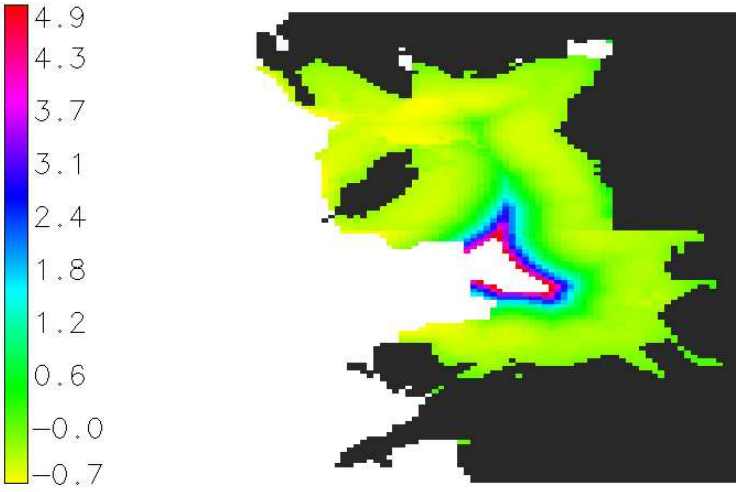

Figure 8.7: Difference in energy cost between farm scales for UK Irish Sea region.

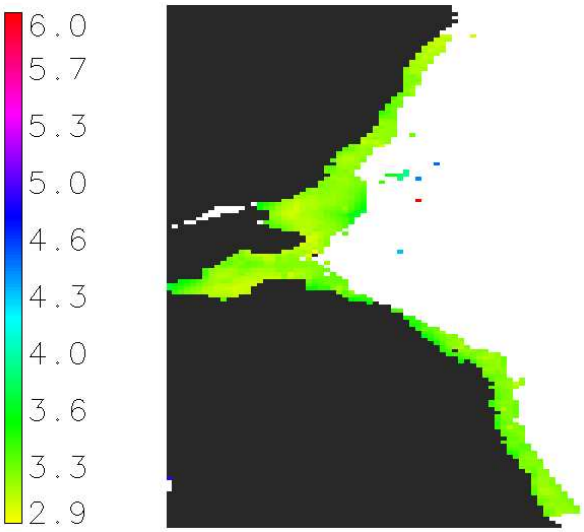

Figure 8.8: Cost of energy for large scale farm in North Sea region with reduced hub height of 60 m.

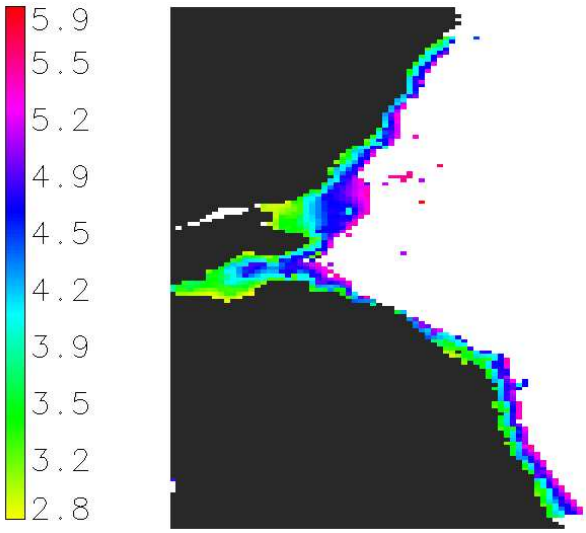

Figure 8.9: Cost of energy for medium scale farm in North Sea region with reduced hub height of 60 m.

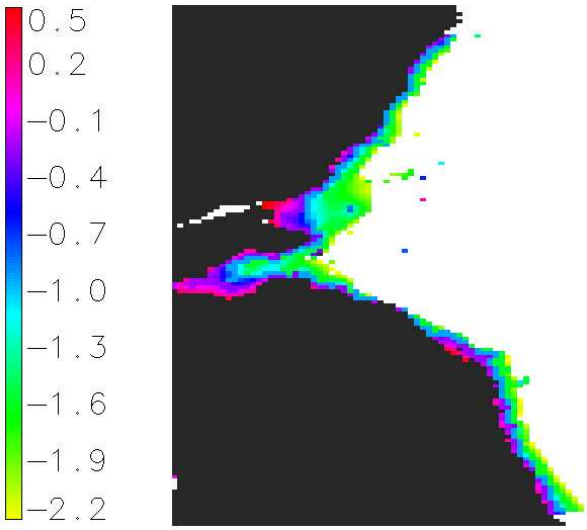

Figure 8.10: Difference in energy cost for large and medium scale farms with reduced hub height in UK North Sea region.

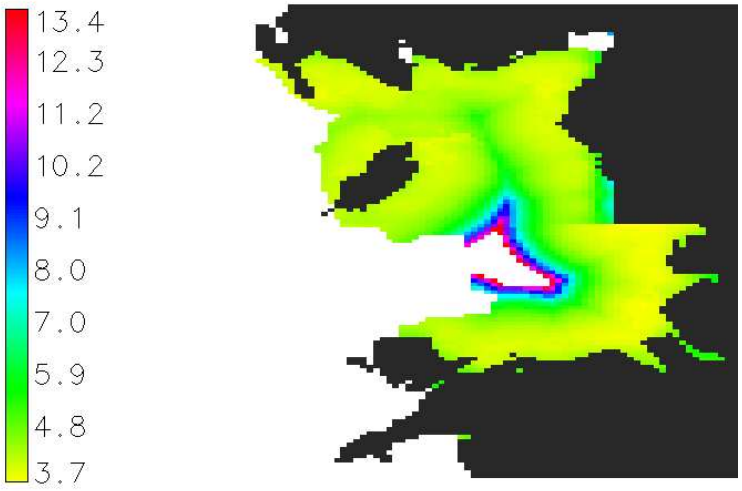

Figure 8.11: Cost of energy for large scale farm in Irish Sea region with reduced hub height of 60 m.

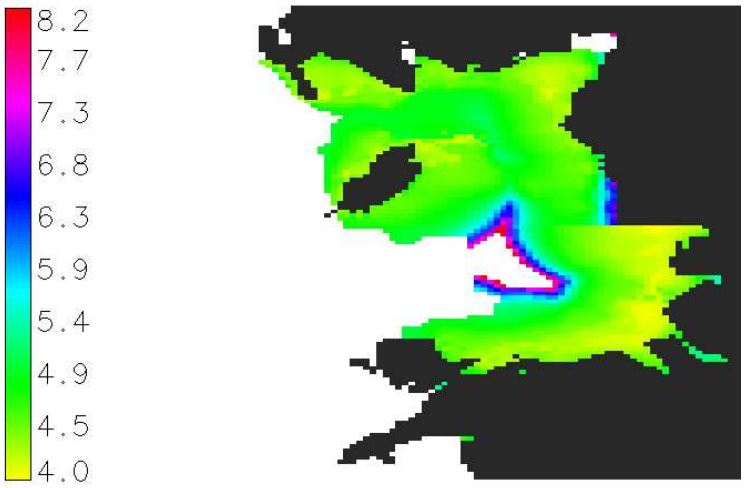

Figure 8.12: Cost of energy for medium scale farm in Irish Sea region with reduced hub height of 60 m.

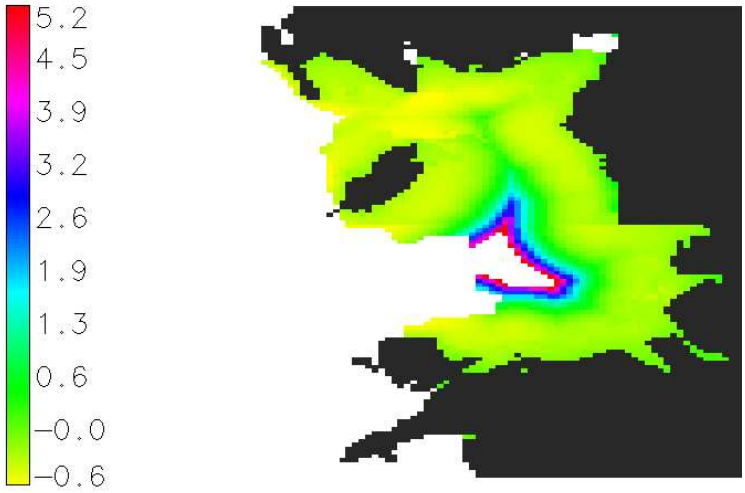

Figure 8.13: Difference in energy cost for large and medium scale farms with reduced hub height in UK Irish Sea region.

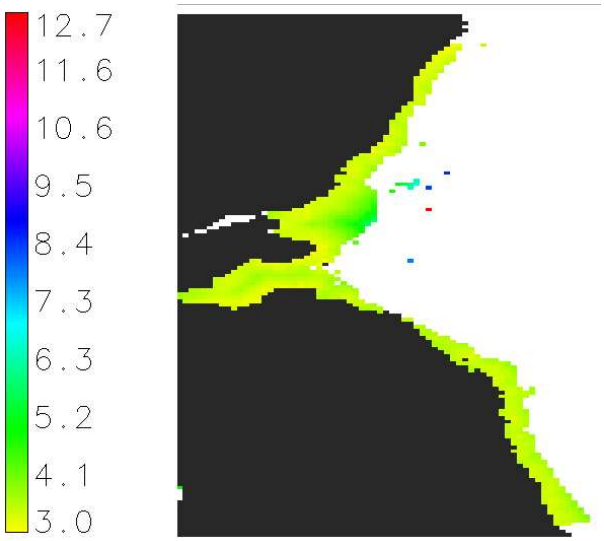

Figure 8.14: Cost of energy for large scale farm in North Sea region with reduced maintenance spend.

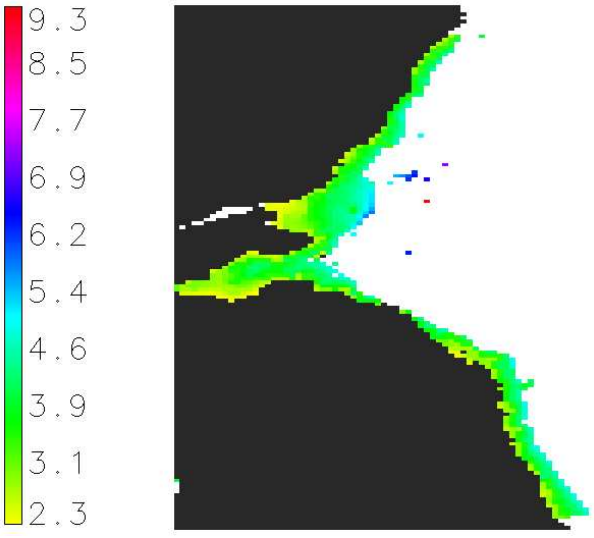

Figure 8.15: Cost of energy for medium scale farm in North Sea region with reduced maintenance spend.

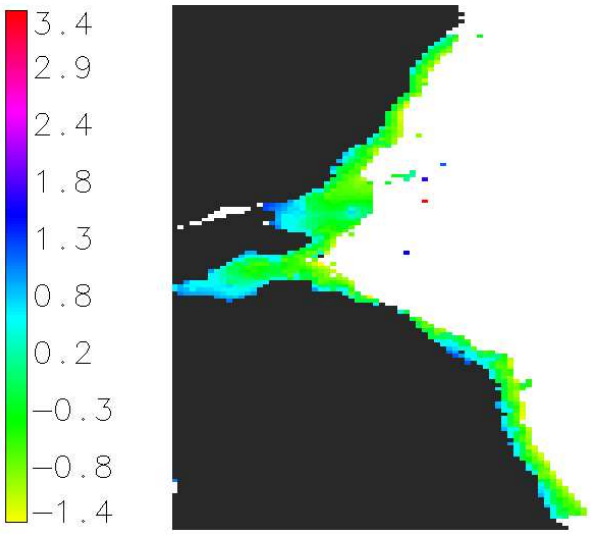

Figure 8.16: Difference in energy cost for large and medium scale farms with reduced maintenance spend in UK North Sea region Negative values denote locations at which the large scale farm produced cheaper energy.

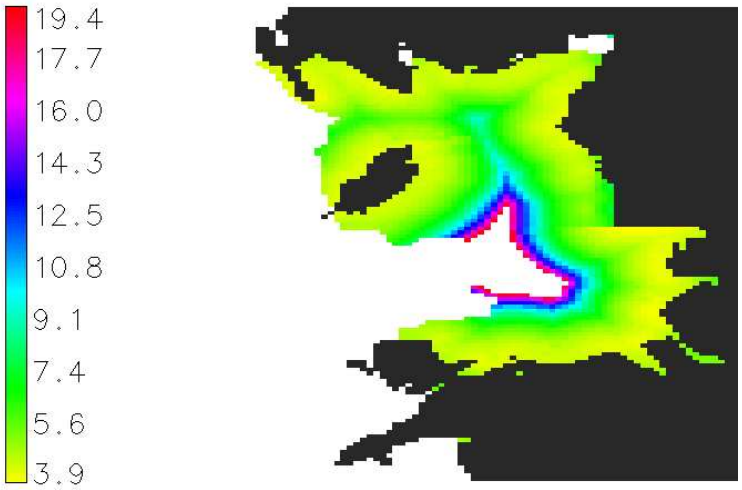

Figure 8.17: Cost of energy for large scale farm in Irish Sea region with reduced maintenance spend.

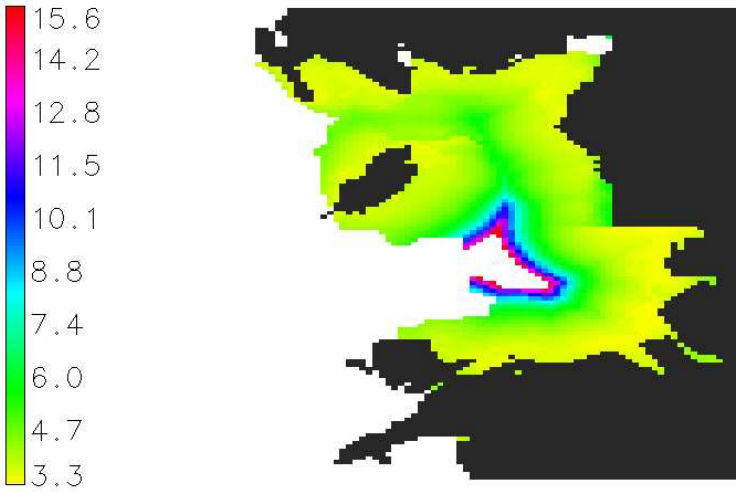

Figure 8.18: Cost of energy for medium scale farm in Irish Sea region with reduced maintenance spend.

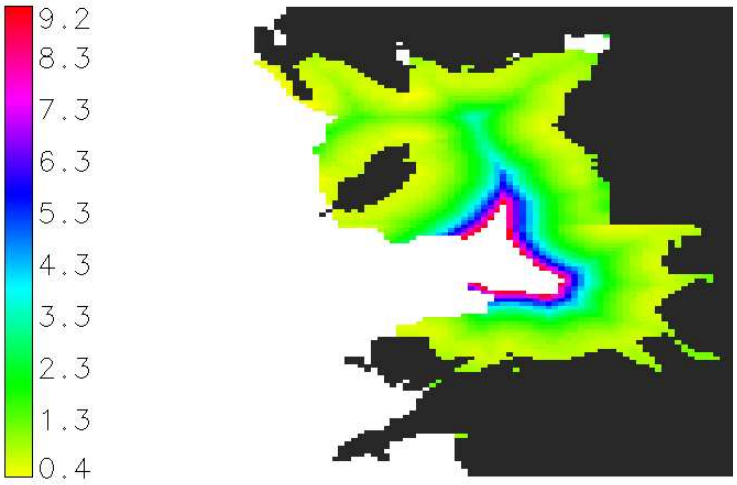

Figure 8.19: Difference in energy cost for large and medium scale farms with reduced maintenance spend in UK Irish Sea region.

Chapter 9

Conclusion

9.1 Review of work completed

The work described in this thesis has investigated the environmental and engineering parameters that influence the engineering economics of offshore wind energy converter systems in Northern Europe. Analysis of some existing data revealed several general features that characterise offshore wind farms, and served to highlight influences on their economic performance. Taken together with a survey of the literature, the analysis also demonstrated that there are no simple methods for predicting the economic performance of an offshore wind farm. The only realistic methodology for understanding the cost trends is through a bottom up approach, wherein detailed models are formulated for each farm component.

In this light, a framework for the cost modelling of offshore wind energy systems was proposed. The modelling approach attempts to account for the effects of fatigue in a more more rigorous way than previously.

An offshore wind farm cost model was written in FORTRAN, realising the framework. The focus of the model is on the structural aspects of offshore farms, but the impacts of maintenance and the need to construct a grid connection are taken into account. The structural elements of the model comprise routines that evaluate the loads experienced by an offshore turbine using established engineering approaches. Preliminary design of components is then undertaken based on the calculated loads, the loads re-evaluated and if necessary components redesigned. A series of optimisation algorithms identify the component dimensions that minimise the cost of the energy produced by the farm. The completed model was used to investigate the sensitivity of the cost of energy from two offshore farm configurations at four locations around Northern Europe.

It was recognised from the outset of this work that the problems of optimal offshore wind farm design and site selection are strongly interlinked. Locations

with the best wind conditions also tend to be those in which it is most difficult to build, having the most demanding wave conditions, the deepest water and being remote from grid connections. The value of the parameter studies for environmental parameters is limited therefore, because in practice the parameters are not independant and vary in a manner linked by geography.

To tackle these difficulties, the cost model was linked with a GIS database of offshore conditions. The completed system was used to plot cost of energy contour maps for wind farms with installed capacities of 150 MW and 400 MW located in two areas around the UK. The results produced by the GIS and cost model combination demonstrate how the methodology can be used to identify economically appealing locations for future offshore farm developments.

9.2 The cost model

The overall design of an offshore wind farm draws on a wide range of technical disciplines. Collation of a set of design procedures and development of algorithms for the design of the several components represents a worthwhile outcome. The cost model itself, together with the process by which it has been formulated, represent conclusions of this work, which may be abstracted on five levels:

- Identification of the 'connection points' between the discrete components of an offshore wind farm, and the means by which the component design proceedures may interact,
- Formulation of 'higher' algorithms for the overall cost modelling of offshore wind farms, accounting for the interactions between components,
- Formulation of lower level algorithms for the design and optimisation of individual components,
- Production of a framework of computer code, and a library of detailed component design routines, that could form a basis for future development, and
- Demonstration of elements of the model through a series of calculations.

9.3 Investigation of the offshore wind resource in Northern Europe

The main cost model parameter studies demonstrated the importance of good wind conditions for good wind farm economics. In the same vein, turbine hub

height is also important for wind farm energy production, but it is difficult to draw any general conclusions in this matter. However it is quite clear that wind-wave interactions, as represented by the Charnock coefficient, have negligible impact on the energy production and the economics of offshore farms. The wave climate was also found to have surprisingly little impact on farm economics.

While small changes in the number of turbines in the base case farms had very little influence on the economics, greatly decreasing the number of turbines served to substantially increase the cost of energy. This suggests, therefore, that it is likely that larger farms will reduce the cost of energy from offshore farms below that exhibited by the small existing farms considered at the beginning of this thesis.

The GIS analysis was intended to examine how the individual cost of energy sensitivities might combine in a real setting. It was clear that finding a location with good wind resources is not sufficient for good economics. The small sensitivities to other cost influences can combine to offset the advantage apparently offered by a good resource. Behaviour, however, is specific to individual locations and farms, and it is difficult to generalise.

The analysis also revealed that using turbines with larger rated capacities would in many locations produce a worthwhile saving in the cost of energy. However, for that saving to be realised, the analysis suggested that attention should be paid to devising an effective maintenance regime.

9.4 Suggestions for further work

Firstly possible minor enhancements to the model and further parameter studies that could be performed are considered. Secondly activities aimed directly at improving the utility of the cost model itself will be discussed. In the main, these are possible new model features that rely on well understood theory, but that it has not proved possible to implement during this project.

9.4.1 Use and enhancement of the model

The following could be undertaken with relatively small changes to the model code:

- The model could be used to study other areas. In fact this has already been undertaken for the Dutch and Danish waters considered in chapter 6, but space and time constraints prevent it being reported here.

- The relatively low impact of the wave climate on the cost of energy was surprising and is worthy of further investigation.
- The GIS work has produced a large quantity of data, effectively costing offshore farms at many locations all at once. There is scope for applying data mining techniques to this data in order to find if simple relations between the cost of energy and the input parameters can be established for each region.
- The impact on the calculations of uncertainties in the input parameters should be evaluated in more detail. This would allow 'error bars' to be associated with the results, which in turn would allow rational commercial decisions to be made on the basis of the model predictions. Ultimately the existing model could be used within a Monte-Carlo method approach to formulating degree of belief distributions for the predicted variables from uncertain input variables.
- Rather than relying on the look up table based grid connection evaluation, the model could be coupled with a first principles grid connection designer, such as that developed at the University of Delft [170]. A modified version of the Delft model has been developed by the author for this very purpose, but time constraints have not allowed integration of the code.
- A cost model for gravity foundation farms was developed and implemented, but was not used for detailed parameter studies. There is scope for using the model for the optimisation of gravity structures in order to see if their economics can be improved. Equally, the gravity foundation model could be developed to account for diffraction in a more rigorous manner.

9.4.2 Further development of the model

Formulation of more detailed cost functions

When the work reported here was started, only three small offshore wind farms had been constructed. As a result, only very limited cost data was available. While this data could be supplemented by information from several 'paper-only' studies, in general these only considered costs in an approximate manner. In view of the limited range and poor quality of the available data, a decision was made to employ relatively simple cost functions for the analysis. As the work has progressed, many more offshore farms have been designed and developed. This in turn should allow the development of more sophisticated cost functions, which

would add to the value of the work. A possible obstacle however is the increasingly commercial nature of the offshore wind industry, which makes developers reluctant to release cost data.

Improvement of fatigue load calculations within the model

The treatment of turbine generated fatigue loads relies on a relatively simple parametric description of the interaction between the turbine blades and wind turbulence. Parametric descriptions of fatigue are not widely regarded as very reliable [59], and in general require empirical tailoring to the characteristics of particular turbines.

At the outset to this work, the possibility was considered of deriving fatigue information from a first principles turbine simulation of the type implemented in the detailed wind turbine design codes summarised in tables 2.2 and 2.3. This approach offers the considerable advantage of providing a perfectly general model, able to account directly for changes in turbine detail. Preliminary investigations showed this to note be a feasible approach due to the time consuming nature of the calculations required. Furthermore time domain turbine simulation is not sufficiently developed such that the design codes are thoroughly reliable tools. As with many research oriented time domain computer codes, there are circumstances in which the calculations have to be 'nursed' to convergence.

A further possibility examined was to derive a look-up table of tower top fatigue spectra, through a series of parameter studies using one of the detailed simulation tools. For any particular turbine, a database of spectra could be developed based on a range of parameters, for instance, hub height windspeed, turbulence intensity and the fundamental frequency of the support structure. Each spectrum would be represented as a set of samples detailing the tower top load component at a large number of discrete frequencies. Tower top spectra for any prevailing conditions could be realised by multi-dimensional interpolation between the spectra stored in the database.

A number of experiments were conducted with the 'FAST' code in this regard, with a view to developing such a database for the turbines considered here. It was found that the data management requirements for the approach to be successful were formidable and thus it is was abandonded in favour of the methodology described in chapters 4 and 5. The main advantages to the database oriented method is that it would have provided accurate tower top fatigue spectra rapidly for use in the cost model, and would have avoided the need to explicitly check for resonance. To set against this, there is the considerable disadvantage that application of the model to other turbines would have required that a very substantial parameter study of the tower top fatigue loads be undertaken. In comparison,

the parametric method implemented allows much more flexibility for what is at best an outline design tool.

The model could usefully be further developed using either of the alternative approaches outlined in this section. There is also scope for improved specialisation of the parametric model employed. However of much greater value would be the wider objective of development of validated means for the rapid evaluation of wind turbine fatigue loads.

Calibration of the structural model

While elements of the structure model have been validated against test data, there remains some uncertainty as to the extent to which the design drivers are correctly captured. In particular it was found that fatigue played a smaller role in the design than had been anticipated from the literature. As part of another project [56], a means of calibrating wind turbine support structure cost models against real data has been developed. The methodology should be applied to the model described here, and the data recalculated.

Appendix A

Influence of economic parameters on qualitative project comparisons

A.1 Discounted cash flow analysis

Conventional discounted cash flow (DCF) analysis [208] of energy projects proceeds by first calculating the life cycle cost, *LCC*, of the costs C_j anticipated in each year of the project j until the end of its economic life n_e using

$$LCC = \sum_{j=0}^{n_e} \frac{C_j}{(1+r)^j} \tag{A.1}$$

where r is the test discount rate. The NPV is then converted to an equivalent annual payment, the levelised cost L, using

$$L = LCC \times \frac{r\,(1+r)^{n_e}}{(1+r)^{n_e} - 1}, \tag{A.2}$$

and the levelised energy production cost, C, referred to in this document as simply the energy cost, calculated from the estimated annual energy production E with

$$C = \frac{L}{E} \tag{A.3}$$

to give a price per unit of energy at which produced power must be sold in order for the project to break even.

Most energy projects exhibit a simple cost structure with a large initial cost incurred during construction before any energy is produced, followed by a series of equal annual on-going costs during each subsequent year of operation. In these circumstances the above analysis can be simplified to produce an expression recommended by the International Energy Agency [183] for discounted cash flow

calculation of the cost of energy:

$$C = \frac{I}{aE} + \frac{M}{E} \tag{A.4}$$

where

I	=	Initial cost
M	=	Annual on-going cost
E	=	Annual energy production
a	=	Discounting factor. (defined below)

The discussion in this appendix focuses on the characteristic features of DCF analysis rather than details of particular projects, and thus it is convenient to define a 'specific' investment cost i and a 'specific' on-going cost m as follows:

$$i = \tfrac{I}{E} \quad m = \tfrac{M}{E} \ . \tag{A.5}$$

The DCF expression used in the remainder of this appendix is therefore

$$C = \frac{i}{a} + m. \tag{A.6}$$

It is also convenient to refer to the capital intensiveness Π of a project which here is defined as

$$\Pi = \frac{i}{aC} \tag{A.7}$$

which in turn implies that

$$m = (1 - \Pi)C. \tag{A.8}$$

A.2 Impact of economic parameters on the cost of energy

The discounting factor a is calculated from two economic parameters, the test discount rate r and the economic lifetime n_e in years, as follows:

$$a = \frac{1 - \left(\frac{1}{1+r}\right)^{n_e}}{r}. \tag{A.9}$$

The relative importance of the initial cost to the overall cost of energy decreases with increases in the discounting factor. When using parameters that give a large discounting factor therefore, economic comparison of projects tends to be domi-

nated by the on-going costs. By the same token a small discounting factor tends to be more favourable to projects with low initial costs irrespective on the on going costs.

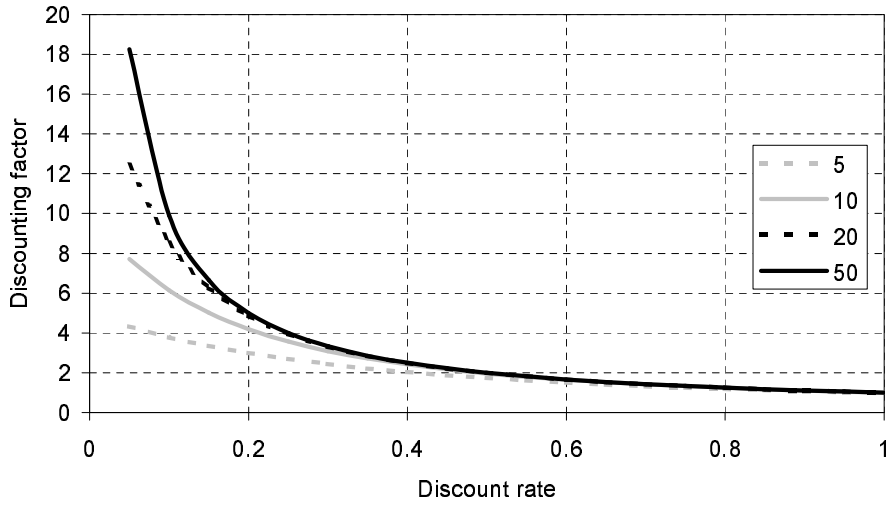

Figure A.1: Discounting factors as a function of discount rate and economic lifetime.

As figure A.1 shows, low discounting factors are associated with short lifetimes and high discount rates. Employing high discount rates and short lifetimes tends to favour projects with relatively low initial costs, in other words projects with a low capital intensity, and vice-versa. In all cases, increasing the discount rate or decreasing the lifetime acts to increase the energy cost. However, the rate of increase is faster for higher capital intensity projects, with the sensitivity of the cost of energy, given by

$$\frac{dC}{da} = \frac{-i}{a^2} \tag{A.10}$$

being proportional to the specific investment cost.

The outcome of comparing projects with differing capital intensities *can* depend on the economic parameters used therefore. There are a range of clear cut cases that are independent of the economic parameters. If two projects, respectively, have specific initial and on-going costs of i_1, i_2 and m_1,m_2 then the outcome of comparison will only depend on the economic parameters used if either $i_1 < i_2$ and $m_1 > m_2$ or $i_1 > i_2$ and $m_1 < m_2$. For all other cases the outcome of any comparison is independent of the economic parameters.

A.3 Sensitivity of economic decisions to changes in the discounting factor

For what range of discounting factors are the results of a particular comparison unchanged, where the comparison is one that depends on the discounting factor? In this section a general analysis will be developed and then applied to a comparison representative of those found elsewhere in this thesis.

Suppose two projects assessed with a discounting factor of a_1 have energy costs $C_{1,a1}$ and $C_{2,a1}$such that

$$C_{2,a2} = f\ C_{1,a1} \tag{A.11}$$

where $0 < f < 1$. Each cost is composed of an initial cost component i_1,i_2 and an annual ongoing cost component m_1, m_2 so that

$$\frac{i_2}{a_1} + m_2 = f \times \left(\frac{i_1}{a_1} + m_1 \right). \tag{A.12}$$

If $C_{1,a1}$ is regarded as fixed, this equation gives the locus of combinations of $i_2$and m_2 for which $C_{2,a1}$ is a proportion f of $C_{1,a1}$.

$C_{1,a}$ and $C_{2,a}$ are energy costs evaluated respectively with the same initial and ongoing cost components as $C_{1,a1}$ and $C_{2,a1}$ but at a generalised discounting factor of a. For the second project to remain more economic than the first, irrespective of the economic parameters, a condition on the discounting factor may be derived from the inequality

$$C_{2,a} < C_{1,a}. \tag{A.13}$$

It is convenient to express the condition in terms of a factor x on the initial discounting factor defined such that

$$a = x\, a_1 \tag{A.14}$$

and to refer to a critical factor x_c at which the first and second energy costs become equal. The critical factor is then given by

$$x_c = \frac{i_2 - i_1}{m_1 - m_2} \frac{1}{a_1}. \tag{A.15}$$

Eliminating m_2 between A.12 and A.15 gives an expression for the critical factor

$$x_c = \frac{i_2 - i_1}{a_1 m_1 (1 - f) - f\, i_i + i_2} \tag{A.16}$$

that can be used to investigate the range of discounting factors for which the outcome of economic comparison of the two projects remains unchanged.

We are interested in the economic comparison of projects of similar and differing character. It is convenient to use the capital intensity of a project, calculated at a specific discounting factor as a measure of its character. The cost of energy for projects with a similar capital intensity is split in a comparable way between the initial and on-going costs.

Figure A.2 shows the factor by which the discounting factor can be increased without influencing the qualitative result for comparison of two projects for which $f = 0.9$, as a function of the discount rate of initial comparison and the ratio of the capital intensities evaluated at the initial discount rate. The results, in terms of these variables, are independent of the specific costs. Where the capital intensity of the projects are similar, that is π_2/π_1 is close to unity, then irrespective of the discounting factor used for the initial comparison, it can be varied over a considerable range with impacting on the outcome. Where the capital intensity of the projects is markedly different, such that project 2 is initially much less capital intensive than project 1 then the range over which the discounting factor can be varied is considerably reduced.

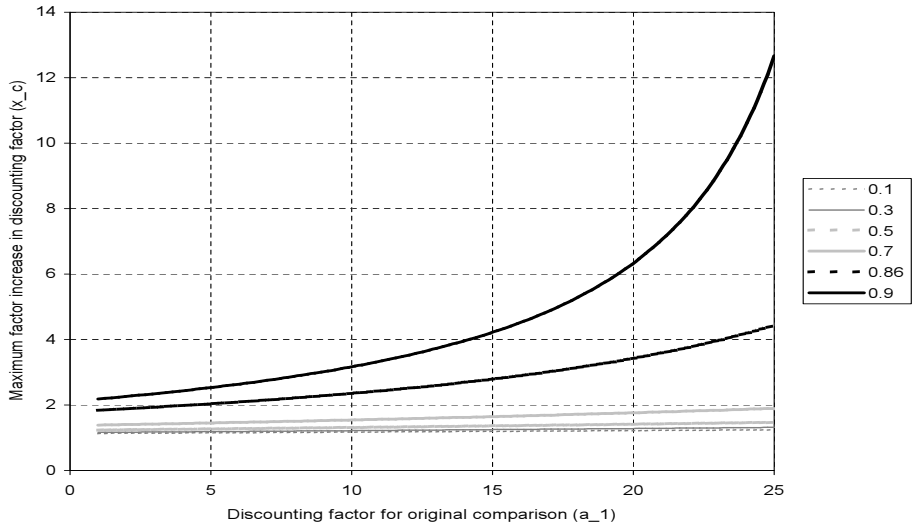

Figure A.2: Maximum multiplier by which discounting factor may be increased without changing the conclusion of an economic comparison, as a function of the discounting factor of initial comparison (horizontal axis). Data plotted is for an initial cost difference factor f of 0.9 and for a range of ratios of capital intensity ($\frac{\pi_1}{\pi_2}$) listed in the key. This figure only considers cases where the capital intensity ratio is less than unity.

Figure A.2 only considers cases where the initially cheaper project is less cap-

ital intensive than the first, so that increasing the discounting factor eventually makes the two energy costs equal. It is conceivable that the cheaper project could be more capital intensive than the more expensive, in which case reducing the discounting factor could change the outcome of a comparison. Figure A.3 deals with these cases again assuming $f = 0.9$, where the critical factor is now less than unity reflecting the need for a reduction in the discounting factor to change the outcome of comparison. Note that for cases where the capital intensiveness of the initially cheaper project is slightly greater than that of the more expensive, then it is never possible for the outcome of the economic comparison to be altered by the discounting factor. For this reason the diagram does not consider values of π_2/π_1 below 1.1. When the lower cost project has a higher capital intensity than the more expensive, it is not possible to achieve the specified ratio of energy costs, f, at low discounting factors. The curve for each ratio of capital intensity in the figure starts at the lowest discounting factor for which $f = 0.9$ is possible.

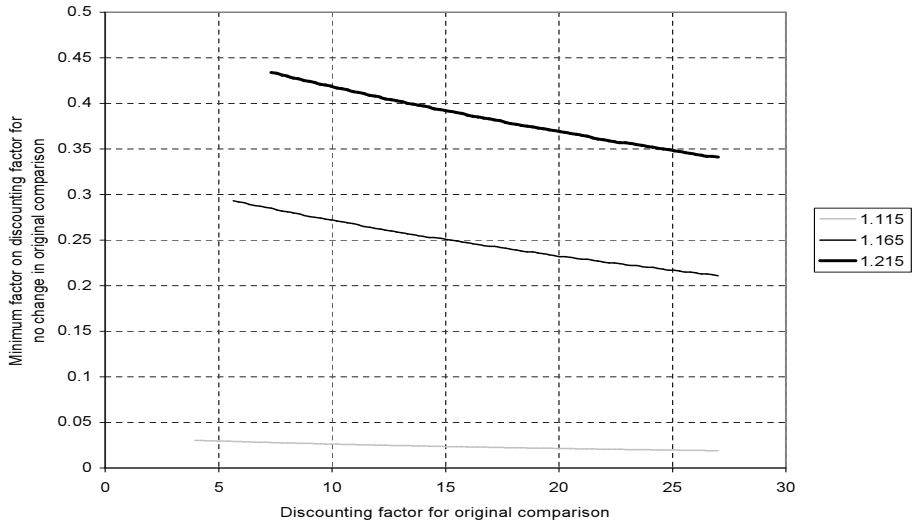

Figure A.3: Maximum multiplier by which discounting factor may be reduced without changing the conclusion of an economic comparison, as a function of the discounting factor of initial comparison (horizontal axis). Data plotted is for an initial cost difference factor f of 0.9 and for a range of ratios of capital intensity ($\frac{\pi_1}{\pi_2}$) listed in the key. This figure only considers cases where the capital intensity ratio is greater than unity.

Increasing the initial cost difference between the two projects, setting $f = 0.8$ for example decreases the sensitivity of the comparison to the discount rate, illustrated in figure A.4.

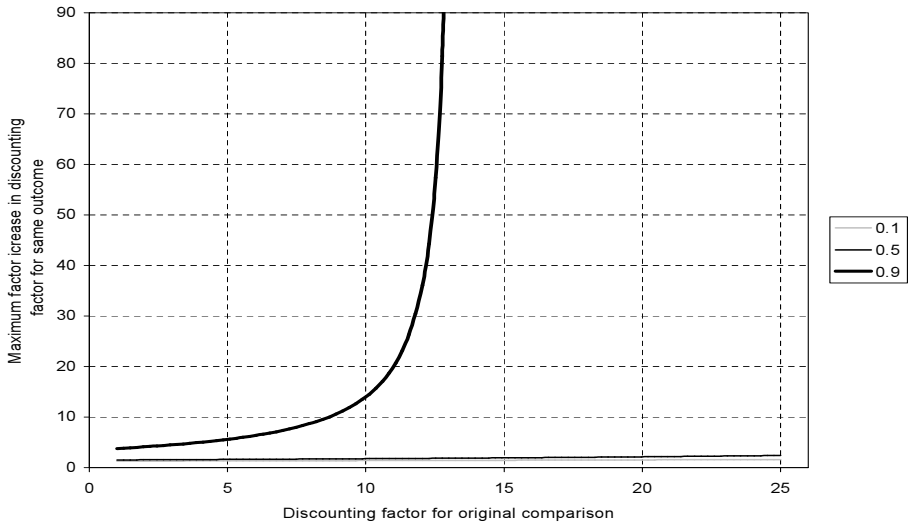

Figure A.4: Maximum multiplier by which discounting factor may be increased without changing the conclusion of an economic comparison, as a function of the discounting factor of initial comparison (horizontal axis). Data plotted is for an initial cost difference factor f of 0.8 and for a range of ratios of capital intensity ($\frac{\pi_1}{\pi_2}$) listed in the key. This figure only considers cases where the capital intensity ratio is less than unity.

A.4 Implications for comparison of offshore wind projects

The analysis has demonstrated that the outcome of the DCF comparison of projects with similar capital intensiveness is not very sensitive to the discounting factor, and by implication the economic parameters employed. Since this thesis deals exclusively with offshore wind projects with comparable capital intensity, the conclusions herein are unlikely to be changed by even quite large changes to the discount rate or economic lifetime assumed.

The outcome of comparing projects with very different capital intensity is rather more strongly influenced by the economic parameters assumed. Such circumstances might arise if the economic results from this work were compared with a fossil fuel plant. Were such comparisons to be made, considerable effort would be required to determine the appropriate discount rate and economic lifetime that provides a fair comparison.

Appendix B

Turbines considered in the analysis

B.1 Introduction

To limit the scope, the analysis in this thesis considers only two types of turbine. Two contrasting machine types were chosen to allow comparison of the impact of turbine characteristics on offshore support structures and comparative economics. Two machines were selected, a generic 1.5 MW concept drawing on data taken from a range of sources and intended to be representative of machines in the class, and a 4 MW version of the Kvaerner-Turbin WTS-80 machine.

The turbines were selected early on in the work. Recent developments in large turbine technology for offshore use make the choices seem conservative and even obsolete. This is an unavoidable problem in a quickly developing field.

B.2 1.5 MW Turbine

B.2.1 Description

The data is intended to represent a 'typical' Danish style 3 bladed pitch controlled turbine of the 1.5 MW class. It has been assumed that the machine was originally designed for onshore use and that a minimal degree of marinisation has been applied to adapt it for use offshore. Data has been obtained from a range of literature sources, and also by consultation with manufacturers.

B.2.2 Overall specification

The basic description of the turbine used by the cost model is as shown in table B.1.

Rotor diameter	64 m
No. of blades	3
Rotation speed	20 rpm
Cut in wind speed	3 m/s
Cut out wind speed	25 m/s
Rated wind speed	13.13 m/s
Rated wind power	1500 kW
Generator efficiency (assumed constant)	96.7
Gearbox efficiency(assumed constant)	96.5
Nacelle vertical dimension	8 m
Nacelle frontal area	22.4 m^2
Effective blade area	147.75 m^2
Nacelle drag factor	1.2
Blade drag factor (operating case)	0.4
Blade drag factor (fail case)	1.3
Aerodynamic damping (% critical)	1.31
Compatiblt diameters for tower top	1.8-2.0 m
Mass (incl. blades)	75,000 kg
Purchase cost (2002)	1,000,000 Euro

Table B.1: Description of the 1.5 MW turbine used for the parameter studies.

B.2.3 Aerodynamic performance and blade description

Estimation of the annual energy output requires information on the aerodynamic performance of the turbine. For the cost model, this is represented by a $Cp - \lambda$ curve. The performance curve used for the 1.5 MW turbine is shown in figure B.1.

The aerodynamic damping is estimated from a description of the blade configuration using equation B.1, which requires the chord and twist distributions for the turbine blade. Figure B.2 shows the distributions assumed for the 1.5 MW turbine.

B.3 4 MW Turbine

B.3.1 Description

This turbine concept is an uprated version of the Kvaerner-Turbin WTS-80 design, with the rated power increased to 4 MW, and the rotor diameter extended to 90 m, together with a new blade layout optimised for offshore application. The WTS-80 design itself was derived from the Kvaerner-Turbin Nasudden II prototype. The

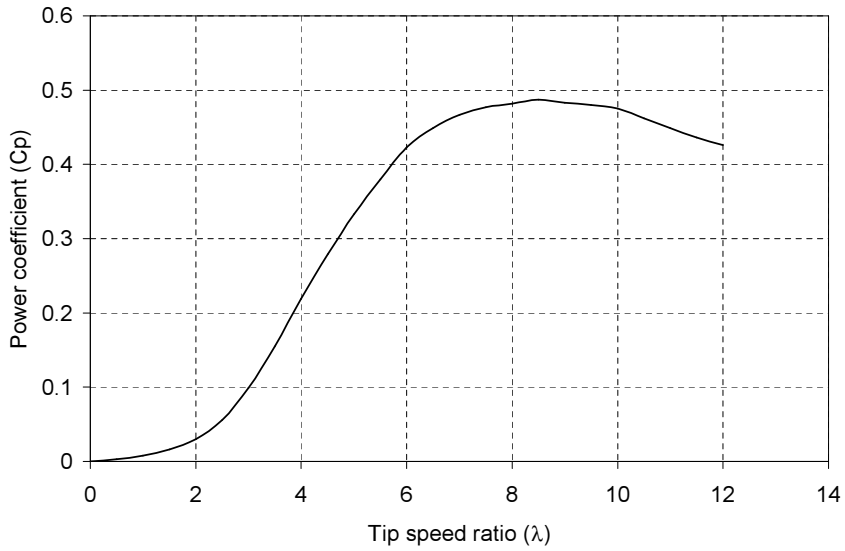

Figure B.1: $Cp - \lambda$ curve for 1.5 MW Turbine.

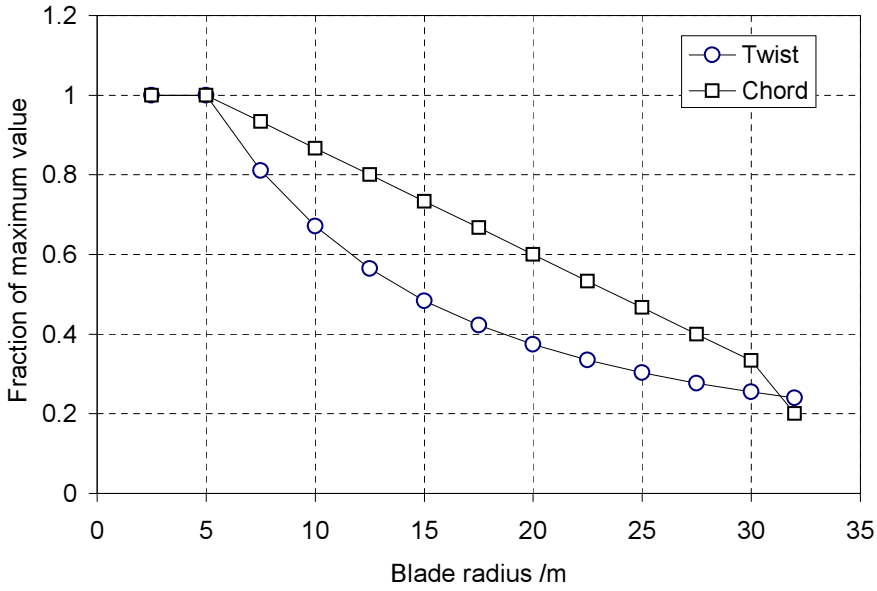

Figure B.2: Chord and twist distributions for 1.5 MW Turbine. Values are plotted relative to the maximum chord of 2.5 m and the maximum twist of 22 degrees.

2 bladed machine employs full span pitch control, and has been marinised for offshore use. Data for this machine was obtained from Kvaerner-Turbin, Delft University and the Opti-OWECS project.

B.3.2 Overall specification

The specification of the 4 MW turbine used for the parameter studies is shown in table B.2.

Rotor diameter	45 m
No. of blades	2
Rotation speed	20 rpm
Cut in wind speed	5 m/s
Cut out wind speed	25 m/s
Rated wind speed	13.3 m/s
Rated wind power	4000 kW
Generator efficiency (assumed constant)	94.9
Gearbox efficiency(assumed constant)	94.9
Nacelle vertical dimension	10 m
Nacelle frontal area	35 m^2
Effective blade area	187 m^2
Nacelle drag factor	1.2
Blade drag factor (operating case)	0.4
Blade drag factor (fail case)	1.3
Aerodynamic damping (% critical)	1.02
Compatible diameters for tower top	2.2-2.4 m
Mass (incl. blades)	141,000 kg
Purchase cost (2002)	2,550,000 Euro

Table B.2: Description of the 4 MW turbine used for the parameter studies.

B.3.3 Aerodynamic performance and blade description

The performance curve and blade configuration assumed for the 4 MW turbine are shown in figures B.3 and B.4 respectively.

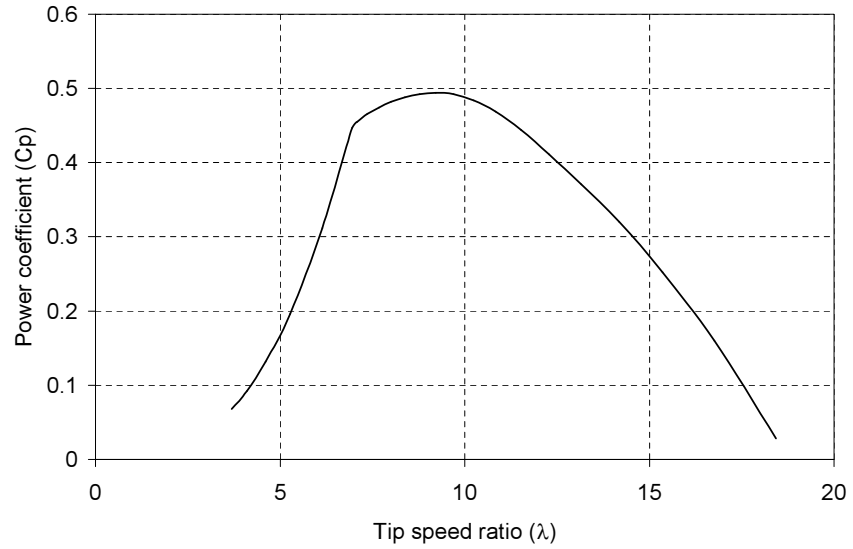

Figure B.3: $Cp - \lambda$ curve for 4 MW Turbine.

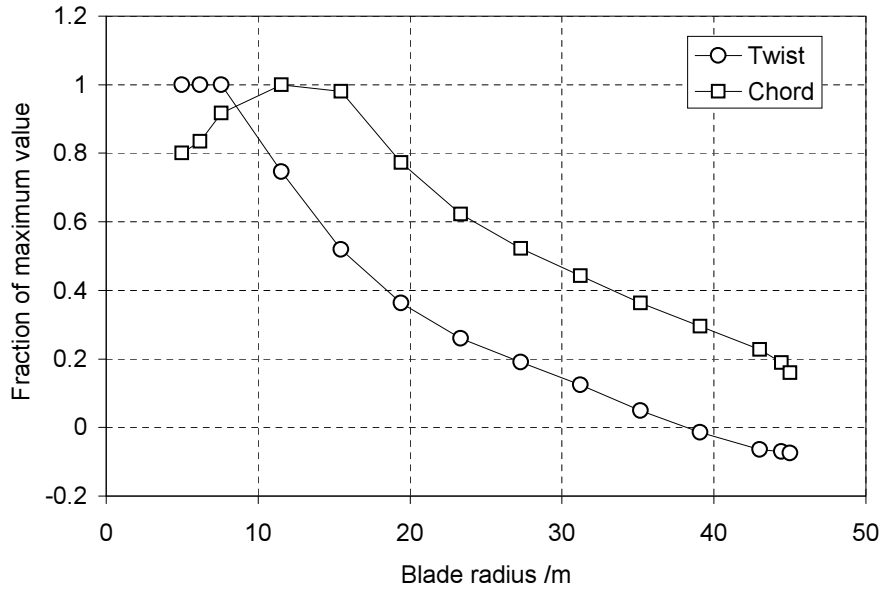

Figure B.4: Chord and twist distributions for 4 MW Turbine. Values are plotted relative to the maximum chord of 4.4 m and the maximum twist of 13.4 degrees.

B.4 Estimating aerodynamic damping

The rotor derived aerodynamic damping of the structure is estimated according to the relation [129]

$$\xi_c = \frac{N_b \rho \Omega_R}{8\pi f_1 m_1} \int_{r_{root}}^{r_{tip}} \left(\frac{dC_l}{d\alpha} \right)_r c\,(r)\, r dr. \tag{B.1}$$

where

ξ_c	Aerodynamic damping as a fraction of critical damping
N_b	Number of blades
ρ	Density of air
Ω_R	Rotor speed
f_1	Frequency of the first mode
m_1	Modal mass for the first mode
r	Spanwise co-ordinate along a blade
r_{root},r_{tip}	Extremities of blade
$c\,(r)$	Chord length at r
$\frac{dc_l}{d\alpha}$	Slope of lift coefficient with angle of attack.

The value of the integral depends on the geometry of the turbine and the flow conditions. So long as the flow remains attached over the blades, the slope of the lift coefficient against angle of attack relationship remains approximately constant. If the flow separates, during blade stall, then the slope reduces. It thus is possible to estimate an upper limit on the aerodynamic damping by evaluating expression B.1 assuming attached flow conditions over the blade. Table B.3 shows values computed for the two turbines investigated here using the data above.

Turbine	Value of integral
1.5 MW	4,426
4 MW	11,318

Table B.3: Value of integral in expression for aerodynamic damping of first mode of structure.

Appendix C

Miscellaneous data

Physical etc. data	
Density of air	1.2 kg/m^3
Density of water	1000 kg/m^3
Acceleration due to gravity	9.81 m/s^2
Von Karman constant	0.4
Charnock constant	60
Material properties	
Steel modulus (tower and pile)	210 GPa
Steel density (tower and pile)	7860 kg/m^3
Steel max. stress	2 MPa
Endurance relation constant (tower and pile)	$2x10^{14}$
Endurance relation slope (tower and pile)	4
Tower surface roughness	0.4
Concrete density	3000 kg/m^3
Safety factors	
Above water bending safety factor	1.35
Below water bending safety factor	1.35
Above water fatigue safety factor	1.25
Below water fatigue safety factor	1.35
Economic data	
Test discount rate	5%
Economic lifetime	20 years

EUR:GBP Exchange rate	1.5
Total 'Other' costs	13 % of total investment
Coefficients in Morison Equation	
Drag coefficient	1.25
Drag coefficient	2.0

Appendix D

Grid connection model

D.1 Introduction

As discussed in chapter 2, the grid connection comprises the following major components:

- Inter-turbine connections and switch gear,
- Main switch gear, transformer and support platform,
- Cable from farm to shore,
- Cable from shore to grid,
- Equipment for connection to the grid.

The type of connection concepts employed, for example whether AC or DC equipment is used, or the topology of the connections between the turbines will have a strong influence on the cost of the grid connection. For any particular farm configuration, there will be a connection technology that provides the least cost solution.

For each connection technology, the capital cost will be influenced by:

- Turbine rated power
- Number of turbines
- Distance between turbines
- Distance to shore
- Distance from shore to grid.

D.2 'Bottom-up' detailed cost model

A detailed 'bottom-up' cost model for offshore wind farm grid connection systems, designing connections on a component by component basis, was developed as part of the work reported here. The FORTRAN implemented model draws substantially on a Microsoft Excel spreadsheet model developed at the University of Delft [170], but contains a number of corrections and some updated costs. As with the main cost model, the grid connection model searches over a range of connection options to identify the most economic solution for any particular offshore farm grid connection scenario.

It was originally planned to use the grid connection model as a direct component of the whole system model described in the main chapters of this thesis. Time constraints have prevented the full integration and debugging of the integrated models. The results reported here rely therefore on a simpler look-up table based model, developed by undertaking parameter studies with the developed model.

D.3 Look-up table model used in the reported analysis

For the look-up table model, costs are considered in the following categories only:

- Internal connection costs within the farm and ancillary equipment, including transformers, transformer support platform and switchgear,
- Connection cable from the farm to the shore,
- Connection cable from the shore to the grid,
- Cost of connecting to the grid.

The internal connection costs and ancillary equipment are dealt with by means of a look-up table specifying the capital investment as a function of the number of turbines in the farm and the rated output of each turbine. Linear interpolation is used to estimate the internal grid connection costs for intermediate cases.

Parameter studies for the range of farm configurations considered here demonstrated that the costs of connection cables, both onshore and offshore, scaled linearly with the distance covered. These costs are estimated therefore using a cost per unit distance multiplier.

Again for the range of farm configurations considered here, the cost of the equipment required to connect to the grid is constant. Thus the fourth item is treated as a fixed cost.

Figures D.1 and D.2 summarise the grid connection costs predicted by the look up table model for farms comprising 1.5MW and 4MW turbines respectively.

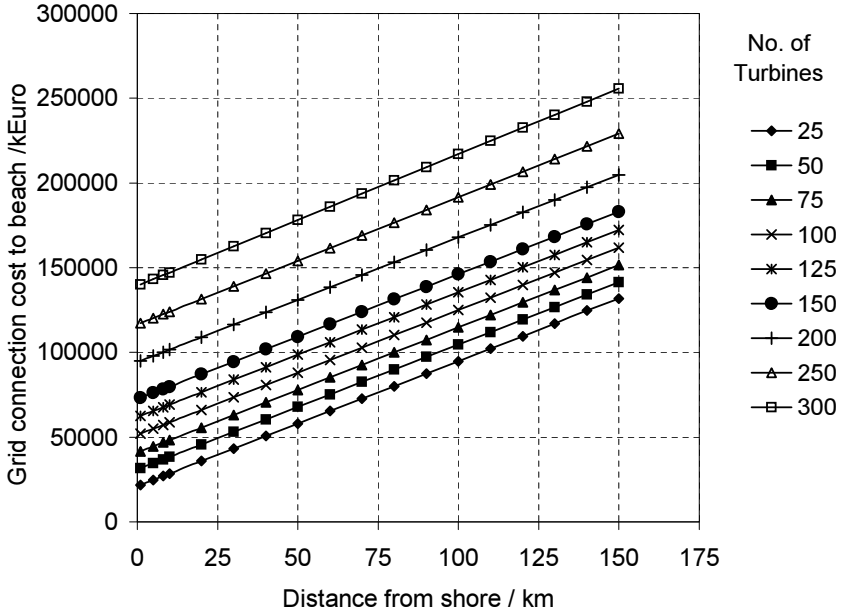

Figure D.1: Grid connection costs for farm of 1.5MW turbines as a function of the distance from the shore and the farm size.

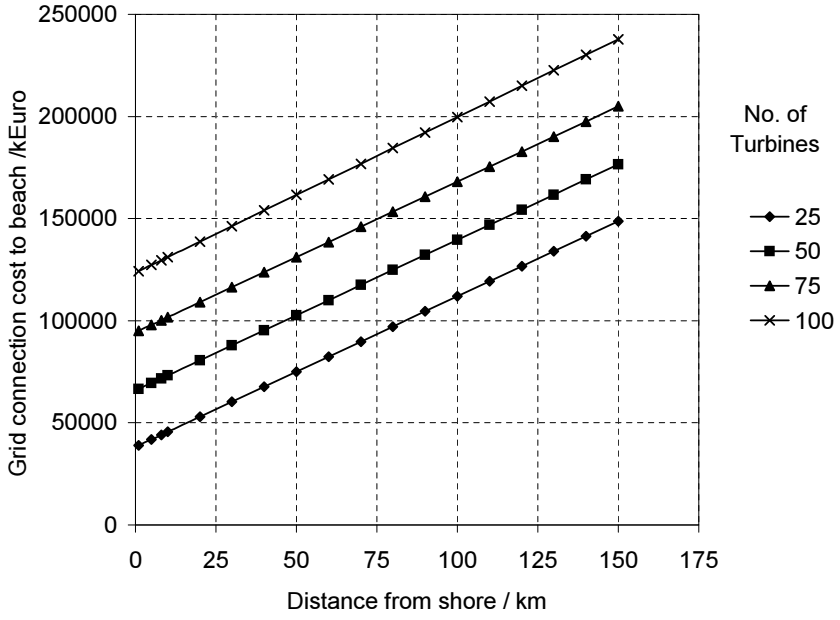

Figure D.2: Grid connection costs for farm of 4MW turbines as a function of the distance from the shore and the farm size.

Appendix E

Model of on-going costs

E.1 Introduction

The on-going costs model is adapted from work undertaken at the University of Delft, primarily by van Bussel and Schontag [132]. The author had some involvement in this work, but it is reported here purely by way of explanation.

A detailed Monte-Carlo simulation of the interactions between turbine failures, maintenance effort, and the occurrence of storms sufficiently severe to prevent maintenance was developed. This was used in turn for a series of parameter studies to investigate the impact on turbine availability and maintenance costs of the following parameters:

- Distance to shore
- Climatic conditions
- Farm size
- Reliability of individual turbines.

Using the results of the study, a set of parametric relationships were formulated. These were implemented as FORTRAN code for use in the cost modelling study.

E.2 Details

The overall farm availability is estimated from three parameters

- The reliability of the wind turbines themselves, which here will be denoted η_{avail},
- The impact that maintenance provision has on the overall availability, which is symbolised as η_{crew},

- The impact of storms on access to the wind farm for maintenance, η_{storms},

such that the overall farm availability is given by

$$\eta_{avail,farm} = \eta_{storms}\eta_{crew}\eta_{avail} \tag{E.1}$$

and the annual energy production is a fraction $\eta_{avail,farm}$ of that estimated without considering availability at all.

E.2.1 Impact of storms

The impact of storms is estimated using

$$\eta_{storms} = 1 - \frac{1}{2}\left(F_{storm}^2 + F_{storm}^3\right) \tag{E.2}$$

where the proportion of time during which storms prevent maintenance access is given by

$$F_{storm} = e^{-\left(\frac{10.48}{a_w}\right)^{2.2}} \tag{E.3}$$

and

$$a_w = \frac{\bar{u}}{0.8855} \tag{E.4}$$

with $\bar{u}$ being the annual hourly mean wind speed at the hub height.

E.2.2 Impact of maintenance actions

The parameter study found that the effect of maintenance actions on the farm availability could be modelled using

$$\eta_{crew} = 1 - e^{\frac{-T_{work}C_{maint}}{1.08}}. \tag{E.5}$$

In this expression C_{maint} is the annual expenditure on maintenance operations, measured in 2002 MEuro, including the cost of replacement parts. Clearly the number of turbines and their size will have an impact on the effectiveness of any maintenance expenditure, but this influence was not investigated. It is assumed here that expression E.5 remains valid if reformulated in terms of the proportion of the total turbine investment cost spent annually on maintenance. In the original study, the total turbine investment cost was 71 MEuro, and thus equation E.5 is transformed into

$$\eta_{crew} = 1 - e^{\frac{-71T_{work}C_{maint}}{1.08C_{turb}}} \tag{E.6}$$

where C_{turb} is the total turbine investment cost. T_{work} is the proportion of each assumed twelve hour shift available for the maintenance crew to work on the

farm, allowing for 1 hour embarkation and disembarkation time at the beginning and end of each shift and travel using a boat with an average speed of 10 km/h, which gives

$$T_{work} = \frac{1}{6}\left(6 - \left(1 + \frac{L_{maintbase}}{10}\right)\right). \tag{E.7}$$

The further the farm is from the maintenance base, $L_{maintbase}$ in kilometres, the lower the availability for a given annual maintenance expenditure C_{main}, as more and more of the work time is consumed simply by travelling to and from the wind farm. Figure E.1 demonstrates one instance of how the value of η_{crew} declines with distance from the shore. For the calculations within this thesis, it has been assumed that the distance from the maintenance base is equal to the distance from the shore, and this is reflected in the figure.

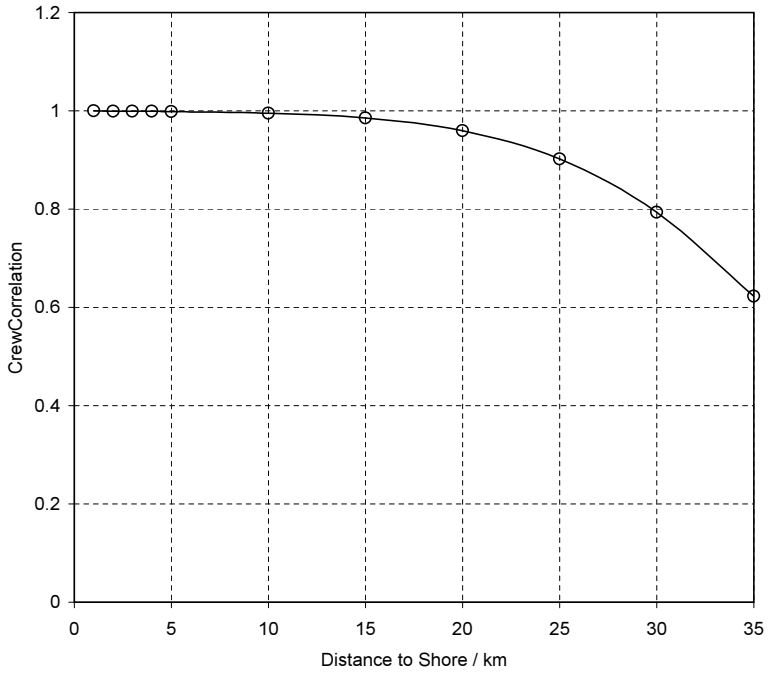

Figure E.1: Variation of η_{crew} (here denoted 'CrewCorrelation') with distance from the shore.

E.2.3 Integration into the cost model

The maintenance calculation is implemented within the cost model as a series of functions. Figures E.2 and E.3 show model predictions for how the overall farm availability $\eta_{farm,avail}$ varies with distance from shore for annual maintenance expenditures of 1 MEuro and 2 MEuro respectively, assuming a farm with a turbine

investment cost of 1 MEuro, and each turbine having an individual reliability η_{avail} of 95%.

For any particular farm configuration and location, there will be an optimum annual expenditure C_{maint} on maintenance that minimises the overall cost of energy, that is

$$C = \frac{C_{tot}}{aE\eta_{avail,farm}} + \frac{C_{maint} + C_{other}}{E\eta_{avail,farm}} \tag{E.8}$$

where in this case E is the annual energy production before accounting for availability, a is the annuity factor, C_{tot} is the total investment cost and C_{other} are any ongoing costs other than maintenance operations. The cost model maintenance routines search over annual expenditures between 0.1 MEuro and 6 MEuro, and return the optimum annual expenditure.

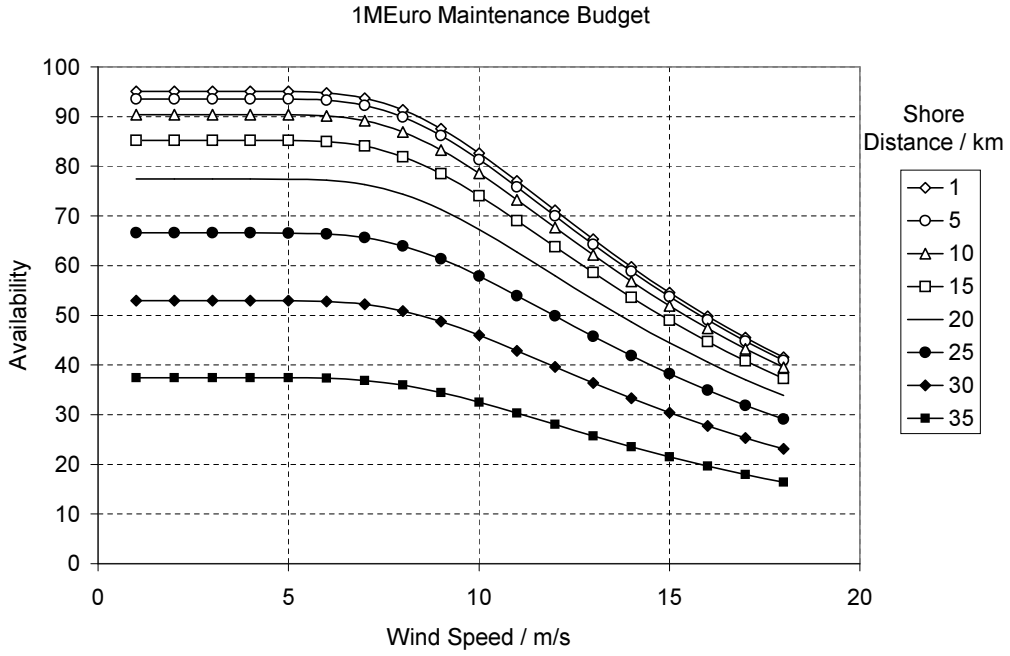

Figure E.2: Variation of farm availability with distance from the shore and hub height annual mean hourly wind speed as predicted by the model for an annual maintenance expenditure of 1 MEuro at a farm with a total turbine investment cost of 71 MEuro.

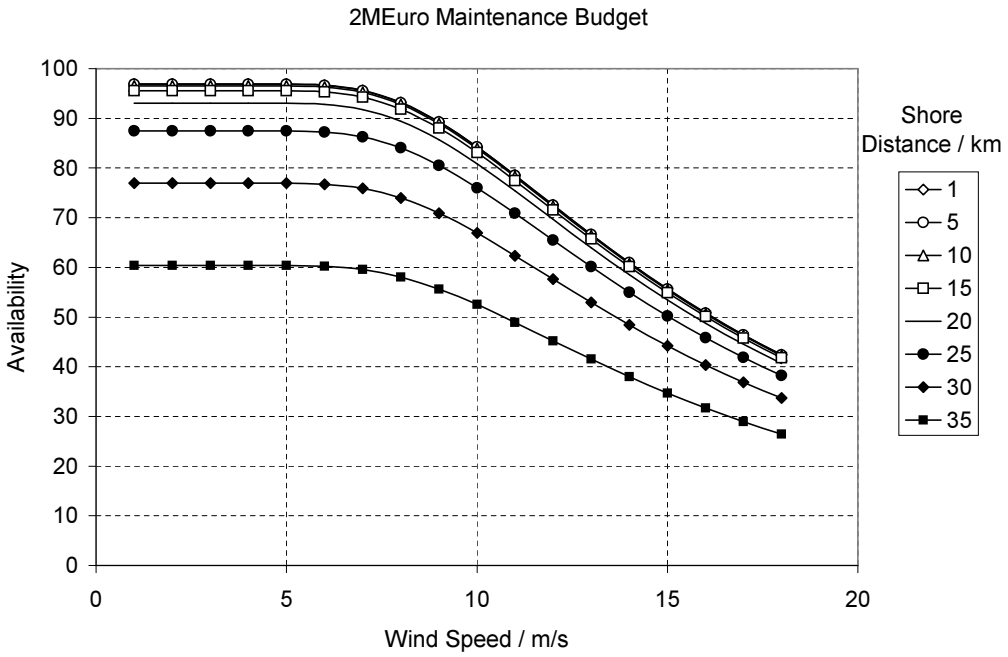

Figure E.3: Variation of farm availability with distance from the shore and hub height annual mean hourly wind speed as predicted by the model for an annual maintenance expenditure of 2 MEuro at a farm with a total turbine investment cost of 71 MEuro.

Appendix F

Farm cost breakdown data

F.1 Introduction

Chapter 3 discusses the conclusions that may be drawn from an analysis of cost data for several existing offshore farms and desk studies. This appendix describes the sources of the data used and presents several diagrams that were omitted from the main text for clarity.

F.2 Farms/Studies considered and data sources

Table F.1 lists the recent farms and studies considered in chapter 3 along with the data sources used for information.

Data was also available for the so called "Phase IIC" study [210]. This was not included in the main analysis because it may have been unrepresentative for two reasons. Firstly a large proportion of the work reported was derived from the much older Phase IIB [211] study, which was completed before the first offshore farm was built and therefore must be regarded as quite unreliable. Secondly most of the Phase IIC study investigated the use of very large wind turbines with diameter up to 120 m. These diameters are much larger than those available commercially at the time of the original study, typically 40m diameter machines with rated powers below 500 kW, and the results are dominated by assumptions made about the cost and design of future large turbines. The RES study in contrast focussed on commercially available turbines, and is thus judged to be more representative despite producing high cost estimates.

Farm/Study	Year	Brief description	Sources for cost and environmental data
Vindeby	1991	Early Danish farm in sheltered Baltic waters	[13], [209],[15]
Lely	1994	Dutch farm in inland sea	[209], [16], [15]
Tunø-Knob		Danish demonstration farm in Baltic	[17], [209],[15]
Middelgrunden	2001	Semi-commercial Danish farm	[24], [184], [15]
Horns Rev	2003	Large 'commercial' danish farm	[28], [184], [15]
OptiOWECS	1998	EU funded desk study	[16]
RES	1993	UK DTI funded desk study	[10]
Thyssen		German desk study	[11]
SKPower		Danish desk study	[12]

Table F.1: Farms and studies considered for the analysis in chapter 3 and data sources used.

F.3 Turbine cost correlation

Figure F.1 shows the turbine unit cost in kEuro as a function of the total farm rated power in Megawatts.

F.4 Grid connection cost correlations

Figures F.2 and F.3 respectively show the total grid connection cost (including connections between turbines) as a function of the farm rated power and the shortest distance from the shore.

F.5 Operation and maintenance costs

Information on operation and maintenance costs is even readily available than that for capital costs. Much of the literature quotes annual maintenance costs as a proportion of the initial investment cost. Typical figures from the offshore wind farms and studies listed above range from 1.2% to 2.84%.

Operation and maintenance plays a greater role in the energy cost than these

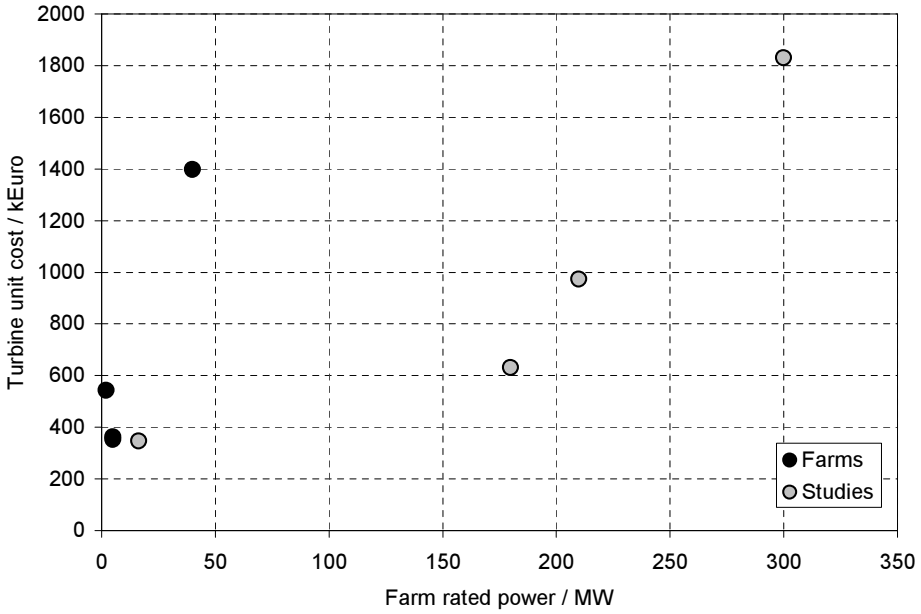

Figure F.1: Relationship between grid connection cost and farm rated power for several offshore farms and recent studies.

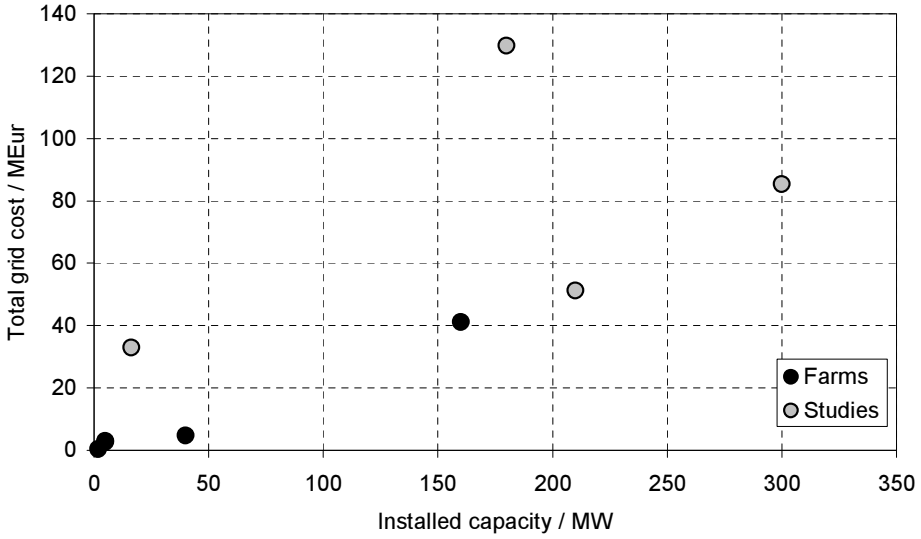

Figure F.2: Relationship between grid connection cost and farm rated power for several offshore farms and recent studies.

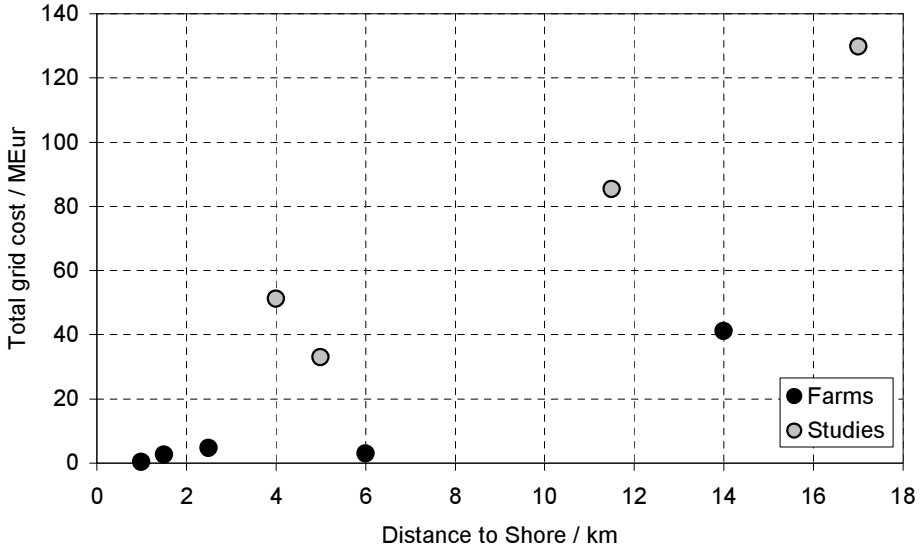

Figure F.3: Relationship between grid connection cost and distance to shore for several offshore farms and recent studies.

figures superficially suggest. Manipulation of equation 3.1 shows that the proportion of the total cost of energy attributable to an annual maintenance cost equal to a fraction x of the total investment cost is given by $\frac{ax}{ax+1}$. With a discount rate of 5% and a lifetime of 20 years, the discounting factor is equal to 12.46, meaning that a 1% annual maintenance cost represents approximately 11% of the total energy cost.

Table F.2 lists the contribution to the energy cost made by operation and maintenance for several of the farms and studies listed earlier in this appendix. The figures show that operation and maintenance costs are of approximately equal importance to the grid connection costs in many cases, and hence cannot be completely ignored in evaluating the suitability of a location. Maintenance costs depend on the details of the farm and its location in much the same way as the grid connection and the support structure. They are not considered in any detail in this work, with appendix E describing an externally developed model that was used here.

Farm/Study	Fraction of energy cost
Vindeby	13.0%
Lely	15.7%
Middelgrunden	15.5%
OptiOWECS	23%
Phase IIC	26-31%
Thyssen	22.7%
RES	16.3%

Table F.2: Contribution to energy cost made by operation and maintenance for several farms and studies.

Appendix G

Mathcad model used in chapter 3

The following pages present the Mathcad version 11 model used to produce figure 3.18.

Basic Tower Frequency Model for Wind Turbines

Set top forces

$M_{top} := 2000 \cdot 10^3$

$F_{top} := 400 \cdot 10^3$

Set dimensions

$r_{top} := 2$

Material propertes

$\sigma_m := 80 \cdot 10^6$

$M_{turb} := 79000$ turbine mass

$E := 200 \cdot 10^9$ Youngs Modulus

$\rho := 7800$ Density

$pois := 0.3$

$P := \frac{1}{2}$ Rotor freq

Linear radius distribution (for now)

$$r_o(h, r_{bot}, H) := \left| \begin{array}{l} d_r \leftarrow \frac{r_{top} - r_{bot}}{H} \\ r_{bot} + d_r \cdot h \end{array} \right.$$

Bending moment distn

$$M(h, H) := M_{top} + F_{top} \cdot (H - h)$$

Distributions down the tower

$r_i(r_o, t) := r_o - t$ Inner radius function

$I(r_o, t) := \frac{\pi}{4} \cdot \left[r_o^4 - (r_i(r_o, t))^4 \right]$ Second moment of area

Local buckling calcukation

$tb := 0.1$

Given

$$\frac{M \cdot r_o}{I(r_o, tb)} = \frac{0.4E}{\sqrt{3} \cdot \sqrt{1 - pois^2}} \cdot \frac{tb}{r_o}$$

$buckthick(M, r_o) := Find(tb)$

$t_{buckle}(h, r_{bot}, H) := buckthick(M(h, H), r_o(h, r_{bot}, H))$ *More convenient form*

Bending minimum thickness at any location

$tt := 0.1$ This is the trial thickness to start with

Given

$$I(r_o, tt) = \frac{(M \cdot r_o)}{\sigma_{max}}$$

Bendthick returns the bending thickness

$bendthick(r_o, M, \sigma_{max}) := Find(tt)$

More convenient form

$t_{bend}(h, \sigma_{max}, r_{bot}, H) := bendthick(r_o(h, r_{bot}, H), M(h, H), \sigma_{max})$

Combine the two with a function that gives the largest

$$\text{minthick}(h,\sigma_{max},r_{bot},H) := \max\left(t_{buckle}(h,r_{bot},H),t_{bend}(h,\sigma_{max},r_{bot},H)\right)$$

Get the actual thickness using a thickness factor tf

$$\text{thick}(tf,h,\sigma_{min},r_{bot},H) := tf\cdot\text{minthick}(h,\sigma_{min},r_{bot},H)$$

Define the tower volume function

$$XSArea(r_o,t) := 2\cdot r_o\cdot t - t^2$$ Gives the X_sect area of each section

$$TowerXSA(h,r_{bot},tf,\sigma_{min},H) := XSArea\left(r_o(h,r_{bot},H),thick(tf,h,\sigma_{min},r_{bot},H)\right)$$

$$Vol(r_{bot},tf,\sigma_{min},H) := \int_0^H TowerXSA(h,r_{bot},tf,\sigma_{min},H)\,dh$$ Generic expression for tower volume

Frequency calculation using simple raleigh method

First define the shape function

$$\psi(h,H) := 1 - \cos\left(\pi\cdot\frac{h}{2\cdot H}\right)$$

$$\psi dd(h,H) := \frac{d^2}{dh^2}\psi(h,H)\rightarrow$$ Second differential

Generalised stiffness

$$GenStiff(r_{bot},tf,\sigma_{min},H) := \int_0^H E\cdot I\left(r_o(h,r_{bot},H),thick(tf,h,\sigma_{min},r_{bot},H)\right)\cdot\left(\psi dd(h,H)^2\right)dh$$

Generalised mass

$$m(h,r_{bot},tf,\sigma_{min},H) := \rho\cdot TowerXSA(h,r_{bot},tf,\sigma_{min},H)$$ This is mass distribution

$$GenMass(r_{bot},tf,\sigma_{min},H) := 0.5\cdot\left[M_{turb}\cdot\left(\psi(H,H)^2\right) + \left[\int_0^H m(h,r_{bot},tf,\sigma_{min},H)\cdot\left(\psi(h,H)^2\right)dh\right]\right]$$

$$\text{freq}(r_{bot}, tf, \sigma_{min}, H) := \frac{1}{2\cdot\pi}\cdot\sqrt{\frac{\text{GenStiff}(r_{bot}, tf, \sigma_{min}, H)}{\text{GenMass}(r_{bot}, tf, \sigma_{min}, H)}}$$

This is the frequency

Get the expressions into a form for plotting

$$\text{FreqPlot\_RH}(H, r_{bot}) := \frac{\text{freq}(r_{bot}, 1, \sigma_m, H)}{P}$$

$$\text{FreqPlot\_RH2}(H, r_{bot}) := \frac{\text{freq}(r_{bot}, 2, \sigma_m, H)}{P}$$

Divide by P makes relative to rotor

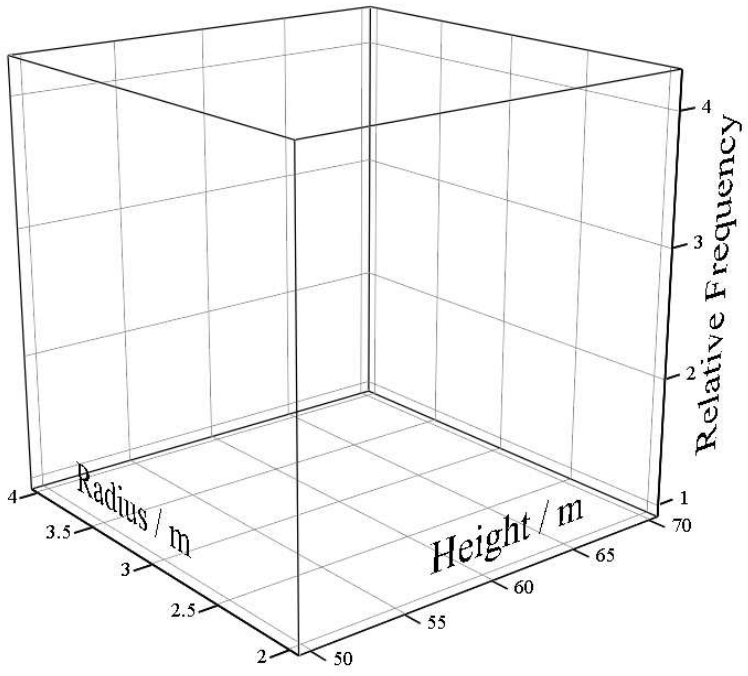

FreqPlot_RH, FreqPlot_RH2

Appendix H

Finite element methodology

H.1 Approach

A simple finite element methodology is employed for deflection and eigenfrequency calculations for the structure. For the FE calculations a structure is treated as a simple beam of varying cross section and material properties. The approach is based on that described by Fenner [212]. No assumptions are made as to the cross section and as such the calculations are essentially exact for the structure as described in the model. It must be kept in mind though that the model treats the structure geometry in a simplified manner.

As discussed in the main text, the structure is treated as being divided into a number of sections. Within each section the properties do not change. These sections form 'natural' elements for the finite element analysis, directly amenable to deflection calculation. Matters are not so simple for the eigenfrequency calculations, which require that a 'mass-spring' type model of the structure be constructed. While the already defined sections make 'natural' spring elements, the formation of the mass elements requires further consideration.

H.2 Finite element theory

Consider a generalised element of the modelled structure experiencing bending about one axis of symmetry as shown in figure H.1. This element, the m^{th} from the base of the structure, has length L_m and its left hand boundary (as shown) coincides with the i^{th} node along the structure, with the right hand boundary coincident with the j^{th} node. A set of local co-ordinates x and y are defined to be respectively along and normal to the neutral axis of the element.

When the structure is subjected to load, the force and moment applied to the element at node i are V_i and M_i, and at node j, V_j and M_j. Let the variation of the

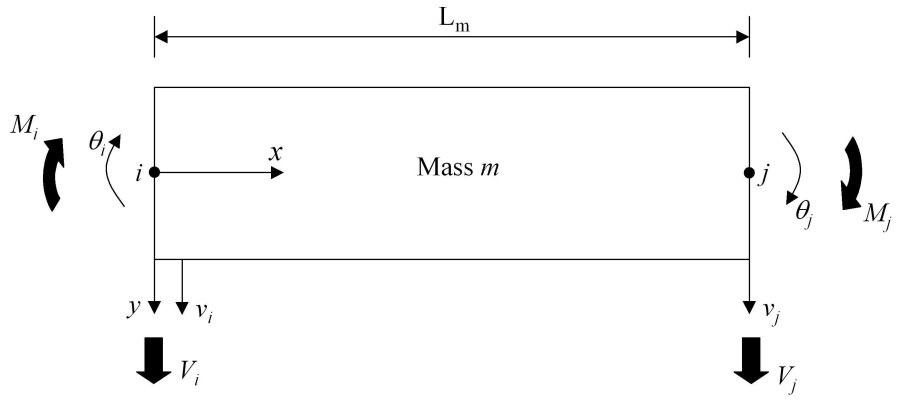

Figure H.1: Beam element for FEA model.

displacement in the y-direction along the length of the element in co-ordinates local to the element with origin at the i^{th} node be given by

$$v(x) = C_1 + C_2 x + C_3 x^2 + C_4 x^3 \tag{H.1}$$

The clockwise rotation at any point of the element is then

$$\theta = \frac{dv}{dx} = C_2 + 2C_3 x + 3C_4 x^2 \tag{H.2}$$

Substituting the conditions at the i^{th} node into these relationships gives, for the deflection

$$v_i = v\,(0) = C_1 \tag{H.3}$$

and for the rotation

$$\theta_i = \theta\,(0) = C_2 \tag{H.4}$$

Conditions at the j^{th} node similarly imply for the deflection there

$$v_j = v\,(L_m) = C_1 + C_2 L_m + C_3 L_m^2 + C_4 L_m^3 \tag{H.5}$$

and for the rotation

$$\theta_j = \theta\,(L_m) = C_2 + 2C_3 L_m + 3C_4 L_m^2 \tag{H.6}$$

Relations H.3 to H.6 may be used to express constants C_3 and C_4 in terms of the boundary deflections and rotations. Through a series of substitutions it may be

shown that

$$C_3 = \frac{3v_j}{L_m^2} - \frac{3v_i}{L_m^2} - \frac{2\theta_i}{L_m} - \frac{\theta_j}{L_m} \tag{H.7}$$

and

$$C_4 = \frac{\theta_j}{L_m^2} + \frac{\theta_i}{L_m^2} - \frac{2v_j}{L_m^3} - \frac{2v_i}{L_m^3}. \tag{H.8}$$

Consider now that the element is subjected to a moment N and a shear force Q. By simple bending theory, the hogging moment at any point is given by

$$N = E_m I_m \frac{d^2 v}{dx^2} \tag{H.9}$$

i.e.

$$N = E_m I_m \left(2C_3 + 6C_4 x\right) \tag{H.10}$$

where E_m is the Young's Modulus of the element and I_m is the second moment of area. Similarly the shear force is

$$Q = \frac{dN}{dx} = 6E_m I_m C_4. \tag{H.11}$$

Applying the conditions at the nodes i and j gives:

$$V_i = Q\left(0\right) = 6C_4 E_m I_m \tag{H.12}$$

$$M_i = -N\left(0\right) = -2C_3 E_m I_m \tag{H.13}$$

$$V_j = -Q\left(L_m\right) = -6C_4 E_m I_m \tag{H.14}$$

$$M_j = N\left(L_m\right) = E_m I_m \left(2C_3 + 6C_4 L_m\right) \tag{H.15}$$

which may be written collectively in matrix form:

$$\begin{bmatrix} V_i \\ M_i \\ V_j \\ M_j \end{bmatrix} = E_m I_m \begin{bmatrix} 0 & 6 \\ -2 & 0 \\ 0 & -6 \\ 0 & 6L_m \end{bmatrix} \begin{bmatrix} C_3 \\ C_4 \end{bmatrix}. \tag{H.16}$$

Using expressions H.7 and H.7, the matrix of polynomial coefficients may be written as

$$\begin{bmatrix} C_3 \\ C_4 \end{bmatrix} = \begin{bmatrix} \frac{-3}{L_m^2} & \frac{-2}{L_m} & \frac{3}{L_m^2} & \frac{-1}{L_m} \\ \frac{2}{L_m^3} & \frac{1}{L_m^2} & \frac{-2}{L_m^3} & \frac{1}{L_m^2} \end{bmatrix} \begin{bmatrix} v_i \\ \theta_i \\ v_j \\ \theta_j \end{bmatrix}. \tag{H.17}$$

Combining H.16 and H.17 gives

$$\begin{bmatrix} V_i \\ M_i \\ V_j \\ M_j \end{bmatrix} = \frac{E_m I_m}{L_m^3} \begin{bmatrix} 12 & 6L_m & -12 & 6L_m \\ 6L_m & 4L_m^2 & -6L_m & 2L_m^2 \\ -12 & -6L_m & 12 & -6L_m \\ 6L_m & 2L_m^2 & -6L_m & 4L_m^2 \end{bmatrix} \cdot \begin{bmatrix} v_i \\ \theta_i \\ v_j \\ \theta_j \end{bmatrix} \tag{H.18}$$

which provides an analytic relationship between the forces and the deflection and rotation at both ends of the element. For conciseness this relationship will be written as

$$\mathbf{R}_m = \mathbf{k}_m \delta_m \tag{H.19}$$

where $\mathbf{k}_m$ is the element stiffness matrix, i.e.

$$\mathbf{k_m} = \frac{E_m I_m}{L_m^3} \begin{bmatrix} 12 & 6L_m & -12 & 6L_m \\ 6L_m & 4L_m^2 & -6L_m & 2L_m^2 \\ -12 & -6L_m & 12 & -6L_m \\ 6L_m & 2L_m^2 & -6L_m & 4L_m^2 \end{bmatrix}. \tag{H.20}$$

The overall structure, comprising many such elements, must be in equilibrium. In other words, the sum of the externally applied forces and moments at the nodes must be equally to the sum of the forces and moments on the structural elements at the nodes. These two force sets must in turn be compatible with the deflection and rotation of the structure. Thus, mathematically,

$$\mathbf{F} = \sum \mathbf{R_m} \tag{H.21}$$

and

$$\sum \mathbf{R_m} = \sum \mathbf{k_m} \delta_\mathbf{m} = \mathbf{K} \delta \tag{H.22}$$

where K is the overall stiffness matrix for the structure, vector F contains the externally applied loads and δ represents the corresponding linear and rotational displacements. Clearly we can write

$$\mathbf{F} = \mathbf{K} \delta. \tag{H.23}$$

The means by which the overall stiffness matrix is composed warrants further

explanation. Let the elemental relation H.18 represented by

$$\begin{bmatrix} V_i \\ M_i \\ V_j \\ M_j \end{bmatrix} = \begin{bmatrix} k_{11} & k_{12} & k_{12} & k_{14} \\ k_{21} & k_{22} & k_{23} & k_{24} \\ k_{31} & k_{32} & k_{33} & k_{34} \\ k_{41} & k_{42} & k_{43} & k_{44} \end{bmatrix} \begin{bmatrix} v_i \\ \theta_i \\ v_j \\ \theta_j \end{bmatrix} \tag{H.24}$$

such that the elements of the element stiffness matrix relating the loads and displacement of nodes 1 and 2 may be referred to as $k_{1,11,}k_{1,12}$ etc., with the elements of the matrix relating nodes 2 and 3 being denoted $k_{2,11}$ etc., and elements of the matrix relating the n^{th} and $n+1^{th}$ nodes being $k_{n,11}$ and so on. Using this notation, relationship H.23 when written out in full has the general form of equation H.27. In practice the overall stiffness matrix departs from this form due to the influence of boundary constraints, as discussed in the next section.

For a structure with a known stiffness matrix, the nodal displacements caused by a force set F can be calculated from

$$\delta = \mathbf{K}^{-1} \cdot \mathbf{F}. \tag{H.25}$$

H.3 Application of boundary conditions

The boundary conditions on the structure comprise the free upper end which carries the mass of the nacelle and the lower end which is constrained by the behaviour of the foundation.

Since the upper end of the tower is free, no modification of the relationships is required. However, for the eigenmode calculations described later, the mass of the nacelle and rotor must be added to the mass of the upper node.

At the lower end, the response of the foundation, irrespective of type, is modelled by a rotational and lateral stiffness. Thus the lowest node of the tower, the 1^{st} node in the above analysis, may be thought of as being connected to the rigid ground through a lateral and rotational spring, allowing both lateral motion and rotation of the lowest node. To include this behaviour in the model an extra node, the 0^{th} node, is introduced representing the rigid sea-bed. A lateral spring of stiffness k_{lat} and a rotational spring of stiffness k_{rot} link the first node to the 0^{th} node such that the relationship between the forces, moments and deflections of the 0^{th}

and 1^{st} nodes is given by

$$\begin{bmatrix} V_0 \\ M_0 \\ V_1 \\ M_1 \end{bmatrix} = \begin{bmatrix} k_{lat} & 0 & 0 & 0 \\ 0 & k_{rot} & 0 & 0 \\ 0 & 0 & k_{lat} & 0 \\ 0 & 0 & 0 & k_{rot} \end{bmatrix} \begin{bmatrix} 0 \\ 0 \\ v_1 \\ \theta_1 \end{bmatrix} \tag{H.26}$$

where the deflection and rotation of the 0^{th} nodes has been pre-constrained to zero. Note that the external force V_0 and moment M_0 exerted on the foundation do not influence the calculation since the deflection of 0^{th} node has been constrained. Adding this boundary condition to expression H.27 gives equation H.28.

H.4 Deflection calculation

The finite element calculation is implemented within the model as an independent subroutine fea_beam contained within Fortran source code file fea3.f. The subroutine must be provided with arrays containing

- The position of each node,
- Young's modulus for each element
- Section moment of area in the bending direction for each element
- Force applied at each node
- Moment applied at each node.

The overall stiffness matrix is evaluated, and then the resulting deflection calculated by solving equation H.25 using the SGESV routine from the LINPACK [213] numerical library. The implementation is general in that it may be used to solve simple bending problems for any similar beam type structure.

H.5 Application to eigenfrequency calculation

For the calculation of eigenfrequencies, the model treats the structure as a simple nodal mass spring system. Each element is treated as a mass-less spring connecting together masses lumped at the nodes. Solving the general equation of motion for a freely vibrating nodal system

$$\mathbf{Kv} = \omega^2 \mathbf{mv} \tag{H.29}$$

$$\begin{bmatrix} V_1 \\ M_1 \\ V_2 \\ M_2 \\ V_3 \\ M_3 \\ V_4 \\ M_4 \\ \vdots \end{bmatrix} = \begin{bmatrix} k_{1,11} & k_{1,12} & k_{1,13} & k_{1,14} & 0 & 0 & 0 & 0 & \cdots \\ k_{1,21} & k_{1,22} & k_{1,23} & k_{1,24} & 0 & 0 & 0 & 0 & \cdots \\ k_{1,31} & k_{1,32} & k_{1,33}+k_{2,11} & k_{1,34}+k_{2,12} & k_{2,13} & k_{2,14} & 0 & 0 & \cdots \\ k_{1,41} & k_{1,42} & k_{1,43}+k_{2,21} & k_{1,44}+k_{2,22} & k_{2,23} & k_{2,24} & 0 & 0 & \cdots \\ 0 & 0 & k_{2,31} & k_{2,32} & k_{2,33}+k_{3,11} & k_{2,43}+k_{3,12} & k_{3,13} & k_{3,14} & \cdots \\ 0 & 0 & k_{2,41} & k_{2,42} & k_{2,43}+k_{3,21} & k_{2,44}+k_{3,22} & k_{3,23} & k_{3,24} & \cdots \\ 0 & 0 & 0 & 0 & k_{3,31} & k_{3,32} & k_{3,33}+k_{4,11} & k_{3,34}+k_{4,12} & \cdots \\ 0 & 0 & 0 & 0 & k_{3,41} & k_{3,42} & k_{3,43}+k_{4,21} & k_{3,44}+k_{4,22} & \cdots \\ \vdots & \vdots & \vdots & \vdots & \vdots & \vdots & \vdots & \vdots & \ddots \end{bmatrix} \begin{bmatrix} v_1 \\ \theta_1 \\ v_2 \\ \theta_2 \\ v_3 \\ \theta_3 \\ v_4 \\ \theta_4 \\ \vdots \end{bmatrix} \tag{H.27}$$

$$\begin{bmatrix} V_0 \\ M_0 \\ V_1 \\ M_1 \\ V_2 \\ M_2 \\ V_3 \\ M_3 \\ \vdots \end{bmatrix} = \begin{bmatrix} k_{lat} & 0 & 0 & 0 & 0 & 0 & 0 & 0 & \cdots \\ 0 & k_{rot} & 0 & 0 & 0 & 0 & 0 & 0 & \cdots \\ 0 & 0 & k_{lat}+k_{1,11} & k_{1,12} & k_{1,13} & k_{1,14} & 0 & 0 & \cdots \\ 0 & 0 & k_{1,21} & k_{rot}+k_{1,22} & k_{1,23} & k_{1,24} & 0 & 0 & \cdots \\ 0 & 0 & k_{1,31} & k_{1,32} & k_{1,33}+k_{2,11} & k_{1,43}+k_{2,12} & k_{2,13} & k_{2,14} & \cdots \\ 0 & 0 & k_{1,41} & k_{1,42} & k_{1,43}+k_{2,21} & k_{1,44}+k_{2,22} & k_{2,23} & k_{2,24} & \cdots \\ 0 & 0 & 0 & 0 & k_{2,31} & k_{2,32} & k_{2,33}+k_{3,11} & k_{2,34}+k_{3,12} & \cdots \\ 0 & 0 & 0 & 0 & k_{2,41} & k_{2,42} & k_{2,43}+k_{3,21} & k_{2,44}+k_{3,22} & \cdots \\ \vdots & \vdots & \vdots & \vdots & \vdots & \vdots & \vdots & \vdots & \ddots \end{bmatrix} \begin{bmatrix} 0 \\ 0 \\ v_1 \\ \theta_1 \\ v_2 \\ \theta_2 \\ v_3 \\ \theta_3 \\ \vdots \end{bmatrix} \tag{H.28}$$

produces values for the eigenfrequencies ω and the corresponding eigenvectors **v** of displacement where **m** and **K** are respectively mass and stiffness matrices for the structure. The solution uses the RGG routine from the public domain EISPACK [214] library of mathematical functions.

The stiffness matrix employed is identical to that formulated above, in equation H.27 for example. To produce a mass matrix, it is assumed that half of the mass of a segment is associated with the node on one segment boundary, and the other half of the mass with the other node. Thus the mass associated with each node is equal to the half the sum of the masses of the adjoining segments.

Appendix I

Implementation of the Dirlik equation

I.1 Introduction

Well known solutions exist for the calculation of fatigue damage from narrow band stress spectra (see for example [215]). Their applicability is limited however, because most real stress spectra, including those encountered in the current work, do not fulfil the criteria to be regarded as narrow band. Some workers have investigated means to correct calculations for non-narrow banded features, however their validity is also rather limited.

There are two 'accurate' approaches to calculating fatigue damage from stress spectra. One is to transform the stress spectrum into a time series and apply rainflow counting in the conventional manner. This is a time consuming and cumbersome process. Attention has thus turned to means by which to calculate rainflow stress ranges directly from the properties of stress spectra. The Dirlik equation, developed empirically during an extensive numerical study [86] in 1985, is a widely accepted technique in the wind industry. The rainflow ranges produced by the Dirlik equation can be used directly to assess the fatigue life of components, via the Palmgren-Miner [74] law.

The Dirlik technique has been employed in this work for the evaluation of fatigue damage from computed stress spectra. This appendix describes the methodology, drawing entirely on the literature, and also explains how the calculations have been implemented numerically in the cost model.

I.2 The Dirlik expression

Dirlik showed that rainflow ranges could be computed from the zeroeth m_0, first m_1, second m_2 and third m_3 and fourth m_4 moments of stress spectra using

$$p_{RF}(\sigma_R) = \frac{\frac{D_1}{Q}e^{-z/Q} + \frac{D_2 Z}{R^2}e^{-z^2/2R^2} + D_3 Z e^{-z^2/2}}{2(m_o)^{1/2}} \tag{I.1}$$

where

$$D_1 = \frac{2(x_m - \beta^2)}{1+\beta^2} \tag{I.2}$$

$$D_2 = \frac{1-\beta-D_1+D_1^2}{1-R} \tag{I.3}$$

$$D_3 = 1 - D_1 - D_2 \tag{I.4}$$

with

$$\beta = \left(\frac{m_2^2}{m_0 m_4}\right)^{1/2} \tag{I.5}$$

$$x_m = \frac{m_1}{m_0}\left[\frac{m_2}{m_4}\right]^{1/2} \tag{I.6}$$

$$R = \frac{\beta - x_m - D_1^2}{1-\beta-D_1+D_1^2} \tag{I.7}$$

$$Q = \frac{1.25(\beta - D_3 - (D_2 R))}{D_1} \tag{I.8}$$

$$Z = \frac{\sigma_r}{2\sqrt{m_0}} \tag{I.9}$$

I.3 Calculating fatigue damage

Using Dirlik's empirical equation to evaluate the Rainflow ranges, the damage accumulated in time T can be calculated from the stress spectrum [139] by

$$D = \frac{T}{T_c}\frac{1}{A}\int_0^\infty \sigma_r^m p_{RF}(\sigma_r)\, d\sigma_r \tag{I.10}$$

assuming a fatigue endurance curve of the form

$$N = AS^{-m} \tag{I.11}$$

which is as used in the main sections of this work. The mean time between stress peaks T_c can be estimated from moments of the spectrum [139] via

$$T_c = \left[\frac{m_2}{m_4}\right]^{\frac{1}{2}} \tag{I.12}$$

I.4 Numerical implementation

Starting with a stress spectrum in units of ${}^{MPa^2}/_{Hz}$ produced as described in Chapter 5, moments are calculated via numerical integration. Moments are given by the general formula

$$m_n = \int_0^\infty f^n S_{\sigma\sigma}(f)\, df \tag{I.13}$$

and integration is performed using an adaptive Simpson's rule routine taken from Numerical Recipes [90]. In practice, the numerical integration is only continued until the frequency beyond which the spectrum has no significant components rather than until infinity.

Next, a numerical representation of the Rainflow probability density function is produced using equation I.1 by considering stress transition ranges from zero up to the stress range at which the probability of occurrence falls below 0.01. Transition ranges are considered at intervals of 0.2 MPa. As is common in preliminary studies [59], the impact of mean stress is ignored, so that in effect a Rainflow vector rather than a matrix is produced.

Once the Rainflow probability distribution has been calculated, the damage is computed using further numerical integration of equation I.10. In this case, the integrand is not available as a continuous function and thus the integration is performed using a trapezium rule. $\sigma_r^m p_{RF}(\sigma_r)$is calculated at each value of σ_r for which the Rainflow distribution was evaluated and the trapezium rule then applied to give the damage.

Appendix J

Numerical solution of the pile deflection equation

J.1 Formulation

Consider a pile of length L embedded in an elastic soil as shown in figure J.1 where z is a co-ordinate denoting the distance along the pile from the mudline. When the pile is subjected to a lateral load F and moment M at the mudline, let the lateral deflection of the pile be denoted by x, where $x = x(z)$.

When subjected to a pile deflection, the reaction of the soil may in general be expressed as

$$p = -E(x, y)x \tag{J.1}$$

where p is the soil reaction force per unit length of pile. The soil elastic modulus E will vary with both depth and deflection, however these effects are ignored here as there is insufficient data to treat them thoroughly within the study. Using conventional beam bending theory, the structural behaviour of the pile may be written

$$E_p I_p \frac{d^4x}{dz^4} = p \tag{J.2}$$

where E_p and I_p are the modulus and second moment of area of the pile, assumed constant down its whole length. This expression in turn may be re-written as

$$E_p I_p \frac{d^4x}{dz^4} + Ex = 0 \tag{J.3}$$

This homogenous differential equation must be solved to give the pile deflection as a function of depth, subject to the boundary conditions that at the pile head, i.e. $z = 0$

$$E_p I_p \left.\frac{d^3x}{dz^3}\right|_{z=0} = F \tag{J.4}$$

$$E_p I_p \left.\frac{d^2x}{dz^2}\right|_{z=0} = M \tag{J.5}$$

Since the pile tip is free, it can carry no force or moment and hence two further boundary conditions are:

$$E_p I_p \left.\frac{d^3x}{dz^3}\right|_{z=L} = 0 \tag{J.6}$$

$$E_p I_p \left.\frac{d^2x}{dz^2}\right|_{z=L} = 0. \tag{J.7}$$

J.2 Numerical Solution

The numerical solution described here draws on standard approaches used by the offshore industry [135]. The pile is discretised into n internal elements of length l as shown in figure J.1. Central differencing of equation J.3 then yields a general relation for the deflection x_i of node i that is

$$E_p I_p \left(\frac{x_{i-2} - 4x_{i-1} + 6x_i - 4x_{i+1} + x_{i+2}}{l^4}\right) + Ex_i = 0 \tag{J.8}$$

which can be rearranged, using the obvious relation

$$l = \frac{L}{n} \tag{J.9}$$

to give

$$x_{i-2} - 4x_{i-1} + \varphi x_i - 4x_{i+1} + x_{i+2} = 0 \tag{J.10}$$

where

$$\varphi = 6 + \frac{EL^4}{E_p I_p n^4}. \tag{J.11}$$

Equation J.10 in turn may be re-arranged to make x_i the subject. Gauss-Siedel [90] iteration can then be used to solve for the deflection profile, repeatedly evaluating the deflection at each internal node from the pile top to the pile bottom until convergence is obtained.

A difficulty with this approach is calculating the deflection on the two top and bottom nodes of the pile, which cannot be calculated using equation J.10. The application of boundary conditions at either end of the pile however provides a solution

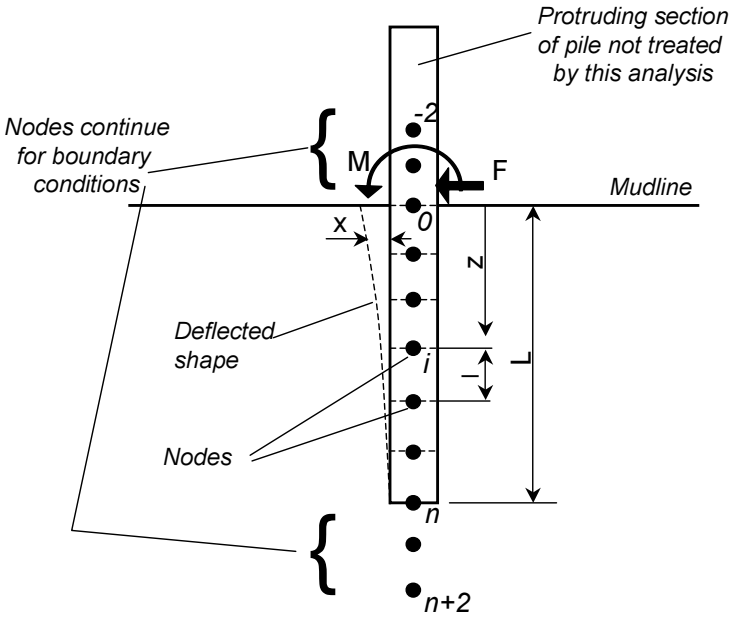

Figure J.1: Representation of the pile foundation.

J.2.1 Application of boundary conditions

To ease the application of boundary conditions and produce consistent results for all of the pile, the discretisation is extended for two nodes beyond the upper and lower ends of the pile. These nodes have no physical significance beyond their use in applying the boundary conditions.

At the pile top, according to conventional bending theory the imposed bending moment and shear force dictate

$$M = E_p I_p \frac{d^2x}{dz^2} \tag{J.12}$$

and

$$F = E_p I_p \frac{d^3x}{dz^3}. \tag{J.13}$$

The first of these relations may be discretised as

$$M = E_p I_p \frac{x_1 - 2x_0 + x + -1}{l^2} \tag{J.14}$$

which on re-arrangement gives

$$x_{-1} = \frac{Ml^2}{E_p I_p} + 2x_0 - x_1. \tag{J.15}$$

Similar treatment of equation J.13 shows

$$x_{-2} = \frac{-2Fl^3}{E_p I_p} + x_2 - 2x_1 + 2x_{-1}. \tag{J.16}$$

Before each Gauss-Siedel iteration of the pile nodes, equation J.15 is used to calculate a new value for x_{-1} based on the current values for the deflection at the internal nodes. Equation J.16 is then used to give a value for x_{-2}, allowing the deflection of the first two internal nodes to be calculated.

At the pile bottom, the free tip means that both the bending moment and shear force must be zero, such that

$$EI\frac{d^2x}{dz^2} = 0 \tag{J.17}$$

and

$$E_p I_p \frac{d^3x}{dz^3} = 0. \tag{J.18}$$

Analysis similar to that for the pile top nodes yields

$$x_{n+1} = 2x_n - x_{n-1} \tag{J.19}$$

and

$$x_{n+2} = x_{n-2} - 2x_{n+1} + 2x_{n-1} \tag{J.20}$$

which are used to generate values that allow the deflection of the bottom two internal nodes to be calculated.

Appendix K

Diffraction analysis of the gravity foundation

K.1 Introduction

In a statistically described sea state, the largest force experienced by a structure can be considered to be the most probable maximum force. The most probable maximum diffraction uplift force on the gravity base subjected to a sea state with significant wave height H_s may be determined from

$$mpm\left(F\right) = 0.925\frac{\sigma_F}{\sigma_\eta}H_s \tag{K.1}$$

where σ_η is the standard deviation of the wave height spectrum $S_{\eta\eta}\left(\omega\right)$ for the sea state given by

$$\sigma_\eta = \sqrt{\int_0^\infty S_{\eta\eta}\left(\omega\right)d\omega}. \tag{K.2}$$

The standard deviation of the spectrum of the forces $S_{FF}\left(\omega\right)$ that the foundation is subjected to, σ_F may be calculated from

$$\sigma_F = \sqrt{\int_0^\infty S_{FF}\left(\omega\right)d\omega}, \tag{K.3}$$

noting that the force and wave spectra are related by

$$S_{FF}\left(\omega\right) = \left[RAO_F\left(\omega\right)\right]^2 S_{\eta\eta}\left(\omega\right). \tag{K.4}$$

The Force Response Amplitude Operator, $RAO_F(\omega)$, may be defined as

$$RAO_F = \frac{F(\omega)}{\xi(\omega)} \tag{K.5}$$

where $\xi(\omega)$ represents the wave amplitude at frequency ω. It may be thought of as a transfer function that relates the amplitude of the diffraction force at a certain frequency to the amplitude of driving waves at the same frequency. Calculating $RAO_F(\omega)$ for a particular foundation geometry essentially defines the diffraction response of that foundation.

K.2 RAO_F for the gravity foundation

Vugts and Harland [198] investigated RAO_F for variations of the 'base' gravity foundation considered in chapter 5, using the DELFRAC software of the Delft University of Technology Ship Hydrodynamics group. DELFRAC is a sophisticated diffraction analysis package that computes the wave driven flow field around the gravity base by solving a Poisson equation and integrates the resulting pressure field to calculate forces.

Figure K.1 shows representative results for bases of varying thickness, and figure K.2 has results for varying water depth. It can be seen that the base thickness has little impact on RAO_F, although the water depth plays a more significant role. The value of RAO_F as the wave frequency approaches zero, in other words for very long waves, is approximately constant. It may be estimated from the additional hydrostatic force exerted on the foundation of area A_{base} when covered by a very long wave crest of amplitude $\xi(0)$ above the mean sea level, that is

$$F(0) \approx \rho_w g A_{base} \xi(0). \tag{K.6}$$

The corresponding response amplitude operator is therefore

$$RAO_F(0) = \frac{F(0)}{\xi(0)} = \rho_w g A_{base} \tag{K.7}$$

with ρ_w representing the density of water.

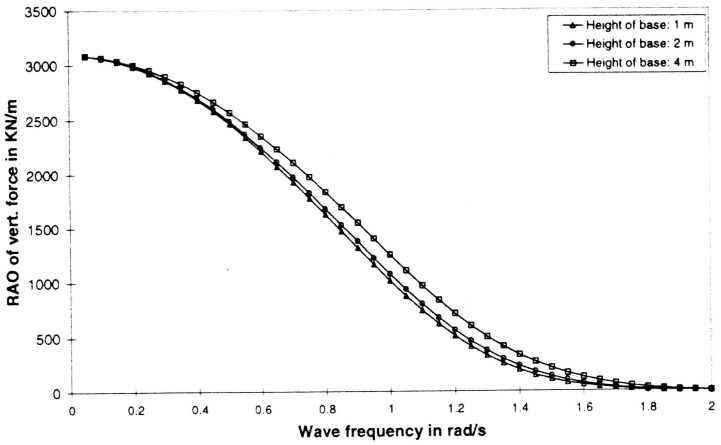

Figure K.1: Force response amplitude operator for gravity foundations of varying thickness in 15m water depth produced by [198].

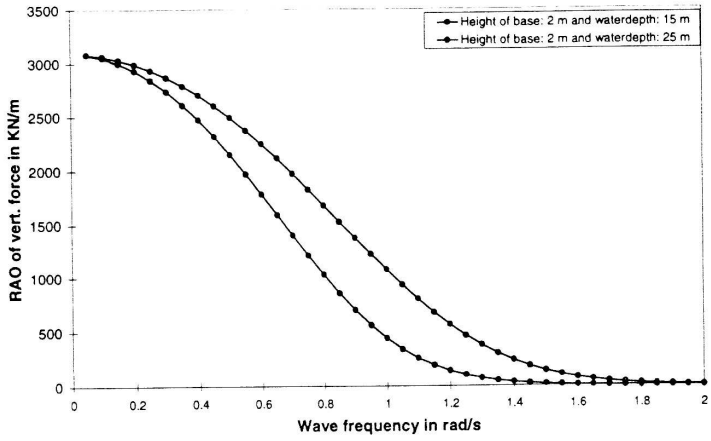

Figure K.2: Force response amplitude operator for gravity foundations in varying water depth produced by [198].

K.3 Approximate representation of RAO_F

For a given foundation geometry, the response amplitude operator could be approximately represented by a function of the form

$$RAO_F(\omega) = RAO_F(0)\, f(\omega) \tag{K.8}$$

or

$$RAO_F(\omega) = \rho_w g A_{base} f(\omega). \tag{K.9}$$

where $f(\omega)$ has value unity at $\omega = 0$ and is fitted to the form of figures K.1 and K.2. No such fitting will be performed here, but it is noted that the single function would be valid for all gravity bases which have the same general form of $RAO_F(\omega)$. The detailed parameter study demonstrated that base thickness has very little influence on the foundation response, and thus the analysis can be applied without regard to thickness so long as the upper surface of the base remains well below the water level. Water depth had a more significant effect, but the intention here is only to modify an existing foundation design for a limited number of locations in which the depth will vary by only a few metres from case to case. The impact of water depth is ignored here except in so far as it also limits the maximum wave height encountered by the foundation. Base diameter will also influence the form of $RAO_F(\omega)$, but again the impact will be small for relatively small changes.

K.4 Implications for diffraction uplift force

With the approximate representation of $RAO_F(\omega)$, by equation K.4, the standard deviation of the force spectrum on the foundation becomes

$$\sigma_F = \rho_w g A_{base} \sqrt{\int_0^\infty f^2(\omega)\, S_{\eta\eta}(\omega)} \tag{K.10}$$

and thence the most probable maximum force is

$$mpm(F) = 0.925 \frac{\sqrt{\int_0^\infty f^2(\omega)\, S_{\eta\eta}(\omega)}}{\sqrt{\int_0^\infty S_{\eta\eta}(\omega)}} \rho_w g A_{base} H_S. \tag{K.11}$$

This result shows that for gravity bases of similar shape and size in the same depth of water, the most probable maximum uplift force due to diffraction scales approximately linearly with both the wave height and the base area. Thus the

cost model assumes, for the purposes of modifying the detailed foundation, that the total structure weight required to resist diffraction is directly proportional to both the plan area os the base and the extreme significant wave height.

Appendix L

Summary of the model code

L.1 Overview

The cost model comprises more than 6000 lines of Fortran-90 code, excluding the source code numerical libraries employed. The code compiles under the Intel Fortran compiler. It does not make use of any proprietary extensions, and thus should compile with other compilers, although this has not been tested extensively.

L.2 Model structure

The model code is well structured. To provide some guidance for any future developments, this section offers a brief guide to the main subroutines of the model. There are many smaller routines that are not discussed here. So far a practicable the code is well commented, and so the function of the smaller routines not mentioned here should become obvious on reading the source code.

Revisions of each routine are denoted by a number suffix added to the subroutine name, so that, for example ANNENERGY10 is the 10^{th} major revision of the routine that estimates the annual energy output of a single wind turbine. The numerical suffixes are omitted in this description.

MASTER is the 'main' routine that co-ordinates the program operation, handling all input and output, and coupling together the various detailed subroutines that perform individual component design. The only calculations within MASTER are those required to converted data in the formats required by the top-level subroutines, for example unit conversions. The following 'top-level' subroutines are called in the order listed:

- REMOTECLIM

- ANNENERGY
- ARRAYEFFICIENCY
- STRUCDIAOPT
- SIMPLEGRID
- MAINOPT
- LPC

L.2.1 Top level subroutines

REMOTECLIM

This subroutine generates the climate data used for the structural calculations, but not the energy production estimation. The wave/wind speed occurrence table is generated by subroutine GENCLIMATE, which is called from REMOTECLIM, but this routine applies the effects of shoaling and breaking to account for the fact that the wave Weibull data may be for a distant point.

ANNENERGY

Calculates the annual energy output for a single turbine based on the Weibull parameters for the windspeed at the hub height, the $C_p - \lambda$ curve, and other information about the turbine.

ARRAYEFFICIENCY

Estimates the array efficiency using the method outlined in chapter 3

STRUCDIAOPT

Returns the cost and other properties of the structure with the optimum diameter distribution. The routine makes multiple calls to the main structure design subroutine STRUCDES with different support structure diameter profiles, and keeps track of the current lowest cost design that is also free from any risk of turbine induced resonance. Tests for resonance are carried out within this routine. The following subroutines are called:

- STRUCDES
- EIGENMATRICES
- EIGEN

1	Lower extent of wind speed band at hub height
2	Upper extent of wind speed band at hub height
3	Representative value of windspeed at hub height
4	Lower extent of wind speed band at reference height
5	Upper extent of wind speed band at reference height
6	Representative value of windspeed at reference height
7	Upper extent of corresponding sig. wave height band
8	Lower extent of corresponding sig. wave height band
9	Representative value for sig. wave height
10	Band probability
11	Sea surface roughness
12	Hub height Turbulence intensity (EDSU)

Table L.1: Meaning of indices in array ClimMat.

SIMPLEGRID

Look up table based grid connection cost estimating subroutine.

MAINOPT

Deduces the optimum annual maintenance cost and the corresponding farm availability factor, by undertaking a numerical search of the predictions of subroutine MAINT

LPC

Calculates the energy cost from the output of the other top-level subroutines using the discounted cashflow approach described in chapter 3.

L.2.2 Second level subroutines

GENCLIMATE

GENCLIMATE is a subroutine that generated the wind speed / wave height occurrence table required for the fatigue calculations. The generated data is stored in matrix ClimMat(200,12). The first index of the matrix is used to identify the climate combination, and provision is made for up to 200 combinations. The second index denotes the data item describing each combination of conditions, according to the convention in table L.1.

The following major subroutines are called:

- WINDSHEAR

- WEIBULLEX
- EDSUTURB

STRUCDES

This subroutine is responsible for the design of a single support structure, and including the many further subroutines called, accounts for the bulk of the model code. There are more than 40 separate parameters that must be passed to the routine, which returns a comprehensive description of the designed structure.

Data about the tower is returned within a series of arrays, giving the outer diameter (dout), the wall thickness (tout), the mass per unit length (mout) and other information at a series of stations along the tower. The number of stations into which the tower is divided can be defined in the input to the model, and the output arrays are sized appropriately using the allocatable arrays feature of FORTRAN-90. The output arrays are arranged so that the element 1 of each refers to the tower station nearest to the seabed, with the final element referring to the tower where it joins the nacelle.

The following main subroutines are called:

- EXMOM
- FATIGUELOADS
- DESIGNPILE
- DESIGNGRAV
- TOWERDESIGN
- INTIALPILE
- INITIALTOWER
- INITIALGRAV
- COSTPILETOWER
- COSTGRAVTOWER

L.2.3 Third level subroutines

WINDSHEAR

Calculates the wind speed at specified height from data at a reference height. The routine first iteratively solves the Charnock and Prandtl relations to estimate the

sea surface roughness from the reference height data. Next the Prandtl relation is used to estimate the wind speed at the specified height.

WEIBULLEX

Returns the probability that a value is exceeded by a single sample taken from a Weibull distribution with specified parameters.

EDSUTURB

Returns the turbulence intensity for a given set of wind conditions, either using the EDSU formula, or the approximation employed here:

$$\sigma_u = 2.5u_* \tag{L.1}$$

EXMOM

Calculates the extreme wind and wave forces on the support structure, applying each load case in turn and selecting the largest forces and moment at each station on the support structure. The following main subroutines are called:

- WINDEXCALC
- COORDWAVES

FATIGUECOORD

Returns an array detailing the total cross-section independent fatigue damage generated by subjecting a specified support structure to specified climate, as generated by REMOTECLIM. The returned array gives the total damage at each station in the support structure.

First the routine evaluates the structural dynamics from a description of the current structure passed as parameters. The mode shapes are calculated using the finite element routines, and then the participating mass, stiffness and damping estimated for each mode considered by the analysis. In principle the routine can work with up to six modes, but as noted in the main text, all the analysis presented here relies on analysis of the first lateral mode only. A transfer function, representing the displacement response of each structural mode to excitation forces is calculated based on the participating mass and stiffness, and the damping factor. The transfer function is held in array, with each element representing the magnitude of the response at a specified frequency. The number of elements

used to represent the transfer function, and the range of frequencies across which it is evaluated can be specified in the model input.

For each combination of wave/wave conditions generated by REMOTECLIM, the calculation proceeds by first producing a tower top load spectrum. The spectrum is held in array in a manner exactly similar to that used for the modal transfer functions. Next, wave force spectra for each defined station on the structure below the mean sea level are generated. The spectra are represented in a similar way to the tower top load spectrum.

A composite spectrum, representing the impact of each nodal force spectrum on each mode of vibration is prduced using the mode shapes computed earlier. The modal displacement response of each structural mode is then evaluated using the transfer function and the composite spectrum.

From the modal displacement response spectra, and the mode shapes evaluated from the structural dynamics, a bending moment, and thence stress, spectrum may be calculated at each station in the support structure. Finally, the numerical implementation of the Dirlik equation is used to estimate the rate at which fatigue damage would be received by each tower station as a result of the computed stress spectra.

The spectral calculations are repeated for each combination of wind speed and eave height supplied to the subroutine, to produce a damage rate at each station on the structure for each climate combination. Finally the damage rates are combined with reference to the probability of each climate combination occurring to produce a composite damage rate for each station on the structure.

The following main subroutines are called

- EIGENMATRICES
- EIGEN
- TTFAT1
- PMSPECS
- WAVEXFER
- WAVEFORCESPECTRUM
- MODALFORCESPECTRUM
- BMSPEC
- SPECTODAMAGE

DESIGNPILE

Co-ordinates the design of the pile, accounting for overturning moment and shear force at the base, vertical load, and the various influences on the pile wall thickness. The penetration depth, diameter, wall thickness and stiffness/damping of the least cost pile are returned.

Many subroutines and functions are called, some of which are listed below, but not further described because of their specialised nature:

- PILEDESIGN : Identifies optimum combination of diameter and length for a pile, assuming a known wall thickness.
- PILEDEFLN : Finite difference based calculation of internal pile bending moments that influences the minimum wall thickness for any case.
- PILELENGTH : Returns the minimum length of pile of fixed diameter required to support a given horizontal and vertical load in a known soil. This is achieved by a numerical search calling PILERESISTANCE and PILEHCAPACITY.
- PILERESISTANCE: Returns the vertical load that can be supported by a particular pile, with specified diameter and length, in a known soil.
- PILEHCAPACITY: Returns the horizontal load that can be supported by a particular pile, with specified diameter and length, in a known soil.
- PILESECSTIFFNESS: Returns the secant stiffness of a known pile in a given soil.
- PILETANSTIFFNESS: Returns the tangent stiffness of a known pile in a given soil.

DESIGNGRAV

This subroutine designs the gravity foundation with respect to overturning moment, base pressure and diffraction induced uplift.

TOWERDESIGN

Performs the mechanical design of the tower, essentially estimating the wall thickness, based on the extreme loads from EXMOM and the damage rates from FATIGUECOORD. An iterative procedure is used in order to account for changes in vertical loading brought about by changes in the tower self-weight, in turn arising from wall thickness changes.

The following main routines are called:

- FATIGUETHICKNESS
- BUCKLINGTHICK
- EXTREMETHICK

INTIALPILE

Sets the 'guessed' pile design used to start the iterative support structure design process.

INITIALTOWER

Sets the 'guessed' tower design used to start the iterative support structure design process.

INITIALGRAV

Sets the 'guessed' gravity foundation used to start the iterative support structure design process.

COSTPILETOWER

Returns the cost of a support structure with a pile foundation in 2002 UK pounds.

COSTGRAVTOWER

Returns the cost of a support structure with a gravity foundation in 2002 UK pounds.

L.2.4 Fourth level subroutines

WINDEXCALC

Calculates extreme wind loads down the structure from a given hub height wind speed.

COORDWAVES

Calculates extreme wave moments down the structure from given wave height and time period information.

FATIGUETHICKNESS

Returns the minimum wall thickness for a circular section of known diameter to resist a given cross-section independent fatigue damage.

BUCKLINGTHICK

Returns the minimum wall thickness for a circular section of known diameter to resist buckling.

EXTREMETHICK

Returns the minimum wall thickness for a circular section of known diameter to resist a given bending moment.

TTFAT1

Returns an array giving the tower top load spectrum for given hub height wind speed and turbulence intensity.

PMSPECS

Returns the Pierson-Moskowitz sea surface displacement spectrum.

WAVEXFER

Calculates the transfer functions to convert wave sea surface displacement spectra into velocity and acceleration spectra.

WAVEFORCESPECTRUM

Returns the wave force spectrum at a point on the support structure, starting from velocity and acceleration spectra produced by WAVEXFER, and using the Borgman linearisation of the Morison equation.

MODALFORCESPECTRUM

Produces a modal forcing spectrum from a mode shape and nodal forcing spectra.

BMSPEC

Produces bending moment and stress spectra from a mode shape and a modal displacement spectrum

SPECTODAMAGE

Converts a stress spectrum to a damage rate using the Dirlik approach.

L.2.5 Selected other routines used throughout the model

FWAVET

Returns estimated periods for wave for fatigue calculations based on their height.

EWAVET

Returns estimated periods for wave for extreme load calculations based on their height.

APPLYBREAKLIMIT

Tests whether a specified wave is at risk of breaking based on a depth criterion, and if so, returns the maximum wave height for which breaking will not occur

HSHOAL

Returns the height of a wave moving from water of depth d_1 to water of depth d_2.

WAVENO

Estimates the wave number of a wave from its time period and the local water depth using linear wave theory.

WAVESPEED

Returns the speed of a wave from its time period, wavelength and the local water depth based on linear wave theory.

EIGENMATRICES

Generates the mass and stiffness matrices for the finite element analysis, starting from a description of the second moment of area and mass per unit length distributions over the length of the support structure.

EIGEN

Returns the eigen-frequencies and normalised eigen-modes of the structure from the stiffness and mass matrices produced by EIGENMATRICES.

L.3 Input files

The model relies on a number of input files, which separately describe the local environment, the turbine, overall engineering parameters, physical constants, economic parameters, and various model control options. The input files are structured in this way to facilitate parameter studies that only involve changing one major component of the farm.

Each file has a rigid format that must be adhered to. In the example files that follow, lines preceded by exclamation marks are comments to ease use of the model. The comments are intended to be self explanatory, so in general no further description is provided.

clim.in

This file describes the local environment, primarily the climate but also other site dependent features such as the distance from the shore.

```
!TITLE:Climate parameters IRISH SEA
! charnock
60.
! wind_c
8.9
! wind_k
1.83
! wind reference height (m)
25.
!wave_c
1.2
!wave_k
1.31
! depth
12.
! rdepth
12.
! A0
0.0
! A1
4.0
!SoilGamma
8.15
!SoilShear
0.01
!SoilCohere
0.01
!Esoil
```

```
5.E4
!SoilType
'S'
!SoilPhi
37.
!EstimateClimateExtremes(1=yes)
0
!WindExtreme1
40.5
!WindExtreme2
29.7
!WaveExtreme1
8.
!WaveExtreme2
5.85
!LoConstantForExtremePeriod
3.2
!HiConstantForExtremePeriod
3.6
!DistanceToShore(km)
15.
!DistanceToGrid(km)
5.
```

turb.in

This file describes all the turbine features. An example file is shown below:

```
Turbine values 1.5MW Final
!CutInSpeed
3
!CutOutSpeed
25
!RatedWindSpeed
13.13
!RatedWINDPower (kw)
1500
!BladeRadius
32.
!No_Of_Lambda_Cp_Values
27
!Lambda CP
0. 0.
0.5 0.003
1. 0.008
1.5 0.016
2. 0.03
```

```
2.5 0.056
3. 0.099
3.5 0.155
4. 0.219
4.5 0.279
5. 0.333
5.5 0.38
6. 0.423
6.5 0.449
7. 0.467
7.5 0.477
8. 0.482
8.5 0.487
9. 0.483
9.5 0.48
10. 0.475
10.5 0.462
11. 0.449
11.5 0.436
12. 0.426
841.5 0.
8491.5 0.
!No_Of_Power_Geneffy_Values
10
!P(kW) Effy
0     0.967
500   0.967
1500  0.967
2000  0.967
2500  0.967
3000  0.967
3500  0.967
4000  0.967
4500  0.967
5000  0.967
!No_Of_Power_GBXeffy_Values
10
!P(kW) Effy
0     0.965
500   0.965
1500  0.965
2000  0.965
2500  0.965
3000  0.965
3500  0.965
4000  0.965
4500  0.965
```

```
5000  0.965
!TurbineCapCost
1000000.
!Omega rpm
20.
!NoBlades
3
!NacelleHeight
8.
!TowerTopMass (kg)
75000.
!TurbCDnacelle
1.2
!TurbCDoperate
0.4
!TurbCDfail
1.0
!NacelleArea(m2)
22.4
!BladeArea(m2)
67.4
!MinTTDia
2.2
!MaxTTDia
2.4
```

eng.in

The 'eng.in' file contains miscellaneous engineering parameters, mostly relating to the tower design. A representative file is as follows:

```
Engineering values
! Hub height (rel to MSL)
80.
!NoOfTurbines
100
!TurbineSpacing(m)
400.
!MinTowerBotDia(m)
2.2
!MaxTowerBotDia(m)
4.
!Tower_E(SI)
210.E9
!Tower_Density(kg/m3)
7860.
!TowerRough
```

```
0.4
!Pile_Density
7860.
!Pile_E(SI)
210.E9
!Tower_MaxSigma
60000000.
!Tower_Bend_FS
1.2
!UsePile
.TRUE.
```

ctrl.in

The 'ctrl.in' file sets various administrative options within the model.

```
CONTROL PARMAMETERS
! No of windspeeds for fatigue calculations
20
! EuroToGBP
1.5
!NoTowerDivs
40.
!NoOfTowerTopDias
2.
!NoOfTowerBotDias
10.
!NoOfExtremeWavePeriods
10.
!FreqAvoidBandWidth
0.1
!UseFDPile
TRUE
```

econ.in

This file sets the economic parameters, and is composed as follows:

```
CostModelEconomicInputFile
! DiscountRate
0.05
! Lifetime
20
!GBPtoEURConversionRate
1.5
```

Appendix M

Estimation of foundation stiffnesses

M.1 Pile foundation

The dynamic calculations depend on information about the behaviour of the designed pile. For the protruding section, the second moment of area and mass per unit length distributions are necessary. These are calculated in the same way as for the tower and passed to the dynamic model.

The treatment of the foundation behaviour in the dynamic model is shown in figure M.1. Rotational and lateral stiffnesses are required for the penetrating section of the pile. In principle stiffness can be estimated using the numerical model of the pile described in section 5.3.5. This predicts a non-linear response (figure M.2), where the stiffness depends on the applied load, as indeed would be found from measurements on a real pile. The structural models are only formulated to deal with linear behaviour.

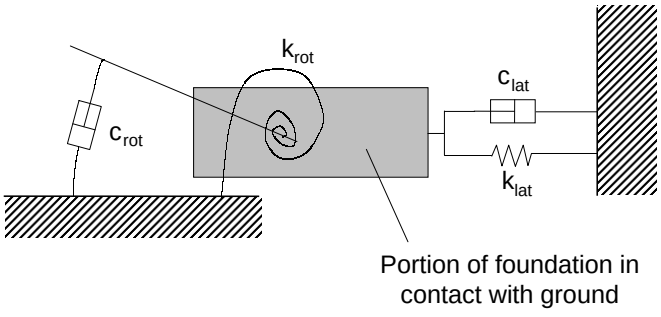

Figure M.1: Idealisation of foundation dynamic behaviour.

Two linearisation procedures are separately used to estimate foundation stiffness values for use in the structural models. For fatigue calculations, secant lin-

earisation as described by Barltrop and Adams [139] is applied with an effective stiffness being calculated at a particular load. The resulting value is used for all subsequent fatigue calculations irrespective of the load. Barltrop and Adams suggest that the linearisation be carried out at the loading which produces the maximum fatigue damage. In practice this load cannot be determined without actually performing the fatigue analysis. A simplification is used here, with the loading determined as that produced by the individual wave for which has the highest product of the probability of occurrence, predicted from the local wave Weibull distribution, and static load, calculated using the Morison equation and linear wave theory. The appropriate wave is determined by the model from a numerical search.

Tangential linearisation is used to model the foundation stiffness for the extreme load response calculation. In this case the loading is simply that calculated by the methodology of chapter 4.

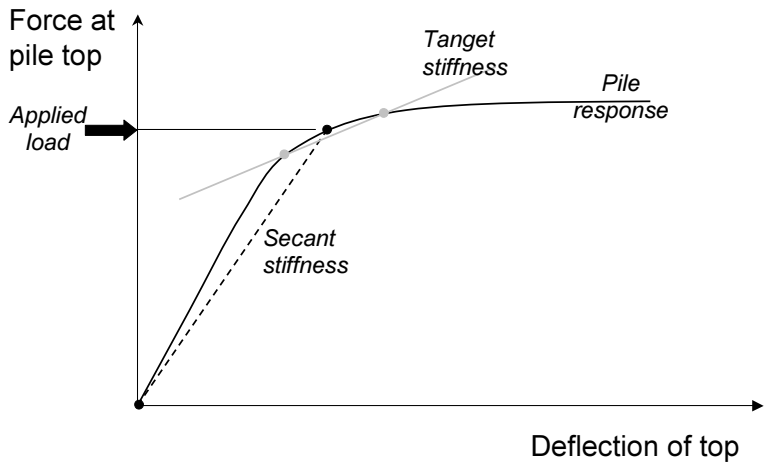

Figure M.2: Non-linear pile response (solid line) showing secant (dashed line) and tangential (dotted line) linearisation proceedures.

M.2 Gravity foundation

As with the pile, horizontal and rotational stiffnesses and damping factors are required for the designed foundation. A simple approach to the foundation dynamics is adopted, relying on analytic results derived for an elastic half space

[25]. Lateral and rotational stiffness as defined in figure M.1 are respectively

$$k_{lat} = \frac{8G_{dyn}R}{1-\nu} \tag{M.1}$$

and

$$k_{rot} = \frac{8G_{dyn}R^3}{3\left(1-\nu\right)} \tag{M.2}$$

with corresponding damping factors

$$c_{lat} = \frac{4.6R^2}{1-\nu}\sqrt{\rho_{soil}G_{dyn}} \tag{M.3}$$

and

$$c_{rot} = \frac{0.8R^4\sqrt{\rho_{soil}G_{dyn}}}{\left(1-\nu\right)\left(1+\frac{2(1-\nu)\Theta_{rot}^{cog}}{8\rho_{soil}R^5}\right)} \tag{M.4}$$

where

R	Radius of foundation
G_{dyn}	Soil dynamic shear modulus
ν	Soil poisson ratio
ρ_{soil}	Undrained soil density
Θ_{rot}^{cog}	Inertia of structure with respect to centre of gravity.

Appendix N

Validation of model and results

N.1 Introduction

The cost model is a representation of the design process for an offshore wind farm, with the primary function of allowing design options to be compared. To provide confidence in the results, some validation of the model has been carried out.

Purely physical models, such as Computational Fluid Dynamics (CFD) simulations of physical processes can be rigorously validated against measurements from well defined test cases. Validation of a model of the type described here is a more difficult task, since it is intended as a predictive tool, for investigation of the costs and design of farms yet to be built. There is therefore a very limited empirical data set against which test of the whole model can be made. To make matters worse, most of the empirical data available was used to inform the model development. The whole point of the model is that it extrapolates from such data as is available to investigate cases yet to be constructed.

It is not practical, therefore, to currently assess the prediction accuracy of the model. There are, nevertheless, a number of validation measures that can be undertaken to try to produce some confidence in the results, and in particular to ensure:

- That the design methods chosen are suitable and capture the design drivers for the cases considered,
- That the programmed model algorithms perform correctly, for example that the numerous optimisers do identify optimum cases,
- That the model code is free from errors so far as possible, so that various physical calculations programmed produce correct results,

- That the scope of the utility of the model is defined, to avoid the risk of drawing overly detailed conclusions unwarranted by the precision of the data.

N.2 Relevance of design methods

Model predictions will only be valid if the design drivers for each component are correctly captured. The performance of the model in this regard could only be quantitatively assessed by comparing model predictions to a large empirical data set. As has already been established, no such data set exists. Even if there were many large offshore farms against which model predictions could be compared, it is unlikely that the designers would be willing to reveal the design drivers in each case.

The discussions of the first five chapters of this work attempted to establish the range of possible design drivers for the components of offshore farms. All the drivers identified have been implemented in the cost model, albeit to differing levels of sophistication. To verify that all the identified drivers can in principle play a role in the model calculations, a series of 'numerical experiments' were undertaken wherein input parameters were set to very high levels and the model output examined to ensure that the expected changes were exhibited. By way of example, were the tower top fatigue spectrum set to represent very high loads, it would be expected that the entire tower design would be driven by fatigue. To assist in this assessment, the cost model returns a report of the design driver for each component, in addition to the physical and cost data discussed elsewhere in this thesis.

A second related issue is whether the design methods employed are appropriate for use in the design of offshore farms. As the discussion in the first five chapters has shown, there is some debate in the community regarding the appropriateness of methods. The fundamentals of all the methods chosen for the model are based on procedures and theory described in the relevant literature. Methods have also be chosen to provide the most sophisticated analysis possible, subject to the constraints of a time limited study. Thus there can be no doubt that the design methods programmed are appropriate. While interpreting the results, however, It must be kept in mind that the model represents a single 'philosophy' for offshore farm design, and that other 'philosophies' may yield a different outcome.

Direct assessment of the validity of published design methods is outside of the scope of this work. It is worth pointing out, that the cost model provides a framework that could easily be adapted to compare the implications of differing

design methods on offshore farm costs and performance.

N.3 Input data and model scope

The design methods programmed into the model rely on a large amount of input data. For the purposes of this discussion, the input data will be divided in to two classes:

- External data, which comprises the main environmental data and overall design parameters contained in the input files and of primary interest to the model user.
- Internal data, which mainly comprises the detailed engineering and cost multiplier data, most of which is hard coded into the model, and is of lesser interest to the typical user.

Uncertainties in the external data will of course have implications for uncertainties in the cost predictions. For commercial site selection or design optimisation work, these uncertainties must be well defined. The analysis within this thesis is intended to uncover trends and indicative cost sensitivities. Indeed, one of the objectives for investigating sensitivities is to identify which of the external parameters have a large impact on the cost of energy and therefore need to be rigorously defined. The results herein rely on 'broad-brush' environmental data for which no uncertainty estimates are available. Thus the impact of uncertainties in the external data has not been considered any further.

Uncertainties in the internal data will also have implications for uncertainties in cost predictions. These uncertainties, however, represent a form of systematic error in that all the results will be influenced in the same way. For example, if the cost per unit weight multiplier for the tower material is ten percent too high, then all tower costs will be over predicted by a similar amount. The uncertainties in the absolute cost predictions are rather large, and this the absolute predictions should be regarded with some caution. This does not diminish the power of the model as a comparative tool. Thanks to the correlation in the errors arising from uncertainties in the internal data, the cost differences between farm configurations are rather more reliable.

N.4 Physical calculations

The model relies on a large number of physical calculations. The FORTRAN code has been carefully structured such that each physical calculation is contained with

a discrete subroutine. Each physical subroutine was validated against analytic or published solutions while the model was developed.

N.5 Optimisers

Several optimisers and other search routines are used to identify optimum parameter values for component configurations. These are difficult to validate completely as the performance of the optimisers depends on the mathematical behaviour of the objective function being optimised. The optimisation approaches adopted are mostly fairly simple, and could be caught out by objective functions that exhibit many false minima.

So far as is practicable, the behaviour of the objective functions has been investigated over a wide range of parameters using manual parameter studies. In general the objective functions showed smooth behaviour, meaning the that the optimisation routines would work reliably. In a few cases, for example with the gravity foundation diameter, it was found that false optima would sometimes be identified. For all such cases identified, it was discovered that the false optima varied in a predictable way, and the risk of returning false optima could be avoided by the careful setting of limits on the search range.

To verify that the optimisers identified correct optimum values, test cases were run to ensure that the routines returned the optima shown by the manual parameter studies. By way of illustration, figure N.1 illustrates two test cases run on the pile model.

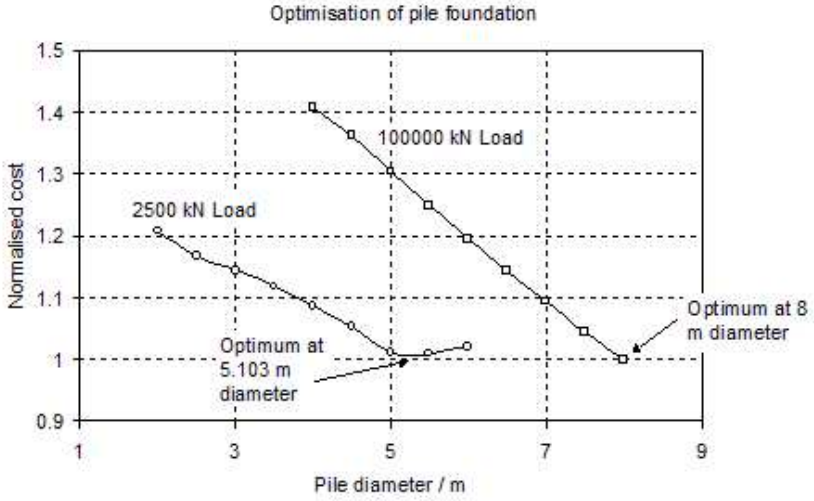

Figure N.1: Illustration of tests run on pile design optimiser. The solid lines with points were derived using a manual parameter study. The points highlighted with arrows show the optima identified by the search routine.

Appendix O

Detailed parameter studies

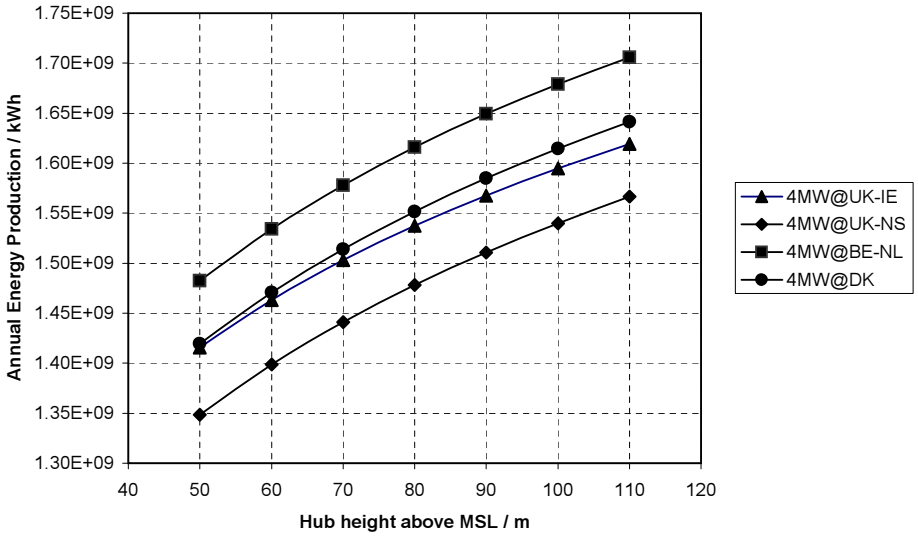

Figure O.1: Variation of 4 MW base case farm annual energy production with hub height, neglecting the influences of turbine availability and transmission losses. A Charnock constant of 60 is assumed.

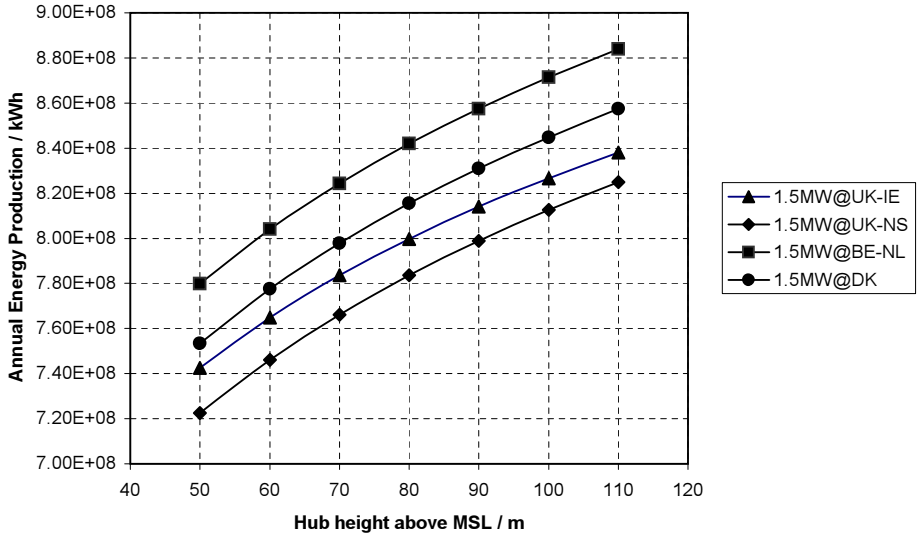

Figure O.2: Variation of 1.5 MW base case farm annual energy production with hub height, neglecting the influences of turbine availability and transmission losses. A Charnock constant of 60 is assmued.

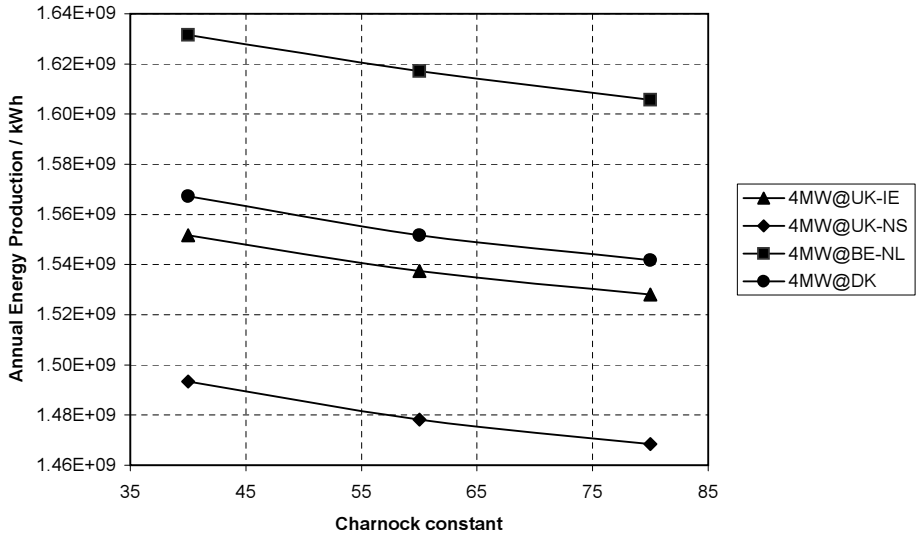

Figure O.3: Variation of 4 MW base case farm annual energy production with Charnock constant, neglecting the influences of turbine availability and transmission losses. A hub height of 80 m is assumed.

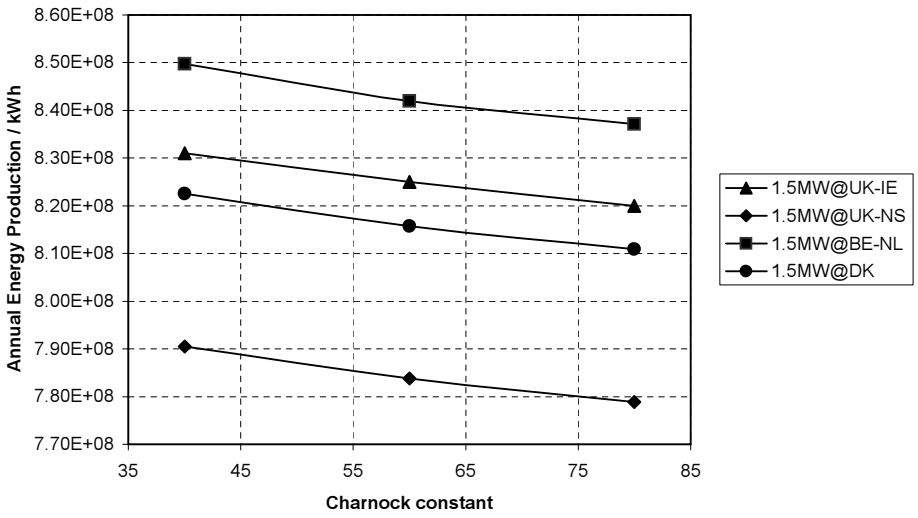

Figure O.4: Variation of 1.5 MW base case farm annual energy production with Charnock constant, neglecting the influences of turbine availability and transmission losses. A hub height of 80 m is assumed.

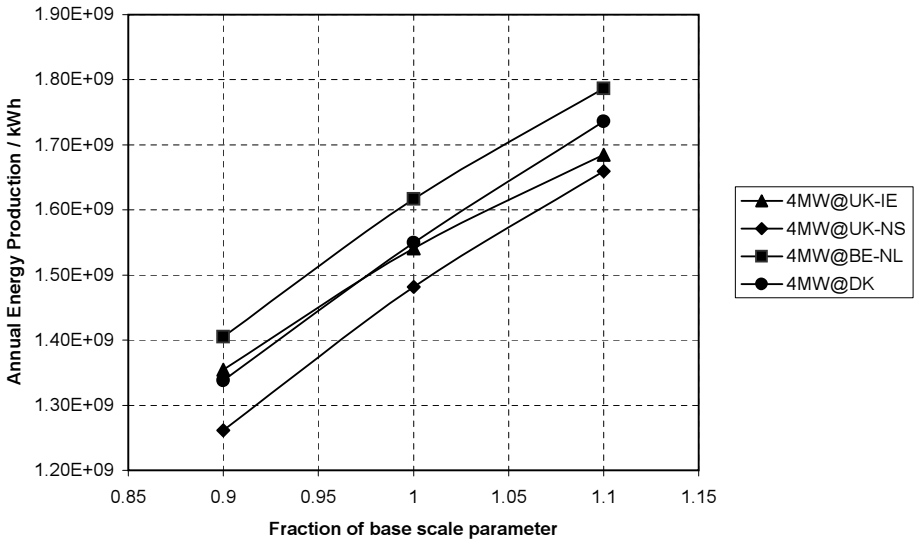

Figure O.5: Variation of 4 MW base case farm annual energy production with Weibull scale parameter, neglecting the influences of turbine availability and transmission losses. A hub height of 80 m and a Charnock constant of 60 is assumed.

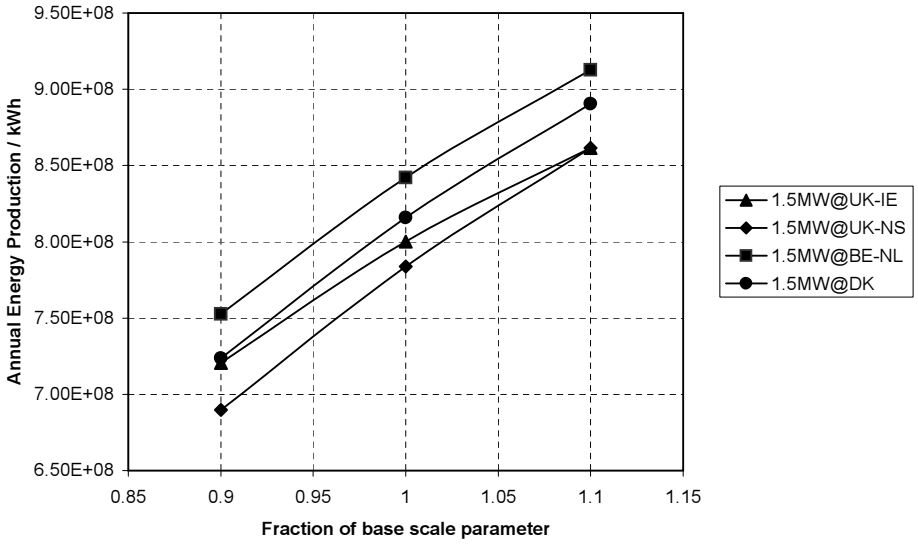

Figure O.6: Variation of 1.5 MW base case farm annual energy production with Weibull scale parameter, neglecting the influences of turbine availability and transmission losses. A hub height of 80 m and a Charnock constant of 60 is assumed.

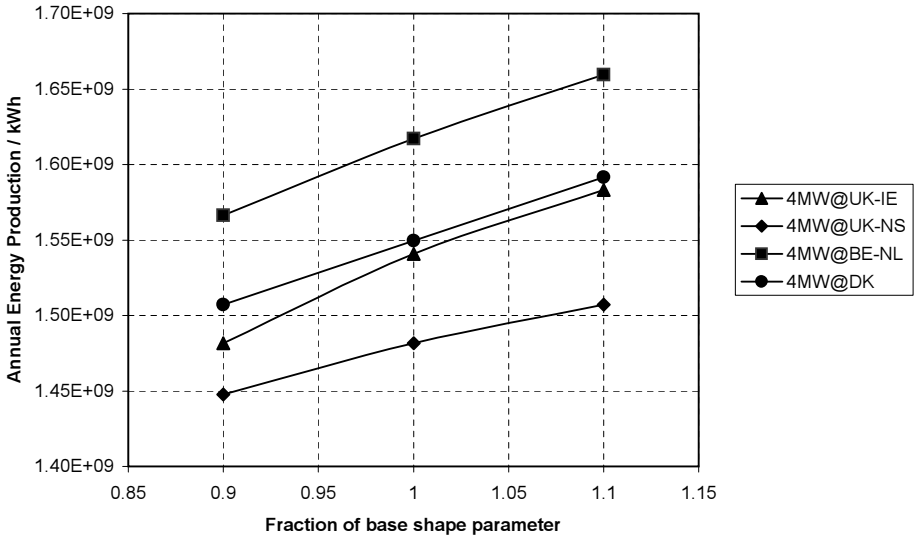

Figure O.7: Variation of 4 MW base case farm annual energy production with Weibull shape parameter, neglecting the influences of turbine availability and transmission losses. A hub height of 80 m and a Charnock constant of 60 is assumed.

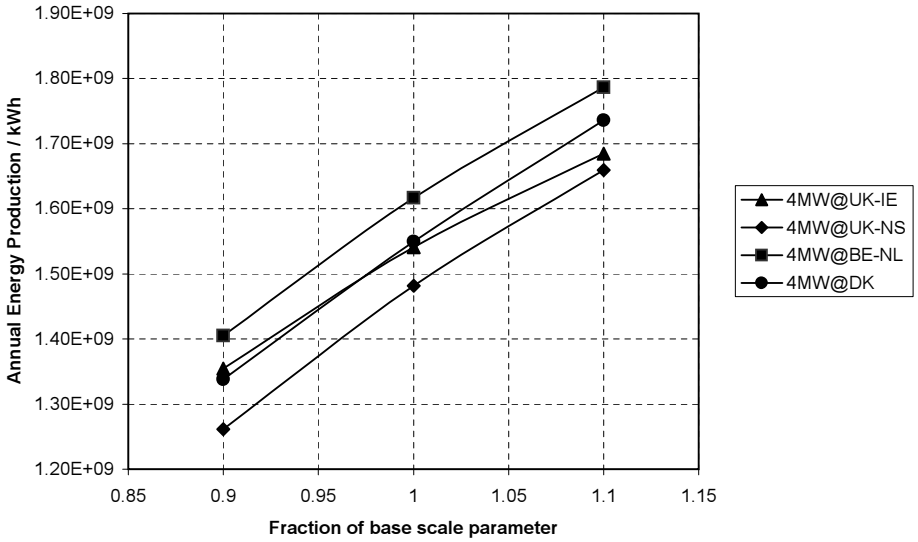

Figure O.8: Variation of 1.5 MW base case farm annual energy production with Weibull shape parameter, neglecting the influences of turbine availability and transmission losses. A hub height of 80 m and a Charnock constant of 60 is assumed.

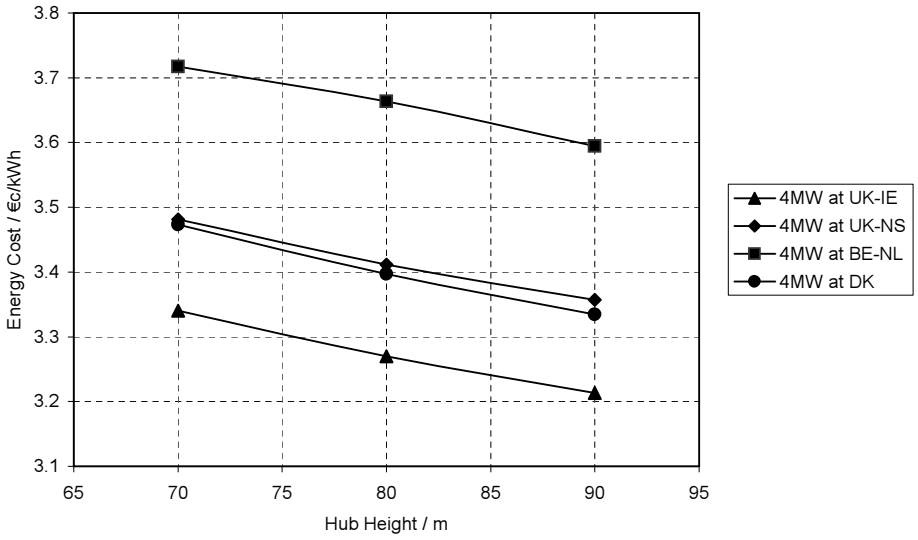

Figure O.9: Influence of hub height on 4 MW base case energy cost.

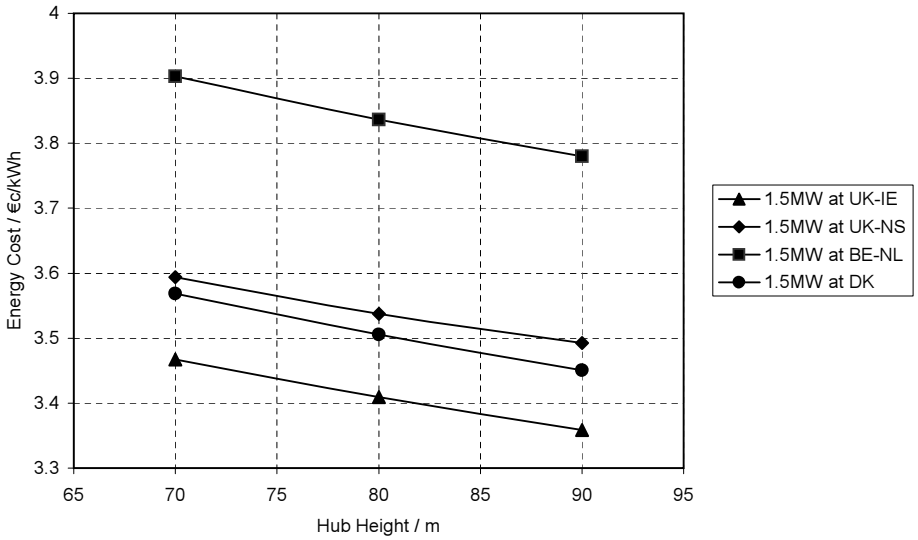

Figure O.10: Influence of hub height on 1.5 MW base case energy cost.

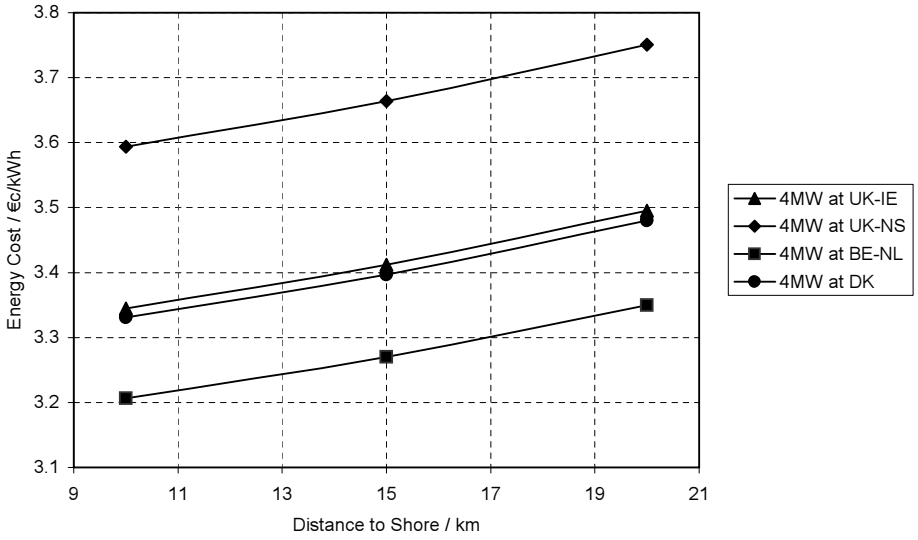

Figure O.11: Influence of distance to shore, in kilometers, on 4 MW base case energy cost.

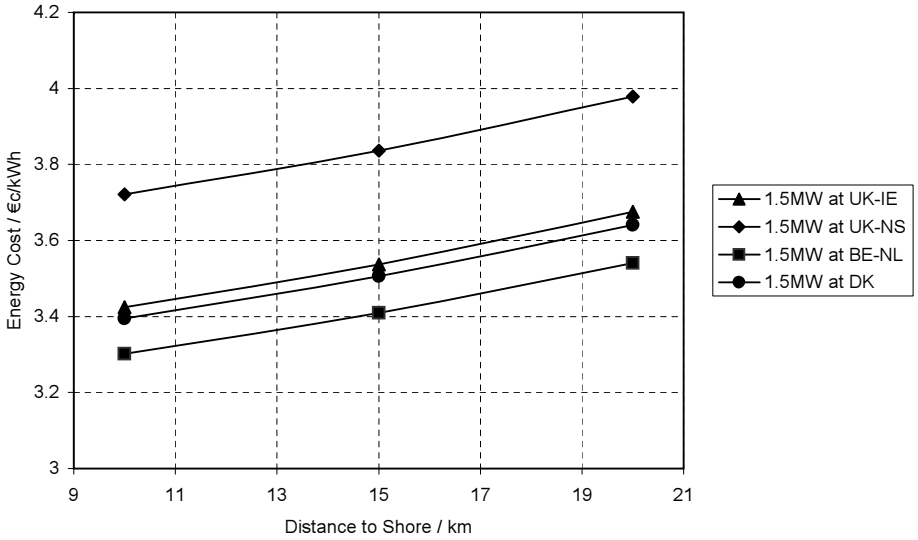

Figure O.12: Influence of distance to shore, in kilometers, on 1.5 MW base case energy cost.

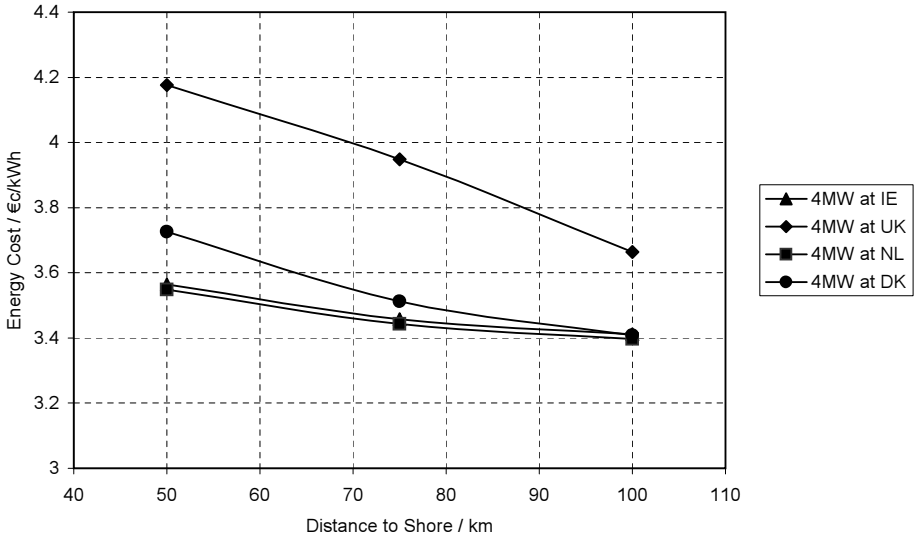

Figure O.13: Influence of number of turbines on 4 MW base case energy cost.

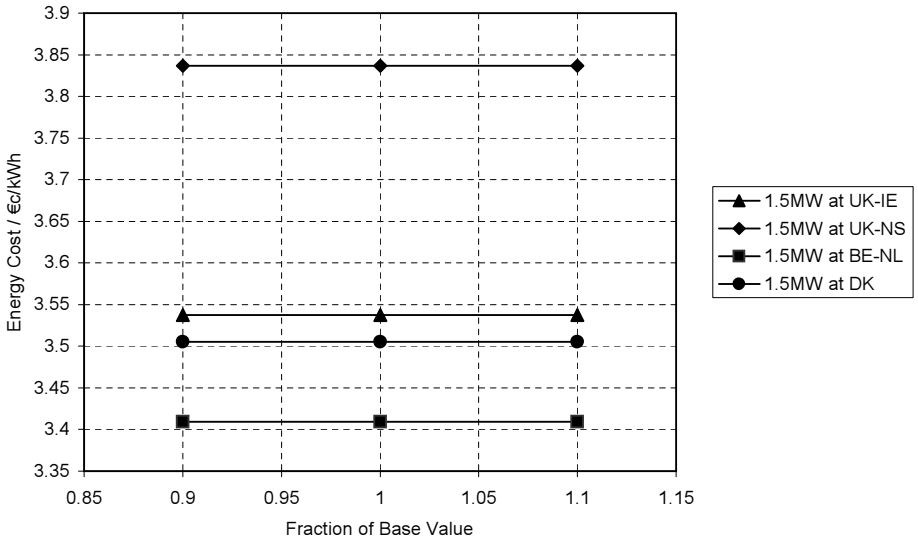

Figure O.14: Influence of 1 year return significant wave height on 1.5 MW base case energy cost.

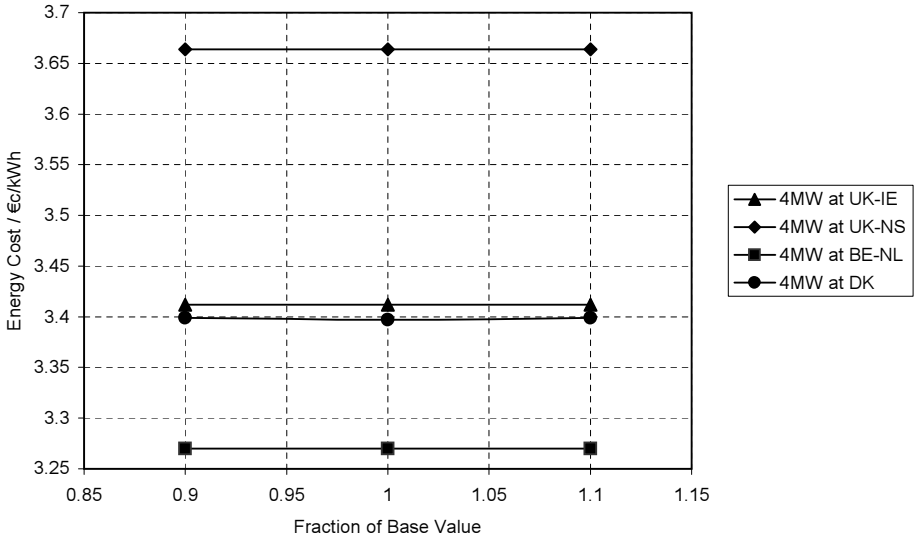

Figure O.15: Influence of 1 year return significant wave height on 4 MW base case energy cost.

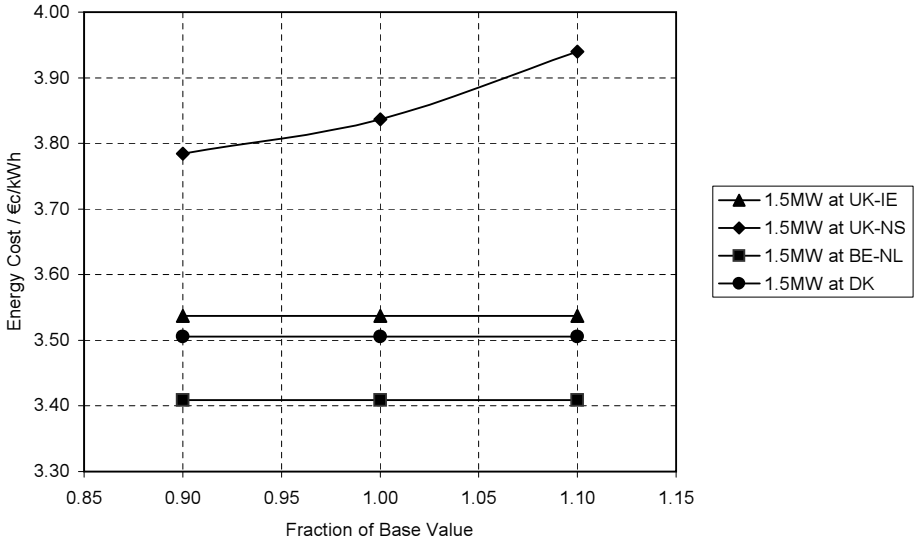

Figure O.16: Influence of 50 year return significant wave height on 1.5 MW base case energy cost.

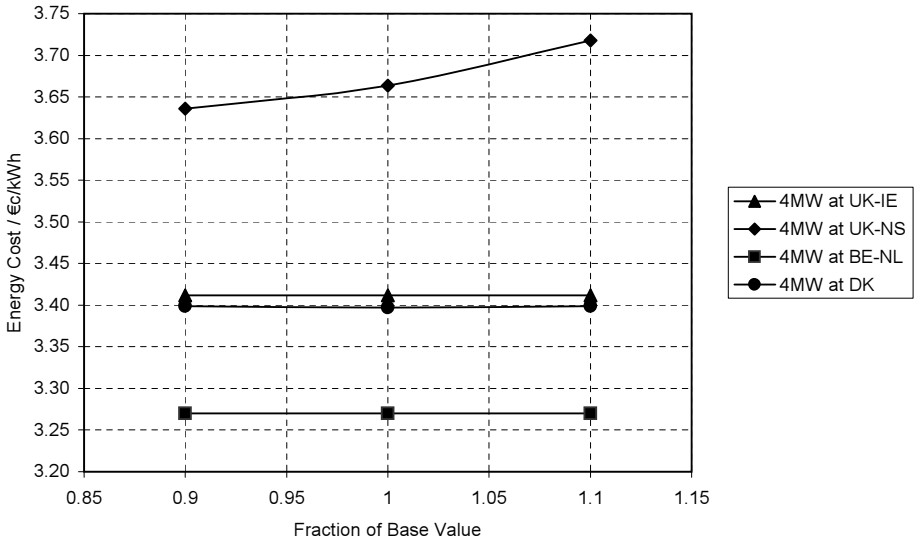

Figure O.17: Influence of 50 year return significant wave height on 4 MW base case energy cost.

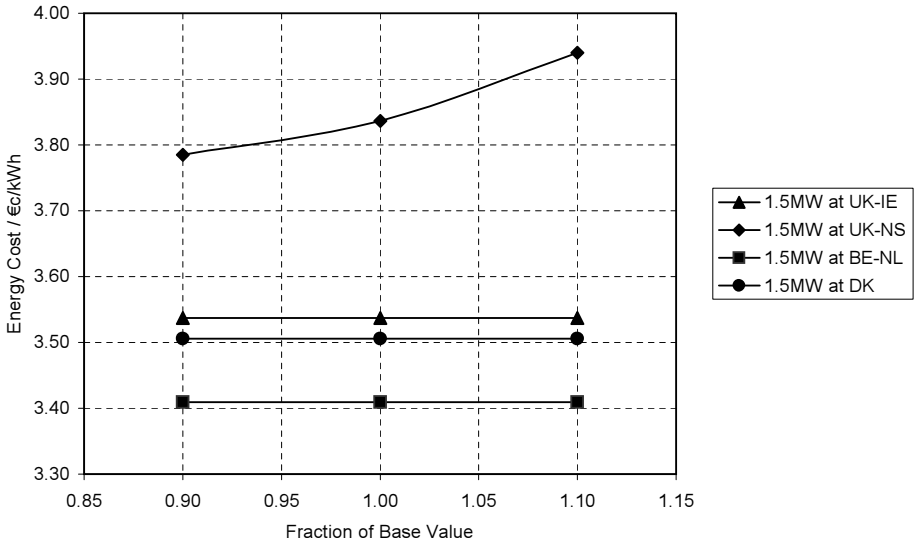

Figure O.18: Influence of 1 year return extreme wind speed on 1.5 MW base case energy cost.

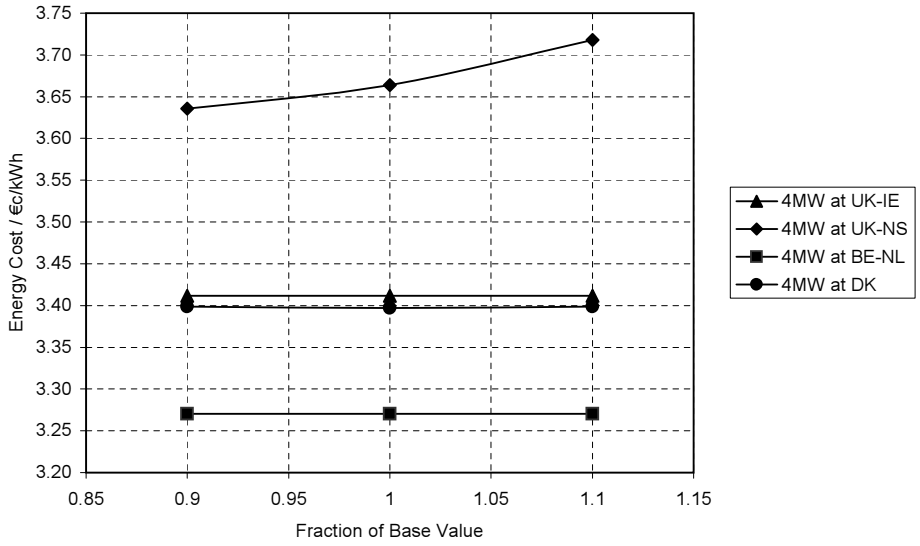

Figure O.19: Influence of 1 year return extreme wind speed on 4 MW base case energy cost.

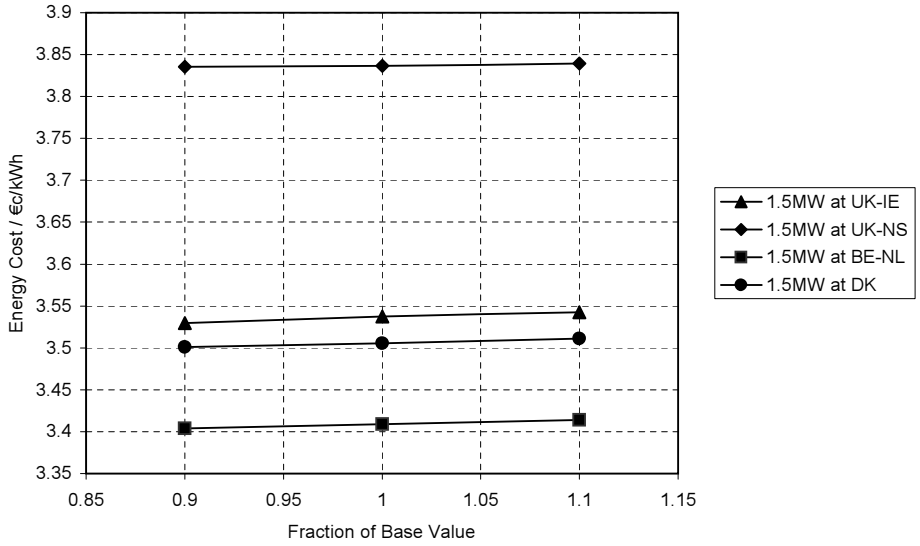

Figure O.20: Influence of 50 year return extreme wind speed on 1.5 MW base case energy cost.

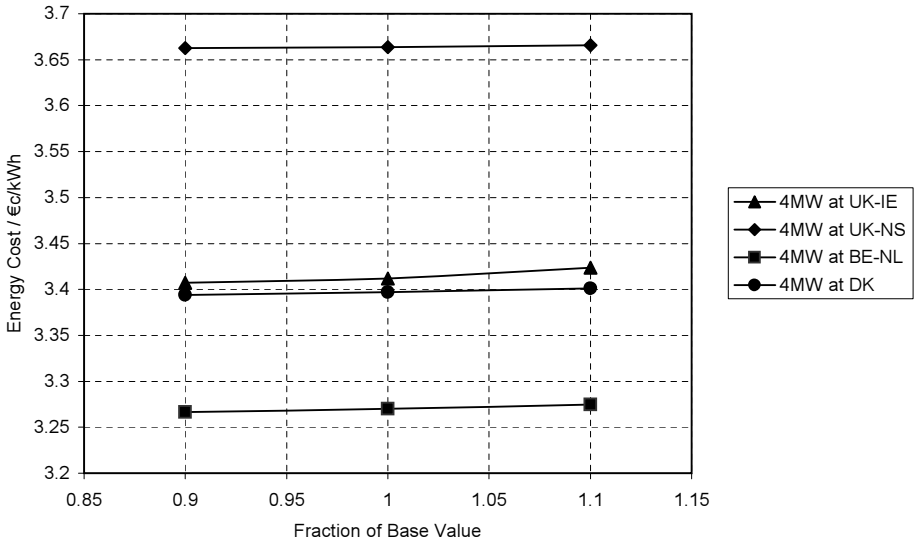

Figure O.21: Influence of 50 year return extreme wind speed on 4 MW base case energy cost.

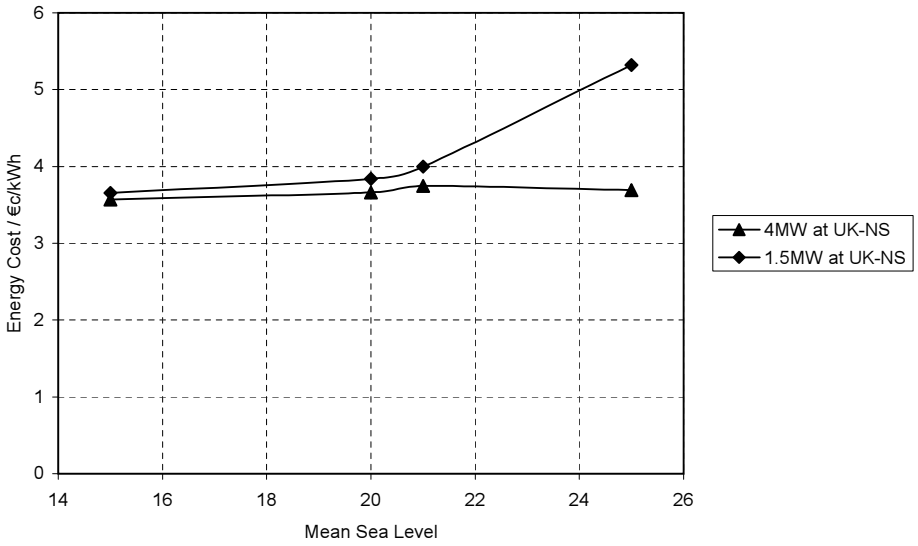

Figure O.22: Influence of depth on base case energy cost at the UK North Sea Site.

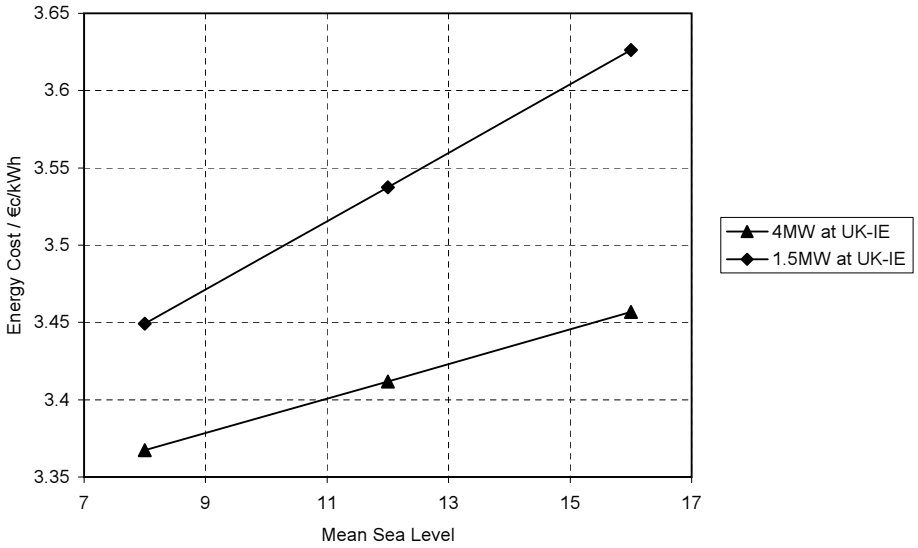

Figure O.23: Influence of depth on base case energy cost at the UK Irish Sea Site.

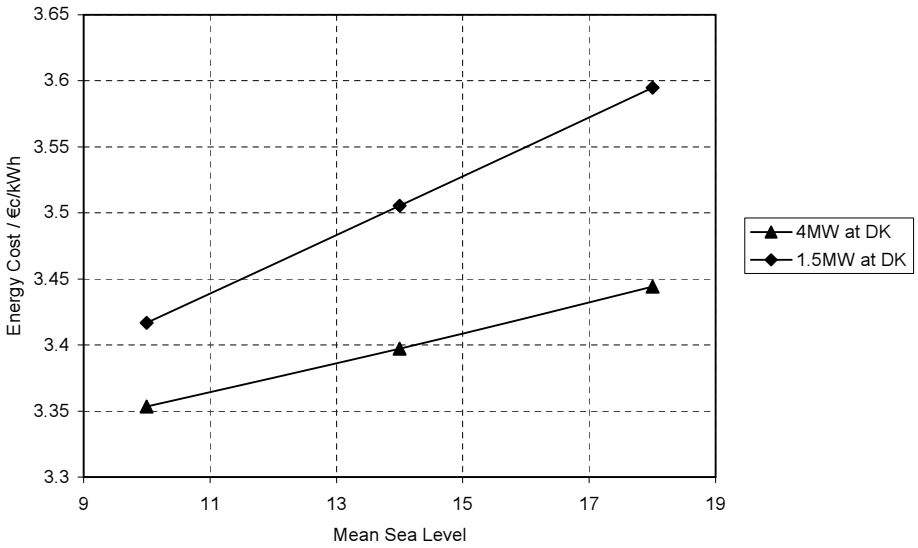

Figure O.24: Influence of depth on base case energy cost at the Baltic Sea Site.

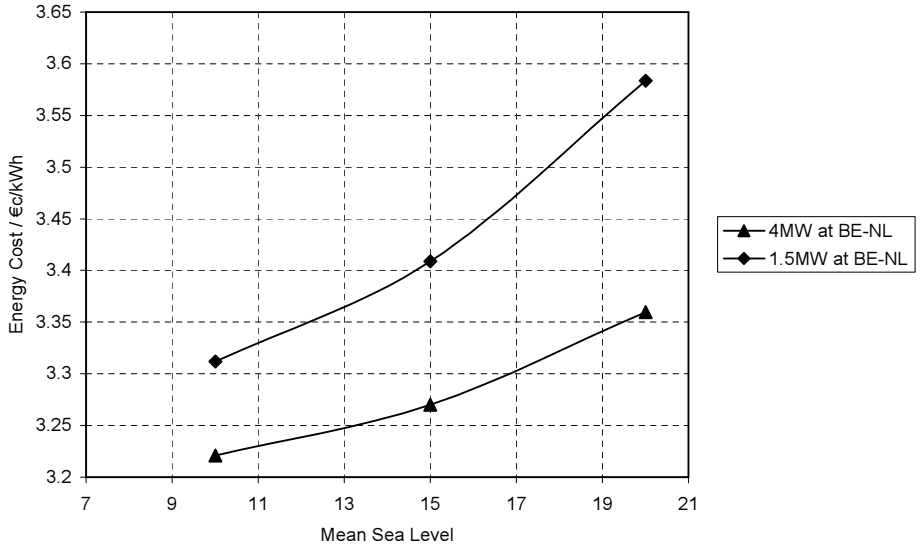

Figure O.25: Influence of depth on base case energy cost at the Dutch North Sea Site.

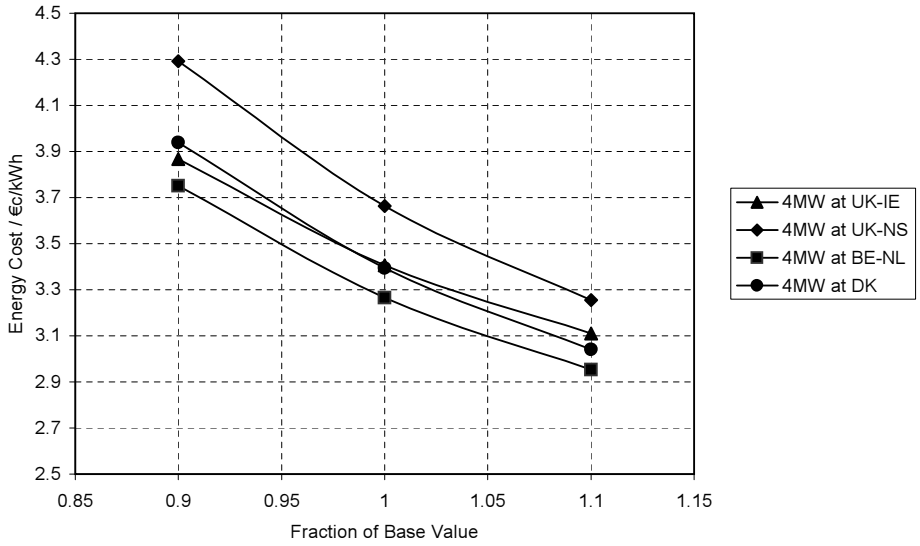

Figure O.26: Influence of annual mean wind speed on base energy cost for large scale farms.

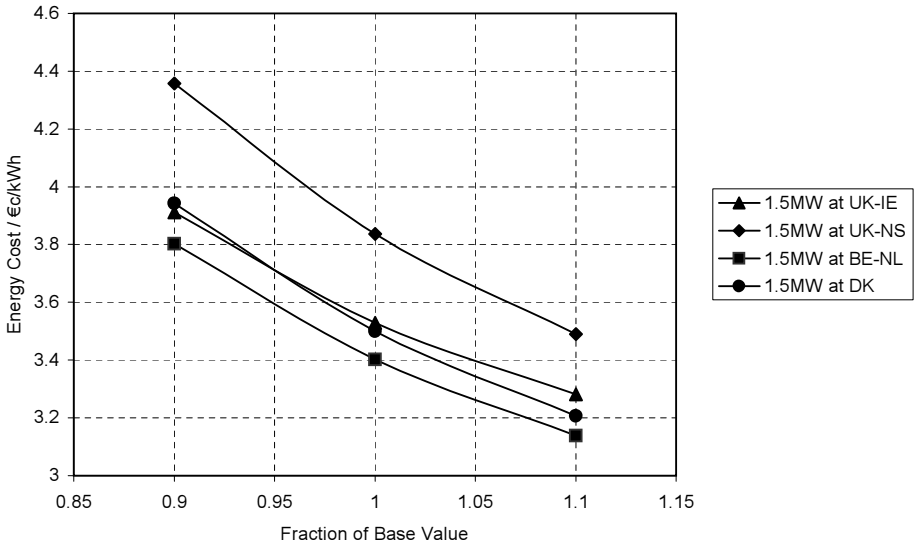

Figure O.27: Influence of annual mean wind speed on base energy cost for medium scale farms.

Appendix P

Fitting relationships to the NEXT data

P.1 Weibull distribution

The cumulative (i.e. exceedance) Weibull distribution is given by

$$P(v > V) = e^{-(v/C)^k} \tag{P.1}$$

where C is the scale parameter, k is the shape parameter and V is the windspeed exceeded. Taking logarithms twice yields

$$\ln(-\ln P) = k\ln(V) - k\ln(C) \tag{P.2}$$

so that plotting $\ln(-\ln P)$ as the ordinate against $\ln(V)$as abscissa produces a straight line of gradient k and intercept $-k\ln(C)$.

The NEXT data [207] was provided as a list of annual exceedances, such as that shown in table P.1 for NEXT location 15920. Parameters were estimated directly by a version of the above procedure using a linear least-squares fitting routine written in the Mathcad environment, included in a separate appendix.

P.2 Wind speed distributions

The NEXT wind data was provided for a height of 10 m above mean sea level. For compatibility with the DWD derived data, the values were first scaled to represent a height of 25m. This was achieved by first using the Prandtl log-law relationship and the Charnock relationship to estimate a value for the water surface roughness at each wind speed, using a value for the Charnock constant of 54 suggested by Lange [216]. The wind speed at 25 m was then estimated using from

Wind Speed at 10 m		**Wave Height**	
Hourly Mean (m/s)	**Exceedance probability (%)**	**Sig. Height (m)**	**Exceedance probability (%)**
0	100	0	100
0.3	100	0.5	73.13
1.6	99.87	1	40.29
3.4	89.56	1.5	21.37
5.5	69.13	2	10.83
8	43.2	2.5	4.68
10.8	21.51	3	1.89
13.9	7.28	6.5	0
17.2	1.58		
20.8	0.23		
24.5	0.04		
28.5	0		
32.7	0		

Table P.1: Wave and wind speed exceedance data for NEXT point reference 15920.

the values at 10 m using the Prandtl log law. Studies in the literature [217] have demonstrated that this is an effective approach to estimating the height variations of annual mean wind speed.

In general Weibull distributions do not perfectly represent wind speed variations at sea which show some curvature in a double logarithmic plot. Figure P.1 illustrates the result of fitting the entire data set from NEXT point 15920, which clearly shows the curvature. To accommodate this, the procedure set out in an earlier analysis [206] was adopted, wherein two separate fits were performed. Firstly, to estimate Weibull parameters to represent the climate variation, only data between 3 m/s and 20 m/s was considered. Secondly, to estimate the extreme wind speed, data between 7 m/s and 26 m/s was fitted.

Once the Weibull parameters are known the mean wind speed was estimated from the climate parameters using the result that the mean of the Weibull distribution is:

$$\overline{V} = C\,\Gamma\left(1+\frac{1}{k}\right). \tag{P.3}$$

The relatively short 9 year time extent of the NEXT data means that 50 year return period hourly wind speeds cannot reliably be calculated. With access to the original NEXT data set then well known statistical approaches to extreme value estimation could be applied, however only exceedance information was avail-

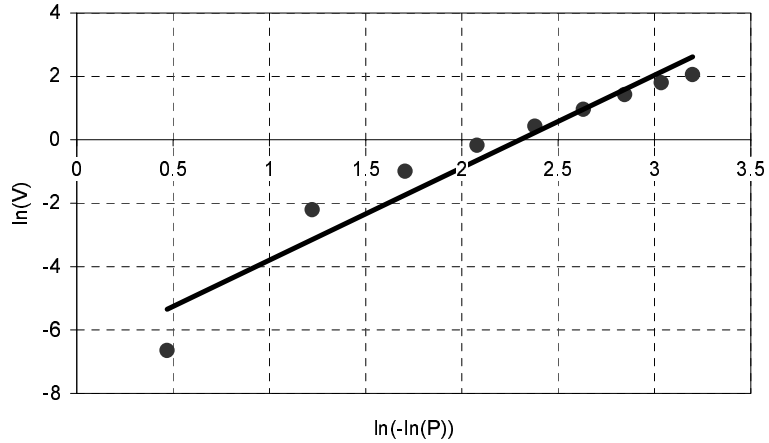

Figure P.1: Wind speed exceedance data from NEXT point 15920, showing form of characteristic curvature.

able. An approximate estimate can be obtained by using the Weibull 'extreme' parameters and solving equation P.1 for V with

$$P(v > V) = \frac{1}{50 \times 8760}. \tag{P.4}$$

This probability is obtained by on the basis that there are 8760 hours per year and the 50 year return period hourly wind speed will be occur only once in 50x8760 hours. This estimate is only valid under the assumption that there are no long-term variations in wind conditions. The results of these procedures for relevant NEXT data are shown in table P.2.

P.3 Wave height distributions

Significant wave height variations may also be approximately represented by a Weibull distribution of the form of equation P.1 where in this case V represents the wave height. Again a published procedure [206] was applied, with fitting only taking place for cumulative data up to an exceedance probability of 0.01. In fact the NEXT data with exceedance probabilities greater than 0.01 is marked as unreliable in any case.

Mean and extreme values were estimated from the Weibull parameters using the same methodology as above. For the 50 year return period wave height it was assumed that sea states last for 6 hours, giving 1460 discrete sea states per year. Thus the probability of the sea state that brings the 50 year return period wave is $\frac{1}{50 \times 1460}$. Results are also shown in table P.2.

Long.	Lat.	Annual mean wind speed			Significant wave height				Ref. No.
		Scale	***Shape***	***50 yr return***	***Mean***	***Scale***	***Shape***	***50 yr return***	
-1.583	56.748	1.128	2.426	33.174	1.472	1.110	1.523	7.981	15194
0.797	53.529	1.127	2.521	31.978	0.998	1.114	1.586	5.102	15631
2.304	52.528	1.128	2.400	32.389	1.126	1.106	1.477	6.390	15697
-1.65	50.413	1.129	2.206	33.067	1.160	1.081	1.290	8.164	16357
-4.657	49.773	1.128	2.377	33.074	1.978	1.118	1.647	9.591	16700
-3.805	53.741	1.129	2.176	33.272	0.993	1.086	1.317	6.750	15920

Table P.2: Weibull distribution data derived from NEXT data. The columns labelled Long. and Lat. give the Longitude and Lattitude respecitvely of the locations while the Ref. No. column gives the reference number assigned to the location in the offshore technology report. The scale parameters shown have been normalised by the distribution mean.

P.4 Wave time period modelling

For each NEXT location functions to estimate wave steepness from wave height were developed of the form discussed in chapter 7. Several functional forms were considered to provide an empirical K-H_s relationship. After trial fittings of all the data and considering the limited precisions of the raw data, a simple relationship was selected such that

$$K(H_s) = A_0 + A_1\sqrt{H_s} \tag{P.5}$$

Each dataset showed two distinct trends for the smaller and larger waves, such as that for point 16700 in figure P.2. Two separate analyses were carried out for each location therefore. The constants for each location were derived from a simple linear least squares fit of the published data.

Several complications arise in this procedure. Firstly the scatter diagrams (see table P.3) show a range of periods associated with each wave height class. To resolve this, UK Department of Energy [137] recommendations are adopted and the modal period is used for each wave height class. Since the period values are binned, a single value is determined as follows. It is assumed that the number of observations in the adjacent period bins (at the same significant wave height) reflects the balance of the observations in the modal bin, and a weighted average of the bin boundaries is calculated as the modal value.

The NEXT data lists spectral peak periods, T_p. While these are in many ways

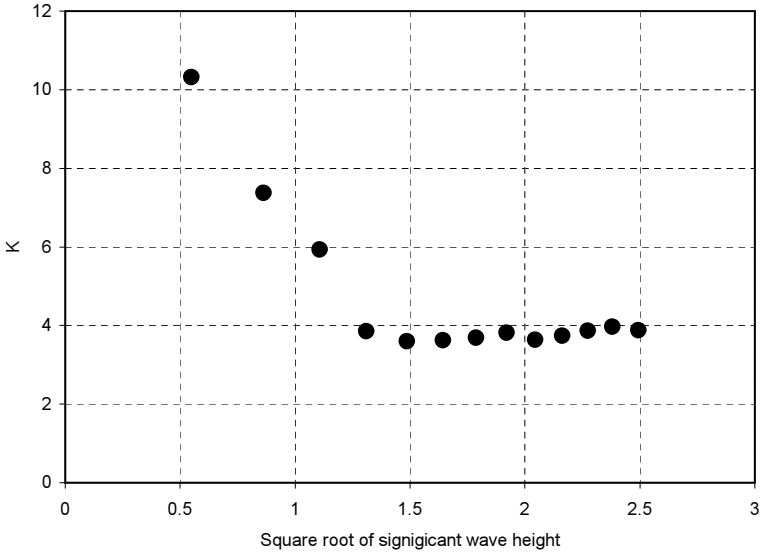

Figure P.2: Period data from NEXT point 16700 showing two trends.

	Spectral peak period / s																
Significant wave height / m	0	1	2	3	4	5	6	7	8	9	10	11	12	13	14	15	16
0		376	2235	9800	3247	1704	1403	1090	773	334	118	9	2	2	2	2	
0.5				7939	14711	1646	478	360	274	172	95	13					
1				41	5782	8584	435	46	16	8	4	1					
1.5					74	5465	2738	34									
2					1	473	3804	513									
2.5							827	1385	4								
3							104	734	575	71	6						
6.5																	

Table P.3: Wave period scatter diagram for NEXT point reference 15920

preferable for a fatigue analysis, the cost model uses zero-up crossing periods T_z and a conversion must be effected. Using the properties of the JONSWAP spectrum it may be shown that [139] :

$$\frac{T_p}{T_z} \approx 0.327e^{-0.315\gamma} + 1.17 \tag{P.6}$$

which was used with the assumed value of $\gamma = 3$ to estimate the zero up crossing period.

A third issue is what precise value to use for the wave height, since the values are binned. Simply averaging the bin bounds is not satisfactory because the wave heights are unlikely to be evenly distributed over the bin extent. Specific wave height values are estimated from the wave height Weibull distribution for the location by calculating the average wave height across the bin using

$$h_{mean,bin} = \frac{\int_{h_1}^{h_2} h\, p(h)\, dh}{\int_{h_1}^{h_2} p(h)\, dh} \tag{P.7}$$

where h_1 and h_2 are the upper and lower bin boundaries respectively, and $p(h)$ is the Weibull frequency distribution for the wave height, specifically

$$p(h) = -\left(\frac{h}{C}\right)^k \frac{k}{h} e^{-\left(\frac{h}{C}\right)^k}. \tag{P.8}$$

The scale parameter C and shape parameter k are those derived by fitting the Weibull distributions as discussed earlier.

Figures P.3 and P.4 show the results of the fitting process as applied to processed data from NEXT point 15920. Figures P.5 and P.6 show results for point 16700. The final constants produced from the analysis are shown in table P.4.

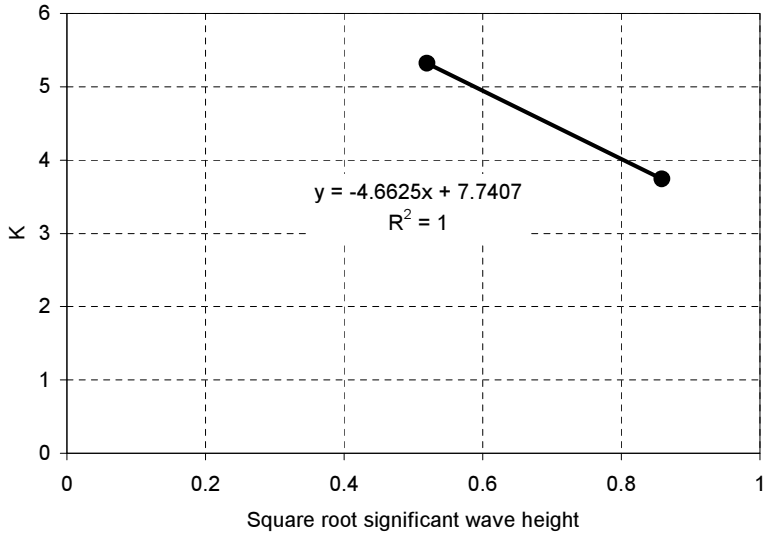

Figure P.3: Period data from NEXT point 15920 with linear fit to lower wave height data.

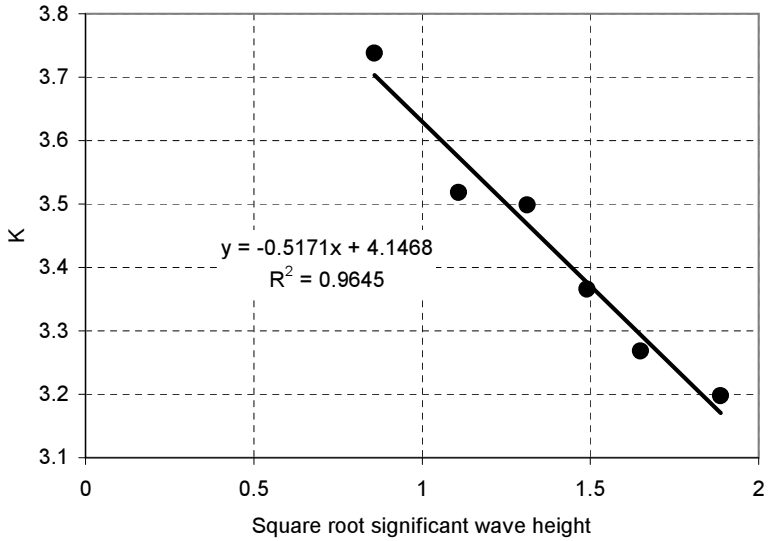

Figure P.4: Period data from NEXT point 15920 with linear fit to higher wave height data.

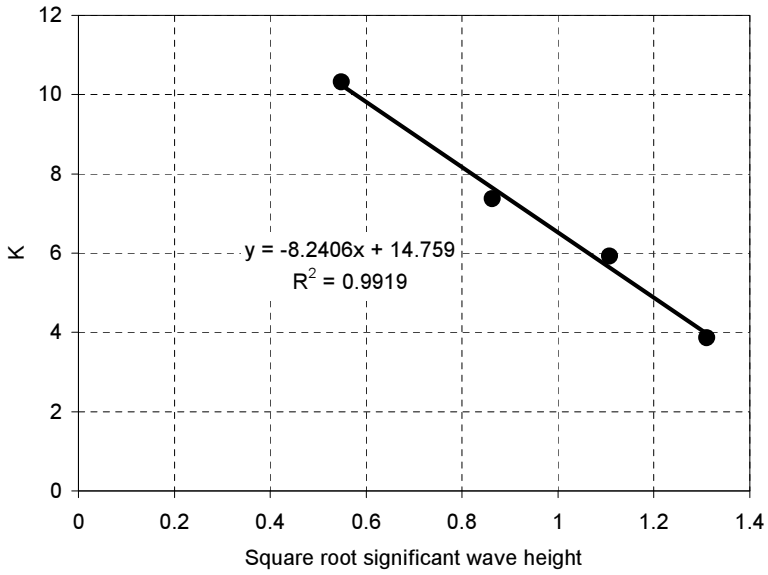

Figure P.5: Period data from NEXT point 16700 with linear fit to lower wave height data.

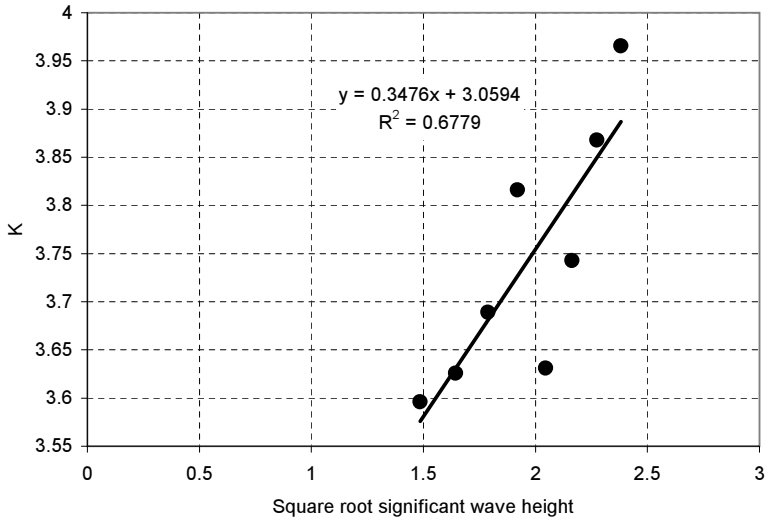

Figure P.6: Period data from NEXT point 16700 with linear fit to higher wave height data.

Ref. No.	Constants for Small waves		Swap over wave height (m)	Constants for Large waves	
	A_0	A_1		A_0	A_1
15194	8.1433	-4.7164	0.742	4.4225	-0.5646
15631	8.34	-5.105	0.743	4.64	-0.8791
15920	7.7407	-4.6625	0.737	4.4147	-0.5171
16357	8.0696	-4.676	0.346	4.2717	-0.3991
16597	8.043	-4.616	1.229	4.6534	-0.8028
16700	14.259	-8.241	1.716	3.0594	0.3476

Table P.4: Wave period representation derived from NEXT data. The Ref. No. column provides the point reference number from the NEXT report. The next two columns give parameters A_0 and A_1 to be used with equation 4.45 for sea states where the significant wave height is smaller than that listed under the 'Swap Over Wave Height' column. The final two columns give parameters to be used in sea states with significant wave heights greater than the swap over value.

Appendix Q

Mathcad worksheet used for fitting Weibull distributions to NEXT data

This chapter contains the Mathcad version 11 program used to drive Weibull distribution parameters for the NEXT wind data. Very similar code was used to derive parameters for the NEXT wave data but is not shown here.

The program is presented here only to indicate how the stages of the analysis were implemented numerically. To ease management of the large quantity of data processed, the Mathcad code was embedded into a Microsoft Excel worksheet, and as such requires modification to be used as a stand-alone program. The Excel worksheet is not shown.

Estimation of weibull parameters from exceedence data (for NEXT WIND data)

$$invals := in0$$

Some definitions

$$data\_height := 10$$

$$reqd\_height := 25$$

$$charnock := 70$$

First scale wind data from 10m to 25m - define the functions

log law $$u(z, ustar, z0) := \frac{ustar}{0.4} \cdot \ln\left(\frac{z}{z0}\right)$$

Relations for iteration soln

$$ustar(u, z, z0) := \frac{0.4 \cdot u}{\ln\left(\frac{z}{z0}\right)}$$

$$z0(ustar, zch) := \frac{ustar^2}{zch \cdot 9.81}$$

Iterative solution for roughness

$$roughness(u, z, zch) := \left| \begin{array}{l} z0old \leftarrow 0.0002 \\ zdiff \leftarrow 1 \\ \text{while } \left|\frac{zdiff}{z0old}\right| > 0.0001 \\ \quad \left| \begin{array}{l} us \leftarrow ustar(u, z, z0old) \\ z0new \leftarrow z0(us, zch) \\ zdiff \leftarrow z0old - z0new \\ z0old \leftarrow z0new \end{array} \right. \\ z0new \end{array} \right.$$

Define scaling u

$$uscale(z, u1, z1, zch) := \left| \begin{array}{l} rgh \leftarrow roughness(u1, z1, zch) \\ us \leftarrow ustar(u1, z1, rgh) \\ u(z, us, rgh) \end{array} \right.$$

Define a fliter to avoid processing zeros

$$\text{uscale2}(z, u1, z1, zch) := \begin{cases} 0 & \text{if } u1 = 0 \\ \text{uscale}(z, u1, z1, zch) & \text{otherwise} \end{cases}$$

Now process each velocity to required height

$$\text{idxmax} := \text{rows}(\text{invals}) - 1$$

$$\text{idx} := 0, 1 .. \text{idxmax}$$

$$(\text{tmpvals})_{\text{idx}} := \text{uscale2}\left[25, \left(\text{invals}^{\langle 0 \rangle}\right)_{\text{idx}}, 10, \text{charnock}\right]$$

copy to vals

$$\text{vals}^{\langle 0 \rangle} := \text{tmpvals} \qquad \text{vals}^{\langle 1 \rangle} := \text{invals}^{\langle 1 \rangle}$$

Analyse for data that cannot be used (i.e. ones and zeros)

$$\text{flter}(a) := \begin{cases} \text{imax} \leftarrow \text{rows}(a) - 1 \\ j \leftarrow 0 \\ \text{for } i \in 0 .. \text{imax} \\ \quad \begin{cases} \text{continue if } a_{i,0} \cdot a_{i,1} = 0 \\ \text{continue if } a_{i,1} = 1 \\ \text{rslt}_{j,0} \leftarrow a_{i,0} \\ \text{rslt}_{j,1} \leftarrow a_{i,1} \\ j \leftarrow j + 1 \end{cases} \\ \text{rslt} \end{cases}$$

$\text{flter}(\text{vals}) =$

	0	1
0	1.697	1
1	3.632	0.964
2	5.911	0.839
3	8.645	0.603
4	11.73	0.347
5	15.172	0.153
6	18.863	0.045
7	22.92	$7.3 \cdot 10^{-3}$
8	27.121	$8 \cdot 10^{-4}$
9	31.697	$1 \cdot 10^{-4}$
10	36.541	$1 \cdot 10^{-4}$

$$fvals := flter(vals)$$

Now split into two data sets for climate and extreme analysis

```
splt(a, lo, hi) := | imax ← rows(a) − 1
                   | j ← 0
                   | for i ∈ 0 .. imax
                   |     continue if a_{i,0} < lo
                   |     continue if a_{i,0} > hi
                   |     rslt_{j,0} ← a_{i,0}
                   |     rslt_{j,1} ← a_{i,1}
                   |     j ← j + 1
                   | rslt
```

$clim\_vals := splt(fvals, 3, 26)$ Climate values

$extr\_vals := splt(fvals, 7, 26)$ Extreme values

Now split into two components

Climate analysis (c)

$Qc := clim\_vals^{\langle 1 \rangle}$ $Vc := clim\_vals^{\langle 0 \rangle}$ $Qe := extr\_vals^{\langle 1 \rangle}$ $Ve := extr\_vals^{\langle 0 \rangle}$

$ye := \ln(-\ln(Qe))$ $xe := \ln(Ve)$

$yc := \ln(-\ln(Qc))$ $xc := \ln(Vc)$

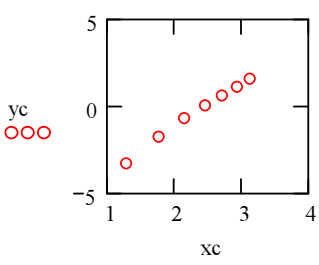

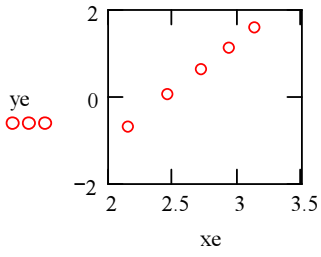

Fit the line

$kc := slope(xc, yc)$

$icptc := intercept(xc, yc)$

$Cc := e^{\left[\frac{icptc}{(-kc)}\right]}$

$ke := slope(xe, ye)$

$icpte := intercept(xe, ye)$

$Ce := e^{\left[\frac{icpte}{(-ke)}\right]}$

kc = 2.613 Cc = 11.937

ke = 2.32 Ce = 11.546

Get the mean of the weibull distribution

$$wp(x,c,k) := k\cdot\left[\left(\frac{x}{c}\right)^{(k-1)}\right]\cdot\exp\left[-1\cdot\left(\frac{x}{c}\right)^{k}\right]$$

$$wmean(c,k) := \int_0^{\infty}\left(\frac{x}{c}\cdot wp(x,c,k)\right)dx$$

$$normC(c,k) := \frac{c}{wmean(c,k)}$$

normC(Cc,kc) = 1.1256972

$c\_resary_0 := normC(Cc,kc)$

kc = 2.6125014

$c\_resary_1 := kc$

wmean(Cc,kc) = 10.6039239

$c\_resary_2 := wmean(Cc,kc)$

normC(Ce,ke) = 1.1286602

$e\_resary_0 := normC(Ce,ke)$

ke = 2.3196023

$e\_resary_1 := ke$

wmean(Ce,ke) = 10.2299897

$e\_resary_2 := wmean(Ce,ke)$

$c\_resary^T = (1.126 \quad 2.613 \quad 10.604)$

$e\_resary^T = (1.129 \quad 2.32 \quad 10.23)$

$out0 := c\_resary^T$ $out1 := e\_resary^T$

Appendix R

GIS Resource analysis results

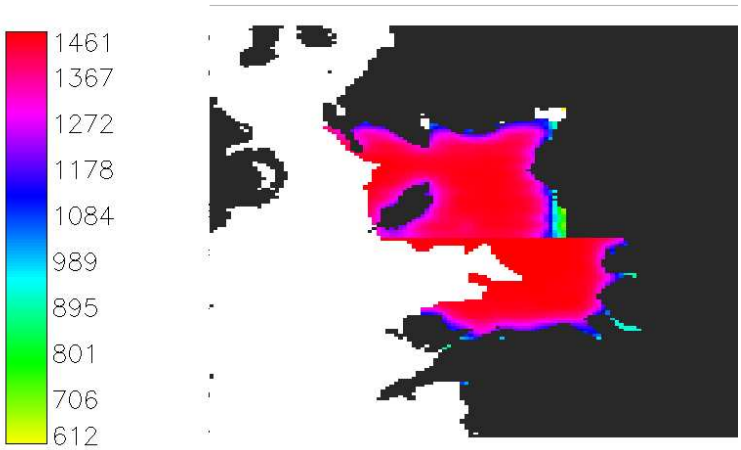

Figure R.1: Annual energy production from 4 MW UK Irish Sea base case farm. The units of the key are GWh/year.

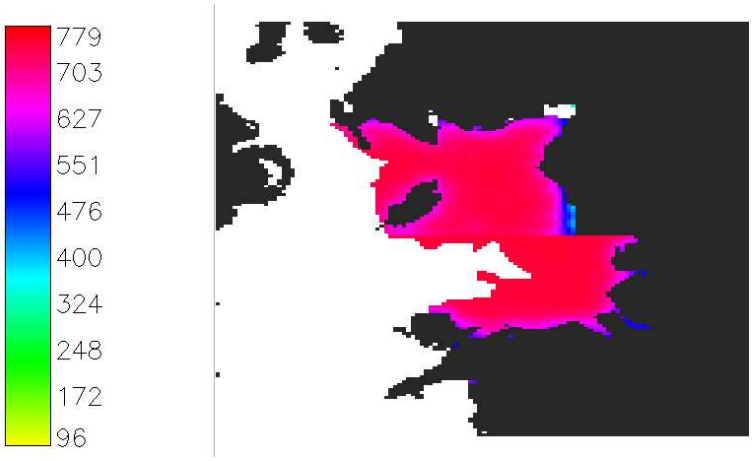

Figure R.2: Annual energy production from 1.5 MW UK Irish Sea base case farm. The units of the key are GWh/year.

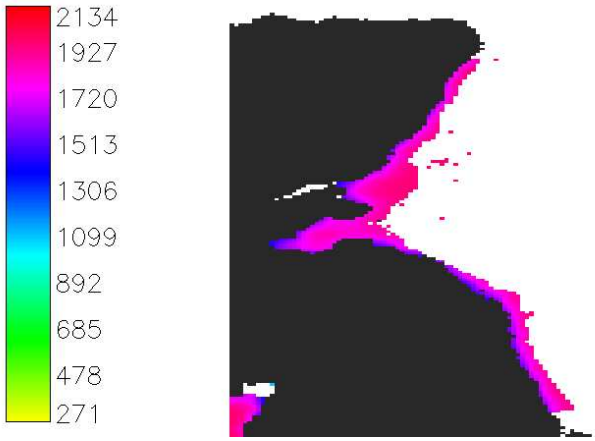

Figure R.3: Annual energy production from 4 MW UK North Sea base case farm. The units of the key are GWh/year.

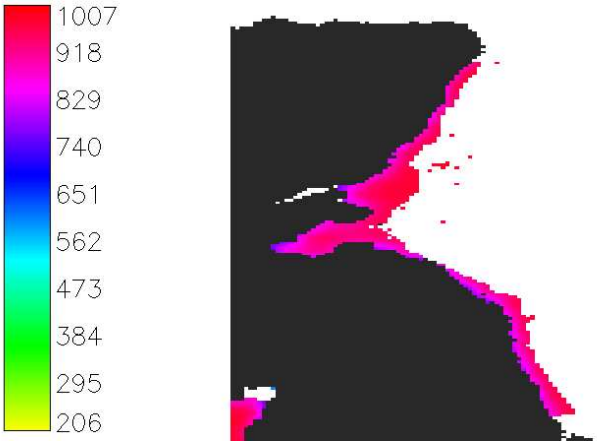

Figure R.4: Annual energy production from 1.5 MW UK North Sea base case farm. The units of the key are GWh/year.

Appendix S

Recently constructed offshore farms

This appendix lists recently constructed offshore wind farms not discussed elsewhere in the text.

Project	Nysted	Arklow Bank	North Hoyle	Scroby Sands
Completion date	2003	2003	2003	2004
Location	DK	IE	UK	UK
No of turbines	72	7	30	30
Capacity (MW)	2.3	3.6	2	2
Distance to shore (km)	9	10	7	2.3
Water depth (m)	6-10	5	12±9	
Hub height (m above MSL)		73.5	67	68

Appendix T

Publications by the author drawing on elements of the thesis

The following publications have drawn on the work described in this thesis:

- Fuglsang P, Bak C, Schepers JG, Bulder B, Cockerill TT, Claiden P, Olesen A & van Rossen R; Site specific design optimisation of wind turbines; Wind Energy vol. 5, pp. 261-279 (October 2002).
- Cockerill TT & Claiden P; A new cost model for the design optimisation of large wind turbines; University of Sunderland Renewable Energy Centre Report; (March 2002), 200 pp.
- Fuglsang P, Bak C, Schepers G, Bulder B, Cockerill TT, Claiden P, Oleson A & Rossen R; Site specific design of wind turbines based on numerical optimisation; European Wind Energy Conference, Copenhagen, Denmark, (July 2001).
- Cockerill TT, Harrison R, K uhn M, Bierbooms WAAM & van Bussel G; Technical and economic evaluation of the Northern European offshore wind resource; Journal of Wind Engineering and Industrial Aerodynamics vol. 89 no.7-8 pp. 689-711 (June 2001).
- Fuglsang P, Bak C, Schepers G, Bulder B, Cockerill TT, Claiden P, Oleson A & Rossen R; Site specific design of wind turbines; Final report on CEC Joule Project JOR3-CT98-0273; Riso National Laboratory, Denmark; (February 2001).
- Kuhn M, Birebooms WAAM, VanBussel GJW, Cockerill TT, Harrison R, Ferguson MC, Goransson B, Harland LA, Vugts JH & Wiercherink, R; Towards a mature offshore wind energy technology - Guidlines from the Opti-OWECS Project; Wind Energy, vol 2, pp.25-48 (1999).

Work for the publications listed was undertaken in collaboration, as the joint authorship demonstrates. Except where explicitly noted, this thesis is based only on those aspects of the work for which the author was responsible.

Bibliography

[1] Royal Commission on Environmental Pollution. Energy - the changing climate (twenty-second report), 2000.

[2] UK Department of Trade and Industry. UK energy sector indicators. Supplement to the Energy White Paper: Our Energy Future - Creating a Low Carbon Economy, 2003.

[3] British Petroleum. BP statistical review of world energy, 2003.

[4] Thomas Ackermann and Lennart Söder. Wind energy technology and current status: a review. Renewable and Sustainable Energy Review, 4:315–374, 2000.

[5] G H Mathies, C Natch, T E Schellin, A D Garrad, M A Wastling, D C Quarton, J Wei, M. Scherweit, and T. Siebers. Study of Offshore Wind Energy in the EC. Verlag Naturliche Energie, Brekendorf, 1995.

[6] D Milborrow and L Harrison. Hydrogen myths and renewables reality. Windpower Monthly, pages 47–52, May 2003.

[7] D Milborrow. Offshore wind plans and developments. Wind Stats Newsletter, 9(4), 1996.

[8] NOVEM. Haalbaarheidstudie demonstratieporject nearshore windpark, 1997.

[9] SEAS Vindkraftdeking Denmark. Havmolle-handlinsplan for de Danske farvande, June 1997.

[10] Renewable Energy Systems Ltd. Feasibility study for a prototype offshore wind turbine. Technical Report W/35/00251/REP/A-C, UK Energy Technology Support Unit, June 1993.

[11] E Hau. Windkraftanlagen - Grundlagen, Technik, Einsatz, Wirtschaftlichkeit. Springer-Verlag, second edition, 1996.

[12] F A Olsen. Feasibility study for a large scale offshore wind farm located in the Baltic Sea. In Proceedings of European Wind Energy Conference, 1994.

[13] F Olsen and K Rasmussen. Experience from the construction and operation of Vindeby offshore wind farm. In Proceedings OWEMES Seminar, Rome, February 1994.

[14] Concerted Action on Offshore Wind Energy in Europe. Resources and economics. Report on activities (also at http://www.offshorewindenergy.org), 2001.

[15] British Wind Energy Association. BWEA offshore wind website. http://www.offshorewindfarms.co.uk/else.html, June 2003.

[16] M Kuhn, W A A M Bierbooms, G J W van Bussel, M C Ferguson, B Goransson, T T Cockerill, R Harrison, L A Harland, J H Vughts, and R Wiecherink. Opti-OWECS final report: Structural and economic optimisation of bottom-mounted offshore wind energy converters volume 0: Executive summary. Technical Report IW-98139R, Delft University of Technology, 1998. ISBN 90-76468-01-X.

[17] P S Madsen. Tuno Knob offshore wind farm. In Proceedings European Union Wind Energy Conference, May 1996.

[18] E Poulson. Vestas experience with offshore installation. In Proceedings European Wind Energy Conference, Dublin, Ireland, October 1997.

[19] Wind Service Holland. Website. http://home.planet.nl/ windsh/, June 2003.

[20] IEA. Website: http://www.iea.org/imporg/ann_reps/wind/sweden.pdf, June 2003.

[21] Amec Wind. Website http://www.amec.com/wind/where/where_2ndlevel.asp?pageid=8035, June 2003.

[22] Middelgrunden Wind Turbine Cooperative. Website. http://www.middelgrunden.dk, August 2003.

[23] H C Sorensen, J Hansen, and P Volund. Experience from the establishment of Middelgrunden 40 MW offshore wind farm. In Proceedings European Wind Energy Conference, Copenhagen, Denmark, 2001.

[24] Middelgrunden wind farm website. http:// www.middelgrund.dk, June 2003.

[25] M Kuhn. Dynamics and Design Optimisation of Offshore Wind Energy Conversion Systems. PhD thesis, Delft University of Technology, 2001.

[26] Anon. High-tech wind turbines hit the high seas. Power Magazine, March 2002.

[27] Elsam. Horns Rev offshore wind farm. Publicity Flyer.

[28] J Jones. Horns Rev 160MW offshore wind. Renewable Energy World, 5(3):77–87, 2002.

[29] T Strandgaard and L Vandenbulcke. Driving monopiles into glacial till. Conference paper copy on website, December 2002. http://www.geoline.dk/Driving%20Monopiles%20into%20Glacial%20Till.pdf.

[30] M French. Conceptual design for engineers. Springer Verlag, November 1998. ISBN 1852330279.

[31] R Harrison, H Snel, and E Hau. Large Wind Turbines Design and Economics. Wiley, 2000. ISBN 0471494569.

[32] P F Ostwald. Engineering Cost Estimating. Prentice-Hall, 1991. ISBN 0132766272.

[33] P-E Consulating Group. Appraisal of mass production costs for wave energy devices. Technical report, Energy Technology Support Group, UK Department of Energy, March 1980.

[34] R Harrison and P Doherty. Cost modelling of hot dry rock systems. Technical report, Sunderland Polytechnic, 1991. UK Department of Energy Contractor Report ETSU G 138F-1.

[35] L J Campbell and J R Darnell. Cost estimates for large wind turbines. Technical Report EPRI AP-3276, Bechtel Group, San Francisco, CA, USA, November 1983. Prepared for Electric Power Research Institute.

[36] D J Egan, M Hulme, and N D Mortimer. Cost data for renewable energy systems. Technical Report ETSU GEN 6069, Sheffield City Polytechnic, 1992. UK Department of Energy Contractor Report.

[37] Yard Ltd. Electricity producing renewable energy technologies common costing methodology Volume 1: Initial development study. Technical Report ETSU GEN 2006-P1, UK Energy Technology Support Unit (ETSU), 1989.

[38] Yard Ltd. Electricity producing renewable energy technologies common costing methodology Volume 2: Final report. Technical Report ETSU GEN 2006 - P2, UK Energy Technology Support Unit (ETSU), 1989.

[39] R W Black. Electricity producing renewable energy technologies common costing methodology Phase II: Final report. Technical Report ETSU GEN 2013, UK Energy Technology Support Unit, 1992.

[40] M Rais-Rohani and Z Huo. Analysis and optimisation of primary aircraft structures based on strength, manufacturability and cost requirements AIAA-99-1328-CP. In Proceeding of the 40th AIAA/ASME/ASCE/AHS/ASC Structures, Structural Dynamics and Materials Conference, 1999.

[41] N. Y. Lao, T. J. Mosher, and J. M. Neff. Small Satellite Cost Model Version 98 INTRO: Users Guide. The Aerospace Corporation, June 1998.

[42] NASA. Parametric Estimating Handbook, second edition, 1999.

[43] Headquarters, Department of the Army. Programming Cost Estimates for Military Construction, May 1994. No: TM 5-800-4.

[44] US Army Cost and Economic Analysis Center. Department of the Army Cost Analysis Manual, May 2002.

[45] Boeing Engineering and Construction. MOD-5B Wind Turbine System: Concept and Preliminary Design Report Volume II: Detailed Report. US DOE report DOE/NASA-00200-02 and NASA Contractor Report CR-168047, sept 1982.

[46] R Harrison, G Jenkins, and R J Taylor. Cost modelling of horizontal axis wind turbines - results and conclusions. Wind Engineering, 13(6):315–323, 1989.

[47] R Harrison and G Jenkins. Cost modelling of horizontal axis wind turbines. Technical Report E/5A/CON/6006/2037, University of Sunderland for ETSU, December 1993.

[48] A. N. Macrae. Economic and cost engineering aspects of wind turbine generators. PhD thesis, Robert Gordon Institute of Technology, 1990.

[49] G R Collecut and R G J Flay. The economic optimisation of horizontal axis wind turbine design. Journal of Wind Engineering and Industrial Aerodynamics, 61:87–97, 1996.

[50] A J Pretlove and R Meyer. Rotor size and mass - the dilemma for designers of wind turbine generating systems. Wind Engineering, 18(6):317–328.

[51] M Kuhn, W A A M Bierbooms, G J W Van Bussel, T T Cockerill, R Harrison, M C Ferguson, B Goransson, Harland L A, J H Vugts, and R Wiecherink. Towards a mature offshore wind energy technology - guidelines from the Opti-OWECS project. Wind Energy, 2:25–28, 1999.

[52] P Fuglsang and H A Madsen. Numerical optimisation of wind turbine rotors. In Proceedings of the European Union Wind Energy Conference, Gothenburg, Sweden, May 1996.

[53] B Hendricks, J G Schepers, T G van Engelen, A J Stern, and G K Boerstra. Aeroelastically optimised cost efficient wind turbine: a case study. In Proceedings of the European Union Wind Energy Conference, Gothenburg, Sweden, May 1996.

[54] P Fuglsang, C Bak, J G Schepers, B Bulder, A Olesen, R van Rossen, T T Cockerill, and P. Claiden. Site specific design optimisation of wind turbines - Final report on EU Joule project JOR3-CT98-0273. Technical report, Riso National Laboratory, Denmark, November 2000.

[55] P. Fuglsang, C. Bak, J.G. Schepers, B. Bulder, T.T. Cockerill, P. Claiden, A. Olesen, and R. van Rossen. Site-specific design optimisation of wind turbines. Wind Energy, 5(4):261–279, 2002.

[56] T T Cockerill and P Claiden. SITEOPT project cost model report. Technical report, University of Sunderland, April 2002. Report on CEC JOULE III Project JOR3-CT98-0273.

[57] T T Cockerill, P Claiden, and P Fuglsang. A new approach to wind turbine cost modelling. (In preparation), 2005.

[58] P P Benham, R J Crawford, and C G Armstrong. Mechanics of Engineering Materials. Longman, 1998. ISBN 0582251648.

[59] H J Sutherland. On the fatigue analysis of wind turbines. Technical report, Sandia National Laboratories, Albuquerque, New Mexico, USA., June 1999.

[60] Kurt I Ronold, Jacob Wedel-Heinen, and Carl J Christensen. Reliability-based fatigue design of wind-turbine rotor blades. Engineering Structures, 21:1101–1114, 1999.

[61] H M Negm and Maalawi K Y. Structural design optimization of wind turbine towers. Computers and Structures, 74:649–666, 2000.

[62] Germanischer Lloyd. Regulations for the certification of offshore wind energy conversion systems, 1995.

[63] Tatjana Pauling. Economic optimization of offshore wind farms. Student thesis, Report IV-96.098R, Institute for Wind Energy, TU Delft., September 1996.

[64] Deutches Institut fur Bautechnik. Richtline fur windkraftanlangen - einwirkungen und standardsicherheitsnachweise fur turm und grundung:., June 1993.

[65] M F Ashby and D R H Jones. Engineering Materials 1: An Introduction to their Properties and Applications. Butterworth-Heinemann, 1996. ISBN 0750630817.

[66] O H Basquin. The exponential law of endurance tests. Proceedings American Society for Testing and Materials, 11:625–630, 1910.

[67] British Standards. BS 7608:1993 Code of Practice for Fatigue Design and Assessment of Steel Structures, 1993.

[68] Anita Sandstrom. Kvaerner-Turbin fatigue dimensioning method. Personal communication, June 1996.

[69] R Soderberg. Working stresses. Journal of Applied Mechanics, 2(3), 1935.

[70] Warren C Young. Roark's Formulas for Stress and Strain. McGraw-Hill, sixth edition, 1989.

[71] S Suresh. Fatigue of Materials, chapter 7, pages 222–256. 2000.

[72] A R Henderson. Analysis Tools for Large Floating Offshore Wind Farms. PhD thesis, Department of Mechanical Engineering, June 2000.

[73] A Palmgren. Die lebensdauer von kugellagern. Zeitschrift des Vereins Deutscher Ingenieure, 68:339–341, 1924.

[74] M A Miner. Cumulative damage in fatigue. Journal of Applied Mechanics, 12:159–164, 1945.

[75] P S Veers. Simplified fatigue damage and crack growth calculations for wind turbines. In Eighth ASME Wind Energy Symposium, page 133. ASME, 1989.

[76] Det Norske Vertias. Rules for Classification.

[77] S D Downing and D F Socie. Simple rainflow counting algorithms. International Journal of Fatigue, 4(1):31, 1982.

[78] R E Akins. Rainflow counting based on predicted stress spectra. In Eighth ASME Wind Energy Symposium, page 131. ASME, 1989.

[79] P H Madsen, S Frandsen, W E Holley, and J C Hansen. Dynamic analysis of wind turbine rotors for lifetime prediction. Contract Report 102-43-51, RISO National Laboratory, Denmark, 1983.

[80] J M Tunna. Fatigue life prediction of Gaussian random loads. Fatigue and Fracture of Engineering Materials and Structures, 9(3):169–184, 1986.

[81] R E Hoskin, Warren J G, and Draper J. Prediction of fatigue in wind turbine rotors. In Wind Energy Conversion Proceedings BWEA 1989, pages 389–394, 1989.

[82] N W M Bishop, H Zhihua, and F Sherratt. The analysis of non-gaussian loadings from wind turbine blades using frequency domain techniques. In Quarton DC; Fenton VC, editor, Wind Energy Conversion : Proceedings of the Thirteenth BWEA Wind Energy Conference, pages 317–324, London, April 1991. Mechanical Enegineering Publications Ltd.

[83] N W M Bishop, Z Hu, and R Wang. Fast frequency domain fatigue life asessment of wind turbine blades. In Wind Energy Conversion Proceedings of Fourteenth BWEA conference, pages 299–305, 1992.

[84] N W M Bishop, Z Hu, R Wang, and D Quarton. Methods for rapid evaluation of fatigue damage on the Howden HWP330 wind turbine. In Proceedings of the Fifteenth BWEA Conference, 1993.

[85] A Halfpenny. A frequency domain approach for fatigue life estimation from finite element analysis. In International Conference on Damage Assessment of Structures (DAMAS), Dublin, 1999.

[86] T Dirlik. Application of Computers to Fatigue Analysis. PhD thesis, University of Warwick, 1985.

[87] N W M Bishop. The Use of Frequency Domain Parameters to Predict Structural Fatigue. PhD thesis, 1988.

[88] N W M Bishop and F Sherratt. Fatigue life prediction from power spectral density data. Environmental Engineering, 2, 1989.

[89] R W Clough and J Penzien. Dynamics of Structures. McGraw-Hill, second edition, 1993.

[90] W H Press, B P Flannery, A T Saul, and T Vetterling. Numerical Recipes in FORTRAN 77: The Art of Scientific Computing Volume 1. Cambridge University Press, 1993.

[91] L S Etube, F P Brennan, and W D Dover. Modelling of jack-up response for fatigue under simulated service conditions. Marine Structures, 12:327–348, 1999.

[92] A D Garrad and U Hassan. The dynamic response of wind turbines for fatigue life and extreme load prediction. In Proceedings EWEA Conference, Rome, October 1986.

[93] D C Quarton, M A Wastling, A D Garrad, and U Hassan. The calculation of wind turbine loads. a frequency or time domain problem? In Wind Energy Conversion Proceedings of Fourteenth BWEA Conference, pages 307–314, 1992.

[94] M L Buhl, J M Jinkman, A D Wright, R E Wilson, Walker S N, and P Heh. FAST User's Guide. NREL, Golden, Colorado, USA, September 2002.

[95] H Glauert. Airplane propellers. In Aerodynamic Theory, pages 169–360. Julius Springer, 1935.

[96] M S Selig, C A Lyon, P Giguere, Ninham C P, and J Guglielmo. Summary of Low Speed Airfoil Data, volume 3. Soartech Publications, 1996.

[97] Mark Drela and Harold Youngren. XFOIL User Primer 6.94. Department of Aeronautics and Astronautics, MIT, December 2001.

[98] C Yan, Y Zhiquan, X Lijun, and Y Dajun. Numerical study of two dimensional flow past an airfoil for hawt rotors. In Proceedings European Wind Energy Conference, Dublin, 1997. Irish Wind Energy Association.

[99] Y G Perivolaris, G D Tzabiras, and S G Voutsinas. Guidelines for an accurate prediction of airfoil characteristics using an advanced navier-stokes solver. In Proceedings European Wind Energy Conference, pages 529–532, Dublin, October 1997. Irish Wind Energy Association.

[100] M O L Hansen. Aerodynamics of Wind Turbines. James and James, London, 2000.

[101] D A Spera. Wind Turbine Technology. ASME Press, New York, USA, 1994.

[102] David-P. Molenaar and Sjoerd Dijkstra. State of the art of wind turbine design codes: main features overview for cost-effective generation. Wind Engineering, 23(5):295–311, 1999.

[103] L Prandtl and O G Tietjens. Applied Hydro- and Aeromechanics. Dover Publ. inc., 1957.

[104] S Goldstein. On the vortex theory of screw propellors. Proceedings of the Royal Aeronautical Society, 123:440–465, 1929.

[105] H Snel, R Houwink, and J Bosschers. Sectional prediction of lift coefficients on rotating wind turbine blades in stall. Technical Report ECN-C-93-052, Netherlands Energy Research Foundation (ECN), December 1994.

[106] L A Viterna and R D Corrigan. Fixed pitch rotor performance of large horizontal axis wind turbines. In DOE/NASA Workshop on Large Horizontal Axis Wind Turbines, pages 69–85, Cleveland USA, 1981.

[107] T S Beddoes and J G Leishman. A semi-empirical model for dynamic stall. Journal of the American Helicopter Society, 34(2):3–17, July 1989.

[108] B Montgomerie. Dynamic stall model called simple. Technical Report ECN-C-95-060, Netherlands Energy Research Foundation (ECN), January 1996.

[109] A S Elliot. ADAMS/WT 2.0 Users Guide. Mechanical Dynamics Inc, Meza, Arizona, USA, 1998.

[110] David J Laino and A Craig Hansen. User's Guide to the Wind Turbine Aerodynamics Computer Software AeroDyn Version 12.43. Windward Engineering, Salt Lake City, Utah, USA, April 2002.

[111] Garrad Hassan Limited. BLADED for windows: A design tool for wind turbine performance and loading. Advertising flyer.

[112] L N Xu, G ans Sankar. Application of a viscous flow methodology to the NREL Phase VI rotor. In Proceedings of the 21st ASME Wind Energy Conference, pages 83–93, Reno, NV, USA, 2002.

[113] W Johnson. Helicopter Theory. Princeton University Press, USA, 1980.

[114] W A A M Bierbooms. A dynamic model of a flexible rotor - part 1: Description of the mathematical model. Technical report, Institute for Wind Energy, Delft University of Technology, May 1990. IW89.034R.

[115] S Oye. Dynamic stall - simulated as time lag of separation. In IEA Symposium in the aerodynamics of wind turbines, UK, November 1990.

[116] L G J Janssen, K Rossis, G Athanassoulis, T T Cockerill, and Others. Focus6: Integrated wind turbine design tool. Proposal submitted to the European Union FP6 Programme, March 2003.

[117] V A Riziotis and S G Voutsinas. GAST: A general aerodynamic and structural prediciton tool for wind turbines. In Proceedings of the European Wind Energy Conference, pages 448–452. Irish Wind Energy Association, October 1997.

[118] A Suzuki and A C Hansen. Dynamic inflow models with nonlinear induced velocity distributions for YawDyn/AeroDyn codes. In Proceedings Windpower 1999, Burlington, VT, USA. American Wind Energy Association.

[119] U Hassan and D M Sykes. Wind structure and statistics. In Wind Energy Conversion Systems. Prentice Hall International, 1990.

[120] M L Buhl, Jr. SNWind User's Guide. National Wind Technology Center, National Renewable Energy Laboratory, Golden, Colorado, USA, June 2002.

[121] D J Tritton. Physical Fluid Dynamics. Oxford University Press, 1988.

[122] H Charnock. Wind stress on a water surface. Quarterly Journal of the Royal Meterological Society, 81:639–640, 1955.

[123] R I Harris and D M Deaves. The structure of strong winds. In Wind Engineering in the Eighties. CIRIA, 1981.

[124] W J Duncan, A S Thom, and A D Young. Mechanics of Fluids. Edward Arnold, second edition, 1970.

[125] W A A M Bierbooms and J B Dragt. SWING 4: A stochastic 3d wind field generator for design calculations. In Proceedings of European Union Wind Energy Conference, pages 942–945, Gothenburg, Sweden, May 1996.

[126] ESDU. Characteristics of atmospheric turbulence near the ground Part II: Single point data for strong wind. Technical report, Engineering Sciences Data Unit, 1974. ESDU Technical Report 740310.

[127] J C Kaimal, Y Wyngaard, Izumi, and O R Cote. Spectral characteristics of surface-layer turbulence. Quarterly Journal Royal Meteorological Society, 98:563–589, 1972.

[128] International ElectroTechnical Committee. IEC1400-1:1994 wind turbine generator systems Part 1: Safety requirements, 1994.

[129] A D Garrad. Forces and dynamics of horizontal axis wind turbines. In Wind Energy Conversion Systems, pages 119–144. Prentice Hall International, 1990.

[130] F M Sinclair and B R Clayton. Excitation and damping forces on offshore wind turbines. Wind Engineering, 13:276–292, 1989.

[131] British Standards Institute. BS 6349-1: Maritime Structures - Part 1: Code of practice for general criteria, 2000.

[132] M Kuhn, G W van Bussel, C Schontag, T T Cockerill, R Harrison, L A Harland, and J H Vugts. Opti-OWECS final report Volume 2: Methods assisting the design of offshore wind energy conversion systems. Technical Report IW-98141R, Institute for Wind Energy, Delft University of Technology, August 1998.

[133] M Kuhn. Modal analysis of the NedWind 40 tower - comparison of measurements and calculations for the sites Oostburg and Lely (Ijsselmeer). Technical Report IW96.029R, Delft University of Technology, 1996.

[134] M C Ferguson, M Kuhn, G J W van Bussel, W A A M Bierbooms, T T Cockerill, B Goransson, L A Harland, J H Vugts, and R Hes. Opti-OWECS final report Volume 4: A typical design solution for an offshore wind energy converter system. Technical Report IW-98143R, Institute for Wind Energy, Delft University of Technology, August 1998.

[135] M Patel. Dynamics of Offshore Structures. Butterworth, 1989.

[136] J R Morison, M P O'Brien, J W Johnson, and S A Schaaf. The forces exerted by surface waves on piles. Petroleum Transactions, 1950.

[137] UK Department of Energy. Offshore Installations: Guidance on Design, Construction and Certification, 1990.

[138] James Lighthill. Waves in Fluids. Cambridge University Press, 1980.

[139] N D P Barltrop and A J Adams. Dynamics of Fixed Marine Structures. Butterworth Heinemann, 1991.

[140] R G Dean. Stream function representation of non-linear ocean waves. Journal Geophysical Research, 70, 1965.

[141] G G Stokes. On the theory of oscillatory waves. Mathematical and Physical Papers Volume 1, 1880.

[142] UK Health and Safety Executive. Overview of the work carried out during the North European storm study: The hindcasting of North Sea metocean parameters (Offshore Technology Report - OTO 97051), July 1997.

[143] D J Peters, C J Shaw, C K Grant, J C Heiderman, and D Szabo. Modelling the North Sea through the North European storm study. In Offshore Technology Conference, Houston, Texas, USA, May 1993.

[144] NOAA National Data Bouy Center. Website: http://www.ndbc.noaa.gov, June 2003.

[145] British Maritime Technologly Limited. Global wave statistics, 1986.

[146] British Maritime Technology Limited. Global wave statistics online, June 2003. Website: http://www.globalwavestatisticsonline.com.

[147] G Neumann and Pierson W J. Principles of Physical Oceanography. Prentice Hall, 1966.

[148] P N Simpson, M Hancock, and U B M Kuhn. A re-appraisal of the cost of UK offshore wind energy. In Proceedings of the thirteenth BWEA conference, March 1991.

[149] W J Pierson and L Moskowitz. A proposed spectral form of fully developed wind seas based on the similarity theory of S A Kitaigorodskii. Journal of Geophysical Research, 1964.

[150] K Hasselman. Measurements of wind wave growth and swell decay during the JONSWAP project. Erganzungsheft zur Deutschen Hydrographischen Zeitschrift, Reihe A, 8(12), 1973.

[151] G Watson and J A Halliday. Floating offshore wind energy - resource assessment and estimation of electricity generation costs. Internal report, Energy Research Unit, Rutherford Appleton Laboratory, UK, March 2000.

[152] A Halfpenny, S Kerr, M Quinlan, and N W M Bishop. A technical feasibility study and economic assessment of an offshore floating wind farm. In Proceedings European Wind Energy Conference, 1995.

[153] K Tong and C Cannell. Technical and economical aspects of a floating offshore wind farm. In Proceedings OWEMES Seminar, Rome, February 1994.

[154] J Kemp. The OWEL wave energy converter. Website: http://www.owel.co.uk/paper.htm, June 2003.

[155] W B Byrne. Investigation of Suction Caissons in Dense Sand. PhD thesis, University of Oxford, 2000.

[156] G T Houlsby, B W Byrne, and C M Martin. Novel foundations for offshore wind farms. Research proposal to EPSRC, August 2001.

[157] SLP Engineering Ltd, Shell Renewables Ltd, Enron Wind Overseas Development Ltd, Fugro Ltd amd Aerolaminated Ltd, Garrad Hassan, Oxford University, HR Wallingford, and Marine Operations. The application of suction caisson foundations to offshore wind turbines. Proposal to DTI.

[158] G T Houlsby and B W Byrne. Suction caisson foundations for offshore wind turbines and anemometer masts. Wind Engineering, 24(4):249–255, 2000.

[159] B M Das. Principles of Foundation Engineering. PWS Publishing, fourth edition, 1998. ISBN 0534954030.

[160] J E Bowles. Foundation Analysis and Design. McGraw-Hill, fifth edition, 1996. ISBN 0071148116.

[161] A Crosby, CC Graham, N A Ruckley, H M Pantin, and R H Belderson. Sea bed sediments around the UK. British Geological Survey Map, 1987.

[162] G J W van Bussel and C Schontag. Operation and maintenance aspects of large offshore windfarms. In Rick Watson, editor, Proceedings of the European Wind Energy Conference, pages 272–275, 1997.

[163] C Schontag. Optimisation of operation and maintenance of offshore wind farms. Master's thesis, Institute for Wind Energy, Delft University of Technology, 1996.

[164] S D Wright, A L Rogers, J F Manwell, and A Ellis. Transmission options for offshore wind farms in the United States. In Proceedings AWEA, 2002.

[165] V G Agelidis and C Madernlis. Technology of offshore wind turbines and farms and novel nultilevel converter-based hvdc systems for their grid connections. Wind Engineering, 26(6):383–395, November 2002.

[166] PB Power. Concept study - Western offshore transmission grid. Technical Report K/EL/00294/00/00, UK Energy Technology Support Unit (ETSU), 2002.

[167] W Grainger and N Jenkins. Offshore wind farm electrical connection options. In Wind Energy - Switch on to Wind Power : Proceedings of the 20th BWEA Conference, 1998.

[168] P Gardner, L M Craig, and G J Smith. Electrical systems for offshore wind farms. In Wind Energy - Switch on to Wind Power : Proceedings of the 20th BWEA Conference, 1998.

[169] Paul Gardner. Meeting at Garrad Hassan Glasgow. Personal Communication, 2002.

[170] C A Gunther. Optimisation of the grid connection of offshore wind farms. Master's thesis, Institute for Wind Energy, Delft University of Technology, 1997.

[171] W A A M Bierbooms. Personal communication, 1997.

[172] I Troen and E L Peterson. European wind atlas. Technical report, Riso National Laboratory, Roskilde, Denmark, 1989.

[173] R M Traci, G T Phillips, and P C Patnaik. Developing a site selection methodology for wind energy conversion systems. Technical Report DOE/ET/20280-3, Science Applications Inc. for US Department of Energy, 1978.

[174] N G Mortensen, L Landberg, I Troen, and E L Petersen. Wind atlas analysis and application program. Technical Report RISO-I-666, Risoe National Laboratory, Denmark, 1993.

[175] R Lange and J Hojstrup. Estimation of offshore wind resources - The influence of sea fetch. In Wind Engineering into the 21st Century: Proceedings of the 10th International Conference on Wind Engineeing, pages 2005–2012, Copenhagen, Denmark, 1999. A A Balkena.

[176] J Mann, S Ott, B H Jorgensen, and H P Frank. Wasp Engineering 2000. Technical Report R-1356(EN), Risoe National Laboratory, Denmark, August 2002.

[177] J A Halliday. Wind resource - anemometry. In L L Freris, editor, Wind Energy Conversion Systems, pages 33–52. Prentice Hall International, 1990.

[178] British oceanographic data centre. Website: http://www.bodc.ac.uk, June 2003.

[179] Britsh atmospheric data centre. Website: http://badc.nerc.ac.uk/home/, June 2003.

[180] D J Millborrow, D J Morre, N B K Richardson, and S C Roberts. The UK offshore wind power resource. In Proceedings of the 4th International Symposium on Wind Energy Systems, 1982.

[181] G M Watson, J A Halliday, J P Palutikof, T Holt, R J Barthelmie, J P Coelingh, L Folkerts, E J Van Zuylen, and J W Cleijne. POWER - A methodology for predicting offshore wind energy resources. In Proceedings BWEA 21st Conference, September 1999.

[182] G M Watson, J A Halliday, J P Palutikof, T Holt, R J Barthelmie, J P Coelingh, L Folkerts, G F M wiegerinck, E J van Zuylen, J W Cleijne, R J Hommel, G C S Barthelmie, J P Coelingh, L Folkerts, E J Van Zuylen, and J W Cleijne. POWER - A methodology for predicting offshore wind energy resources. In Proceedings OWEMES Conference, September 2002.

[183] J Nitteberg, A A de Boer, and P B Simpson. Recommended practices for wind turbine testing 2. Estimation of cost of energy from wind energy conversion systems. Technical report, International Energy Agency Programme for Research and Development on Wind Energy Conversion Systems, 1983.

[184] C A Morgan, P G Hodgetts, W W Schelz, and C J A Versteegh. Review of offshore wind farm project features. Technical report, Garrad Hassan for US Army Corps of Engineers, July 2003.

[185] W Bierbooms. Private communication, Delft University of Technology, 1998.

[186] T Burton, D Sharpe, N Jenkins, and E Bossanyi. Wind Energy Handbook. Wiley, 2001.

[187] G B Airy. Tides and waves. Encyc. Metrop., pages 241–496, 1845.

[188] L E Borgman. Ocean wave simulation for engineering design. American Society of Civil Engingeers Journal of Waterways and Harbours Division, Nov 1969.

[189] Martin Kuhn. Dynamics of offshore wind energy converters on monopile foundations. Technical Report IW-96.093R, Institute for Wind Energy, Delft University of Technology, November 1996. Preliminary report for Martin Kuhn's PhD.

[190] N J Tarp-Johansen and S Frandsen. A simple offshore wind turbine model for foundation design. Technical report, Risoe National Laboratory, Denmark, 2003.

[191] S Madsen, P H ans Frandsen. Pitch regulation for power limitation. In Proceedings of the European Wind Energy Conference, 1984.

[192] Code of practice for loads and safety of wind turbine constructions. The Danish Society of Engineers and the Federation of Engineers, 1992.

[193] DIN. Din4133: Steel stacks (schornsteine aus stahl). German DIN Standard, 1991.

[194] J Wieringa. Gust factors over open water and built up country. Boundary-Layer Meteorology, 3:424–411, 1973.

[195] M C Ferguson. Series of Private Communications. October 1997 - December 1998.

[196] G G Meyerhof. Behaviour of pile foundations under special loading conditions: 1994 R. M. Hardy keynote address. Canadian Geotechnical Journal, 1995.

[197] NETLIB GO numerical library. Website: http://www.netlib.org, August 2002.

[198] J H Vugts and L A Harland. Diffraction analysis of the opti-owecs monotower. Technical report, Workgroup Offshore Technology, Delft University of Technology, June 1997.

[199] British Geological Survey. Sea Bed Sediments Around the United Kingdom: North and South sheets. British Geological Survey, 1987. ISBN: 0751812145.

[200] National Wind Power Offshore Ltd. North Hoyle: New horizons for sustainable energy. Website http://www.natwindpower.co.uk/northhoyle/northhoyle.htm, January 2004.

[201] V N D Caston. Quaternary sediments of the North Sea. In F T Banner, M B Collins, and K S Massie, editors, North West European shelf seas: the sea bed and the sea in motion. Elsevier, 1979.

[202] Grass Development Team. Grass 5.3.x Reference Manual. Istituta Trentino di Cultura, 2003. Available at http://grass.itc.it.

[203] ESRI Arcview Website. Website http://www.esri.com, November 2003.

[204] Clark Labs IDRISI Website. Website http://www.clarklabs.org, November 2003.

[205] N G Mortensen, L Landberg, I Troen, and E L Petersen. Wind Atlas Analysis and Application Program (WASP) Getting Started. Riso National Laboratory, Roskilde, Denmark, January 1992. ISBN 87-550-1792-4.

[206] H Schmidt and J Puttker. Wind and wave conditions in 55 European coastal sea areas, determined from weather and wave observations of voluntary commercial ships. Technical report, Deutscher Wetterdienst, 1992.

[207] Fugro GEOS. Wind and wave frequency distributions for sites around the British Isles. Offshore Technology Report 2001/030, UK Government Health and Safety Executive, 2001.

[208] S Lumby. Investment Appraisal and Financing Decisions. Chapman and Hall, fourth edition, 1991.

[209] T T Cockerill and M Kuhn. Structural and Economic Optimization of Bottom-Mounted Offshore Wind Energy Converters: Report on the First Phase, chapter 1, pages 6–19. Institute for Wind Energy, Delft University of Technology, 1996.

[210] P B Simpson, M Hancock, S Driver, and G Gardner. Offshore wind energy assessment Phase IIC: Reassessment of costs of offshore HAWTGs and their effect on the cost of energy. Technical report, Wind Energy Group Ltd for UK DTI, 1994.

[211] Taywood Engineering. Report on offshore wind energy assessment Phase IIB study. Technical Report E/5A/CON/5009/560, ETSU for UK DTI, 1985.

[212] R T Fenner. Finite Element Method for Engineers. Imperial College Press, 1997. ISBN 1-86094-095-1.

[213] J Dongarra, J Bunch, C Moler, and P Stewart. LINPACK numerical library. Website: http://www.netlib.org/linpack, August 2002.

[214] EISPACK numerical library. Website: http://www.netlib.org/eispack/ index.html, August 2002.

[215] CA Morgan and AJ Tindal. Further analysis of the Orkney MS-1 data. In Davies TD; Halliday JA; Palutikof J, editor, Wind Energy Conversion: Proc. Twelfth BWEA Wind Energy Conference, pages 325–330, London, March 1990. Mechanical Engineering Publications Ltd.

[216] B Lange, S Larsen, J Hojstrup, and R Barthelmie. Modelling the vertical wind speed and turbulence intensity profiles at prospective offshore wind farm sites. In Proceedings of the Global Wind Power Conference, April 2002.

[217] J P Coelingh and A J M van Wijk. Analysis of wind speed observations over the North Sea. Journal of Wind Engineering and Industrial Aerodynamics, 61:51–69, 1996.